UNIVERSITY OF BELGRADE

FACULTY OF MECHANICAL ENGINEERING

Kaled M. B. Legweel

EFFECT OF BIOMATERIAL ON INTEGRITY AND LIFE OF ARTIFICIAL HIP

Doctoral Dissertation

Belgrade, 2016

UNIVERZITET U BEOGRADU

MAŠINSKI FAKULTET

Kaled M. B. Legweel

UTICAJ BIOMATERIJALA NA INTEGRITET I VEK VEŠTAČKOG KUKA

doktorska disertacija

Beograd, 2016

Mentor of the doctoral dissertation

Dr Aleksandar Sedmak, professor,

University of Belgrade Faculty of Mechanical Engineering

Members of the doctoral dissertation committee:

Dr Zoran Radaković, professor,

University of Belgrade Faculty of Mechanical Engineering

Dr Miloš Đukić, assistant professor,

University of Belgrade Faculty of Mechanical Engineering

Dr Katarina Čolić, research associate,

University of Belgrade, Innovation Centre of Faculty of Mechanical Engineering

Dr Marko Rakin, professor,

University of Belgrade, Faculty of Technology and Metallurgy

Defense date:

ACKNOWLEDGEMENTS

I wish to express my sincere appreciation to prof. dr Aleksandar Sedmak for his guidance and insight throughout the duration of this research.

I would specially like to express my gratitude to associate prof. dr Aleksandar Grbović, dr Katarina Čolić and Uroš Tatić for their useful guidance during my research, especially for their valuable advice during the development of numerical models.

I am very grateful to dr Sanja Petronić, Simon Sedmak and Branislav Djoredjević for their great help throughout the duration of this research.

I would also express my gratitude to prof. dr Marko Rakin, prof. dr Zoran Radaković and assistant prof. dr Miloš Đukić for serving as dissertation committee members and providing positive suggestions and comments.

Author

EFFECT OF BIOMATERIAL ON INTEGRITY AND LIFE OF ARTIFICIAL HIP

Abstract:

Hip replacement is a surgical procedure in which parts of the hip joint are removed and replaced with artificial parts, which is known as the prosthesis. Metallic alloys are used for prosthesis, its femoral head and stem are often made of cobalt-chromium alloy. The thesis shows the basic groups of metallic biomaterials and implants used in orthopedics, as well as problems that occur due to failure of these implants.

This thesis presents an analysis from a mechanical perspective of Co-Cr multiphase alloy materials that are used in total hip replacement implants. Design parameters that should be considered for hip implants are fatigue and fracture. An experimental elastic-plastic fracture behaviour analysis is presented in order to evaluate a resistance of the aged and unaged MP35N alloy. The width of the final stretch zone is considered a fracture mechanics parameter, but it should be noticed that this parameter is quite difficult to measure. Method for stretch zone width determination was analyzed, and beside standard fracture mechanics test, this measuring technique includes scanning electron microscopy (SEM). An attempt has been made to determine the final stretch zone width as a fracture parameter for MP35N alloy. It is shown that critical J_i integral value can be obtained from J-R curve as value that corresponds to the average stretch zone size or average stretch zone width. It is possible to correlate these results with obtained J_{Ic} values, and good agreement between them is shown. Another important task was to investigate SEM microphotograph of fracture surface for various specimens and to analyze microstructure of stretch zone. The results indicate that around the crack tip at the stage of crack propagation mixed loading conditions are predominant.

In this thesis a numerical investigation of replacement implant for partial hip arthroplasty is presented. A finite element analysis (FEA) was performed using 3-dimensional models to examine the mechanical behaviour of the femoral component at forces ranging from 3.5 to 6.0 kN. This implant design was chosen for numerical analysis because stress concentration in femoral component lead to implant fracture. Results show that the force magnitudes acting on the implant are of interest, and that they can cause implant stress field changes and implant stability problems, which can lead to implant failure.

For the simulation of crack propagation extended finite element method (XFEM) was used, as being one of the most advanced modeling techniques for this type of problem. Short theoretical background information on the XFEM is provided, as well as the representation of crack and the stress intensity factors computation.

Keywords:

hip replacement implant, MP35N multiphase alloy, microstructure, final stretch zone width, stress intensity factor, crack growth, numerical simulations, extended finite element method

Scientific field:

Technical sciences – Mechanical engineering

Narrow scientific field:

Material sciences

UDK:

620.172:669.15:539.42(043.3)

615.477.2:539.42:519.6(043.3)

UTICAJ BIOMATERIJALA NA INTEGRITET I VEK VEŠTAČKOG KUKA

Rezime:

Zamena kuka je hirurška procedura u kojoj se najčešće delovi kuka otklonjaju i zamenjuju veštačkim delovima, poznatim kao proteze. Za proteze se koriste legure metala, a najčešće su femoralna glava i stem proizvedeni od kobalt-hrom legura. U ovoj disertaciji su prikazane osnovne grupe metalnih biomaterijala i implantata koji se koriste u ortopediji kao i problemi zbog kojih dolazi do otkaza tih implantata.

Predstavljena je analiza višefaznih Co-Cr legura koje se koriste kod implanata kuka. Faktori koji se uzimaju u obzir pri izradi dizajna kuka su otpornost na zamor i lom materijala. Analizirane su eksperimentalne elasto-plastične osobine materijala u cilju da se odredi otpornost kako legure MP35N izložene strenju, tako i MP35N legure koja prethodno nije bila izožena starenju. Širina zone ukupnog razvlačenja je određena kao parametar mehanike loma. Metoda za određivanje zone ukupnog razvlačenja je razmatrana, korišćenjem SEM mikroskopa i standardnih testova mehanike loma. Prikazano je da kritična vrednost J_i integrala može biti dobijena iz J-R krive kao veličina koja odgovara prosečnoj veličini zone razvlačenja ili prosečnoj širini zone razvlačenja. Pokazano je da je moguće porediti ove rezultate sa dobijenim vrednostima J_{Ic}, pri čemu je pokazano dobro slaganje dobijenih rezultata. Još jedan bitan zadatak je bio da se ispitaju prelomne površine na velikom broju epruveta korišćenjem SEMa i da se izanalizira mikrostruktura zone razvlačenja. Rezultati su pokazali da oko vrha prsline u fazi propagacije prsline dominantni su uslovi mešovitog opterećenja.

Pored eksperimentalne analize u ovoj disertaciji prikazana je i numerička analiza implantata kuka. Proračun metodom konačnih elemenata je izvršen korišćenjem tordimenzionalnih modela za ispitivanje mehaničkog ponašanja femoralne komponente. Opterećenje je zadato je u obliku sile inteziteta 3.5 - 6.0

kN. Otkaz impantata kuka dolazi zbog loma nastalog usled velike koncentracije napona u zoni femorala. Rezultati pokazuju da intezitet sile koja deluje na implantat predstavljaja bitan faktor koja izaziva promenu napona i stambilnosti, i koja može prouzrokovati otkaz implantata.

Za simulaciju propagacije prsline korišćena je proširana metoda konačnih elemenata, kao jedna od naprednih tehnika za modeliranje ovakbih vrsta problema. Prikazana je prslina, proračun faktora inteziteta napona i kratka teoretska osnova proširene metode konačnih elemenata.

Ključne reči:

implat kuka, MP35N legura, mikrostruktura, širina zone konačnog razvlačenja, intezitet faktora napona, rast prsline, numerička simulacija, proširena metoda konačnih elemenata.

Naučna oblast:

Tehničke nauke – Mašinsko inženjerstvo

Uža naučna oblast:

Nauka o materijalima

UDK:

620.172:669.15:539.42(043.3)

615.477.2:539.42:519.6(043.3)

TABLE OF CONTENTS

CHAPTER 1

1. Introduction

Hip joint replacement is one of the most important application of biomaterials in medicine, and also one of the most frequently used surgery worldwide. More than 200,000 surgeries are performed only in Europe each year, based on the first attempt by John Charnley, [1]. Replacing degenerated or fractured hip has been enabled by insertion of metallic femoral support into a channel made inside femoral bone, whereas ultra high molecular weight polyethylene (UHMWPE) has been used for acetabular bone cup, [1-3].

Charnley's primary aim was to adopt use of of polymethylmethacrylate cement to bond femoral support and acetabular cup. More advanced design of this implant included cementless bonding, [4,5]. With development of bioceramics, material choice for total hip replacement is completed after 1970, as shown in Table 1.1, [4].

Table 1.1. Materials for total hip replacement [4]

Component	Material
Femoral Stem	Co-Cr alloys or Ti-6Al-4V
Ball	Co-Cr alloys
Acetabular Cup	Ultrahigh molecular weight polyethylene (UHMWPE)
Cement	Polymethylmethacrylate (PMMA)
Cementless	Porous surface coating or hydroxyapatite coating

Figure 1.1. shows all the components of the hip implant, femoral stem and acetabular cup of the prosthesis.

Prostheses can be monoblock when they consist of one part, or modular when consisting of two or more parts, and where their assembly is necessary during operation, [6-9].

Suffering weight and implant movements can lead to the generation of wear microparticles, which can lead to other problems that are direct indicators for structure integrity problems of a prosthesis. The main source of wear under normal conditions is the bearing surface of the cap, [10-12].
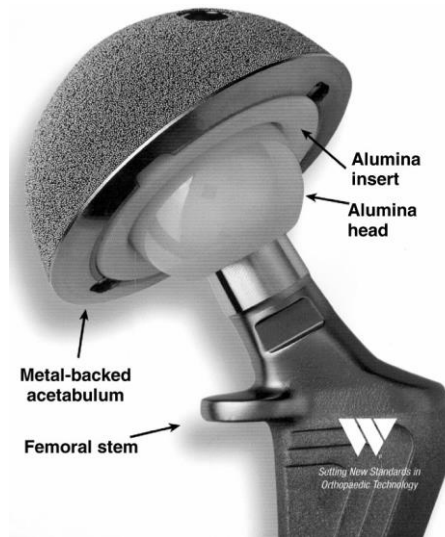
Figure 1.1 Total hip replacement prosthesis, [5]

Recent investigations include numerous efforts to modify the properties of biomaterials in order to improve final surface of the femoral head and to develop other weight supporting couples, such as ceramic-ceramic and metal-metal bearing surfaces, [4,5,13-17].

Contact between the hip prosthesis and the bone in which it is set can be accomplished by two techniques, i.e. the cement and cementless method. By using the cement methods it common problem that crack appears in cement material, what also can be a factor in losing the integrity of an implant, [18].

As the surgery itself develops, the methods for the artificial hip implementation are improving, and therefore the attention must be paid to the materials that are used in these new techniques, [19-25].

1.1 Biomaterials

Biomaterials are used for replacement of tissue or organs, either for medical or for esthetic reasons. Biomaterials can be defined as artificial materials designed to replace living parts in human body and to fulfil their function in certain period of time. Many definitions can be found in literature,[4,5,10]. Let us just state the one from 1987 by Dejvida F. Williams: *„Biomaterial is a material which is not alive on its own, but as a part of implant it interacts with biological systems being in contact with, and in this way it survives."*

Biomaterial science has bloomed recently, whereas biomaterials became everyday clinic practice, including hip replacement. Common property for all biomaterials, regardless on all their differences, is biocompatibility. Biological inertness and mechanical properties should be appropriate, as well, including biocompatible metallic materials, used for implants. Another important request is non-toxicity. In ideal case biocompatible metallic materials should not corrode at all, and should have no damage during entire life. In the case of hip replacement the higher the fatigue strength and corrosion resistance, the better, so that friction and wear produce minimum damage.

Modulus of elasticity of biomaterials is typically 5-10 times higher than the natural one, which is significant problem because of "shielding" effect. Namely, due to this large difference in moudli of elasticity, surrounding bones are almost free from stress, reducing their density and leading to their failure. Therefore, very important request for hip implant is that difference between biomaterial and natural modulus of elasticity is as low as possible, [[25-29]].

Non-toxicity is an extremely important characteristic of implant materials with respect to the release of metal ions and other products may affect the occurrence of cancer, deformities, allergies, necrosis, calcification and inflammatory processes, [30-34]. In practice, the further development of

biocompatible materials, which could be used to develop more adequate biomedical implants, is an area that is constantly evolving, [35-38].

1.2 Integrity and life of hip implants

Hip loading can be as high as body weight multiplied by factor 5 to 7, [9]. Figure 1.2 shows schematically hip joint prosthesis, indicating its capability to move almost without friction, [39-41].
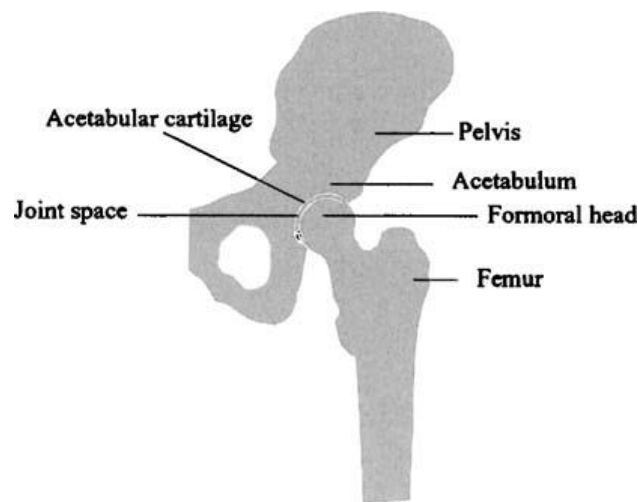
Figure 1.2. Schematic representation of the hip joint

Anyhow, if cartilage is damaged, hip movement causes significant pain and replacement is inevitable, [2,3]. Nowadays this is routine procedure, but implant integrity and life remain significant problem. There are many possible causes for implant premature failure, such as implant loosening and wear, Fig. 1.3, [9,10]. To improve integrity and life of hip implant, two major factor should be considered, design and biomaterial. Therefore, the design of a number of biomedical implants must have a certain degree of reliability as a function of its specific application, [42-46].

Figure 1.3. Failure of hip implant, [10]

Table 1.2. List of the some ISO standards for hip implants

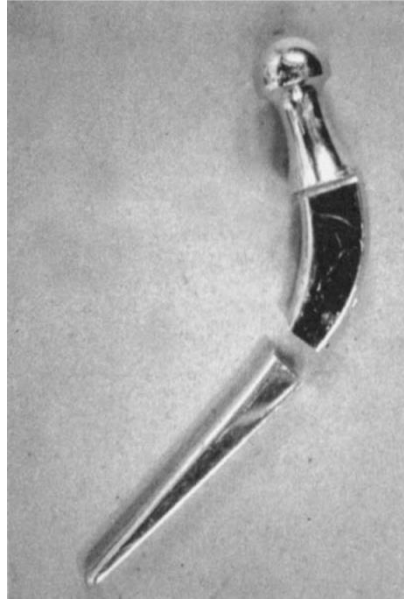| Table 2	List of some of the ISO standards for hip and knee joint prostheses.
ISO/TR 9325:1989	Implants for surgery—Partial and total hip joint prostheses—Recommendations for simulators for evaluation of hip joint prostheses
ISO 7206-1:1995	Implants for surgery—Partial and total hip joint prostheses—Part 1: Classification and designation of dimensions
ISO 7206-2:1996	Implants for surgery—Partial and total hip joint prostheses—Part 2: Articulating surfaces made of metallic, ceramic, and plastic materials
ISO 7206-4:1989	Implants for surgery—Partial and total hip joint prostheses—Part 4: Determination of endurance properties of stemmed femoral components with application of torsion
ISO 7206-6:1992	Implants for surgery—Partial and total hip joint prostheses—Part 6: Determination of endurance properties of head and neck region of stemmed femoral components
ISO 7206-8:1995	Implants for surgery—Partial and total hip joint prostheses—Part 8: Endurance performance of stemmed femoral components with application of torsion
ISO 7207-1:1994	Implants for surgery—Components for partial and total knee joint prostheses—Part 1: Classification, definitions, and designation of dimensions
ISO 7207-2:1998	Implants for surgery—Components for partial and total knee joint prostheses—Part 2: Articulating surfaces made of metal, ceramic, and plastic materials
ISO/TR 9325:1989	Implants for surgery—Partial and total hip joint prostheses—Recommendations for simulators for evaluation of hip joint prostheses
ISO/TR 9326:1989	Implants for surgery—Partial and total hip joint prostheses—Guidance for laboratory evaluation of change of form of bearing surfaces
ISO 14242-1:2002	Implants for surgery—Wear of total hip-joint prostheses—Part 1: Loading and displacement parameters for wear-testing machines and corresponding environmental conditions for test
ISO 14242-2:2000	Implants for surgery—Wear of total hip-joint prostheses—Part 2: Methods of measurement
ISO 14243-1:2002	Implants for surgery—Wear of total knee-joint prostheses—Part 1: Loading and displacement parameters for wear-testing machines with load control and corresponding environmental conditions for test
ISO 14243-2:2000	Implants for surgery—Wear of total knee-joint prostheses—Part 2: Methods of measurement
ISO 14879-1:2000	Implants for surgery—Total knee-joint prostheses—Part 1: Determination of endurance properties of knee tibial trays
ISO 15032:2000	Prostheses—Structural testing of hip units

ASTM has formed Committee for surgical implants, namely ASTM F4, to establish standards and documents for procedure and recommandations regarding safe replacement of hip joint. Standards developed by ASTM F4

Committee can be classified according to: materials, design and dimensions; testing methods; exploitation behaviour, [47-49]. These standards are adopted also by ISO, [50-53], as listed in Table 1.2.

They represent sound basis for any furhter elaboration on the integrity and life of hip implants.

1.2.1. Estimation of implant

Generally speaking, there are four primary attributes for estimtion of reliability, [10,46,54,55]:

- Quality. It specifies standards for materials, processes, production, manufacturing, measurments and control.

- Reliability. It specifies probability for flowless functioning of a product or system in the scope of its operating conditions.

- Safety. Identifies problems and aims of safe design, including the request for safe degradation of product if failure occurs.

- Performance. Defines limit up to which product or system realizes its aim or function in the scope of its technical characteristics and operating conditions.

1.3 Thesis topic

Hip implants still exhibit problem of premature failure, promoting their integrity and life at the top of the list of problems to be solved in near future. Also, wear is still significant problem due to inflamation caused by particles discharged from implant surface. Any damage due to wear and/or corrosion is ideal location for crack inititiation and further futigue growth.

Therefore, this thesis is focused on integrity and life of hip implants with an aim to improve their performance and reliability. Toward this aim, experimental and numerical methods have been applied to analyse problem and provide possible solutions.

Numerical models are based on the finite element method (FEM), including the extended FEM (X-FEM). Experimental testing of fracture mechanics properties has been performed.

Relevant literature also indicate integrity and life as the major problem for hip implants, emphasing fatigue as the main cause of premature failure, [9,10, 56-63].

1.4 Case Report

The patient was an active, 53 year-old man (178 cm, 114 kg) with advanced osteoarthritis of the left hip. [60,62,63] The femoral component was a cemented Exactech Opteon stem, size 3, with a 28-mm 110 Co-Cr femoral head (Exactech). Radiographs showed good implant position, Fig. 1.4.a. The patient returned to his usual work and reported no difficulty until 43 months postoperatively. Radiographs showed a fractured femoral prosthesis at the neck–shoulder junction Fig. 1.4.b.

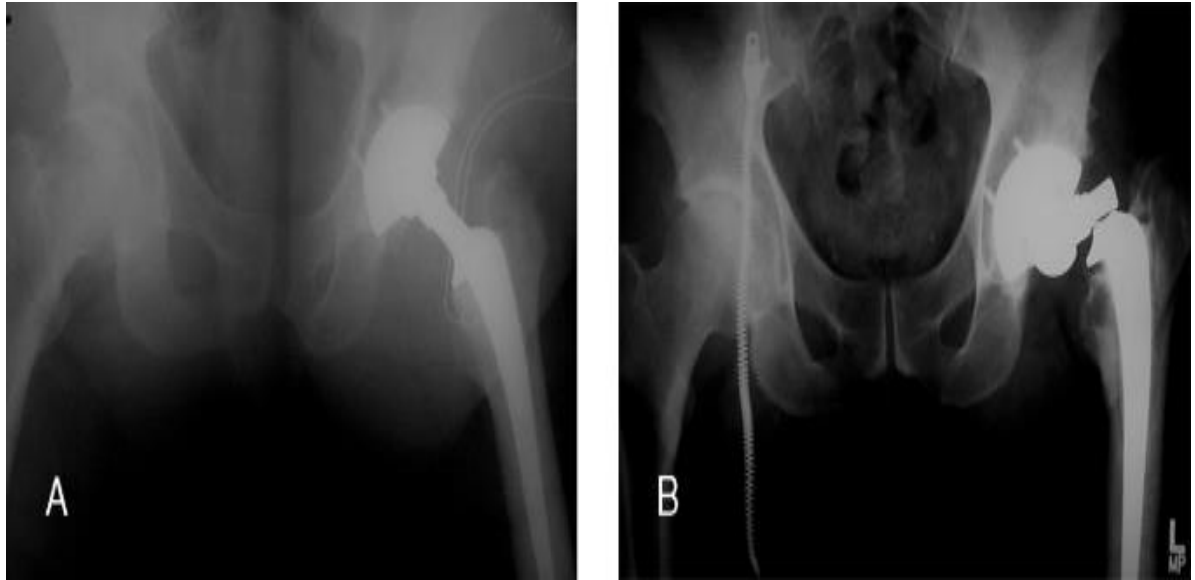*Figure 1.4. (a) Postoperative radiograph. (b) Followup radiograph shows fracture of the well fixed stem at the neck shoulder junction 43 months after implantation.*
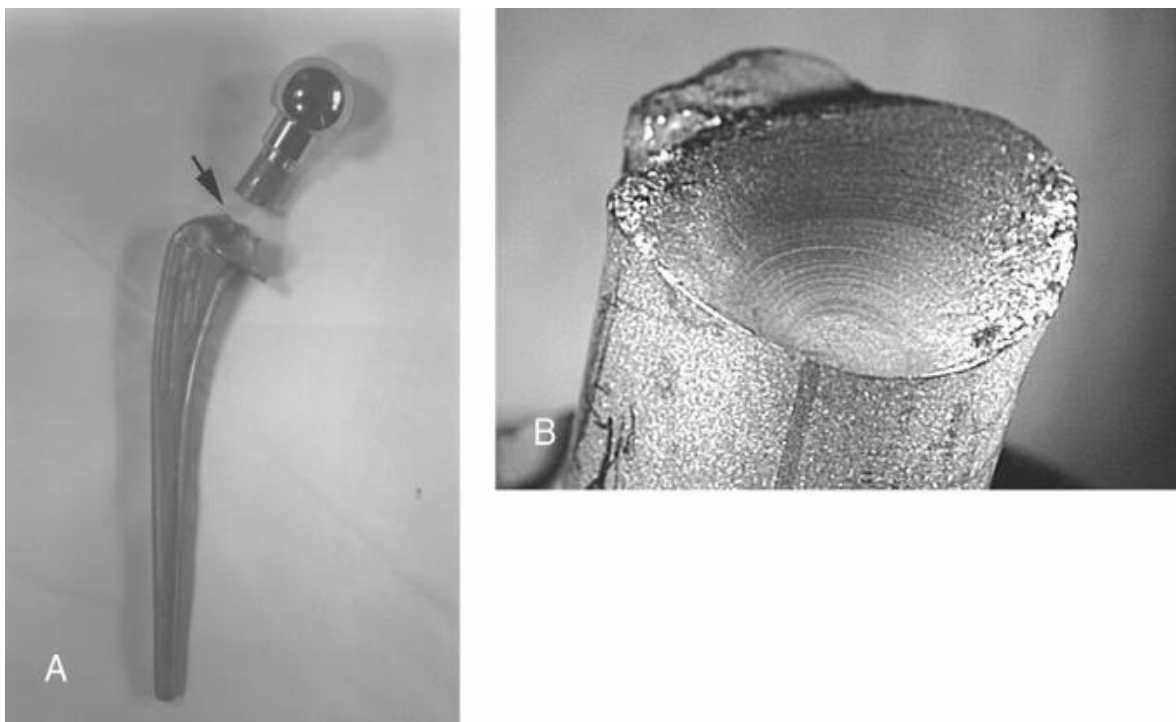
Figure 1.5. (a) Fractured implant from case (b) Magnified view of the implant fracture surface

It was concluded that pronounced laser etching at the lateral neck shoulder junction caused heat induced changes in the material microstructure

and the creation of a local stress riser, [63]. This decreased fatigue resistance in a highly stressed region of the implant, combined with high patient demands, appeared to result in the early fatigue failure of the implant, as is presented in Fig. 1.5.

Taking aforementioned into account, the model shown in Fig. 1.6 has been used for analysis, as being similar to the prosthesis type which failed, Figs. 1.4-1.5.

Figure 1.6. Model used for analysis

Taking into account the material of which prosthesis we made, i.e. CoCr multiphase alloy, for further investigation of the effect of biomaterial on the integrity of the hip prosthesis was chosen precisely this type of material, very often analyzed in the literature, [13,33,34,64-77].

Systemic effects of implanted prostheses made of cobalt-chromium alloys were investigated in [68-73] Systemic effects of Co-Cr alloy/polyethylene hip joint prostheses were investigated using instrumental neutron activation to determine the concentrations of up to 16 elements. In the work reported here, both the prospective and the retrospective investigations of serum and whole blood showed massive Co enrichments as a consequence of implant corrosion. The data show a wide range of individual burdening, ranging from practically no effect to the most extreme values. The analyses of organs revealed significant Co and Cr enrichment in several tissues and organs. Consequently, it can be seen that implant corrosion is not an occurrence of merely local significance, but

one that affects the trace element status of the entire organism, [68]. Particulate titanium and cobalt-chrome metallic debris in failed total knee arthroplasty were investiged in [57]. Titanium exhibited greater abrasive wear and elicited a different cellular response than cobalt-chrome under conditions of polyethylene failure allowing metal-on-metal contact. The variability of this foreign body reaction may be due to important differences in particle size and number, as well as in the material properties of the two alloys.

Considering metal to metal implants, cobalt chromium molybdenum metal combination for modular hip prostheses was investigated, [78]. The development of a metal combination for modular hip systems was motivated by the following observations: (1) wear particles from polyethylene acetabular components can lead to a foreign body reaction and late aseptic loosening and (2) well designed all metal hip prostheses had very low wear rates, usually causing no osteolytic problems. The realization of a metal combination consisted of the stable anchoring of a standard metal lining in a polyethylene insert that, combined, is intended to provide adequate load transfer and fit to either the bone cement bed or the titanium shell. From 1988 to 1995, approximately 40,000 metal combinations (Metasul) were implanted. From these, 44 single components, with a maximum time in situ of 5.5 years, were retrieved and examined. The total linear wear rate averaged 2 to 5 micrometers per year per component after the initial conditioning phase, [78]

Failure cases of CoCr implants are reported in relevant literature, [56-64,74-77]. This study reports an unusual case of late fatigue failure of a cobalt-chromium alloy cementless femoral stem which functioned well for 24 years. The failure occurred at the stem/neck transition radius remote from any modular interface. The crack initiated at the top tensile side at the implant surface following a minor traumatic event. It then propagated transgranularly up to about half of the neck cross section before final fracture occurred, which illustrates the high toughness of the implant, [58].

The results exhibited hot tearing, shrinkage porosity and metal oxide films due to inadequate heat dissipation during solidification process, as a consequence of poor investment casting ceramic mold configuration, [59]. Two femoral neck fractures and one fractured post of a femoral component of a total knee replacements. In all cases, fatigue was the mechanism of failure. The life time of these prostheses was 3-5 years. The porous coating; microstructural features, including large grains, carbides, porosity, inclusions and defects; design and manufacturing defects were all likely causative factors in these fatigue failures, [61]. Intermediate follow-up radiographs before the fracture were available in 7 cases, all of which demonstrated loss of calcar support. Scanning electron microscopy of the fracture surfaces in 3 of the components showed porosity near the initiation site. Metallography of polished and etched cross sections near the fracture surface revealed large grain size, [74]. These fractures occurred immediately adjacent to the base of the modular head. Skirted modular heads were used in 3 of the 4 failed components. This constructs promotes corrosion. Cyclic fatigue-loading in combination with the material factors of course grain microstructure and extensive carbide precipitation along the grain boundaries were also identified as the cause of implant failure, [75].

CHAPTER 2

2.1 Orthopedic biomaterials

To design an implant one has to know human body biomechanics. Resaerach in biomehanics and biomaterials lead to better results in *in vivo* conditions. Orthopedic implants are very successful in regaining movebility and improving quality of life, and they can be classified into two basic groups, table 2.1., [4,5,10,79-81].

Table 2.1. Orthopaedic implants

Implants for fixation after breakage	Joint replacement
Implants for fixation of backbone Wires, screwa and needles Artifitial ligaments Intramedular wedge Platelets	Hip Knee Ancle joint Shoulder Elbow Wrist Fingers

Figure 2.1 shows human sceleton with protheses for joint replacement, [5]. Prostheses can be classified into total and partial. Total protheses are permanent implants with irreverable surgery beacuse large part of bone is replaced. Contrary to that, in the case of partial prosthesis only a part of bone and artilage is removed enabling later interventions.

Implant design and shaping is based on dinamic and kinematic loading characteristic for each joint, [3,40,41].

Oveloading on implant-bone connection or loading constraints can cause bone resorption, and implant loosening and failure.
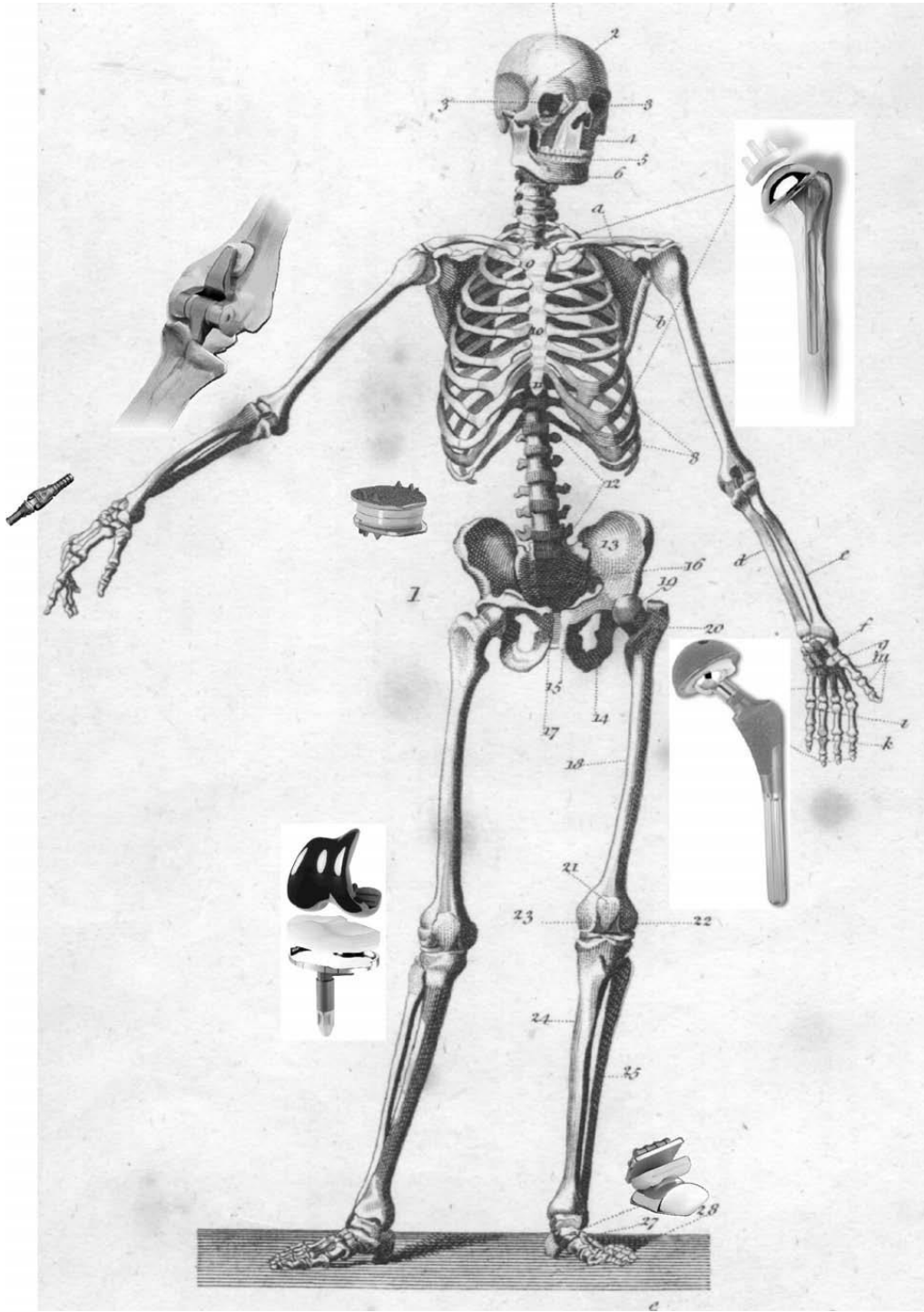
Figure 2.1 Human skeleton with joints and their eventual replacements[5]

2.2 Hip implants

Hip replacement is common orthopedic procedure applied to patients with serious degenerative osteoarthritis or rheumatic arthritis (Fig. 2.2), [10]. These implants comprise the basis, built in femur bone channel to stabilize prothesis, and joint parts. In the case of total hip replacement, femur head prosthesis id made of Co-Cr alloy, whereas basis is made of Ti alloy. Joint surfaces are typically made of Co-Cr alloys and ultra high density poliethilene (UHDP), because this combination results in low friction between sliding surfaces, also providng appropriately shaped joint surface due to UHDP plasticity.

Figure 2.2. Total hip replacement due to osteoarthritis,[10]

Total hip replacement is typical for older patients with serious osteoarthritis. Anyhow, study (Implant Committee of the Japanese Orthopedic Association, 2000) of hip implants has shown that their wear and failure occurafter 5-10 years. Therefore, interity and life of hip implants is still of utmost importance, [82-85].

2.2.1. Total hip prothesis

The hip is one the largest joints in a body, enabling wide range of movements in differnet planes and stability, at the same time. Being in between lower extremities and sceleton, hip supports significant amount of loading, as produced by human body, [6-9,86]. Hip joint consists of femur head (front part of femor bone) positioned in a pelvis hollow named acetabulum, Fig. 2.3, [10].
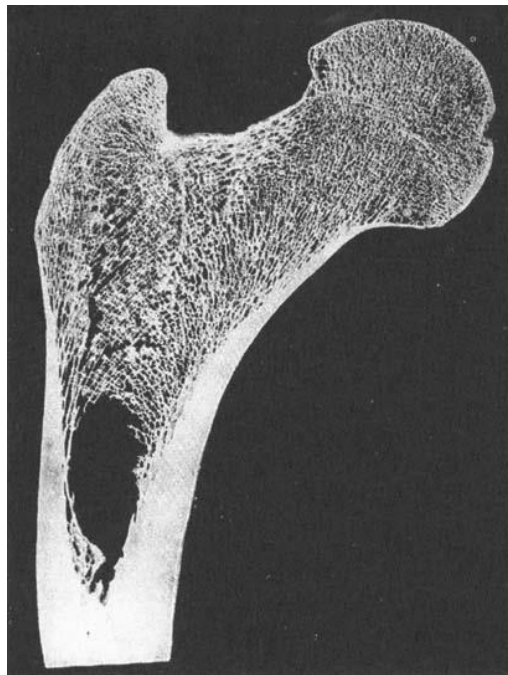
Figure 2.3. Anatomy of a human hip joint

The first documented attempt to replace femoral head dates from 1891, when *Gluck* used prosthesis made of ivory, fixed by screws and cement, but not successfully. Later on, in 1938, prosthesis was made of stainless steel to replace femoral head and acetabulum, while in 1940 implant was made of cobalt-chromium alloy. More advanced version of such an implant named *Austin Moore prosthesis,* is still used taday in some rare cases. In 1960 *Charnley* performed the first total hip replacement, using femoral component of stainless steel and acetabulum of poliethilene, fixed by acryl cement. Finally, in 1970-ies ceramic prosthesis has been introded due to its high wear resistance, but at the expense of low toughness, [16].

2.2.2. Prosthesis types

Prosthesis can be monolite, having just one part, or modular, having two or more parts. Both type have advantages and disadvantages. Monolite prostheses are cheaper, have better corrosion resistance and are not prone to disassembling. Anyhow, in some cases, like prolongation of extremities, modularnu prosthesis is needed in order to use different femur lengths, [4-9,50]. Also in this case, different parts can be made of different materials. Thus, the strongest material is used for femoral basis since it is the most stressed part, both regarding static and dynamic loading, Table 2.2, [52].

Critical parameters for femoral head production are, [53]:

- Surface roughness, affecting friction and wear.
- Maximal outer diameter.
- Resistance to tensile force along joint.

Table 2.2. Materials used for modular prosthesis parts[52]

Component	Material type	material
Femoral basis	Metal	CoCrMo,Ti legure, stainless steel
Femoral head	Metal	CoCrMo, stainless steel
	Ceramics	Alumina, zirconia
Acetabulum	Polymer	UHMWPW, XPLE
	Metal	CoCrMo
	Ceramics	Alumina, zirconia
Acetabulum shell	Metal	CP Titanium, stainless steel

Femoral head made of ceramics has smoother surfacereducing friction, but its maximal diameter is 40 mm, due to production limitations. Larger diameters enable better stability and movability of replaced hip joint. Acetabular part is usually made of two different materials, except in the case of metal on metal hip implant, [15,32,33,87-90].

In the middle of the twentieth century Charnley introduced polymethyl methacrylate as a means of fixation for bones and prostheses. It should be noted that polymethyl methacrylate is not primarily a binder, but the adhesive material which has the task of uniformly distributing load to the hip prosthesis, [91-95].

Cementless prosthesis are fixed using biological method, i.e. natural bone growth, enabled by special design and materials, Fig. 2.4, [5]. Structural part of prosthesis is coated by thin layer of porous metallic alloys, based on cobalt or titanium, or by bioactive materials based on calcium phosphate (calcium hydroxiapatite, tricalcium phosphate), [9,96,97].
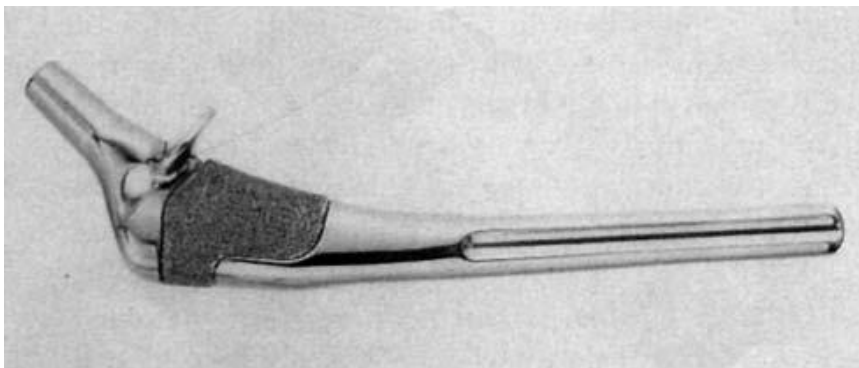
Figure 2.4. Cementless prosthesis, [5]

There are six different types of cementless prosthesis, regarding its shape, Fig. 2.5. Types 1,2,3 are designed for better proximal fixation, type 4 is coated with porous material for better distal fixation, type 5 is modular prosthesis and type 6 is curved, but rarely used, [98,99].
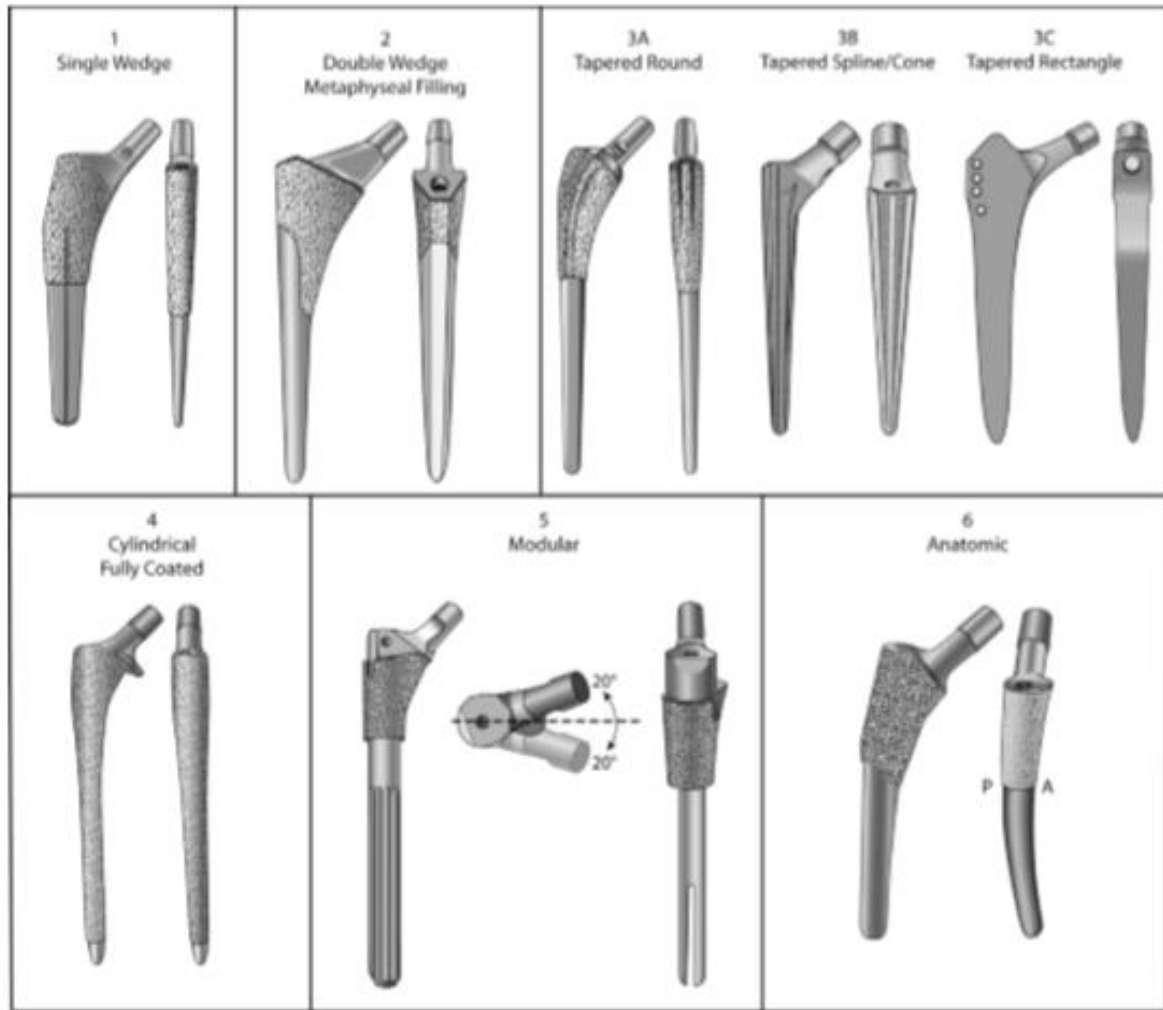
Figure 2.5. Cementless types of prosthesis, [98]

In older patients, with less vital bone tissue, bone cement compensated deficiencies. In younger patients, the benefits of cementless prosthesis is usualy used, mainly beacuse re-operation, which would be complicated in the case of the presence of cement, [98-102].

2.3 Materials used for total hip prosthesis

Orthopedic biomaterials are exposed to fatigue loading, limiting the choice to metallic materials having strength, corrosion and wear resistance, as well as biocompatibility, [4,5]. At the begining the most used metallic materials

were strainless stell 316L and CoCr alloys, but nowadays Ti alloys and CoCr and mostly used for femural component, in combination head of ceramics or CoCr alloy and PMMA as a cement. Acetabulum is made of ceramics or UHMWPEa and positioned in Ti or CoCr layer to be cemented or fixed by screws.

Table 2.3 Mechanical properties of biometerials for hip implant, [4,5]

	Modulus of elasticity (GPa)	Yield stress (MPa)	Tensile Strength (MPa)	Fatigue Strength (MPa)	Hardness (HVN)	Elongation (%)
Bone						
Low stress	15.2	114t	150c 90t	30-45	-	-
High stress	40.8	-	400c 270t	-	-	-
Metallic materials						
Stainless steel	190	792	930t	241-820	130-180	43-45
CoCrMo	210-253	448-841	655-1277t	207-950	300-400	4-14
CPTi	110	485	760t	300	120-200	14-18
Ti-6Al-4V	116	897-1034	965-1103t	620-689	310	8

Mostly used stainless steels are 316L, according to ASTM. Anyhow, since their use in nowdays rare, this type of metallic material will not be discussed

here. The best choice of CoCr alloys is CoCrMo alloy, which will be discussed later, but the focus in this thesis is on commertially pure titanium (CPTi) and, mostly, on Ti-6Al-4V alloy, due to its superior mechanical properties. One big advantage of Ti alloys is its modulus of elasticity, being cca two times less than CoCrMo alloy and stainless steel, as shown in Table 2.3, [4,5]. Proshesis made of Ti alloys are shown in Fig. 2.6.

Figure 2.6. Prosthesis made of Ti alloys [10]

Figure 2.7. Proshesis made of porous material [103]

Porous materials are used for cementless prosthesis to replace cement, since they enable bone to grow into its porous structure and fix the proshtesis in this way, Fig. 2.7. [103]

So far, the only polymer used for implants is UHMWPE, being shaped under high pressure and temperature to produce components as shown in Fig. 2.8., [9,104]. Due to the problems of wear of biomaterial on the acetabulumpart made of polymer, bioceramics, mostly alumina, has been applied for this purpose, [105-107].

Figure 2.8. Component of hip implant made of UHMWPE, [9]

Finally, composite materials has been used recently, e.g. carbon-carbon composite, Fig. 2.9, where carbon fibres are combined with carbon powder during sintering process.

Figure 2.9. Implant made of composite [103].

2.4 Metallic biomaterials

Metallic biomaterials are used to replace or upgrade structural components of human body to cure damage due to aging, desease or incidents. Mainly, they are used for joints and dental implants, as indicated in Fig. 2.10, together with other applications. [10]

In metallic biomaterials used for hip implant corrosion may occur, as the unwanted metal reaction to the environment, i.e. human body. [10,108] As a biomaterial used in orthopedic surgery, only austenitic stailness steels are used. [97,109]
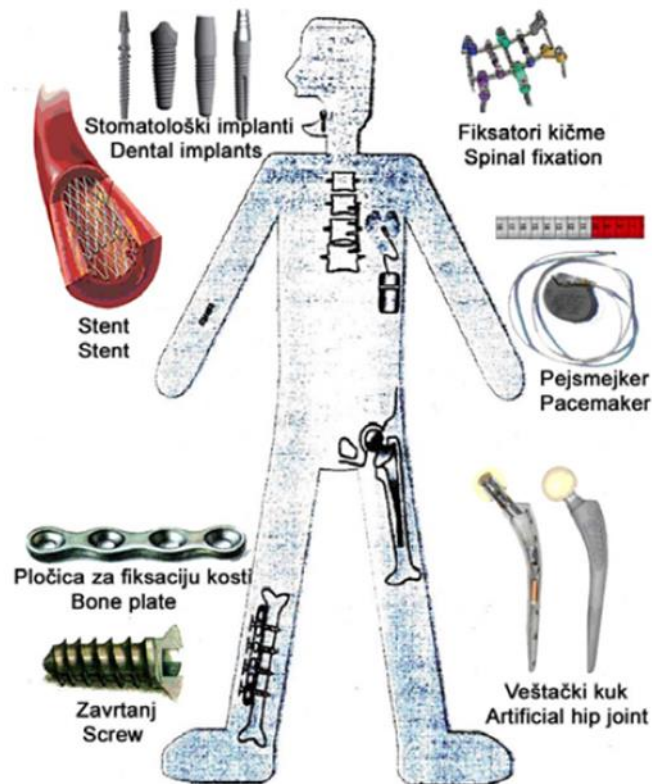
Figure 2.10. Medical implants made of metallic materials [10].

2.4.1. Titanium and its alloys

Titanium is very reactive element, forming strong bonds with oxygen, which is the main reason for its late commertial usage, starting back in 1940-ies in USA. Although being the last to be used for medical purposes, Ti and its alloys are nowadays the best option and the most frequently used metallic materials for hip impants, due to extraordinary combination of their properties: high specific strength, relatively low elasticity modulus, high biocompatibility and extremely low level of toxity. On the other hand side, its tribology properties are inferior comparing to Co-Cr alloys, but benefits of usage of Ti alloys certainly overcome this. [110]

Commertially pure (CP) Ti, has α microstructurom, as opposed to combination of α and β microstructure in Ti alloys. The CP Ti is produced in four basic purities, 1 to 4. It is mainly used for dental implants. . [110,111]
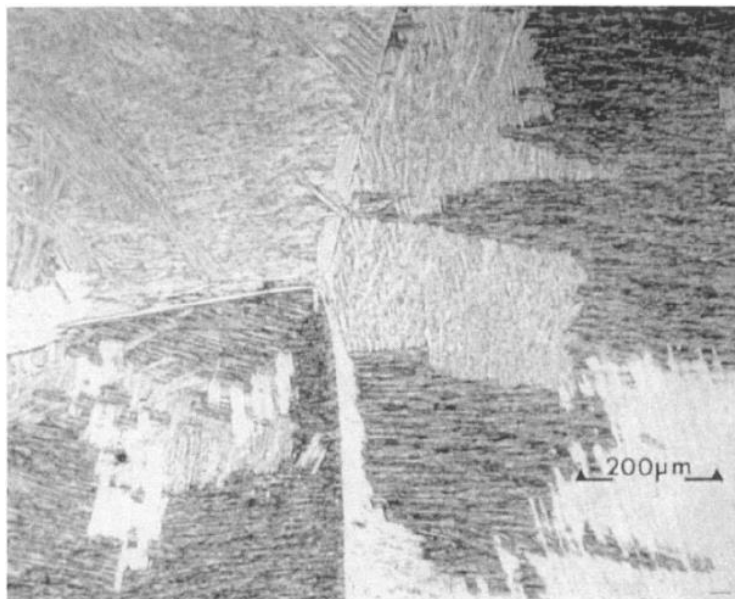
Figure 2.11. Ti6Al4V microstructure. 3 large grains (β faza), a struktura inside [110]

Titanium alloys, especially α + β type, such as Ti-6Al-4V, Fig. 2.11 and 2.12, are the most frequently used biomaterials, but recently have replaced by more advanced Ti alloys, in order to eliminate harmful effect of V, as it turned

out recently to be toxic to human body. Anyhow, this is of no relevance for research performed here, because integrity and life of these alloys are practically the same. . [110]

Figure 2.12. Hip implanr made of Ti alloy, [9].

2.4.2. Cobalt-chromium alloys

Pure Co, has face centered cubic (FCC) lattice above 419 °C, whereas below 419°C hexagonal closed packed (HCP) lattice exists. By alloying Co with Cr, Ni and Mo (e.g. MP35N alloy), microstructure becomes complex and enables transformations to obtain excellent mechanical properties.
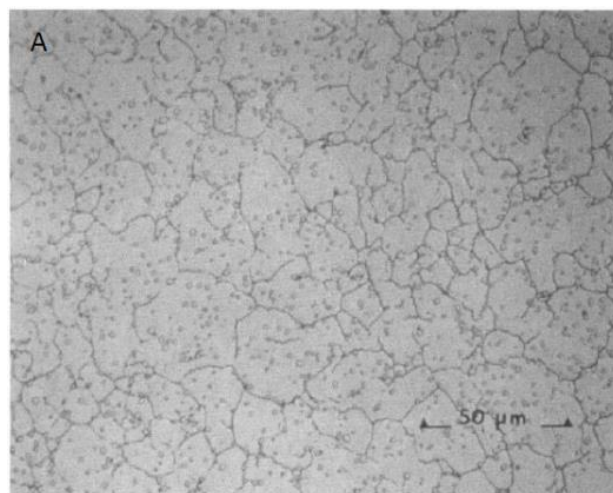
Figure 2.13. Microstructure of CoCrMo alloy obtained by HIP[5]

Development of these (super)alloys has started at the beggining of XX Century, with so-called "Vitalium denture" alloy for dental implants, [112-118] .

Typical microstructure of finegrain homogenous CoCrMo alloy is shown in Fig. 2.13[5]. Table 2.4 shows mechanical properties of different Co-Cr alloys. Mostly used nowadays are casted CoCrMo (F75) and forged CoNiCrMo legura (F562, *[10]*.

Table 2.4. Mechanical properties of biomedical Co-Cr alloys, [4]

Properties	Casted CoCrMo(F 75)	Forged CoCrWNi(F 90)	Forged CoNiCrMo (F562)		
			Annealed	Aged	Totally annealed
Tensile strength (MPa)	655	860	795-1000	1790	600
Yield stress (MPa)	450	310	240-655	1585	276
Elongation (%)	8	10	50	8	50
Contraction (%)	8	-	65	35	65
Fatigue strength (MPa)	310	-	-	-	340

Elasticity modul of Co-Cr alloy is between 220 and 234 GPa, which maked ''stress shielding'' problem even more pronounced than with stainless steel. Figure 2.14 shows hip implant made of Co-Cr superalloy.

Figure 2.14. Hip implant made of Co-Cr superalloy, [10].

CHAPTER 3

3.1 Factors influencing hip prosthetic integrity and life

3.1.1. Mechanical properties of bones

The bone can be defined as a firm endoskeletal connective tissue that adheres to body structure, protects internal organs, and allows movement, [4,5,119-121]. The bones have different shapes and complex external and internal structure and are seen as a viscoelastic material.

Femoral bone (Figure 3.1.), [5] , is the largest and strongest bone in the human body, located between the hip and the knee. This bone has an almost perfect cylindrical shape. It consists of a head, neck and body. The head is in the form of a hemisphere and has a smooth surface. Gate having a flattened pyramidal shape and connects the head and the body of the bone.
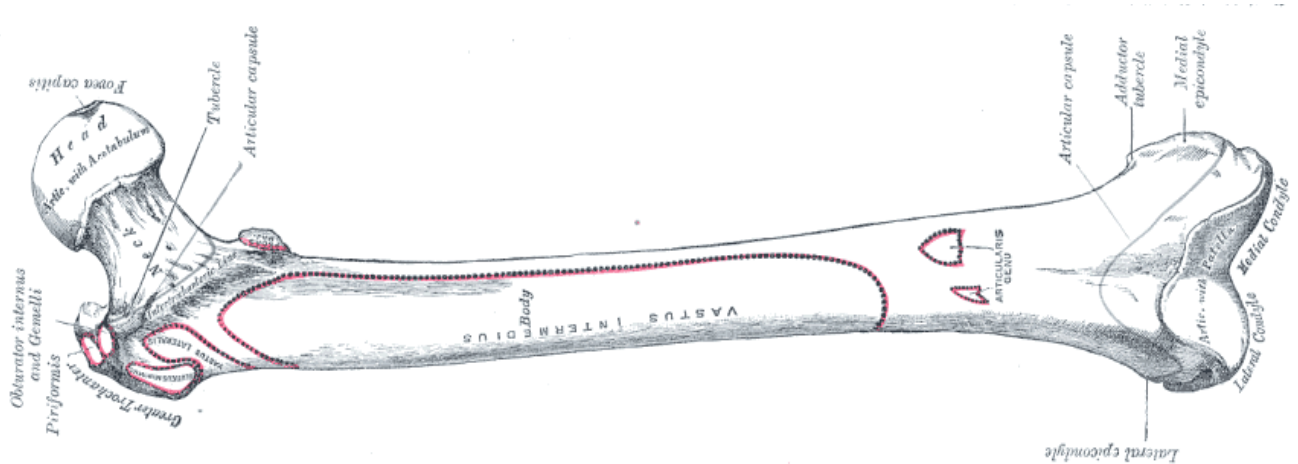

Figure 3.1. Femoral bone, [5]

From the mechanical standpint, the bone can be viewed as relatively sturdy and lightweight composite material formed mainly of collagen and

hydroxyapatite. In order to understand the properties of the bone it is necessary to understanding the organization of the two components.

Femoral bone has a relatively high compressive strength of about 170 MPa, which means it has good resistance to compression force, but not as good resistance to tensile and torsional forces. The modulus of elasticity of bone varies between 0.76 and 19.6 GPa, [4,119-121]. Although the bone is predominantly brittle material, it has a significant degree of elasticity, which is provided by collagen. Characteristics of the femoral bone vary depending on gender, age and level of activity of the individual.

Bones are organs that form part of the endoskeleton in vertebrates. Their role is to push, support the body and protect the organs of the same. The bones produce red and white blood cells and store minerals. The bone structure is similar to the one engineering-fiber composite material. [119-121].
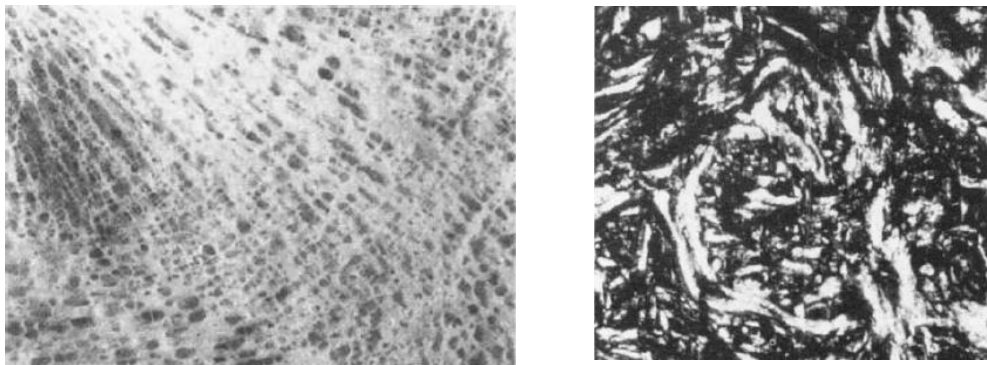
Figure 3.2. Shape of a compact and fibrous bone,[5]

Typical bone consists of a tube, which is also called the cortex. It contains a substantially rigid material and is called the "compact bone" or "kortikularna bone". The space within the tube is, if we look from the perspective of structure, hollow. This cavity is filled with bone marrow. At the ends of bones where the bones connect with other bones through joints, the cortex becomes much thinner and the interior is filled with a porous structure and is called the "kancelarna bone". This is also called the "spongy" bone part. Kancelarna bone

has a very important mechanical role. It receives compressive loads from the joints.

Compact bone (Figure 3.2), [4,5,119], can be displayed as a "primary" or "secondary", according to whether they are formed from the beginning (de novo), or replaces an existing bone. The fibrous bone consists of relatively loose structure that does not have any particular orientation. Collagen fibers are spread in all directions. The amount of the hydroxyapatite is quite small, and the porosity is relatively high. This type of bone is formed only in situations where the material needed to form in a short time, [5,119].

Fibrous bone (Figure 3.2.), [4,5,119], Is also formed during the adaptation of the bone. This means that when you need to come to a very rapid thickening of the bones. This can happen due to the excessive use of a bone or if some other bone becomes unusable because of breakage. Although there are various types of primary bone, there is only one kind of secondary bone called the secondary osteonalna (secondary Haversian) bone. Creating secondary bone begins with the removal of existing bone by the specialized cells called osteoclasts. These large cells dissolve bone, because the release of very strong reagents. This will create a cavity in the bone (or crater in the surface of the bone), which is then often supplement with new bone made by osteoblasts.

It is often said that the unique mechanical properties of bone. None of the individual characteristics is not some special extreme, but it is again very difficult to replicate the exact same characteristics and combinations of characteristics with some artificial material. Metallic materials which are frequently replaced with bone (e.g. hip) have greater strength and endurance (which is preferred), but also greater rigidity, which can lead to problems because they can start reducing the stress adaptation reactions in the surrounding bone. Only composite materials such as CFRP, offer the possibility of matching elastic rigidity because polymers themselves are not sufficiently rigid. Even then it is quite difficult to create composites with carbon fibers

having a modulus of elasticity at low bone (20 GPa) , [4,5]. In addition, they need to maintain adequate strength and durability. And all this should be done in a complex three-dimensional form requested.

3.1.2. Effects of the environment (organism)

Under normal conditions, bodily fluids represent 0.9% saline solutions containing amino acids and proteins. Body fluids are comprised of different types of fluids, such as tissue fluids, lymph and blood, but also contain solid components, such as traveling cells (leukocytes and macrophages) and blood particles (cells, platelets and erythrocytes). Under normal conditions, the pH of body fluids is 7 (although pH value due to the occurrence of inflammatory processes caused by surgery or injury can drop to 4-5), a value of temperature and pressure is 37 ° C and 1 atm (where the internal partial pressure of oxygen is a quarter of an atmospheric pressure of oxygen), [4,5,9].

Described biological environment of the human body is extremely corrosive for metallic materials. First of all, lower partial pressure of oxygen to provide the human body than in air accelerates corrosion of biocompatible metallic materials, as this reduces the speed of recovery of the pacifying oxide film after it is damaged or removed from the surface of the material. In the human organism the concentration of oxygen (such as O_2 or H_2O_2) can be extremely high due to the appearance of the inflammatory process, leading to accelerated corrosion of metals present in the human body. In addition, the man of the day, on average, took a few thousand steps with a frequency of 1 Hz, [122]. For this reason, artificial hips and knees, spinal fixation, bone fixation plates and wires, which are surgically implanted in the human body, suffer variable load, which corresponds to the cycle of walking, but the stress level of the implant, for example, artificial hip, several times higher than the impact of the body weight, [4,5,9].

Until the appearance of fatigue is caused by many years of cyclic stress which occurs due to normal daily activities of the human body. When it comes to fatigue, foreign body (metallic implant) is statically pressed against the surface of the object to which the cyclic strain (bones). The friction which then occurs as a result of the relative displacement of small amplitude of the contact surfaces of two components which are due to the compactness of the oxide layer formed on the surface of the implant, decreases, the surface layer of the crown, which provides education free metal surfaces. At the point of contact occurs cracks, which is expanding rapidly, causing fracture of metallic material. Artificial hips, bone fixation plates and wires, which are used in orthopedic surgery, often suffer due to the load effect of fretting fatigue, [60- 63,122-127].

Within the human body, friction caeses metal material to wear, which further leads to a continuous release of metal ions, metal compounds and wear debris (metal shavings). The release of these products into the tissue surrounding the medical implant, can cause poisoning of local tissue or diseased organs, a good example of this is the emergence of black tissue surrounding the implant, which indicates the occurrence of metallosis (Eng. Metallosis) in clinical orthopedics. When the appearance of fatigue occurs simultaneously with the corrosion of biocompatible metallic material, it is referred to phenomena of corrosion fatigue, although this phenomenon may be accompanied by additional friction which describes the fretting corrosion-fatigue.

The foregoing shows that the human body is an extremely aggressive environment for metallic materials, in chemical terms, and in terms of mechanical stress, thus decreasing the consistency of biocompatible implant metallic materials.

The way in which a suitable material is selected for orthopedic surgery in the first place depends on the number and importance of the requirements and criteria that have been set. In the case of a small number of requests, great

importance, the emphasis is on the qualitative and quantitative analysis of the properties and behavior of a small number of materials that come shortlisted, through information or experiences. The application of quantitative methods of decision-making takes into account a large number of demands and criteria, as it is considered a relatively large number of acceptable materials.

Optimal materials are selected by combining quantitative methods of decision making and expert knowledge. The level of security depends on the coverage of the decision requires reliable quantitative values or objective assessments. Metals, which are mostly used as biomaterials in orthopedics as stainless steel, cobalt-chromium alloys, titanium alloys. Stainless steel (316L) has excellent mechanical properties due to insufficient amount of chromium have a passive resistance to corrosion. Cobalt-chromium alloys are stronger and the passive layer that is resistant to corrosion, has increased strength, but reduced flexibility. Titanium alloys are separated from other metallic biomaterials for implants. Are preferred for their low weight, a greater specific strength and to superior biocompatibility in comparison to the other alloys. However, compared with stainless steel, have a lower flexural stiffness, poor mechanical strength. With the rise of impurities in commercially pure titanium is achieved by greater strength but also decreased flexibility.

Given that biocompatible materials are used not only in orthopedics but also in other areas of medicine, where they are in constant interaction with living tissue, it can be concluded that the development of new materials for application in medicine requires extremely important knowledge and understanding of the interactions mentioned, which biocompatibility and non-toxicity materials are becoming critical factors for further development of implant metallic materials. Also, as a basic guideline for further development of biocompatible metal materials allocated and the need to achieve low values of modern biocompatible metallic alloys, which would ensure that smaller difference between the modulus of elasticity of bone and the implant material

and thus prevent further damage to the bone tissue and reduce bone density. Primary selection of materials for artificial hip prosthesis shows that the application of quantitative methods for making solutions obtained in accordance with today's applications of materials in practice.

3.1.3. Possible complication after hip prosthetic implantation

The phenomenon of resorption of bone tissue around the proximal part of the femoral component of the implant is the most common complications of cementless prosthesis. Osteoresorption manifests itself during the first few weeks and months after installation of the implant. This phenomenon is progressive and leads to loosening of the prosthesis or to periprothetic fractures.

It should be noted that periprosthetic osteresorpcija is part of the adaptive physiological remodeling of bone tissue after implantation of the implant, but when osteoresorption overcome the physiological level and becomes massive, it can lead to rejection of the prosthesis aseptic loosening or fracture the surrounding bones. Use osteodensitometry measurements before surgery measurement of bone mineral density, and then monitoring changes in bone density after surgery, it is possible to detect early where patients will reach osteoresorpcije and timely take appropriate measures necessary to ensure the stability of the prosthesis, [9,10].

Postoperative infection is one of the worst outcomes of surgery, [6,7,128]. Factors that influence the occurrence of infection after total hip replacement were a large amount of foreign material, hematoma formation making its removal more difficult, due to insufficient mobility of the joint. In such cases, it is necessary to remove the implant and the necrotic soft tissue and bone, with the appropriate treatment. Loosening the set of components is one of the long-term and serious complications. Insufficiently precise surgical technique and

poor positioning of implants can accelerate the emergence of loosening, [6,7,128]. As a result of loosening may cause dislocation of the prosthesis. (Figure 3.3), [10].

Figure 3.3. Dislocation of a hip prosthetic, [10]

The following figure shows the proximal femoral osteolysis caused by polyethylene wear discharged products; the wear caused the displacement of the femoral head in relation to the acetabular glass (Fig. 3.4), [10].

Figure 3.4. Femur head dislocatioin relative to the acetabulum, [10]

Total hip arthroplasty is an area where improvements are constantly striving surgical techniques, implant design and materials used for making implants. Total hip arthroplasty is an effective, safe and relatively cheap

method that restores the functionality of the hip joint and relieve the patient's pain. After this operation, the patient needs to change some of their habits, e.g. they will not be allowed to squat to cross their legs, will have to sit and lie on a hard, elevated surface. However, regardless of what will no longer be allowed to work, the patient receives more obtaining relief from pain.

However, despite the fact that the first replacement of the hip joint made back in the 1940's (not counting ivory) still exists room forimprovement and enhancements, which may be able to reduce the number of complications and adverse reactions to the implant.

3.1.4. Influence of biomaterials

Various studies have shown that the metal alloy components used in orthopedics can have toxic and that are soluble in body fluids due to corrosion (1983). Each metal has its own unique internal toxicity to the cells (depending on concentration), wherein the corrosion process which determines the actual concentration. Therefore, in fact, corrosion resistance alloys and toxicity of individual metals in the alloy main factors that determine the biocompatibility.

Corrosion of metals in aqueous solutions occurs due to electrochemical mechanisms. Different metals have different internal prone to corrosion. More noble metals are less prone to corrosion. Corrosion reactions occur on the surface of the metal and in specific conditions (working environment) can cause a radical change in this "theoretical plemenosti". After implantation, the metal ion is surrounded by serum, proteins, and cells, which can modify impact on the local corrosion reaction, Figure 3.5., [5,10,108].

Figure 3.5. Corrosion of a metal implant used for total hip replacement, [5]

Numerous factors influence the corrosion of metals. Porosity and rough surface increases the reactivity of the surface area of the implant and hence overall corrosion resistance. Also loaded implant authorities are much more susceptible to corrosion compared with unladen areas. The composition, structure and thickness of the passive layer is very dependent on the type of metal and the composition of the working environment. Metals contain various errors such as grid faults, impurities and contaminants that can provoke corrosion reaction. Different heat treatment processes of metal processing and changing the grain size and the energy state of the material or cause the occurrence of surface inhomogeneities. All of these factors affect the stability of the surface layer and thus corrosion-proof.

Artificial hip joints of all, bears the greatest burden of alternating loads generated during periodic cycles of walking. Average healthy human make several thousand steps a day at frequency of 1 Hz. Another factor that needs to take into account the friction material of the implant under cyclic loading small amplitudes, which occur during normal walking patient. The emergence of friction causes wear between materials, which results in inflammation of the particles, which can in this way be released. Thus, the inside of the body chemically and mechanically adversely affect the structure of metallic materials, [4,5].

Wear always happens during articulation of artificial joints, as a result of mixed-mode lubrication. Since the beginning of athroplasty, attempts are made to reduce this wear through various combinations of materials and surface treatment. The search for materials with a significantly higher wear resistance is an important aspect of current research and development in the field of implants that are suffering load, and has not yielded satisfactory results, Figure 3.6., [5,10,124].
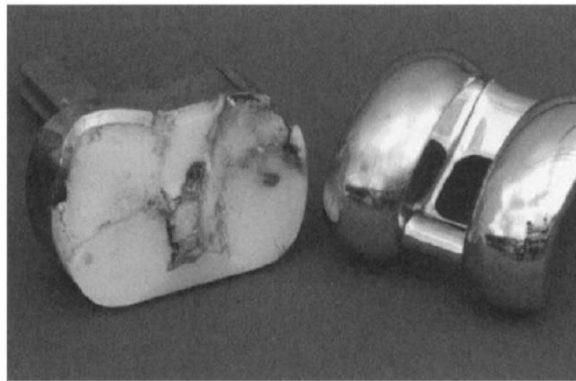

Figure 3.6. Total knee prosthetics failure due to wear in biomaterial, [5]

Particles resulting from wear, friction and fragmentation induce the formation of inflammatory reaction, which at a certain point is promoting granulation tissue response to a foreign body, which can attack the compound bone-implant. When clinical data on wear and tear on the entire population of patients notice significant variations, [106,107].

3.2 Examples of metal hip implants failure

For further analysis of the problem of preserving the integrity, two examples of hip replacement failure due to problems caused by wear and corrosion problems biomaterials are presented. [108, 130]

In the first case there was a problem of failure of the implant due to the appearance of cracks in biomaterials incurred as a result of problems of wear

basics hip replacement. The base is made of cobalt-molybdenum alloy refracted around nine years after implantation (Figure 3.7.)., [130].

Figure 3.7. An example of a broken prosthetic base of a hip prosthetic 9 years after implantation, [130]

Tensile strength of the selected alloy is ~ 900 MPa. Fracture location is approximately at the center of the base, where the stres at the maximum bending. The base is embedded in the femur and fixed to the femur using bone cement. The stress at which the fracture occurred is estimated to be ~ 50 MPa, based on the assumption that the load was five times greater than the weight of the body. The frequency cyclicity is estimated at (1-2) to 107, with the assumption that the patient walked 5 to 103 steps a day for nine years, [130].

From the circumstances of which depend on the evidence mentioned, it can be concluded that the basis of the artificial hip joint failed due to friction between the base and the metal fixators. This then led to the initial crack and its expansion to the base of the center due to cyclic loads while walking. This is clearly a situation where there was friction corrosion between the contact surface under cyclic loads while walking.

In the second case there was a premature cancellation hip replacement due to corrosion problems biomaterials (Figure 3.8.), [5].
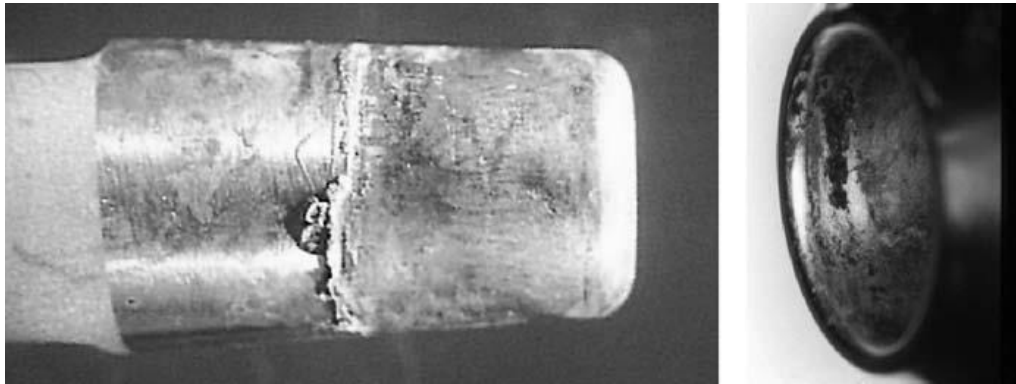

Figure 3.8. Failure of total hip replacement failure due to corrodion, [5].

Analysis of fracture

- The collected medical history, a chronological analysis and x-rays. Analysis of biomaterials and the used constructive solutions.

- Visual inspection of the implant. Irregularities were not spotted.

- Optical micrographs in order to analyze all the details of the damage.

- Chemical and mechanical analysis.

- Scanning electron microscopy to analyze micro-mechanisms of fracture.

- Clearly, the presence of smoothness, pitting and corrosion in scratches on the device, particularly in the area of the head.

- Scanning electron microscopy revealed intergranular attack and pitting that are associated with corrosion and polishing, which is indicative of small movements - fretting.

- Fretting

- Initial gap

- Load in the head (+12 mm door)

- Code prosthesis in which the design tolerance is exceeded, there is instability in the mechanical zone (Jacobs et al., 1998).

- Brown et al. (1995) have demonstrated a correlation between the door extension and fretting corrosion. Longer neck contributes a larger bending moments causing increased relative movement between the head and the socket, or fretting that continuously break the passive film and provokes repasivizaciju with consumption of oxygen in the gap.

- Fractographic analysis shows the presence of polished zone (the result of fretting), the etched microstructures (low pH value) and pitting corrosion due to gaps.

3.3 Methods in the analysis of the integrity of orthopedic implants

One of the key processes that accompanies the product development process is a fundamental analysis of reliability, which is one of the main influencing factors on the integrity of the implant. Designers and manufacturers of medical devices must register its patents, according to existing regulations and directives, [47-53]. Design development process of the medical devices is the first step in the process of manufacturing of medical implants, and sets a major challenge, especially as the initial idea, and after completing the standardization process and the device. Indeed, the development of reliable and durable joint prosthesis resulted in a significant improvement in the sustainable quality of work life in a large percentage of patients.

Also, reliable prosthesis for replacement joints, fully sustainable integrity is very cost-effective from the perspective prices. The cost estimates vary depending on a number of factors such as preoperative status, improvement opportunities, assessment of useful life, coexisting diseases.

The first step in assessing the reliability of orthopedic impalnata collecting physiological data to clinical examinations of. The ultimate success of the surgical treatment when the patient regain physiological kinematics you had before. (Figure 3.9.), [10,54,55]. The physiological data such as deviation, load, force and reaction torques in the wrist can be measured during the patient's normal walking.
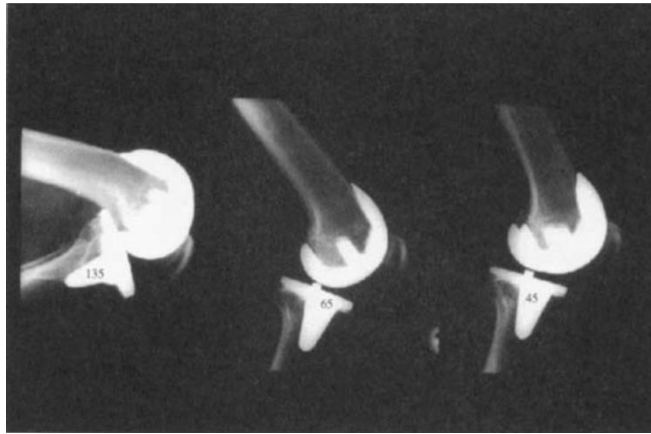

Figure 3.9. An example of a successful physiological kinematics in patients after the prosthetics have been implanted, [10]

Physiological forces in the joint during normal movement are shown in Figure 3.10., [9,10].
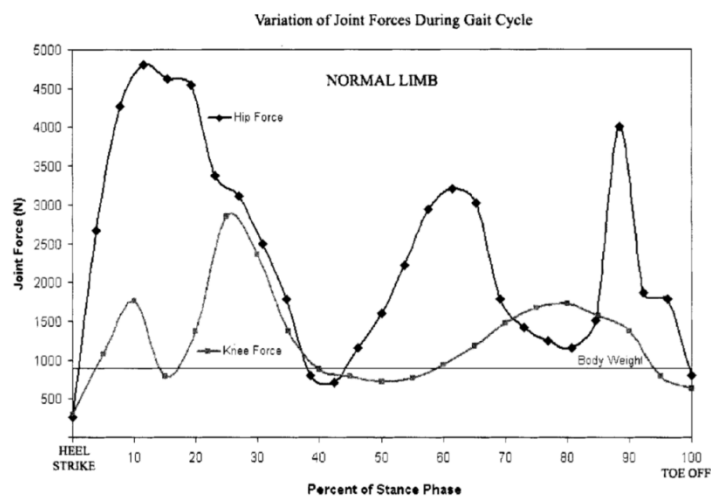

Figure 3.10. Physiological forces in a joint during normal movement, [10]

These data were evaluated using a mathematical model of kinematic and kinetic data were obtained from the analysis of trends in the laboratory using multiple video cameras and force platforms.

A more direct method to obtain data related to the reaction force is the use of joint prostheses equipping and instruments that can be implanted, used by Bergman et al. In one study they recorded the hip joint forces that are larger and up to eight times the weight of the body when the patient accidentally stumbled. Such loads greatly influence the preservation of the integrity of the prosthesis, [131,132]. These data can also be used in the calculation method for assessing the reliability of implants.

In assessing of integrity of the prosthesis is therefore necessary to take into account the physiological forces that may occur in the implant, which can deviate or be significantly greater than the forces prescribed by standards. Weight of the patien has a great influence on the load that can occur on the implant. Sustainability prosthesis, their resistance to fatigue and breakage due to fatigue, depends not only on the material used, but also on the design of the device, [133-135]. The belief that the material is initially eligible for use in the product and its acceptance is the long term aspect of the quality system. Clause 4, ISO 9001: 1987 specifies requirements for quality assurance systems. ISO 9004 gives detailed instructions for designing and manufacturing products.

CHAPTER 4

4.1 Application of numerical methods in design and analysis of orthopedic implant integrity

During the 1960s, engineers used the approximate solution methods in load analysis and other areas. Clou was the first to introduce the term *finite element* in 1960. The first book about finite element method was written by Zienkiewicz and Chung. This method evolved from application in structural engineering to a widespread computational approach to many fields of science and technique. FEM became a powerful and reliable numerical tool for analysis of structures subjected to different types of load in cases where solving of these problems was too complex for exclusively analytical methods.

In FEM, a complex region which defines the continuum is discretized into simple geometric shapes - *elements*. It is assumed that these elements have properties and relations which can be mathematically expressed as unknown quantities in certain points of elements - *nodes*. A process of connecting and combining of individual elements in a given system is applied. After taking into account the influence of load and boundary conditions, a series of linear or non-linear equations is typically obtained. Solving of these equations provides an approximate behavior of a continuum or a system. The algorithm for this method consists of the following steps: continuum discretization, selection of interpolation functions, calculating of system properties, forming of algebraic equations, solving of algebraic equation systems, calculation of necessary influences in nodes for individual finite elements.

The advantages of applying FEM include: it's applicable to complex geometries, complex types of analysis, complex loads, models made of non-homogeneous materials, etc. Types of errors that can occur include

discretization errors, as well as formulation and numerical errors. The basic equation of Fem for static load conditions is $\{F\} = [K] \cdot \{u\}$, where $[K]$ is the general or global stiffness matrix, $\{u\}$ is the global displacement vector, [136-138].

The basic principle of FEM represents the discretization of a complex region, which defines the continuum, into simple geometric shapes - elements. In other words, this method formulates the solution for each element separately, instead of seeking a solution for the domain as a whole. These solutions are then combined to obtain the solution for the whole region, [136-138].

FEM saw its first use in orthopedic biomechanics in 1972, for the purpose of assessing of stresses in human bones. Since then, this method has been applied with increasing frequency in stress state analysis of bones and prosthetics, as well as fracture fixation, for example one model is presented in Figure 4.1. ,[139-151].
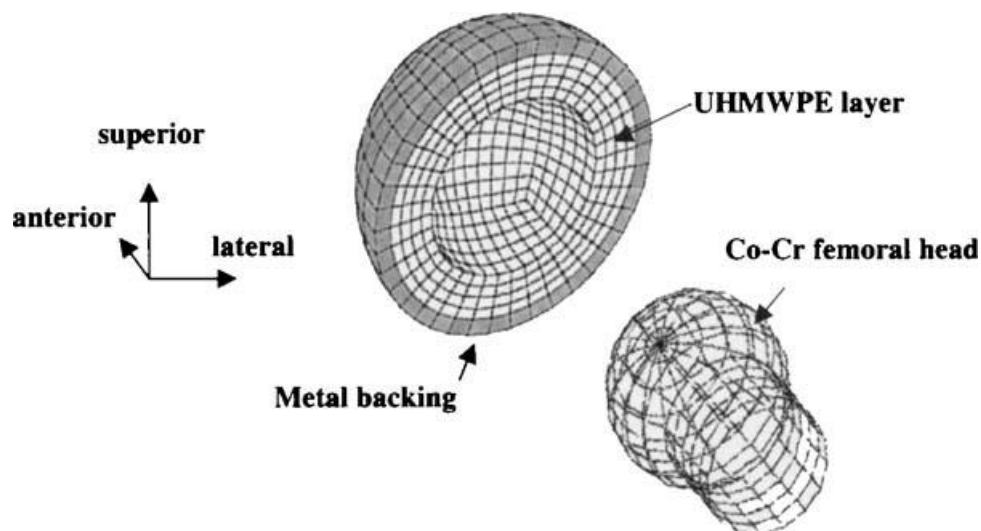

Figure 4.1. Schematic illustration of an FE model of a hip prosthesis containing a UHMWPE acetabular cup with a metal backing and a Co-Cr femoral head[10]

In addition to bones, this method can be used in analysis of numerous other tissues and organs. In case of orthopedics, there has always been a significant interest in stress and load. However, mathematical tools available for stress analysis in classic mechanics were not suitable for calculations of extremelly irregular structural properties of bone. Hence, the use of FEM represented a logical step due to its unique ability to determine the stress state in structures with complex shape, load and material behavior, [150-155]. In this thesis, the basics of finite element method and its application to prosthetics will be presented, with particular attention to modeling of a total hip replacement prosthetic.

4.2 Basic principles of deformation mechanics of orthopedic biomaterials

Mechanical loads of organs and tissues within a human body cause stresses and strains. Stress is defined as force per unit area, wherein the force acts on the area in a given direction. Stresses include normal and shear stress, and the components of real stress depend on the coordinate system, i.e. the direction in which the force acts on a given surface (Figure 4.2). In the case there are no shear stresses, the observed structure is subjected only to normal stresses, which are then referred to as principal stresses, [156,157].

Strain represents changes in shape and dimensions of the observed elements which occur due to loads. They are changes in length which occur due to normal stress and changes in angle due to shear stress. Like stress, strain can be viewed depending on the coordinate system. Tissue stiffness is defined as its resistance to strain, i.e. to change in shape and volume. For simpler geometric shapes, analysis of mechanical behaviour can be determined analytically, wherein for complex cases, it is necessary to apply a numerical method, such as finite element method (FEM), [156,157].

Biomaterials must possess adequate mechanical strength which guarantees good force distribution to surrounding bone structures, along with small electric and thermal conductivity. Biomaterial behavior can be described using two basic quantities: stress and strain. Stress is defined as inner force per unit area for a given cross-section:

$$\sigma = \frac{F}{A} \left[\frac{N}{m^2} \right]$$

(4.1)

Where stress is denoted with σ, force with F, and A is the cross-section area. Stress is defined for a given point within a supported body subjected to loads. Shown in Figure 4.2 are the stress vectors for 1D, 2D and 3D problems.
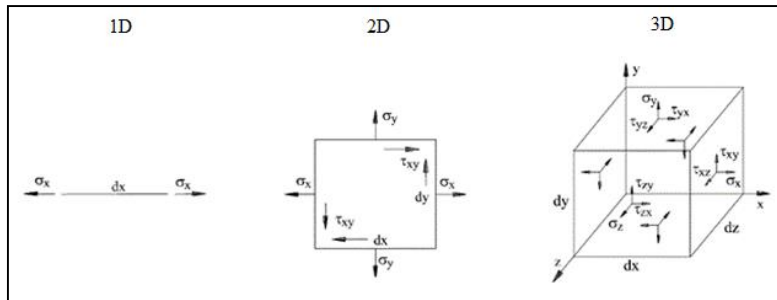

Figure 4.2. Stress vectors for 1D, 2D and 3D problems

Strain can be defined as transformation, i.e. a change in shape of a biomaterial under the effects of a force:

$$\varepsilon = \frac{\Delta l}{l_0}$$

(4.2)

where ε is the strain, $\Delta l = l - l_0$ is the change in length, l the deformed length, and l_0 is the initial length. Strain can be observed as relative displacement, if displacement is defined as the change of a body's dimensions due to load. Shown in Figure 4.3 is the strain in a small element with a volume of dxdydz, along with the calculation of strain components. Longitudinal, i.e. normal components are denoted by ε_x and ε_y, wherein shear components, also referred to as angular, are denoted by γ_{xy}. In order to express strain via displacements u,

v and w, the following assumptions must be made: strain is small and linearly dependent from displacement. The strain-displacement equation in matrix form is:

$$\{\varepsilon\} = [L]\{f\} \tag{4.3}$$

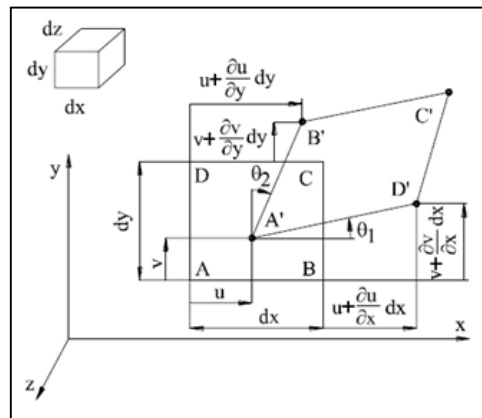where ε is the strain vector, f is the displacement vector, and L is the differential operator matrix.

Figure 4.3. Small element strain,[9]

Table 4.1. Basic continuum mechanics euquations for 1D, 2D or 3D problem

	1D	2D	3D
Displacement $\{f\}$	$\{u\} = \{u(x)\}$	$\begin{Bmatrix} u \\ v \end{Bmatrix} = \begin{Bmatrix} u(x,y) \\ v(x,y) \end{Bmatrix}$	$\begin{Bmatrix} u \\ v \\ w \end{Bmatrix} = \begin{Bmatrix} u(x,y,z) \\ v(x,y,z) \\ w(x,y,z) \end{Bmatrix}$
Strain $\{\varepsilon\}$	$\{\varepsilon_x\}$	$\{\varepsilon_x \varepsilon_y \gamma_{xy} \gamma_{yx}\}^T$ $\gamma_{xy} = \gamma_{yx}$	$\{\varepsilon_x \varepsilon_y \varepsilon_z \gamma_{zy} \gamma_{yx} \gamma_{xz}\}^T$ $\gamma_{ij} = \gamma_{ji},$ $i,j = x,y,z$
Stress $\{\sigma\}$	$\{\sigma_x\}$	$\{\sigma_x \sigma_y \tau_{xy} \tau_{yx}\}^T$ $\tau_{xy} = \tau_{yx}$	$\{\sigma_x \sigma_y \sigma_z \tau_{zy} \tau_{yx} \tau_{xz}\}^T$ $\tau_{ij} = \tau_{ji},$ $i,j = x,y,z$

Given in table 4.1 are the unknown quantities for any points in a body depending on whether the problem is 1D, 2D or 3D, where u, v and w, and x, y and z are the coordinate system axes, [156,157].

Within the field of biomechanics, continuum mechanics deals with determining of changes within the biomaterial as a whole. Continuum can be defined as a solid body which can deform due to mechanical load. Changes which are being considered are related to the changes in strain and stresses in a biomaterial, caused by mechanical load. Such an approach, wherein the history of changes in quantities in material points is monitored, is referred to as Lagrange approach to continuum analysis, and is applied in describing of mechanical behavior of biomaterials, [156,157].
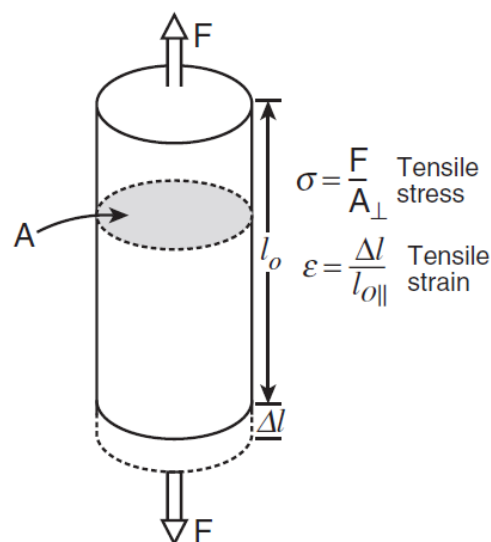

Figure 4.4. Type of tension load that act on the biomaterial, [5]

Load applied to a biomaterial can act in one of the following ways: tension, compression, shear or a combination thereof, Figure 4.4. [5] Tensile stresses are generated by forces which subject the material to tension, whereas as compressive stresses are caused by forces that subject the material to pressure. Loads that lead to deforming or separating of biomaterial by means of molecular layer sliding generate shear stresses. Shear stresses can occur during

uniaxial tension and compression, since maximum shear stress appears in planes which are under the angle of 45° relative to the direction of the force, [156,157].

4.2.1. Stresses in biomaterials

Strain caused by mechanical load produce internal mechanical forces within the body. In order to determine the internal forces, it is necessary to take out a small volume, ΔV, from the biomaterial around an arbitrarily selected point P. Shown in Figure 4.5. is a body subjected to forces F_i, with a denoted small volume ΔV and small area ΔS. Acting on the surface ΔS is a mechanical action of the surrounding biomaterial, [156]. Force per unit area represents the stress vector $t^{(n)}$ and can be written in the following way:

$$t^{(n)} = \lim_{\delta S \to 0} \frac{\Delta F}{\Delta S} = \frac{dF}{dS} \tag{4.4}$$

where n is the external unit perpendicular to ΔS, and ΔF is the force acting on surface ΔS. Stress vector can be decomposed into normal and tangential components: $t^{(n)} = \sigma_n + \sigma_t$. Normal stress component is along the direction of n, normal to the surface, whereas the tangential stress component lies in a plane perpendicular to normal n. Shown in Figure 4.2. are the stress vectors for each individual surface parallel to the axes of a Cartesian orthogonal coordinate system. Each of these stress vectors can be decomposed into components.

$$\left.\begin{matrix} \sigma_{11} \\ \sigma_{22} \\ \sigma_{33} \end{matrix}\right\} \text{ normal stress components}$$

$$\left.\begin{matrix} \tau_{12} \\ \tau_{13} \\ \tau_{21} \\ \tau_{23} \\ \tau_{31} \\ \tau_{32} \end{matrix}\right\} \text{ tangential stress components}$$
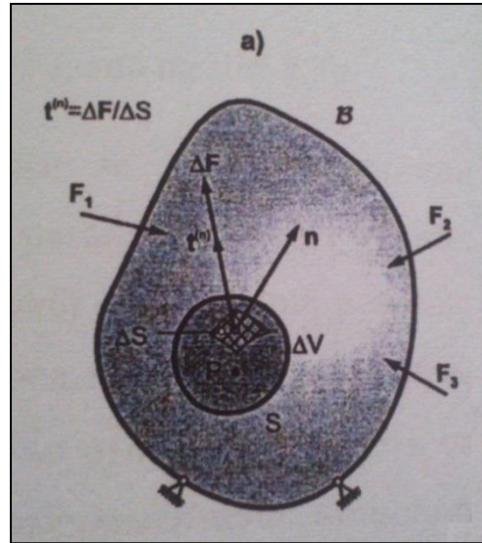
Figure 4.5. Unit volume around point P,[9]

Stress vector can be expressed in matrix form as:

$$\sigma = \begin{bmatrix} \sigma_{11} & \sigma_{12} & \sigma_{13} \\ \sigma_{21} & \sigma_{22} & \sigma_{23} \\ \sigma_{31} & \sigma_{32} & \sigma_{33} \end{bmatrix} \tag{4.5}$$

Principal stresses act in a plane with unit normals p_1, p_2 and p_3 and can be obtained by calculating of eigenvalues. In that case, the stress matrix has the following form:

$$\sigma = \begin{bmatrix} \sigma_1 & 0 & 0 \\ 0 & \sigma_2 & 0 \\ 0 & 0 & \sigma_3 \end{bmatrix} \tag{4.6}$$

Here it can be observed that shear stresses in principal planes equal zero. Maximum shear stresses occur in plane which are rotated by an angle of п/4 relative to principal axes, [156].

Stress components in a continuum must satisfy the equilibrium equations. Equilibrium equations can be external and internal. External equilibrium equations represent the sum of all active and reactive forces which is equal to zero. Internal equilibrium equations are defined for an elementary part of the volume and the sum of internal volume forces as all stress

increments along the corresponding axes is equal to zero. Internal equilibrium equations for 1D, 2D and 3D problems are given as:

$$\text{1D problem: } \frac{\partial \sigma_x}{\partial x} + F_x = 0 \tag{4.7}$$

$$\text{2D problem: } \frac{\partial \sigma_x}{\partial x} + \frac{\partial \tau_{xy}}{\partial x} + F_x = 0, \frac{\partial \sigma_y}{\partial y} + \frac{\partial \tau_{yx}}{\partial y} + F_y = 0. \tag{4.8}$$

$$\text{3D problem: } \frac{\partial \sigma_x}{\partial x} + \frac{\partial \tau_{xy}}{\partial x} + \frac{\partial \tau_{xz}}{\partial x} + F_x = 0, \qquad \frac{\partial \sigma_y}{\partial y} + \frac{\partial \tau_{yx}}{\partial y} + \frac{\partial \tau_{yz}}{\partial y} + F_y = 0,$$

$$\frac{\partial \sigma_z}{\partial z} + \frac{\partial \tau_{zx}}{\partial z} + \frac{\partial \tau_{zy}}{\partial z} + F_z = 0. \tag{4.9}$$

4.2.2. Strain in biomaterials

Strain can be defined as a mechanical quantity which describes the kinematics of shape changes of a biomaterial, [156,157]. Shown in Figure 4.5. is a deformable body, with a denoted unit length *ds*. If the strain is expressed as:

$$\varepsilon = \frac{d(ds)}{ds} \tag{4.10}$$

the expression for determining the change along unit length in the directions of an orthogonal Cartesian coordinate system can be obtained as:

$$\varepsilon_{xx} = \frac{d(dx)}{dx}, \quad \varepsilon_{yy} = \frac{d(dy)}{dy}, \quad \varepsilon_{zz} = \frac{d(dz)}{dz}, \tag{4.11}$$

In addition to strain in direction of coordinate system axes, shear deformation also needs to be introduced, in form of angular strain. Shear strain represents the change in angle between any two segments of a line which were

perpendicular to each other initially. This strain is defined by the following expressions:

$$\gamma_{xy} = \frac{\pi}{2} - \alpha_{xy}, \quad \gamma_{yz} = \frac{\pi}{2} - \alpha_{yz}, \quad \gamma_{xz} = \frac{\pi}{2} - \alpha_{xz} \tag{4.12}$$

where α_{ij} represent the angles between line segments dx_i i dx_j after deforming. Shear strain γ_{ij}, $i \neq j$, $i,j = 1,2,3$ are symmetrical and represent engineering shear strain, [156,157]. In continuum mechanics, real shear strain is used instead, and is expressed as:

$$\varepsilon_{ij} = \frac{1}{2}\gamma_{ij}, \qquad i \neq j, \qquad i,j = 1,2,3 \tag{4.13}$$

Strain components can be calculated the displacement field u_i as well:

$$\varepsilon_{ij} = \frac{1}{2}\left(\frac{\partial u_i}{\partial x_j} + \frac{\partial u_i}{\partial x_i}\right) \tag{4.14}$$
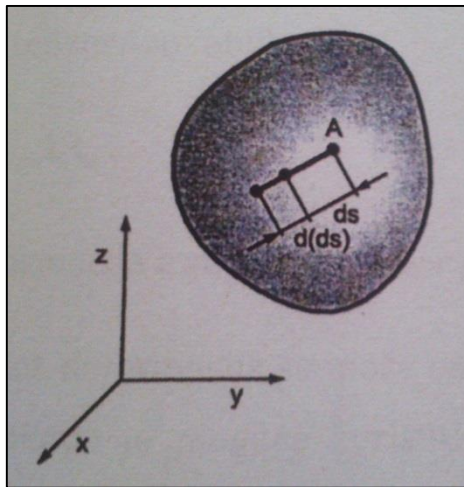

Figure 4.6. Elongation of a longitudinal element, [9]

The relationship between stress and strain is expressed via Hooke's Law according to which the following holds: relative strain in an elastic body, within certain boundaries, is directly proportional to the stress acting on it. For linear elastic materials, the Hooke's Law can be written as:

$$\sigma = E\varepsilon \tag{4.15}$$

where E represents Young's elasticity modulus, σ is the stress and ε is the strain. Stress-strain curve can be represented graphically and is shown in Figure 4.7. Yield limit line divides the stress-strain curve into elastic and plastic zones. In the elastic zone, strain is increased mostly in proportion to stress, and in this zone, relation 4.5. holds. Above the yield limit, in the plastic zone, Hooke's Law no longer applies. In other words, once the force stops acting, the biomaterial will not return to its initial state.
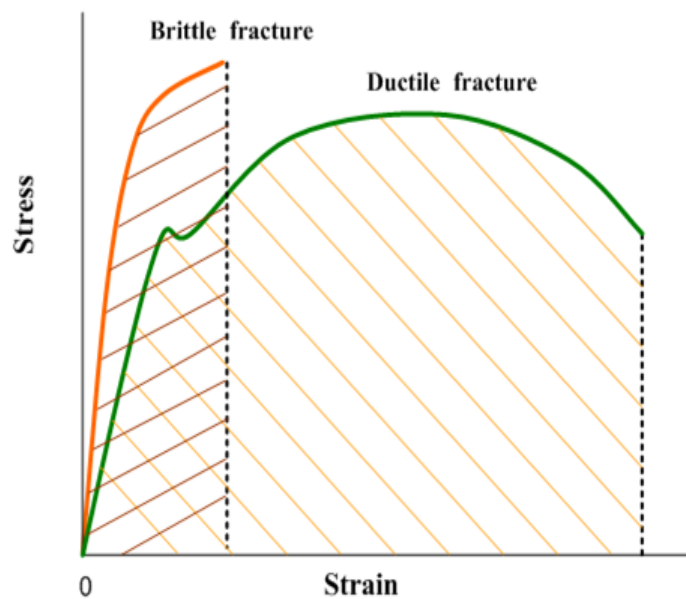
Figure 4.7. Stress-strain curve

Curve E, i.e. Young's elasticity modulus, represents the ratio between stress increment and strain increment in a biomaterial. Stiffer biomaterials are harder to deform and such materials have higher elasticity moduli. It can be observed in Figure 4.7. that the stress is seemingly decreasing immediately before it reaches maximum value. Maximum stress is referred to as tensile strength. When selecting biomaterials for a specific application, elasticity limit is of great importance, since it determines whether the material will deform or not.

Shear modulus G can be defined as the initial slope of the stress-shear strain curve, [157] and can be written as:

$$E = 2G(1 + v) \tag{4.16}$$

where v is the Poisson's ratio which is defined as the negative ratio between lateral and longitudinal dilatation of a truss subjected to tensile or compressive load.

4.3 Fundamental assumptions of finite element method

As was previously mentioned, finite element method, or finite element analysis, represents a numerical methods used for solving of complex geometry problems, for which obtaining of an analytical solution is extremely difficult. FEM is a method based on discretization of complex geometrical domains into much smaller and simpler ones, wherein field variables can be interpolated using shape functions. Such domains are referred to as elements. The field of variables within a finite element is described by approximative functions, whereas terms of this function are defined based on the values of variables in the nodes, [136-138].

Points in which adjacent elements are connected are called node points, or nodes. Each nodes has the property that the displacement of all adjacent elements in that node is the same. In this way, the behavior of a part of the structure can be described through a common node, i.e. the behavior of the structure as a whole can be described by the nodes of the model. Based on the node displacement field, strain and stresses can be determined for finite elements, and consequently, the structure as a whole.

Stress analysis is of great significance, since if the stresses are known, it is possible to calculate the strain within a body, and determine whether the component can withstand the given load. FEM enables the simulation of mechanical behavior of individual parts subjected to external load, assuming that the geometry and material properties are known. The result of this method is the verification of a specific design, assuming it meets the defined requirements and specification.

4.3.1. An overview of finite element method development

First papers in the field of finite element method were written during the 1940s. In 1941, Hrenikof was solving problems related to structural and stress analysis of a solid body. Due to the need to discretize the model into finite elements, further development advanced towards topology and geometric properties. Soon afterwards, finite element method found its application in the aircraft industry. The founders of the method, who have defined its basic concepts, were Kloug, Martin, Top and Tarner. First papers on the matrix concept were published by Argyris et al. These papers were printed in 1960, in a book where the term finite element was used for the first time. First university textbook was written by Cook in 1974, at a time when the method was already widely accepted and significantly developed.

Variation principles of continuum mechanics were of great significance in FEM development, giving it a general approach. Static approach to FEM was established in 1960. In the mid-sixties, White and Friedrich solved partial differential equations by using a mesh of triangular elements and variation principles. After that, Helinger and Reisner established a mixed finite element model, which combined both forces and strain as unknown quantities.

Nowadays, finite element method is widely used in solving of various problems. Despite this, this method is still being developed and new possibilities for its application are being researched.

4.3.2. Basic steps in finite element method

There are two basic approaches in finite element method. First one is the force, or flexibility method. Within this method, forces are the basic unknown quantities in a problem that is being analyzed. In order to obtain structural equations, equilibrium equations need to be set up first. This results in a system of algebraic equations, wherein unknown quantities are the forces determined from these equations. In order to achieve compatibility conditions during the solving of specific problems, the elements must be connected by nodes, along sides or surfaces. Basic structural equations are related to node displacement, and equilibrium equations and relations between forces and displacements are also used. Of the two method mentioned here, the second one is far more commonly used, [136-138]

Finite element method uses structural models which consist of mutually connected finite elements. A displacement function is assigned to each element. All elements are connected directly, or indirectly including nodes and/or common boundary lines/surfaces of elements. Based on known stress and strain values in a node, these values can be determined for any other nodes and elements within the considered structure, assuming its material properties and the applied load are already known. The total number of structural equations describes the behavior of all nodes and represents a system of algebraic equations, which are best represented in matrix form.

4.3.2.1. Domain discretization and selection of element type

Finite element method is based on physical discretization of an observed domain (figure 4.8.). The base of the structural analysis is the subdomain, a part of the structure (domain), called the finite element. A finite element is not of differentially small dimensions, but instead has finite dimensions, and hence its name. Due to this, the equations which describe the state in individual finite elements are of algebraic nature. The first step in structural analysis, i.e. in determining of stresses and strain, is the discretization of the domain (model). It is performed by dividing the domain with lines into subdomains, or finite elements. The selection of finite element size determines the accuracy of obtained results, and the time needed for the analysis.
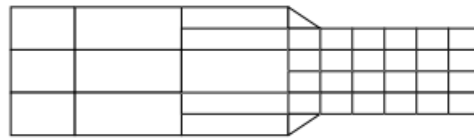
Figure 4.8. Discretization of domain into finite elements

The selection of elements used in FEM analysis depends on the domain geometry. If the domain is planar, two-dimensional plane elements are used, and for spatial domains, three-dimensional elements are used (Figure 4.9.), [136-138]
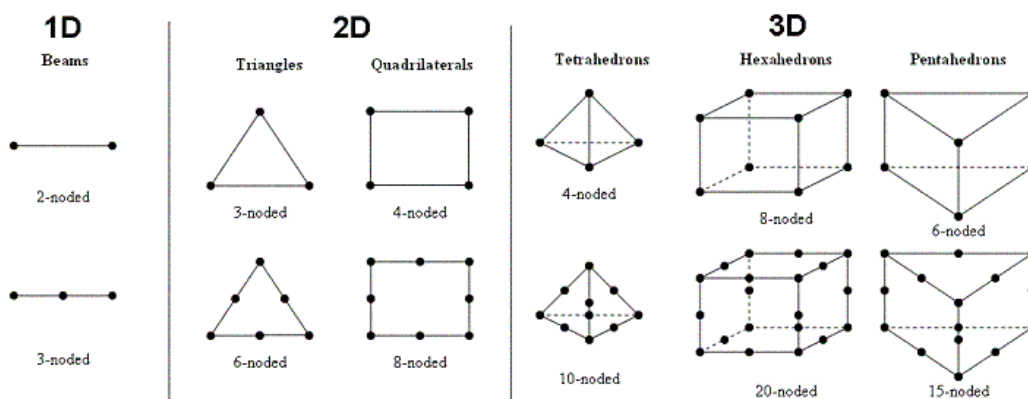

Figure 4.9. Types of finite elements, [138]

4.3.2.2. Selection of displacement functions

The selection of displacement functions is performed for every element. The function is defined within the element and uses values calculated in nodes. Linear, quadratic or cubic polynomials are typically selected as displacement functions. Functions in nodes are unknown quantities. Functions are selected in a way that ensures that FEM can be used to achieve displacement continuity within the body, i.e. between all elements in nodes, along sides and surfaces. Upon selecting the displacement function, the relationship between strain and displacement is established, along with the relationship between stress and strain, [136-138].

4.3.2.3. Defining of relationships between strain and displacement and stress and strain

For every finite element, equations must be set up. If the problem is one-dimensional, i.e. strain only occurs in one direction, for example the x direction (it is related to displacement "u"), then axial strain is defined by the following expression:

$$\varepsilon_h = \frac{du}{dx} \tag{4.17}$$

This equation holds for small strain. Stresses and strain are also related by the so-called constitutive relations. Hooke's Law is one of them. For a one-dimensional problem, the relationship between stress and strain is given by:

$$\sigma_h = E \cdot \varepsilon_h \tag{4.18}$$

where σ_h is the stress in x direction and E is the elasticity modulus. Once the relationships have been established, the stiffness matrix is set up.

4.3.2.4. Stiffness matrix

There are several methods for determining stiffness matrices,[136-138]:

1. Direct equilibrium method - Stiffness matrix relates the forces in element nodes to the nodes. It is obtained from the force equilibrium conditions for each element considered.

2. Variation methods **-** based on the stationary principle. Unlike the direct method, it can be applied to more complex elements.

3. Weight residual method - is based on differential equations for the considered problems. Galerkin method is the most famous one. Based on residual methods, equations are obtained which describe the behavior of elements. In matrix form, this can be written as:

$$\begin{Bmatrix} f_1 \\ f_2 \\ \vdots \\ f_n \end{Bmatrix} = \begin{bmatrix} k_{11} & k_{12} & k_{13} & \cdots & k_{1n} \\ k_{21} & k_{22} & k_{23} & \cdots & k_{2n} \\ k_{n1} & k_{n2} & k_{n3} & \cdots & k_{nn} \end{bmatrix} \begin{Bmatrix} d_1 \\ d_2 \\ \vdots \\ d_2 \end{Bmatrix} \tag{4.19}$$

$$\{f\} = [k] \cdot [d] \tag{4.20}$$

where $\{f\}$ is the force vector in element nodes; $[d]$ is the nodal displacement vector and $[k]$ is the element stiffness matrix.

4. Energy balance method - based on the balance of various types of energy. It is used in thermostatic and thermodynamic continuum analysis.

The stiffness matrix and equations for individual finite elements are obtained using one of the aforementioned methods. By using the direct method and superposition, individual element matrices can be summed. Herein the concept of continuity or compatibility, according to which the structure must be continuous, must be satisfied. Global structural equation in matrix form is:

$$\{F\} = [K] \cdot [d] \tag{4.21}$$

where $\{F\}$ is the force vector in a global coordinate system; $[d]$ is the vector of known and unknown displacement of all nodes within the structure and $[K]$ is the global stiffness matrix.

Global stiffness matrix $[K]$ is a singular matrix, since its determinant is equal to zero. The singularity problem is solved by introducing adequate boundary conditions.

4.3.2.5. Determining of displacement of the whole structure

Matrix equation of the structure, wherein the boundary conditions are defined, represents a system of algebraic equations in the following form:

$$\begin{Bmatrix} F_1 \\ F \\ \vdots \\ F_n \end{Bmatrix} = \begin{bmatrix} K_{11} & K_{12} & k_{13} & \cdots & K_{1n} \\ K_{21} & K_{22} & k_{23} & \cdots & K_{2n} \\ K_{n1} & K_{n2} & k_{n3} & \cdots & K_{nn} \end{bmatrix} \begin{Bmatrix} d_1 \\ d_2 \\ \vdots \\ d_2 \end{Bmatrix} \tag{4.22}$$

where n is the total number of unknown degrees of freedom.

Based on the equations mentioned above, stresses and strain are determined. The conclusion of each analysis is reduced to determining of the correct location where highest stresses and strain occur.

4.4 Finite element method application in orthopedic biomechanics

Finite element method application in orthopedics is of great significance. This method allows the modeling of joints, long bones, spine, skull, [149-155].However, from an engineer's point of view, current biomechanical analyses can be considered too simpe. Non-linear and anisothropic properties are incorporated into some of the more recent models, and have aided in demosntrating the possibilities that FEM can provide.

In this thesis, the application of FEM in designing of artificial hips will be considered. This method can be divided into three basic steps,[9]:

1. Preprocessing
2. Processing
3. Postprocessing

The first step, preprocessing, consists of transforming a physical component which is analyzed into a computer model. Modeling is typically performed using a different software package. This step is illustrated by a number of examples, Figure 4.10., [155].
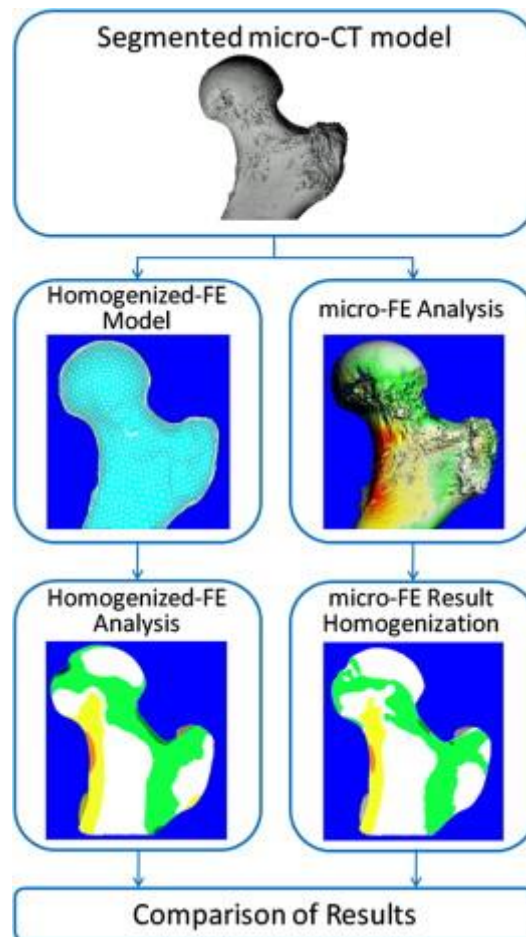

Figure 4.10. Examples of biomechanical models, CT model of a human hip,[155]

Considerable accuracy is required during the modeling of areas which are near the points where the load is acting, as well as in areas where there are significant changes in geometry, [139-144]. In addition, there is a possibility of using an image obtained by computer tomography (CT) or three-dimensional scanners. The next step involves the defining of load. First, boundary conditions are defined as the integral part of the mathematical model that FEM is supposed to solve, and are given in physical form as supports. Physical models with symmetric geometry and boundary conditions require significantly less nodes when the mesh is generated.

In order to divide a domain into smaller subdomains, i.e. elements, the mesh is used. The process of generating the mesh, elements, nodes and the defining of their boundaries is referred to as the discretization of the problem domain, [136-138].
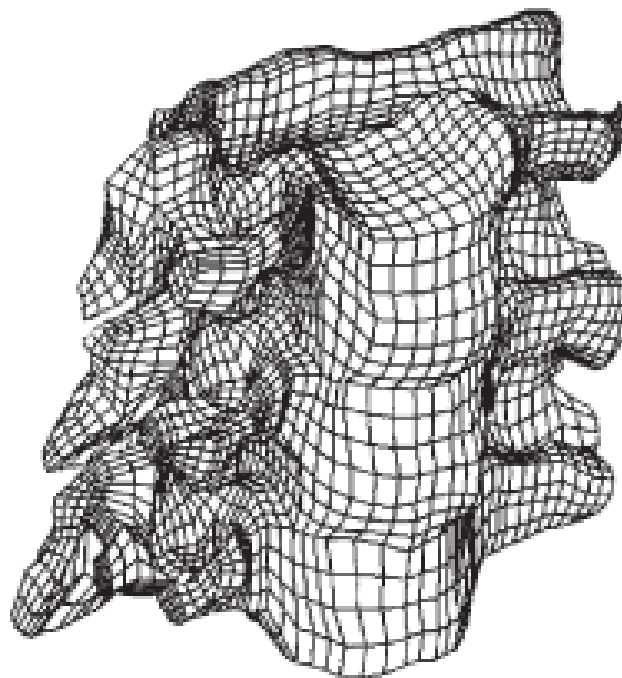
Figure 4.11 Example of mesh generation in bones, [5]

Figure 4.11. shows the mesh, i.e. the distribution of elements on several biomemical examples. The whole domain is divided into a mesh of smaller domains for two reasons: solving of equations in a smaller and simpler domain avoid the solving of complex equations which involve complex geometry, and element decomposition approximates domains characterized by very complex geometry in a very accurate way, [137, 141-153].

Approximation functions, i.e. interpolation functions describe the assumed behavior of the region. Interpolation models are typically in polynomial form.

A general polynomial type of a field of variables $f(x)$ is as follows:

$$f(x) = f\big(u(x)\big) = a_1 + a_2 x + a_3 x^2 + \cdots + a_{n+1} x^n = \{1 \; x \; x^2 \dots x^n\}\{a\}$$

$$= \{\underline{n}\}^T \{a\} \tag{4.23}$$

where $\{\underline{n}\}^T$ are the shape functions of the variable, x is the coordinate of the observed point, $\{a\}$ is the vector of polynomial coefficients. Displacement in any point can be expressed via the product of the displacement shape matrix, $[N]$ and the displacement vector for the points in the region, $\{\delta\}$,[136-138]

$$f(x) = [N]\{\delta\} \tag{4.24}$$

Stiffness matrix and load vector are first defined for a local coordinate system, and then for the global as well. Local coordinate system is a coordinate system of an element, and the global coordinate system is related to the whole model. The stiffness matrix is symmetrical, positively defined and singular. The load vector is defined in nodes, and the load can be initial, surface or volumetric. Defining of the stiffness matrix and load vector for the global system is achieved by using the transformation matrix. Terms in the transformation matrix are the sines on cosines of angles between the local and global coordinate system.

Upon determining the geometry, material properties and load, and after the mesh has been generated, the software can begin looking for a solution.

Postprocessing involves the analysis and evaluation of the solution of algebraic equations. Postprocessing software contains certian operations which involve sorting of acting stresses, display of dynamic model behavior, displaying of the deformed structure, determining of safety factors, [153-155]. Data can be displayed in tabular of graphical fashion.
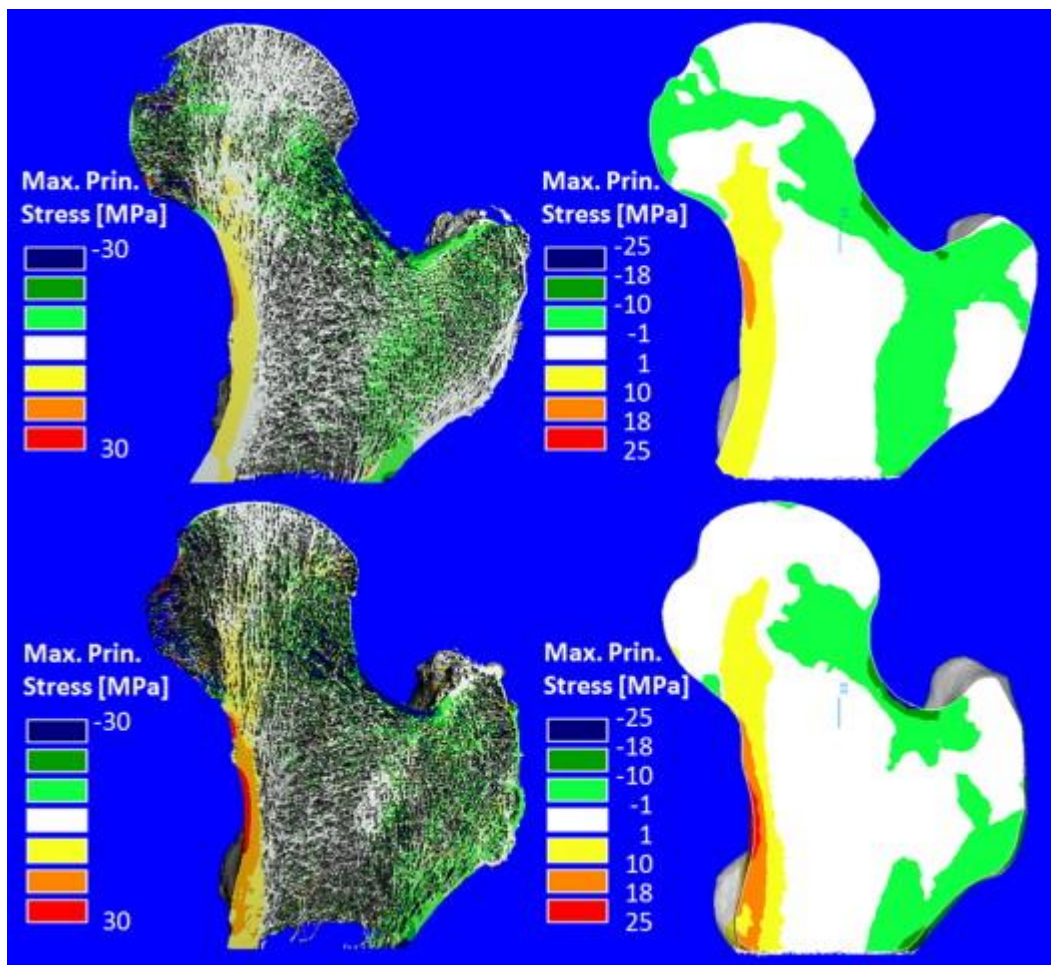

Figure 4.12. Examples of solution displays for the hip,[155]

Even though the equations were solved for nodes only, graphical representation of results covers the whole domain, since results obtained for nodes can be used to approximate quantities which are of interest, but are not located in node.s This makes FEM a very powerful method, since there are no

experimental methods that can determine the quantities of interest in every point of the body. However, this means that even though the results are available in every point, the most accurate solutions are obtained in nodes. In other words, when generating the mesh, it is important to place nodes at the most interesting points.

4.5 Application of FEM in analysis of behavior of biomaterials with cracks

Modeling of fracture mechanics problems requires an adequate treatment of displacement and stress field singularity around the crack tip, wherein the biggest problem is reflected in drastic increase in discretization error, which occurs when using classic FE, such as the eight-node element. The most efficient solution is obtained by using the reduction technique (reducing the error to only 1%) or by applying special FE around the crack tip, which contains the strain field singularity, figure 4.13., [136-138, 158-160]. First papers related to elements around the crack tip were written by Henshell and Shaw, 1975, who have introduced quadrilateral elements, and Barsoum, 1974, 1976, who introduced triangular elements.
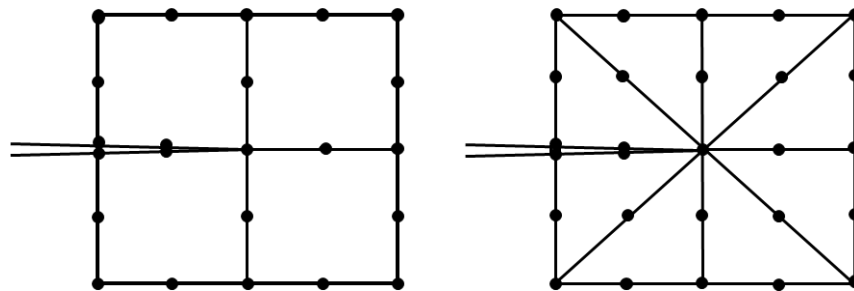
Figure 4.13 Special Crack Tip Elements, quarter-point elements

Properties of an eight-noded isoparametric element, shown in figure 4.14., are described by following equations:

$$N_1 = -\frac{1}{4}(1-\xi)(1-\eta)(1+\xi+\eta)$$

$$N_2 = -\frac{1}{4}(1+\xi)(1-\eta)(1-\xi+\eta)$$

$$N_3 = -\frac{1}{4}(1+\xi)(1+\eta)(1-\xi-\eta)$$

$$N_4 = -\frac{1}{4}(1-\xi)(1+\eta)(1+\xi-\eta)$$

(4.25.a)

$$N_5 = \frac{1}{2}(1-\xi^2)(1-\eta)$$

$$N_6 = \frac{1}{2}(1+\xi)(1-\eta^2)$$

$$N_7 = \frac{1}{2}(1-\xi^2)(1+\eta)$$

$$N_8 = \frac{1}{2}(1-\xi)(1-\eta^2)$$

(4.25.b)
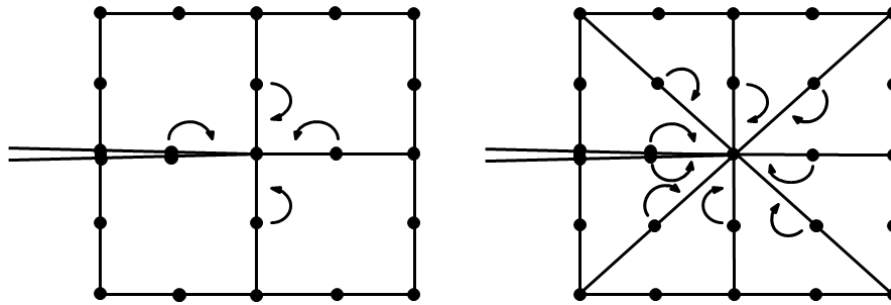
Figure 4.14. eight-noded isoparametric element

Banks-Sills and Bortman (1984) introduced the square-root singular element, figure 4.15.

$$\sigma \sim \frac{1}{\sqrt{r}}$$
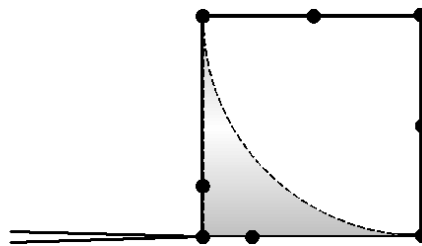
Figure 4.15. square-root singular element

When analyzing the stress state around the crack tip, it is recommended to use triangular isoparametric elements, since such elements, when subjected to load, gives a $1/\sqrt{r}$ strain singularity in the vicinity of the crack tip, and are displayed in nodes "shifted" by 1/4 of the side length. This region is modeled by placing elements in concentric circles, while ensuring that their size decreases as the approach the tip (figure 15). The area which suffers plastic strain must be accurately modeled using a larger number of FE, whereas elastic analysis of stress state does not require a particularly fine mesh, which is important in terms of calculation time.

By applying FEM in order to simulate the behavior of a material with a crack, it is necessary to emphasize that elements which define the elastic state, require special formulation within the software, whereas in the case of elements which define the plastic behavior, it is sufficient to place three nodes around the crack tip in an almost identical position.

Fracture mechanics parameters can be determined in a number of different methods, such us displacement extrapolation, J-Integral, stiffness derivative method, etc.
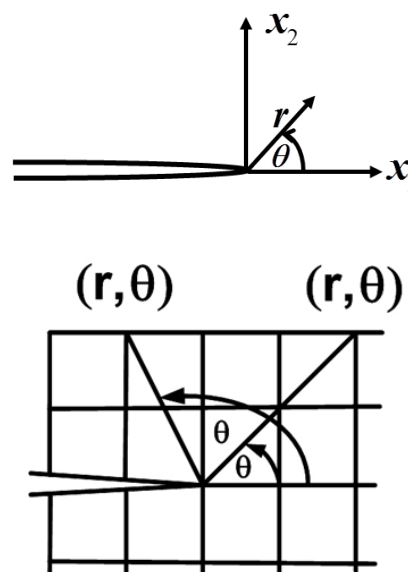

Figure 4.16 displacement extrapolation method

In the case of displacement extrapolation method, figure 4.16., when crack propagation simulation in the material is performed using polar coordinates, the following expressions can be defined for plane strain conditions:

$$v(r,\theta) = \frac{K_I}{2\mu}\sqrt{\frac{r}{2\pi}}\sin\frac{\theta}{2}\left(\kappa+1-2\cos^2\frac{\theta}{2}\right)$$

$$\mu = \frac{E}{2(1+v)}$$

(4.26.)

$$\kappa = \begin{cases} 3-4v & \text{pl } \varepsilon \\ (3-v)/(1+v) & \text{pl } \sigma \end{cases}$$

Equivalent coefficient is determined according to expression 4.27.

$$K_I^* = \frac{\sqrt{2\pi}}{2}\frac{E}{(1+v)}\frac{1}{\sin\frac{\theta}{2}\left[2(1-v)-\cos^2\frac{\theta}{2}\right]}\frac{v(r,\theta)}{\sqrt{r}}$$

(4.27.)

If the angle $\theta = 0$, the following expression is obtained:

$$K_I^* = \frac{\sqrt{2\pi}}{4}\frac{E}{1-v^2}\frac{v(r,\pi)}{\sqrt{r}}$$

(4.28.)

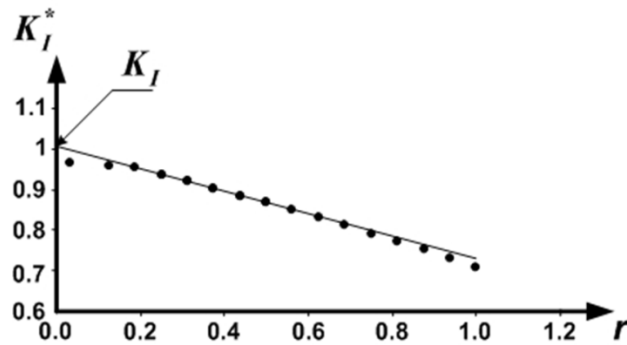As shown in figure 4.17., $K_I = \lim_{r\to\infty} K_I^*$

Figure 4.17. Diagram of dependence of K_I and K_I^*

One of the commonly used methods is the J integral method, shown in figure 4.18., and in this case the J integral can be expressed by 4.29.
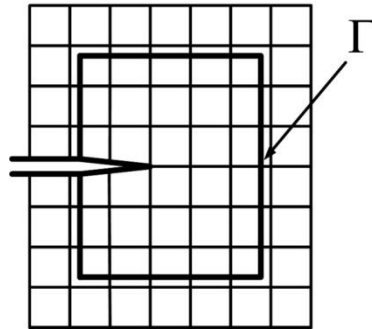

Figure 4.18. J – integral method

$$
\begin{aligned}
J = \int_{\Gamma} \Bigg\{ &\frac{1}{2}\left[\sigma_{11}\frac{\partial u_1}{\partial x_1} + \sigma_{22}\frac{\partial u_2}{\partial x_2} + \sigma_{12}\left(\frac{\partial u_1}{\partial x_2}+\frac{\partial u_2}{\partial x_1}\right)\right]n_1 \\
&- \left[\left(\sigma_{11}\frac{\partial u_1}{\partial x_1}+\sigma_{12}\frac{\partial u_2}{\partial x_1}\right)n_1 + \left(\sigma_{12}\frac{\partial u_1}{\partial x_1}+\sigma_{22}\frac{\partial u_2}{\partial x_1}\right)n_2\right] \Bigg\} \; ds
\end{aligned}
$$
(4.29.)

CHAPTER 5

5.1 Fracture mechanics of metal orthopedic biomaterials

In a more focused sense, the term fracture mechanics is related to investigation of crack propagation conditions. In a broader sense, it includes a part of strength of materials, which is related to the final stage of the deforming process, caused by the load. Based on that, strength of materials and structure failure problems are defined as the main subject of fracture mechanics. Fracture analysis, i.e. fracture surface analysis, provides numerous data about material behavior. A conical fracture indicates plastic tensile fracture, as opposed to a flat surface, which indicates brittle fracture.

Fracture mechanics is a discipline which requires the connecting of theoretical consideration with experimental results, as well as with the occurrence of failures and disasters in structure exploitation. Developed experimental methods for determining fracture mechanics parameters, which include critical value of stress intensity factor, crack opening displacement, Rice's contour integral, were created based on theoretical analyses and mathematical models of differently shaped bodies with a crack, [161]. Back in those days, fracture mechanics achieves its first practical success by explaining the failure of machinery in exploitation. Most famous examples include Liberty type ships and Comet type airplanes. Liberty ships were manufactured by the USA, and exported to Great Britain during the Second World War Since Great Britain had considerable need for supply ships, due to their losses in the Atlantic, engineers decided to connect the ship's hull by welding, rather than rivets, which reduced production time significantly. Such ships started failing during the war36 due to poor welding, which lead to the occurrence of defects in the material (cracks) and stress concentration in weaker locations in the hull, in addition to the use of cheaper steels. A more detailed analysis, aided by

fracture mechanics, revealed critical yield spots, which enabled the repairing of the remaining ships before the war ended, [161-164].

First quantitative relationship between stress and crack propagation was presented by Griffith, in a paper published in 1920. He applied stress analysis to an example of an eliptical crack, in order to explain crack propagation behavior. Griffith's model offered an excelent explanation of the ratio between stress and crack propagation for brittle materials (glass). Modification of the model, which would explain the fracture behavior of metal, appeared as late as 1948, when Irwin took into consideration dissipation energy due to plasti strain in the metal, and added it to the existing model.

Practical application of fracture mechanics has been based since the begining on a two-way interpretation of its parameters: on one hand, they represent load and structure geometry, including the crack geometry, and on the other they are also a property of the material, i.e. it resistance to crack growth, Figure 5.1., [161,162]. In other words, instead of dealing exclusivelly with fracture analysis, fracture mechanics became a valuable tool in the hands of engineers whose task is to prevent failure.
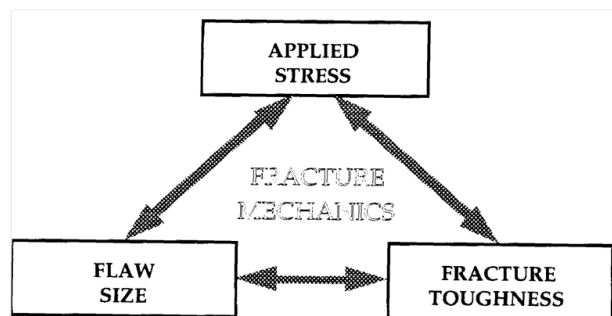

Figure 5.1. Fracture mechanics triangle, [161]

Structure integrity is a relatively new scientific and engineering discipline that, in a broader sense, includes the analysis of state and diagnostics of behaviour and yielding, as well as assessment of structure life and its revitalization. This means that, apart from the usual situation where there is a

need to assess structural integrity after defects were determined by non-destructive test methods, this discipline also includes the analysis of the stress state of the structure without cracks, typically by means of finite element method. Such an approach is of particular importance for structures which are subjected to working conditions in which cracks typically occur, such as fatigue, creep and corrosion.

Fracture mechanics includes various approaches depending on material properties. First papers were able to describe crack behavior in linear elastic materials under quasi-static loading. Elasto-plastic fracture mechanics considers plastic strain under quasi-static loading, whereas dynamic, viscoelastic and viscoplastic fracture mechacnis introduce time as a variable. Materials of lower toughness exhibit brittle behavior during fracture, along with a linear dependence of stress from fracture toughness, Figure 5.2, [161-164].
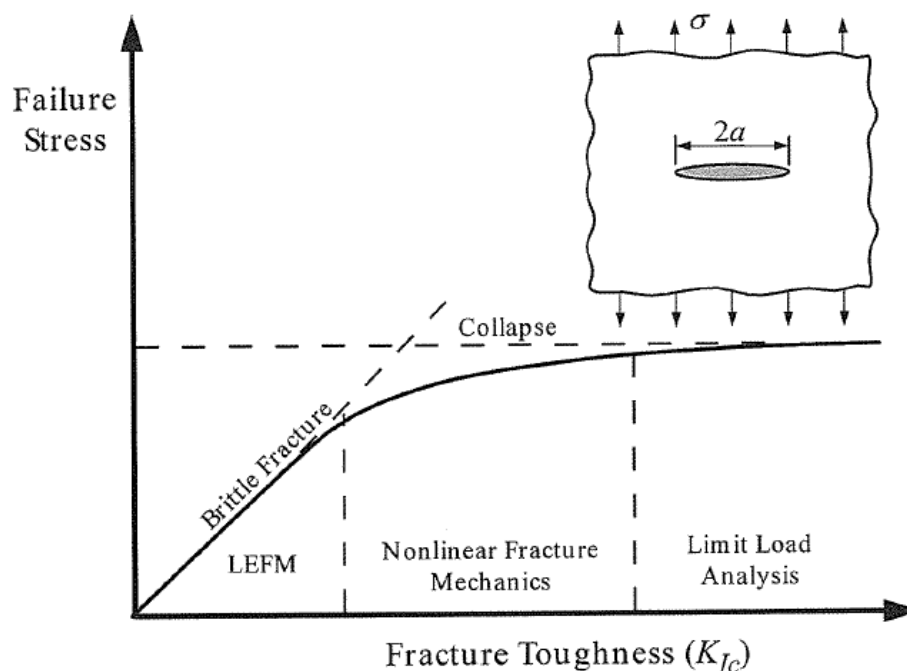

Figure 5.2: Behavior of materials, depending on the fracture toughness, [161]

Analysis and prevention of failure in load bearing components of an artifical hip represents a considerable challenge when fabricating implants.

All material failures begin with crack initiation, which typically occur in locations of highest stress concentration, and which propagtes until failure. For the sake of simplification, linear elastic fracture mechanics is used, as it provides satisfying approximation of the phenomenon. Even though the occurrence of plastic strain at the very tip of the crack in metal materials is inevitable, solutions provided by the elasticity theory are of great significance in both theory and practice when solving problems related to crack initiation and development.

5.2 Derivation of the Elastic Stress Field Equations

A crack is a void within a body which appeared without the removal of material, and is bordered by two opposing surfaces whose distance is significantly less than the other two dimensions, figure 5.3. The common contour line of the crack surfaces is the crack front, [161-164].
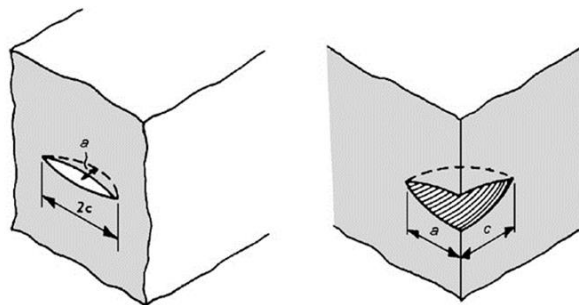

Figure 5.3. Crack types

Linear elastic fracture mechacnis (LEFM), introduces the assumption that a surface which is distant from the crack tip remains elastic, whereas the plastic area around the crack tip is small, [162].

One of the most important initial successes of elasticity theory was the fact that it explained the significant difference between theoretical and real strength of policrystal bodies. Hence, the material fails mostly due to the

breaking of bonds between the atoms of a structure, due to applied load. The strength of the atomic bond depends on the attraction forces between them. Shown in figure 5.4. is the diagram of dependence of potential energy from distance between atoms, [161].
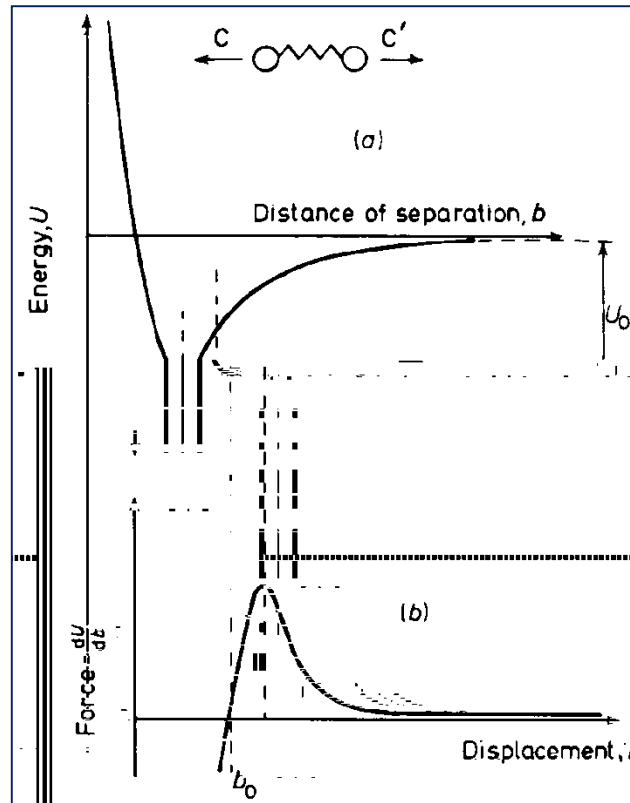

Figure 5.4. Potential energy and applied force as a function of distance between atoms,

[161]

Equilibrium state occurs where potential energy has its minimum value. Bond energy is given in the following way:

$$E_b = \int_{x_0}^{\infty} P dx \qquad (5.1)$$

where x_0 is the equilibrium distance, and P is the force applied.

Applied force can be simply determined by assuming that the force-distance ratio curve (figure 20-down) has a semi-sinusoidal shape:

$$P = P_c \sin\left(\frac{\pi x}{\lambda}\right) \tag{5.2}$$

where P_c represents the cohesion force, and λ is the distance. For small displacements, the force-displacement ratio is linear:

$$P = P_c \left(\frac{\pi x}{\lambda}\right) \tag{5.3}$$

The stiffness of the atomic bond is analogous to the spring model, thus this stiffness (i.e. spring constant) is given as:

$$k = P_c \frac{\pi}{\lambda} \tag{5.4}$$

It can be written that:

$$\sigma_c = \frac{E\lambda}{\pi x_0} \tag{5.5}$$

or

$$\sigma_c = \frac{E}{\pi} \tag{5.6}$$

if it is assumed that λ is approximately equal to the atomic distance.

Surface energy can be evaluated in the following way:

$$\gamma_s = \frac{1}{2}\int_0^\lambda \sigma_c \sin\left(\frac{\pi x}{\lambda}\right) dx = \sigma_c \frac{\lambda}{\pi} \tag{5.7}$$

Surface energy per unit area, γ_s, is equal to one half of fracture energy, since two surfaces form during material failure.

Taking into account the expression for σ_c, the following is obtained:

$$\sigma_c = \sqrt{\frac{E\gamma_S}{x_0}} \tag{5.8}$$

Thus, theoretical cohesion strength of a material is approximately equal to E/π, however experimental fracture strengths of brittle materials are typically three or four orders of magnitude below this value.

Griffith was the first to explain the reasons for this disagreement, by assuming that the material contains a crack type defect, which results in stress concentration, [161,162]. However, fracture cannot occur unless the stress, at atomic level, does not exceed the value of cohesive strength of bonds within the material. Hence, material defects reduce the total strength by increasing local stresses, in the vicinity of the crack.

First quantitative evidence of stress concentration in the vicinity of the crack were given by Inglis. Crack type defect can be replaced with an elliptical opening with the large axis 2a and small axis 2b (figure 5.5). Inglis assumed that the crack behavior is not affected by the size of the plate (specimen), since the plate dimensions are much larger than the dimensions of the crack, [161,162].
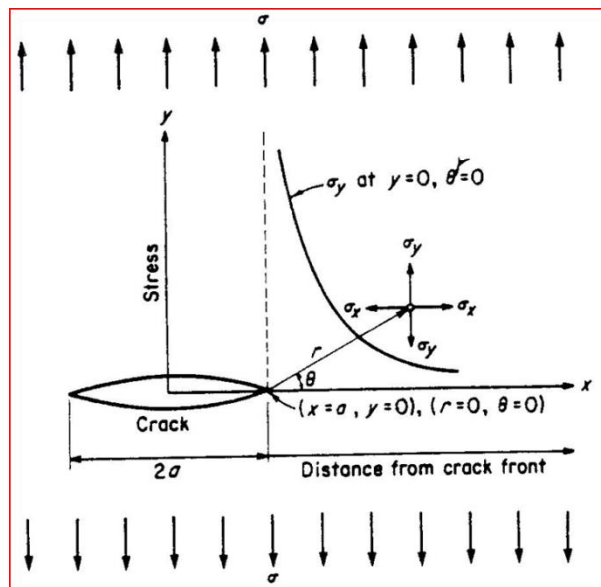

Figure 5.5: Elliptical opening on a plate, subjected to stress σ ,[162]

For this case, Inglis provided a solution using the curvature radisu ρ in the following form:

$$\sigma_A = 2\sigma\sqrt{\frac{a}{\rho}} \tag{5.9}$$

Inglis has shown that equation (5.9) provides a good approximation to stress concentration due to a notch that is not elliptical, except at the tip.

Equation (5.9) predicst infinite stress at the tip of an infinitely sharp crack, where $\rho = 0$. Sharp crack paradox motivated Griffith to develop a fracture theory based on energy, rather than local stress.

For a plate with a crack, Griffith applied stress analysis in order to show that:

$$\Pi = \Pi_0 - \frac{\pi\sigma^2 a^2 B}{E} \tag{5.10}$$

where Π_0 is the potential energy of an uncracked plate and B is plate thickness.

Solving of a brittle fracture problem is given for a plate with crack length 2a, under the effects of remote tensile stress, σ, figure 5.6.
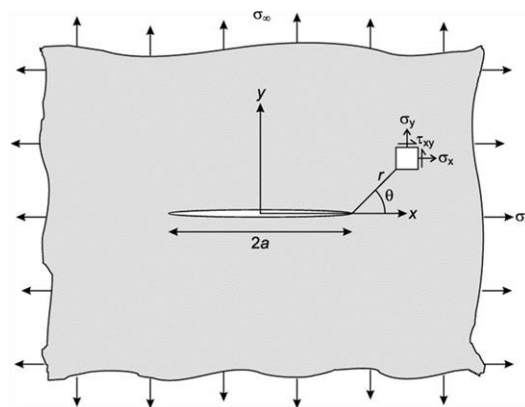

Figure 5.6.: Elliptical opening of a plate, subjected to stress σ

Plate dimensions are significantly larger than crack length, except thickness B, which is sufficiently small to ensure plane stress state. By analyzing an incrementally small crack length growth da, Griffith determined that the crack will grow in an unstable manner if the released potential energy $-dP$ is equal to the work necessary for the initiation of new crack surfaces, dW_s, [161-164].

$$-\frac{d\Pi}{dA} = \frac{dW_s}{dA} \tag{5.11}$$

Since crack initiation requires the forming of two surfaces, W_s is given by:

$$dW_S = 4BdA\gamma_S \tag{5.12}$$

where γ_s is the surface energy of the material.

By applying Griffith's energy criteria, the following is obtained, [161-164]:

$$\frac{\pi\sigma^2 a}{E} = 2\gamma_S \tag{5.13}$$

Left side of the previous expression represents the energy release rate, whereas the right side is the resistance to crack growth of the material. Energy release rate (denoted by G), is also known as the crack growth force, and represents the load and geometry of the body, including the crack geometry, whereas material resistance to crack growth (G$_C$) is its critical value, which is a material property.

By solving for fracture stress, the following expression is obtained

$$\sigma_C = \left(\frac{2E\gamma_S}{\pi a}\right)^{1/2} \tag{5.14}$$

Griffith's approach can be applied to other crack shapes. For example, fracture stress for an elliptical crack in a material is given by:

$$\sigma_f = \left(\frac{\pi E\gamma_S}{2(1-v^2)a}\right)^{1/2} \tag{5.15}$$

where a is the radius of the crack, and v is the Poisson's ratio.

Griffith's theory provides a good explanation for brittle material strength, but its application to extremely plastic materials, such as most metals, requires certain modifications.

Irwin and Orowan have, independent of each other, modified Griffith's solution, in order to explain the behavior of plastic materials, [161-164]:

$$\sigma_C = \sqrt{\frac{E(2\gamma_S + \gamma_P)}{\pi a}} \tag{5.16}$$

where γ_P represents plastic strain work which precedes unstable crack growth, whose values are far above γ_S, which allows further simplification of the equation:

$$\sigma_C = \left(\frac{E\gamma_P}{\pi a}\right)^{1/2} \tag{5.17}$$

Energy criteria is based on a global approach and cannot be applied to local behavior analysis.

For ideally rigid bodies, the crack can be formed only by breaking of atomic bonds, γ_S reflects the total energy of broken bonds per unit area. However, once the crack propagates through the metal, dislocation motion takes place around the crack tip, resulting in additional energy dissipation.

5.2.1. Basic crack propagation models

Determining of stress and strain fields in that zone can be represented by three basic load cases, i.e. three models of crack surface displacement resulting from them, [162-164].
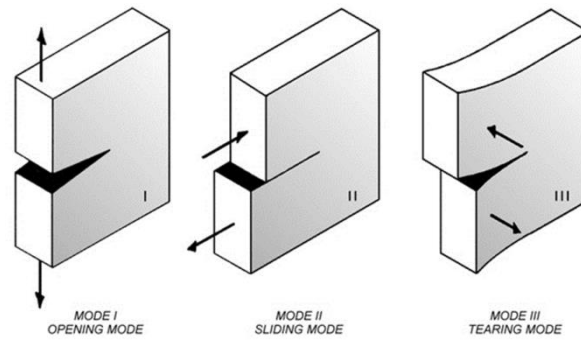
Figure 5.7. Basic crack propagation models: I) Cleaving, II) Sliding and III) Shearing

Irwin, [161-163], had shown that there are three basic shapes of displacement of one crack surface relative to the other, and that they describe the behavior of cracks in all stress states. Shown in figure 5.7. are the basic shapes of displacement of elements which include the crack tip. Displacement shapes of a crack tip which lies in the x-z plane, can be described as follows:

- Shape I - crack propagation by cleaving, characterized by moving of crack surfaces in a way that they open symmetrically relative to the initial crack plane.

- Shape II - crack propagation by sliding, related to local deformation during which one surface slides along the other in the same plane, but in opposite directions.

- Shape III - crack propagation by shearing represents a case of local strain, during which surfaces slide along each other in the direction of the crack so that the points within the material, which were initially in the same vertical plane, are distributed along different vertical planes after crack propagation.

All shapes of crack propagation are solved based on equations derived for a plane elasticity theory problem, and the solutions of the plane problem apply to plane strain and plane stress states. Which of these shapes will be

dominant in real cracks depends on load and factor influenced by geometry and dimensions, [164].

Stress intensity factor determines the magnitude of components for a non-uniform stress distribution. Mathematical derivation of the meaning of this quantity is based on stress state analysis around the crack tip. Shown in fig 5.8 are the stress components near the crack tip in a planar coordinate system of both orthogonal and polar coordinates.
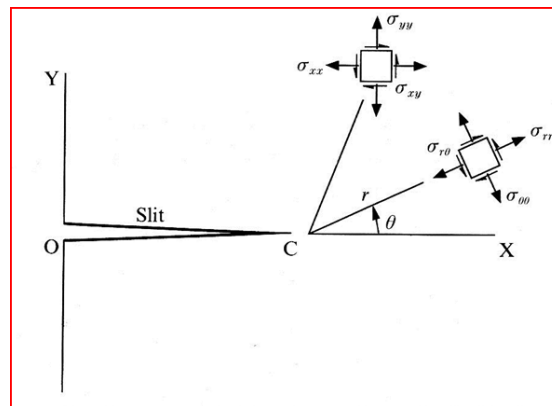

Figure 5.8. Stress components around the crack tip

General expression in tensor form for stress components around the crack tip is given by the expression:

$$\sigma_{ij} = \frac{K_I}{\sqrt{2 \cdot \pi \cdot r}} f_{ij}(\theta)$$
(5.17)

Parameter K_I represents the stress intensity factor. When r→0 (at the very crack tip), stresses become infinite. Taking into account that elastic stresses are being considered, they must be proportional to the external load. In the case of uniaxial tension due to load σ at the infinite distance, K_I will be proportional to σ. Stress intensity factor has the dimension MPa√m and it is proportional to the square root of an adequately chosen length, [164].

In practice, the magnitude of stress intensity factor is of significance for a plate with finite dimensions and a crack of a given length. The solution is then quite complex and approximate solutions are allowed for cases of central or edge crack in a plate with finite dimensions. Geometry correction factor is introduced as:

$$K_I = \sigma\sqrt{\pi a} \cdot f\left(\frac{a}{w}\right) \tag{5.18}$$

Detailed expressions for individual stress fields for load cases I and II, are given in Table 5.1. Ratios of displacement at loads I and II are listed in Table 5.2. Table 5.3. shows stress different from zero and displacement components for load case III, [164].

Table 5.1 Stress field in front of the crack tip for load cases I and II (linear elastic, isotropic material)

	I load case	II load case
σ_{xx}	$\dfrac{K_I}{\sqrt{2\pi r}}\cos\left(\dfrac{\theta}{2}\right)\left[1 - \sin\left(\dfrac{\theta}{2}\right)\sin\left(\dfrac{3\theta}{2}\right)\right]$	$-\dfrac{K_{II}}{\sqrt{2\pi r}}\sin\left(\dfrac{\theta}{2}\right)\left[2 + \cos\left(\dfrac{\theta}{2}\right)\cos\left(\dfrac{3\theta}{2}\right)\right]$
σ_{yy}	$\dfrac{K_I}{\sqrt{2\pi r}}\cos\left(\dfrac{\theta}{2}\right)\left[1 + \sin\left(\dfrac{\theta}{2}\right)\sin\left(\dfrac{3\theta}{2}\right)\right]$	$\dfrac{K_{II}}{\sqrt{2\pi r}}\sin\left(\dfrac{\theta}{2}\right)\cos\left(\dfrac{\theta}{2}\right)\cos\left(\dfrac{3\theta}{2}\right)$
τ_{xy}	$\dfrac{K_I}{\sqrt{2\pi r}}\cos\left(\dfrac{\theta}{2}\right)\sin\left(\dfrac{\theta}{2}\right)\cos\left(\dfrac{3\theta}{2}\right)$	$\dfrac{K_{II}}{\sqrt{2\pi r}}\cos\left(\dfrac{\theta}{2}\right)\left[1 - \sin\left(\dfrac{\theta}{2}\right)\sin\left(\dfrac{3\theta}{2}\right)\right]$
σ_{zz}	**0 (plane stress)** $\nu\,(\sigma_{xx}+\sigma_{yy})$ **(plane strain)**	**0 (plane stress)** $\nu\,(\sigma_{xx}+\sigma_{yy})$ **(plane strain)**
τ_{xz} τ_{yz}	**0**	**0**

Table 5.2 Displacement field around the crack tip for load cases I and II

(linear elastic, isotropic material)

	I load case	II load case
u_x	$\dfrac{K_I}{2\mu}\sqrt{\dfrac{r}{2\pi}}\,cos\left(\dfrac{\theta}{2}\right)\left[\kappa-1+2\,sin^2\left(\dfrac{\theta}{2}\right)\right]$	$\dfrac{K_{II}}{2\mu}\sqrt{\dfrac{r}{2\pi}}\,sin\left(\dfrac{\theta}{2}\right)\left[\kappa+1+2\,cos^2\left(\dfrac{\theta}{2}\right)\right]$
u_y	$\dfrac{K_I}{2\mu}\sqrt{\dfrac{r}{2\pi}}\,sin\left(\dfrac{\theta}{2}\right)\left[\kappa+1-2\,cos^2\left(\dfrac{\theta}{2}\right)\right]$	$-\dfrac{K_{II}}{2\mu}\sqrt{\dfrac{r}{2\pi}}\,cos\left(\dfrac{\theta}{2}\right)\left[\kappa-1-2\,sin^2\left(\dfrac{\theta}{2}\right)\right]$

μ - shear modulus κ=3-4ν (plane strain) κ=(3-ν)/(1+ν) (plane stress)

Table 5.3 Stress different from zero and displacement components for load case III

(linear elastic, isotropic material)

$\tau_{xz}=-\dfrac{K_{III}}{\sqrt{2\pi r}}\,sin\left(\dfrac{\theta}{2}\right)$
$\tau_{yz}=\dfrac{K_{III}}{\sqrt{2\pi r}}\,cos\left(\dfrac{\theta}{2}\right)$
$u_z=\dfrac{K_{III}}{\mu}\sqrt{\dfrac{r}{2\pi}}\,sin\left(\dfrac{\theta}{2}\right)$

When stresses and strain at the crack tip reach critical values, rapid crack growth occurs, along with fracture, and stress intensity factor reaches its critical value K_{Ic}.

Critical stress intensity factor K_c represents the fracture resistance of a material and under certain conditions can be used for predicting of behavior of real structures. In addition, its value depends on the factors such as temperature, strain rate, crack plane orientation, environment in which the material is, and ultimately, element thickness B, [161]   .

Definition of critical stress intensity factor (fracture toughness at plane strain) K_{Ic} is given in a paper by Brown and Srowley, which preceded the ASTM E 399T standard from 1969. Fracture toughness for plain strain K_{Ic} is a material property, which depends on stress intensity factor K for shape I od crack propagation (cleaving) and its dimension is stress x length$^{1/2}$:

$$K_{Ic} = \sigma_c \sqrt{\pi a} \tag{5.19}$$

where: σ_c - stress for which fracture occurs.

In order to determine K_{Ic}, a notched specimen with a crack and of suitable dimensions is subjected to a gradually increasing load, until the crack length reaches a value which results in unstable and quick fracture. The ratio of K_I and the applied load is a function of specimen shape and dimensions. Magnitude of K_I which corresponds to the load which caused unstable crack growth represents the magnitude of K_{Ic}, determined by testing. K_{Ic} depends on the temperature and the rate at which the load is being applied.

5.3 Effect of plastic behavior around the crack tip in biomaterials

Once a plastic zone of considerable size appears around the crack tip, figure 5.9., LEFM methods no longer apply (stress and strain fields can no longer be described by a single parameter, such as the stress intensity factor K, nor can its critical value be used to define fracture toughness of the material), hence EPFM parameters must be utilized, which are not limited to linear elastic material behavior, such as crack tip opening displacement and the J integral.

Crack opening displacement (COD) can be used as a comparative parameter, as suggested by Welds, and defined by the standard DD 19 BSI. The idea is to measure fracture toughness of a material by using crack tip opening displacement - CTOD, figure 5.10. Even though it is of empirical character, CTOD is widely accepted since it is easy to determine even in complex

problems, while providing good results, and in the area of small scale yielding (SSY) it can be related to K_I, [164].
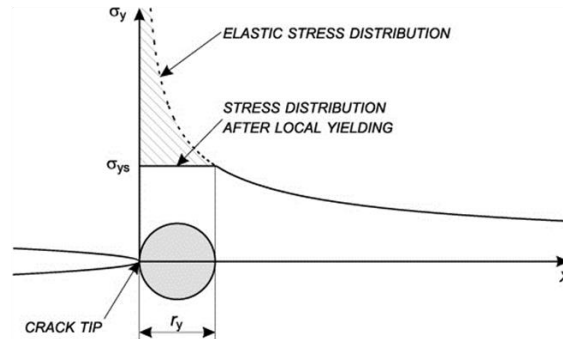

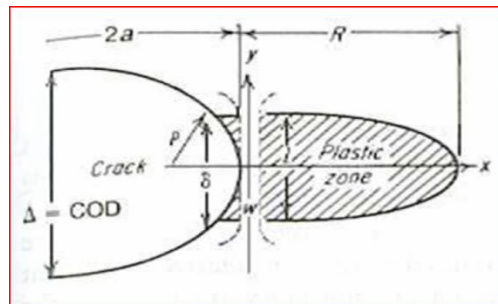*Figure 5.9. Plastic zone around crack tip*

Figure 5.10. The crack tip opening displacement (CTOD)

It should be noted that *m* is a dimensionless constant that depends on the material properties and the stress. The following equations describe CTOD parameter:

$$CTOD = \frac{\rho b}{a + \rho b} COTD_m \, {}^{\circ}\delta = \frac{\rho b}{a + \rho b} \Delta \tag{5.20}$$

$$\delta \approx \frac{b}{2a + b} \Delta \tag{5.21}$$

$$\delta = \delta_{elastic} + \delta_{plastic} = \frac{K_I^2}{m \times \sigma_{ys} \times E} + \frac{\rho_{plastic} \times b}{a + \rho_{plastic} \times b} \Delta \tag{5.22}$$

Irwin had assumed that the crack with a small plastic zone in front of its tip behaves in the same way as a crack with a sharp tip, but of slightly greater length, figure 5.11.
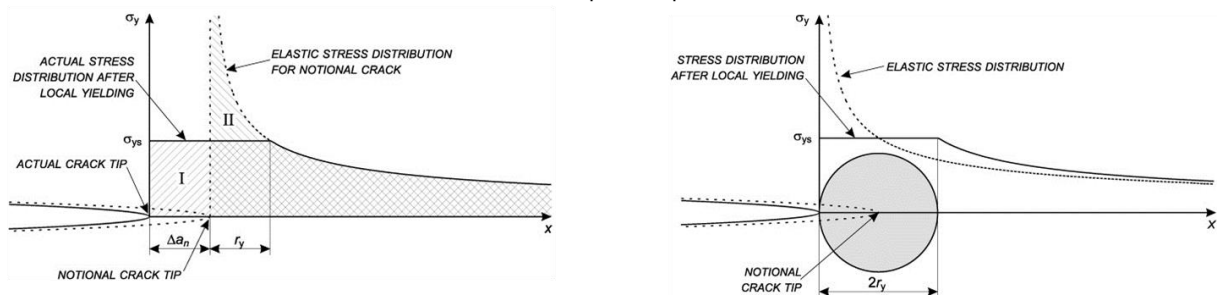
Figure 5.11. Irwins approach

Small plastic strain in the center corresponds to the plane strain, while the outer surfaces have extensive plastic strain corresponding to the plane stress. If material strengthening is neglected, stress is constant in the plastic zone, enabling simple approximation of plastic zone radius, based on an assumption of its increase until balance state is reached. This is the simplest way of introducing the plasticity into the analysis of material behaviour at the crack tip, [161-164].

$$r_p = 2r_y = \frac{1}{\pi}\left(\frac{K_I}{\sigma_{YS}}\right)^2 \quad \text{plane stress;} \tag{5.23}$$

$$r_p = 2r_y = \frac{1}{3\pi}\left(\frac{K_I}{\sigma_{YS}}\right)^2 \quad \text{plane strain} \tag{5.24}$$

As a final result, the following parameter is obtained

$$\delta = \frac{4}{\pi}\frac{K^2}{E\sigma_T} = \frac{4}{\pi}\frac{\mathcal{G}}{\sigma_T} \tag{5.25}$$

Wherein δ is actually CTOD, and in this way it is related to **K** and indirectly to $\mathcal{G}$ in plane strain area, however the suggested model is too simplified.

Strip yield model, suggested by Dugdale provides more realistic and applicable results, [161-164]. The basic concept behind this model is the same as with Irwin, however the effect of the plastic zone is not taken into account only due to an increase in crack length, but also due to the acting of compressive stresses which are at yield stress level, figure 5.12., [161].
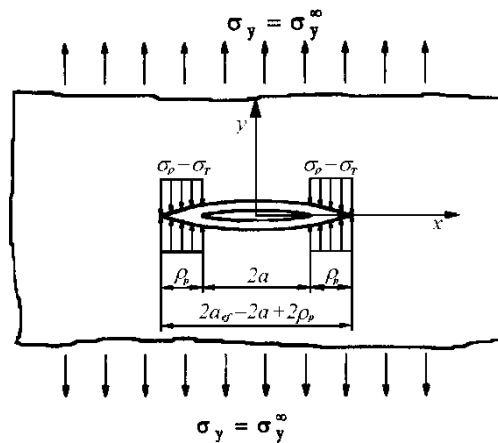
Figure 5.12. Dugdale's model of the plastic zone,[161]

Dugdale took the basic concept from Irwin, while assuming that the plastic zone effect is not caused only by an increase in crack length, but also due to compressive stresses at yield stress level. Dugdale's model holds for plane stress state and the ideal plastic material (hardening equals zero), thus in other cases, with different conditions, correction factor **m** is used:

$$\delta = \frac{K_I^2}{mE\sigma_T} = \frac{\mathcal{G}}{m\sigma_T} \tag{5.26}$$

which represents a non-dimensional constant. For plane stress state and an ideally plastic material, **m** = 1, and for plane strain state and material with hardening, m≈2 ,[164].

The main flaw of CTOD is its empirical nature, i.e. it still represents an insufficiently developed theoretical basis, and this problem was partially solved by J.J. Rice by introducing the so-called, *J-integral*, whose basic features are the following:

1. It does not depend on the integration path, which simplifies its numerical, analytical and experimental determining.

2. It can describe an elasto-plastic stress and strain fields around the crack tip (the same as *K* in LEFM).

3. It can be related to energy release rate.

J-integral only applies to cases where there is no unloading in the plastic strain area, which can be expected for small scale plastic strain and small crack growth.

According to Rice, the *J*-integral is defined as a contour integral, [161-164]:

$$J = \int_{\Gamma} w \times d_y - T_i \frac{\partial u_i}{\partial x} ds \qquad (5.27)$$

where $w = \int_{0}^{\varepsilon_{ij}} \sigma_{ij} d\varepsilon_{ij}$ represents strain energy density; Γ is the integration path; *ds* is an element of arc length; $T_i = \sigma_{ij} n_j$ - tension force on the contour; u_i - displacement and n_i is the unit normal to Γ, 5.13.
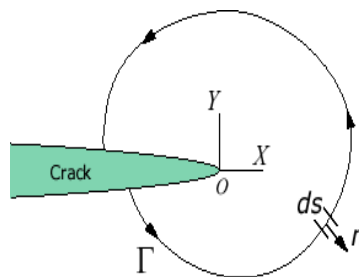
Figure 5.13. J-integral definition

Rice had proven that *J* integral is path independent for two-dimensional problems in the absence of volumetric and inertial forces, in case of a non-linear elastic material, which is homogeneous at least in the direction of the crack.

5.4 Fatigue crack propagation behaviour

The ability to predict the onset of widespread fatigue damage in biomedical implants requires methodologies that predict fatigue crack initiation, crack growth, and residual strength. Valid analytical methodology to predict the onset of widespread fatigue damage in implant structure must be based on actual observations of the physical behavior of crack initiation, crack growth, and fracture, [165-167].

Cyclic fatigue involves the microstructural damage and failure of materials under cyclically varying loads, Fig. 5.14., [166]. Fatigue crack growth of most superalloys is predominantly a cycle-dependent damage process. Structural materials, however, are rarely designed with compositions and microstructures optimized for fatigue resistance, [167,168].
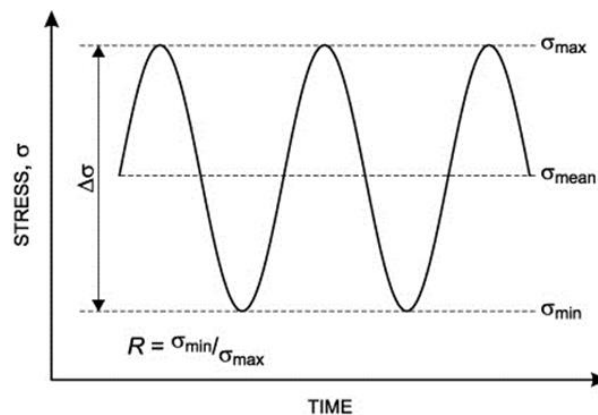
Figure 5.14 Cyclically varying loads

Fatigue crack growth behaviors of superalloys, have received increasing attention in the past several decades because the results of failure analyses indicate that fatigue is one of the major causes of failure in engineering

structures, and the fatigue life of engines is determined by the initiation and the propagation behavior of the cracks, [165-168]. It has been revealed that crack growth is induced by irreversible crack tip plastic flow, Fig. 5.15 which provides the driving force for crack growth, [165-167].
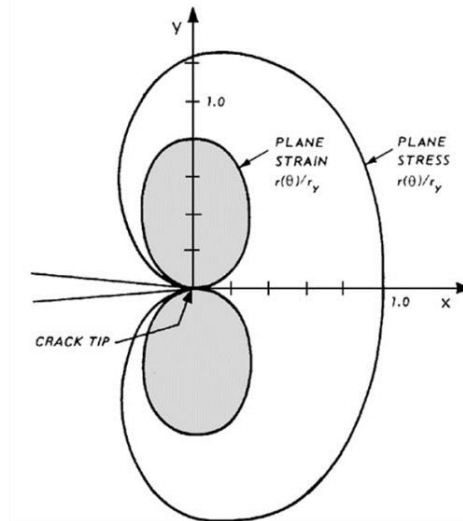

Figure 5.15 Plastic zone shape

Basically, fatigue crack propagation can be divided into three stages: stage I (short cracks), stage II (long cracks) and stage III (final fracture). Once initiated, a fatigue crack propagates along high shear stress planes 45 degrees. This is known as stage I or the short crack growth propagation stage. The crack propagates until it is decelerated by a microstructural barrier such as a grain boundary, inclusions, or pearlitic zones, which cannot accommodate the initial crack growth direction.

When the stress intensity factor K increases as a consequence of crack growth or higher applied loads, slips start to develop in different planes close to the crack tip, initiating stage II. An important characteristic of stage II is the presence of surface ripples known as "striations," which are visible with the aid of a scanning electron microscope. Finally, stage III is related to unstable crack growth. At this stage, crack growth is controlled by static modes of failure and is very sensitive to the microstructure, load ratio, and stress state.

In fracture mechanics, fatigue crack propagation in biomaterials is investigated using CT specimens, wherein it is common in literature to encounter experiments performed in physiological environment conditions.

For prediction of structure life, Paris equation is typically used, [165]:

$$da / dN = C(\Delta K)^m \tag{5.28}$$

where C and m are constants, and ΔK is the stress intensity range. Stress intensity range can be expressed with the following equation

$$\Delta K = Y(\Delta \sigma)(\pi a)^{1/2} \tag{5.29}$$

where Y is a function of geometry, and a is the crack length.

By combining equations ($da / dN = C(\Delta K)^m$

) and ($\Delta K = Y(\Delta \sigma)(\pi a)^{1/2}$

), we obtain:

$$da / dN = C\left\{Y(\Delta \sigma)(\pi a)^{1/2}\right\}^m \tag{5.30}$$

Prediction of biomaterial life can be written as:

$$\int_0^{N_f} dN = \int_{a_i}^{a_f} \frac{1}{YC(\Delta \sigma)^m \pi^{m/2} a^{m/2}} \frac{da}{a^{m/2}} \tag{5.31}$$

where N_f is the total number of cycles to failure, a_i is the initial crack length, and a_f is crack length immediately before a catastrophic failure (this can be assessed by developing on conventional fracture resistance tests, and by using the radio $K_{IC} = Y\sigma / \sqrt{(\pi a_f)}$ to determine a_f for given K_{Ic}, and the applied stress (σ))., figure 5.16., [165-167]

Since *Y* is the function of geometry and crack length, solving of equations during the determining of initial crack length for a given life cycle is best performed numerically.
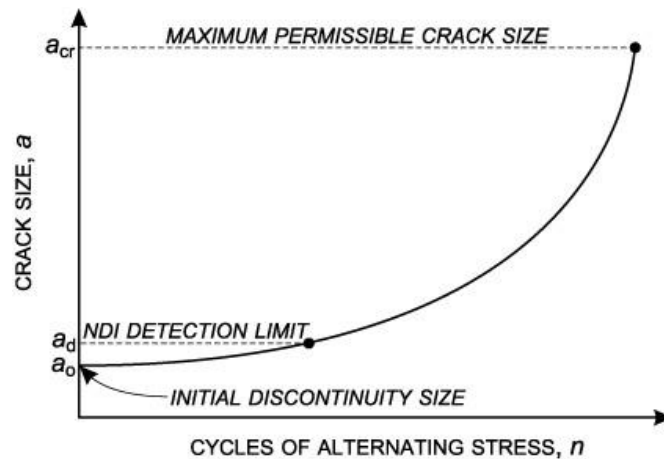

Figure 5.16. Number of stress cycles/crack size diagram

There have been many models developed during the past decades to describe fatigue crack growth,[165-168]. The major difference among these models is the description of damage, such as what constitutes damage, how it accumulates, and what is the best way to describe it. Some of the equations for the crack growth laws are:

Paris Law:

$$\frac{da}{dN} = C(\ \Delta K)^m \qquad (5.32)$$

Forman:

$$\frac{da}{dN} = \frac{C(\Delta K)^m}{(1-R)K_{IC} - \Delta K} \qquad (5.33)$$

Complete curve complete crack growth rate curve

$$\frac{da}{dN} = C(\Delta K)^m \left\{ \frac{1 - \left(\frac{\Delta K_{th}}{\Delta K} \right)^{n_1}}{1 - \left(\frac{K_{max}}{K_{IC}} \right)^{n_2}} \right\}^{n_3} \qquad (5.34)$$

McEvily

$$\frac{da}{dN} = C(\Delta K - \Delta K_{th})^2 \left(1 + \frac{\Delta K}{K_{IC} - K_{max}} \right) \qquad (5.35)$$

5.4.1. Propagation rates

Similarly to the initiation phase, many factors can affect long fatigue crack. Among them, special attention should be given to effects of load ratio and the presence of residual stresses, [165-167]. Generally the effect of increasing load ratio is less significant in the Paris regime than in near-threshold and near-failure regions, Fig. 5.17.
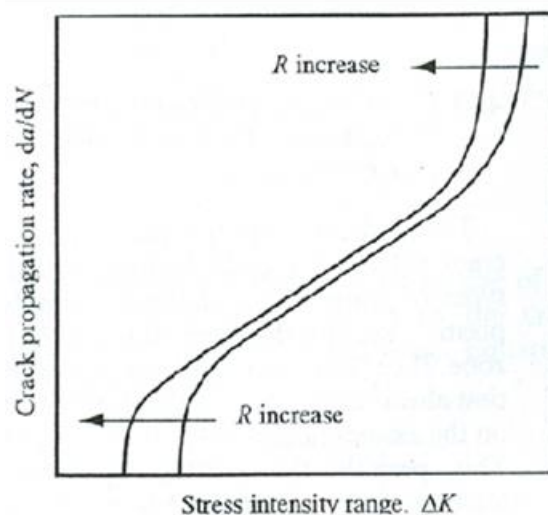
Figure 5.17. The effect of increasing load ratio, [161]

According to LEFM the plastic deformation near the crack tip is controlled by the stress intensity factor (SIF) K, provided the small scale yielding (SSY).

When the stress varied between the max and min then

$$K_{max} = \sigma_{max} \sqrt{\pi a F} \quad K_{min} = \sigma_{min} \sqrt{\pi a F} \tag{5.36}$$

where F is a correction factor of SIF and the stress ratio R ,defined by

$$R = \frac{K_{min}}{K_{max}} = \frac{\sigma_{min}}{\sigma_{max}} \tag{5.37}$$

and $\Delta K = K_{max}$ for R<0 when the tensile part of loading is taken

According to last expression the important factor for fatigue crack propagation is amount of reversal of plastic deformation of crack tip . There are general expiration of fatigue crack propagation rate da/dN in term of SIF will be

$$\frac{da}{dN} = f(\triangle K, R) = g(\triangle K, K_{max}) \tag{5.38}$$

According to Paris and Erdogan

$$\frac{da}{dN} = C(\triangle K)^{m} \tag{5.39}$$

Where C is a weak function of R and m between 2 and 4.

Fatigue crack growth rate curve is given on Fig. 5.18., [165-167].
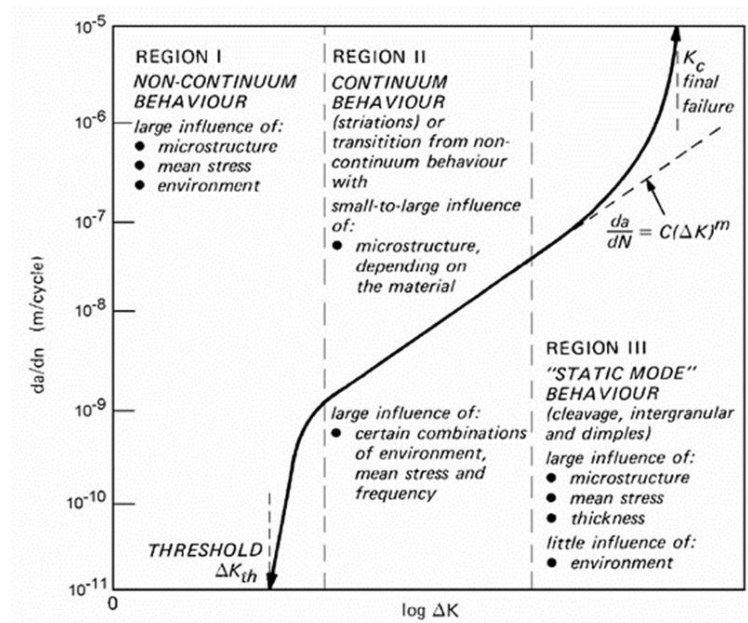
Figure 5.18 Fatigue crack growth rate curve, [161]

In the regime I, there is a threshold SIF range and the rate is practically zero and the regime III where the ΔK is high value, the crack propagation is accelerated. Unstable fracture taken place when the maximum SIF equal the fatigue fracture. The figure illustrates the characteristic of each regime. Near the threshold stress intensity factor, ΔK_{th}, the effects of R ratio are mainly attributed to crack closure effects, in which crack faces contact each other at an applied K_{Ic} that is higher than the minimum applied stress intensity factor, $K_{min.}$, [165-167].

CHAPTER 6

6.1 The Fracture mechanics - Experimental investigation of metallic orthopedic biomaterials

6.1.1. The tests on standard specimens

The first proposals of standards for determining fracture toughness in plane strain have published by American Society for Testing and Materials - ASTM (ASTM E399-70T) and British Standard Institution – BSI (DD 3). There are many common features in experimental determination of fracture mechanics parameters, especially in measuring their critical values and material properties.

As confirmation of the above mentioned can serve the latest standard in this field, ASTM E1820, which combines measurement of fracture toughness as critical value of any of the three basic parameters of fracture mechanics - K_{Ic}, $CTOD_{Ic}$ ili J_{Ic}, [170]. Therefore, the determination of the above parameters, first is described individually, but without some of the details that are given at the end (attached) as the common elements of their measurements. It should also be kept in mind that K_{Ic} is determined directly by definition, and that the standard methods of measuring CTOD and J integral is based on the indirect, ie. approximate relations. In the first case relation CTOD with CMOD, and in the second case relation J integral with the surface under the curve $F\text{-}\delta$.

The first step in planning an experimental determination of fracture toughness in plane strain, K_{Ic}, is the choice of test specimens. Figure 6.1. shows standard single edge notched bend specimen, and Figure 6.2 shows compact tension specimen, [169,170].
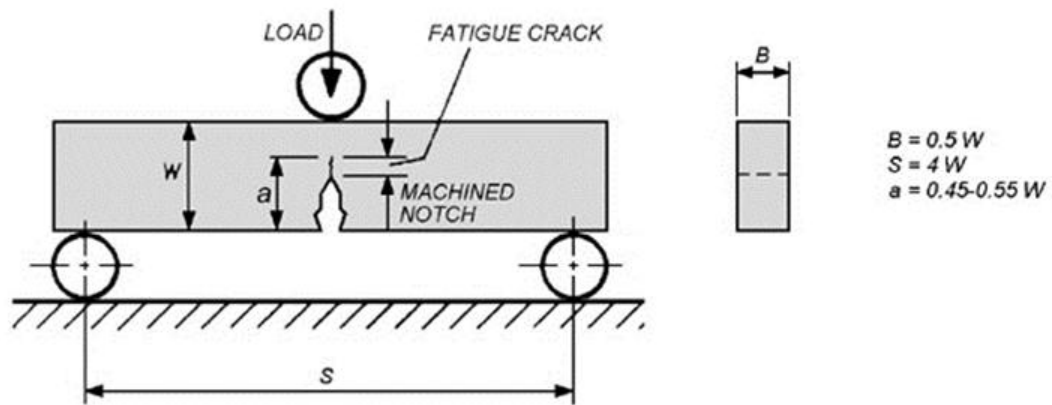
Figure 6.1. ASTM Standard Single Edge notched Bend (SENB) Specimen, [169]

Maximum stress intensity factor for SENB specimen is determined by following formulas, [169,170]:

$$K_I = \frac{LOAD * S}{B * W^{3/2}} * f\left(\frac{a}{W}\right)$$
(6.1.)

$$f\left(\frac{a}{W}\right) = \frac{3\left(\frac{a}{W}\right)^{1/2}\left[1.99 - \frac{a}{W}\left(1 - \frac{a}{W}\right)\left\{2.15 - 3.93\left(\frac{a}{W}\right) + 2.7\left(\frac{a}{W}\right)^2\right\}\right]}{2\left(1 + 2\frac{a}{W}\right)\left(1 - \frac{a}{W}\right)^{3/2}}$$
(6.2.)
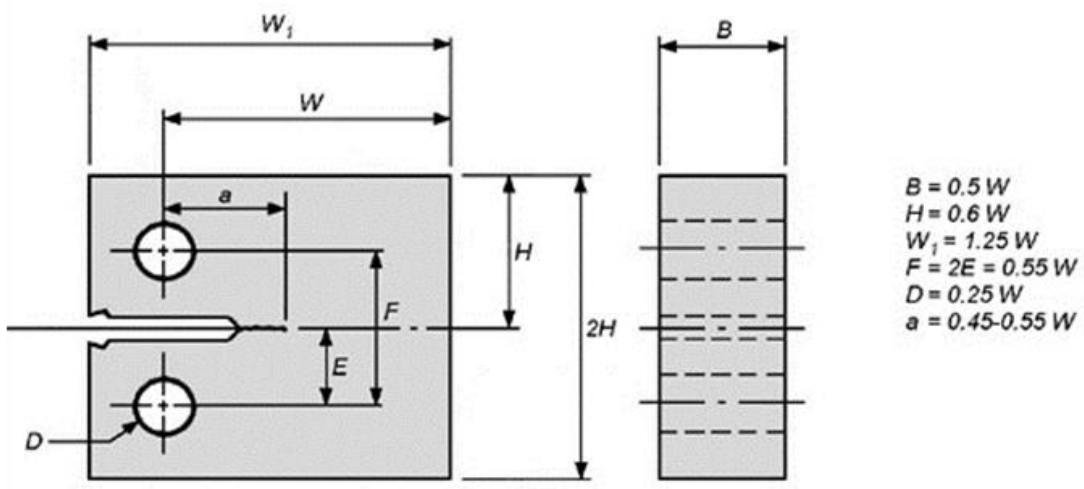
Figure 6.2. ASTM Standard Compact Tension (CT) Specimen, [169]

Maximum stress intensity factor for CT specimen is determined by following formulas:

$$K_I = \frac{LOAD}{B * W^{1/2}} * f\left(\frac{a}{W}\right) \tag{6.3.}$$

$$f\left(\frac{a}{W}\right) = \frac{\left(2 + \dfrac{a}{W}\right)\left\{0.886 + 4.64\left(\dfrac{a}{W}\right) - 13.32\left(\dfrac{a}{W}\right)^2 + 14.72\left(\dfrac{a}{W}\right)^3 - 5.6\left(\dfrac{a}{W}\right)^4\right\}}{\left(1 - \dfrac{a}{W}\right)^{3/2}} \tag{6.4.}$$

The basic requirement that should be complied:

$$B \geq 2,5\left(\frac{K_{Ic}}{R_{p0,2}}\right)^2 \tag{6.5.}$$

Since the critical fracture toughness K_{Ic} is not known before the test, a requirement (6.5) can not be applied. Therefore, there are recommended thickness for different relations of $R_{po,2}/E$. Determined thickness B defines other dimensions of the specimen. For the determination of critical stress intensity factor K_{Ic} there has to be initiated fatigue crack, but on condition that the fatigue crack ensure the relevant requirements. The minimum length of fatigue crack is 1.3 mm and must be achieved by varying the load that ranges between F_{max} i 0,1 F_{max}, so that the maximum stress intensity factor K_{fmax} for fatigue corresponds to Fmax.

For a valid fatigue crack, it must be filled following condition:

$$\frac{K_{fmax}}{E} \leq 0,00032m^{1/2} \quad \text{ili} \quad \frac{K_{fmax}}{K_{Ic}} \leq 0,67 \tag{6.6.}$$

The minimum number of load cycles should be 25 000. In order to ensure the crack length of 1.3 mm, it is necessary that it be achieved in the side surfaces as

the front of fatigue crack has usually arc with the greatest length of the crack in the middle.
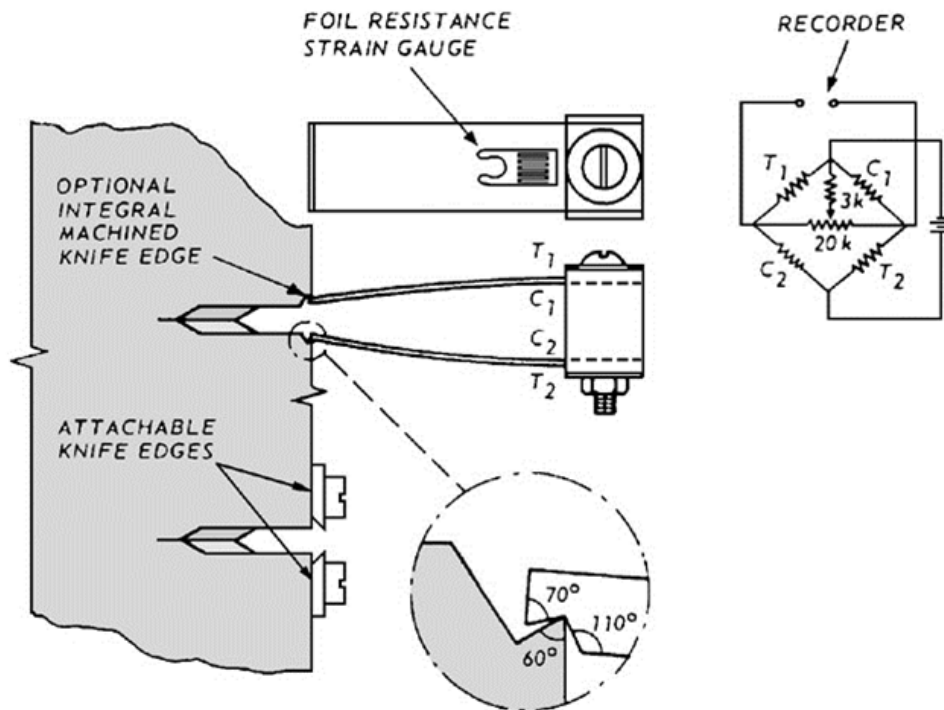

Figure 6.3. Clip gauge and its attachment to the specimen, [169]

Testing of specimens with fatigue crack can be done by bending (or tension) on the testing machine. The load is usually recorded in the form of force. Crack opening displacement is measured with special extensometer, shown in Figure 6.3., [169,170].Example of diagram force - the crack opening displacement is shown in Figure 6.4., [169,170].
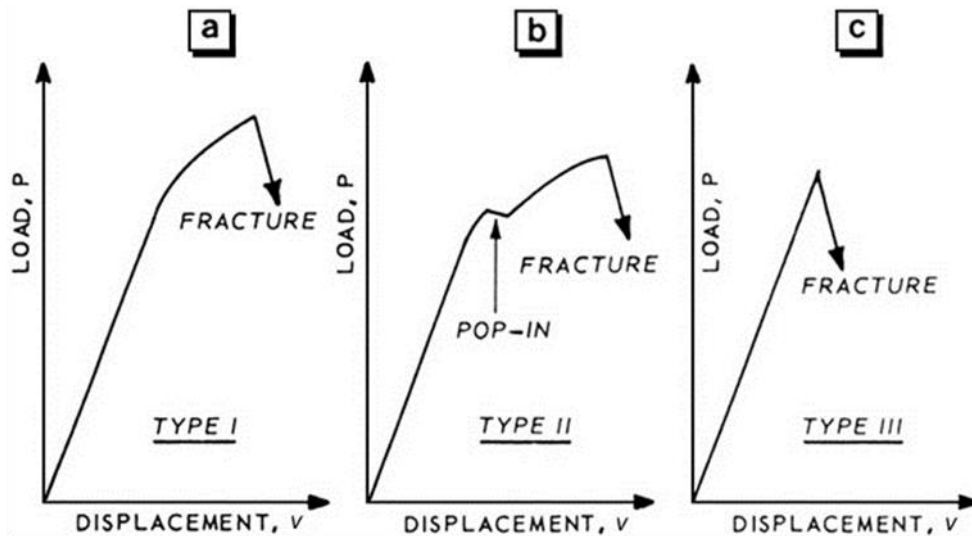
Figure *6.4. Principal types of load displacement plots during K_{Ic} testing, [169,170]*

Besides SENB and CT spesimens for fracture toughness analysis, commonly used is disk-shaped compact tension specimen DC (T), [169,170].

Procedures for experimental analysis that occur in a large number of standards are:

- The specimen is quasi-static loaded up to fracture at a rate of 0,55 to 2,75 MPa·m/s, Epruveta se kvazi-statički opterećuje do loma, brzinom od 0,55 do 2,75 MPa·m/s, with a record on diagram force-CMOD. The force is directly recorded from the test machine, and CMOD from the extensometer.

- K_Q is calculated according to the formulas given in the standard, where is used a force F_Q that was read from the diagram *F-CMOD*, as is shown in Figure 6.5.

- Required conditions should be checked that the obtained result of K_Q was a valid velue of fracture toughness: $t_{min} \geq 2,5(K_Q/\sigma_Y)^2$, which is a requirement for a plane strain state. $P_{max} \leq 1,1 P_Q$, which is the condition of small plastic strain in front of the crack tip.
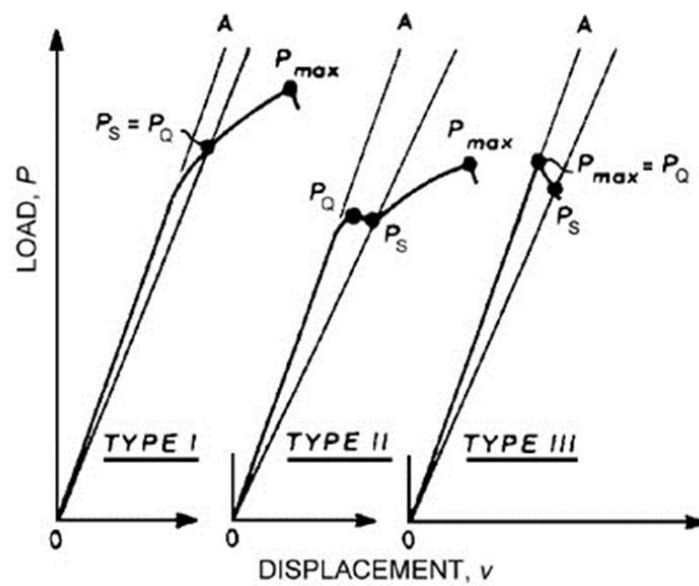
Figure 6.5. Diagrams of force – CMOD, [169,170]

In addition to the above conditions make testing of fracture toughness complex, the final result depends on several factors, which can produce significant overall error, although K_{Ic} is measured directly according to standard. According to [164], errors can be up to 3% during the test, (the inaccuracy of measuring instruments and imprecise positioning of the specimen), up to 5% in force recording F_Q, up to 3% in the measurement of crack length, which can produce a total error greater than 10%.

For components experiencing both plastic and elastic deformation at fracture conditions, another parameter has been developed to define fracture behaviour. A line integral related to energy in the vicinity of crack tip is developed and solved for two-dimensional crack problems and plastic load conditions by Rice, [161-164]. One form of this integral, the J integral, is given by the following equation:

$$J = \int_C (W dy - T \cdot \frac{\partial u}{\partial x} ds)$$

(6.7.)

where: x and y are coordinates normal to the crack front,

T – stress vector acting on the contour,

u – displacement vector,

W – strain energy density and

C – is the line contour surrounding crack tip.

The failure (crack initiation) occurs when J integral reaches some critical value, which is different for different materials and is considered to be material parameter. One can thus define value J_{IC}, which characterizes the toughness of a material near the outset of crack extension, [164]. Several methods based on different specimen configuration and loading conditions were developed for J_{IC} determination. ASTM Standard defines precisely how to determine J_{IC} for each of these standard test methods, [169,170]. The critical J integral value can be obtained from J-R curve as value that corresponds to the average stretch zone size or average stretch zone width (SZW).

6.1.2. Stretch zone width determination method

Apparent increase in crack length during blunting Δa_B is often equated with the stretch zone (SZ), Fig. 6.6., [164].

If the definition of crack tip opening is accepted, then the width of SZ, ω, can be simply expressed through δ_t:

$$\omega = \delta_t / \sqrt{2} \tag{6.8.}$$

Considering that $2\Delta a_B = \delta_t$, it follows that:

$$J = \sqrt{2} m \omega \sigma_Y = 2m \Delta a_B \sigma_Y \tag{6.9.}$$
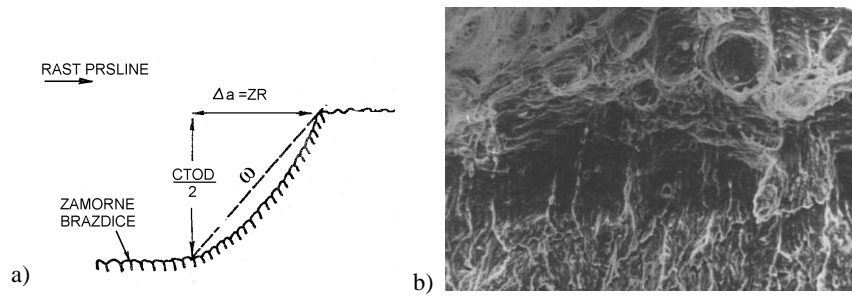
Figure 6.6. Final stretch zone: a) schematic representation b) SEM, [164]

If the definition of crack tip opening is accepted, then the width of SZ, ω, can be simply expressed through δ_t:

$$\omega = \delta_t / \sqrt{2} \tag{6.8.}$$

Considering that $2\Delta a_B = \delta_t$, it follows that:

$$J = \sqrt{2} m \omega \sigma_Y = 2 m \Delta a_B \sigma_Y \tag{6.9.}$$

This relation is mostly used in the form of $J = 2\Delta a_B \sigma_Y$, where the hardening is addressed by using the arithmetic mean of yield strength and tensile strength, instead of yield strength σ_Y; m is set to a value corresponding to plane stress conditions ($m=1$), for stretch zone cannot develop under plane strain conditions, and therefore no crack blunting can occur, [161-164].

The width of the final stretch zone is considered a fracture mechanics parameter, corresponding to the initiation of the stable crack growth δ_i. This parameter is quite difficult to measure, and so does not have a widespread use. It is nevertheless standardized, at least at the level of recommendation (ESIS P2-92), [171]. Figure 6.7. schematically represents stretch zone width determination.

$$SZW_L = \sum_{i=1}^{m} SZW_i \, / m \quad \textbf{(m=5-10)}$$
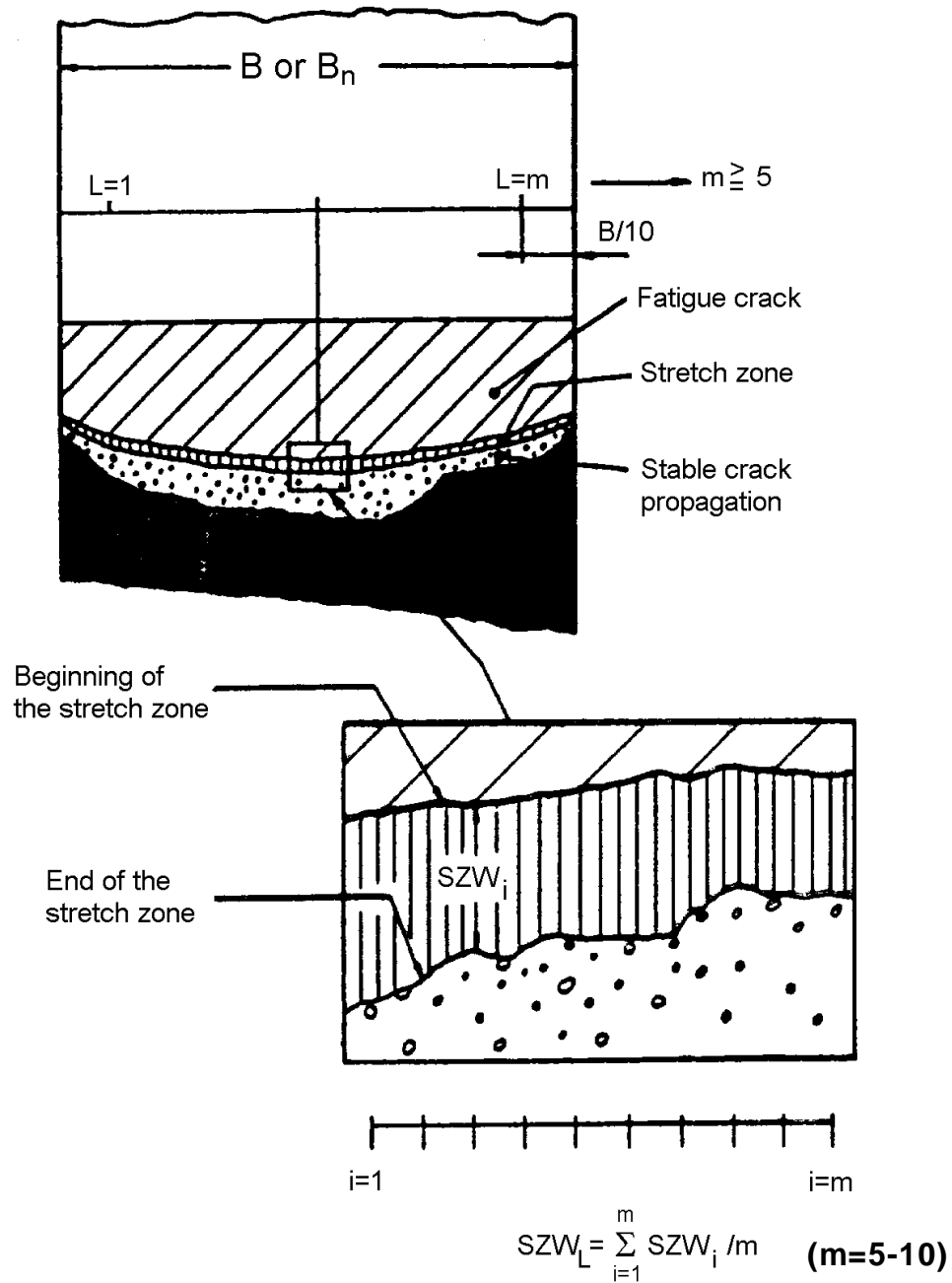
Figure 6.7. Stretch zone measurement. , [171]

On the SEM microphotograph of fracture surface one can distinguish the following areas (zones):

1. Fatigue crack zone – this zone is present due to specimen preparation: specimens are initially fatigue-loaded in order to extend the machined notch a prescribed amount.
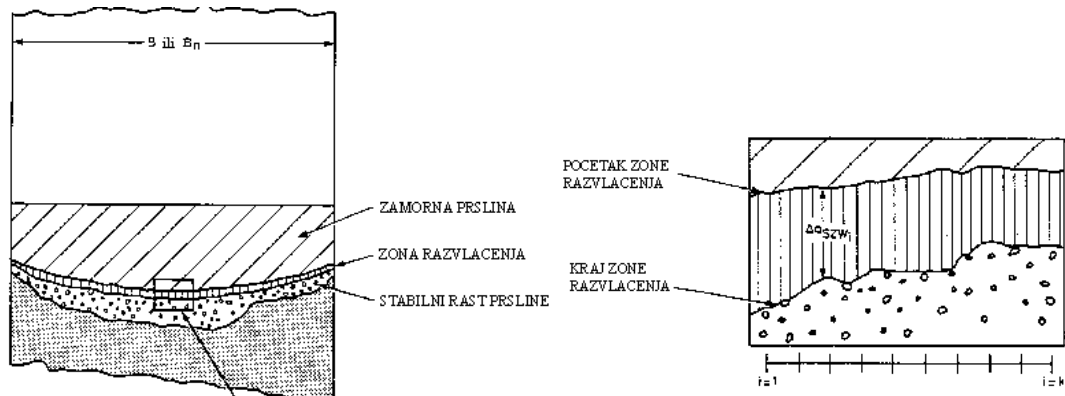
2. Stretch zone – this zone is found to stretch between fatigue crack and stable crack propagation. Size of this zone depends on the toughness of material around the crack tip and thus is in correlation with K_{IC}.

3. Stable crack propagation – zone of stable crack propagation continues beyond stretch throughout the whole cross section until the specimen fails.

The best results are obtained if average value of SZW and the deviation are taken into account. These values can be calculated from values obtained from SEM fracture surface image at several points usually equally spaced along the specimen width. When SZW is known the corresponding critical J_i integral value could be determined, as shown in Figure 6.8.

Figure 6.8. Determination of critical J_i integral from stretch zone size. , [171]

Measuring of the critical SZW at nine points is schematically shown in Figure 6.9.

Figure 6.9. Width measurement of final stretch zone: a) global view b) local view , [164]

With every SEM measurements it is necessary to be defined the start and end of final SZ. It is necessary to do at least five measurements at each point to obtain the local value of the critical SZW, [164,171]:

$$\Delta a_{L,szw} = \frac{1}{k} \sum_{i=1}^{k} \Delta a_{szw}^{i} \qquad k \geq 5 \tag{6.10.}$$

Based on the measured nine local values, critical SZW is obtained.

$$\Delta a_{szw} = \frac{1}{9} \sum_{i=1}^{9} \Delta a_{L,szw}^{i} \tag{6.11.}$$

This size can be used to determine the value of J integral at the initiation of stable crack growth, J_i, as is shown in the diagram J-Δa in Figure 6.10.   `
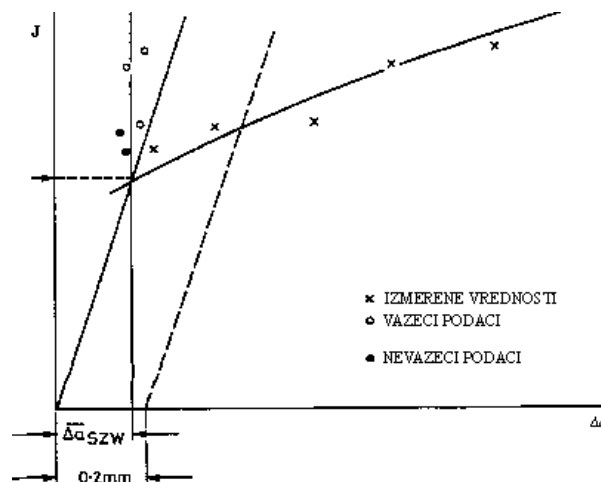
Figure 6.10. Determination of the value J_i by using Δa_{szw}, [164]

Determined value of J_i in this way is not always accurate enough because there is a possible large dissipation of the measured values of the critical SZW Δa_{szw}. It is therefore understandable that the parameters such as J_i, δ_i i Δa_{szw} have not yet been standardized, and there are working on establishing alternative parameters, for example su $J_{0,2}$ i $\delta_{0,2}$ ili $J_{0,2/BL}$ i $\delta_{0,2/BL}$, [164,171].

6.2 Experimental tests on selected biomaterials

6.2.1. Biomaterials selection for experimental tests

The multiphase Co-Cr alloy (35% Ni, 35% Co, 10% Mo, 20% Cr) is biomaterial that is used for hip implants, because it exhibits a superior combination of strength, toughness, and corrosion resistance.

The Co-Ni-Cr-Mo alloy (MP35N) can be cast or forged. The mechanical properties of both alloys are better of those of the cast Co-Cr-Mo alloy considering wear resistance and corrosion resistance, [79]. The MP35N alloy has workability as high as the 316L stainless steel.

While the strengthening mechanisms in MP35N are now reasonably well understood, as well as the influence of cold-work and aging on strength and ductility, there is very little information in the literature on the fracture toughness of this alloy. Several attempts have been made in the literature to determine the plane strain fracture toughness of MP35N, using either 3-point bending specimens (L/T direction, according to ASTM specification), or the Short Rod specimens with chevron slot (T /L direction), [164, 171] .

Most of the previous studies have failed to obtain a valid and consistent measurement according to ASTM E399 standard, [169], because of insufficiently thick sections. This is because, unlike other high strength materials that obtain their strength from aging treatments, MP35N gets its strength mainly from cold-working processes that usually yield final shapes possessing limited cross-

sectional dimensions. Furthermore, it was also reported that the crack often propagated at a large angle with respect to the plane of symmetry in the sample (which is the intended plane of crack propagation in these test methods).

Tested material of interest is MP35N multiphase alloy (35% Co, 35% Ni, 20% Cr and 10% Mo), which exhibits impressive combination of high strength and toughness after extensive plastic strain (e.g. 53% of cold-working) and subsequent aging at about 600°C for 4 hours, positioning it second only to TRIP steels at the suitably plotted diagram, Fig. 6.11., [4,5,79].

Previous studies of MP35N properties, including fracture toughness testing, have indicated further possibility for toughness enhancement, which underline the importance of better understanding of fracture behaviour of this material, [60,172,173]. Therefore, an extensive investigation of the elastic-plastic fracture behaviour of commercially cold-drawn MP35N in both un-aged and aged conditions has been done.
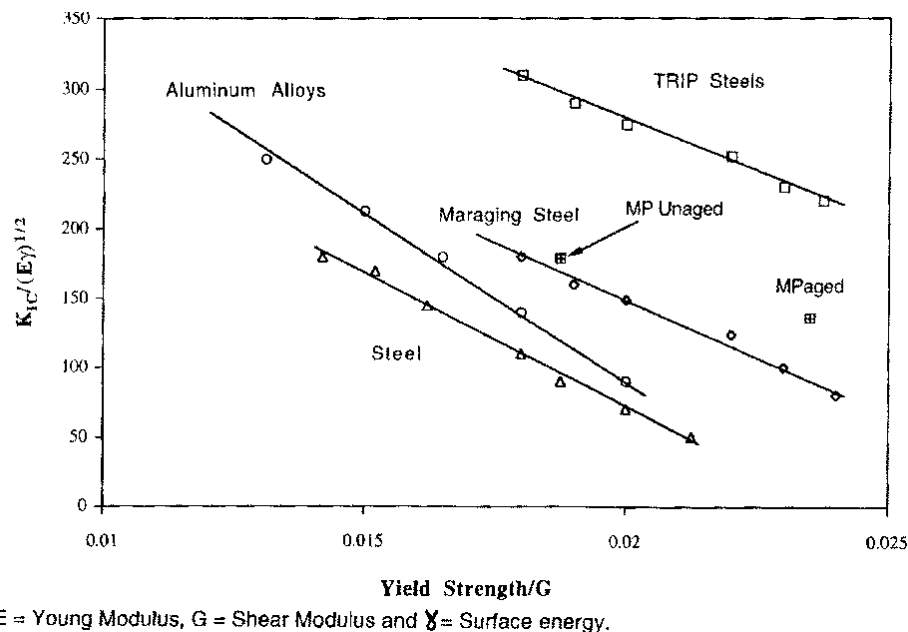
Figure 6.11. Normalized strength-toughness curves of MP35N vs other materials, [10]

During the examination of this alloy it is necessary to take into account the anisotropy of biomaterials. To provide a common scheme for describing

material anisotropy, ASTM standardized the following six orientations, Fig 6.12., L-S, L-T, S-L, S-T, T-L, and T-S.
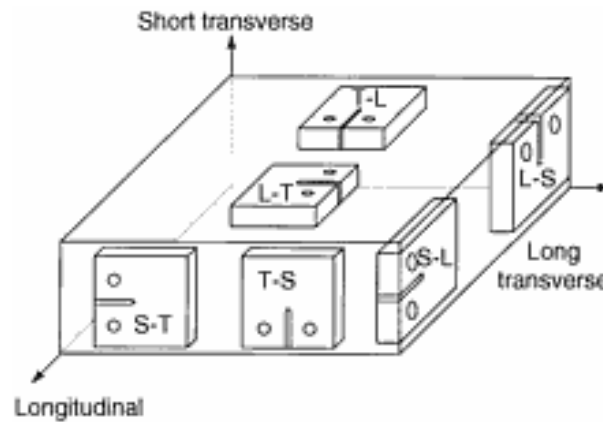
Slika 6.12. Definisani pravci uzimanja epruveta iz materijala, [169,170]

The first letter denotes the direction of the applied load; the second letter denotes the direction of crack growth. In designing for fracture toughness, consideration of anisotropy is very important, as different orientations can result in widely differing fracture-toughness values.

When the crack plane is parallel to the rolling direction, segregated impurities and intermetallics that lie in these planes represent easy fracture paths, and the toughness is low. When the crack plane is perpendicular to these weak planes, decohesion and crack tip blunting or stress reduction occur, effectively toughening the material. On the other hand, when the crack plane is parallel to the plane of these defects, toughness is reduced because the crack can propagate very easily.

6.2.2. Determination of biomaterials fracture parameters with standard specimens

A typical semi-product alloys MP35N is the rod (largest diameter of 38.1 mm), obtained by cold-drawn, which is then, if necessary, subjected to heat treatment (aging) to a maximum strength, [79].

Dimension limitations of available samples, anisotropy and two different states of materials (cold-deformed and aged - CDA or just cold deformed - CD) were significantly compounded the determination of fracture toughness of this alloy

Fracture toughness was measured in two directions, L-T i T-T, Fig. 6.13., which required different forms of a tube, DC (T) for T-T and C (T) L-T. The method of sampling is schematically shown in Fig. 6.13., where due to limited quantities of materials T-L specimens are not been made and tested.
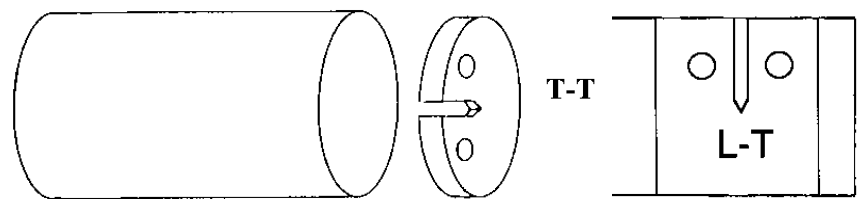
Figure 6.13. Specimen orientation and preparation, [164]

The tubes are made by using electro erosion and fatigue cracks from 1.2 mm by using cyclic loading on the servo-hydraulic machine. In the T-T case, it is possible to achieve a plane strain state, as the thickness of the specimen depends directly on the length of rod. For L-T direction, a relatively small value of fracture toughness, (Table 6.1.) has enabled the use of C (T) specimens, [164].

Table 6.1. Minimum thickness for plane strain state, [164]

orientation	state	K_{Ic} (MPa√m)	σ_Y (MPa)	min. thickness (mm)
L-T	CD	128	1440	19,1
L-T	CDA	98	1790	7,5

During the specimen preparation there has been irregularly fatigue crack growth that has occurred in CDA samples; an angle, the more cracks, Fig. 6.14. This problem is solved by making a fatigue crack before aging, and not afterwards.
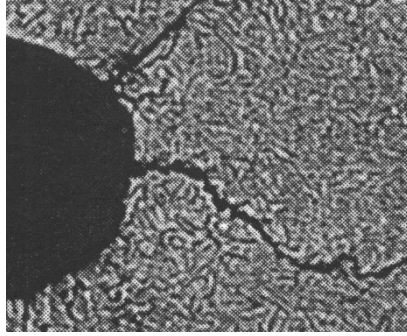
Figure 6.14. Irregular fatigue crack growth, [164]

In this thesis, the issue of measuring K_{Ic} in high toughness materials was addressed with limited cross-sectional dimensions, in L-T direction. We have modified the standard compact tension specimen (CTS) geometry to allow us to measure K_{Ic} of commercially drawn MP35N in both the unaged and the aged conditions. Since this involved a significant modification of the specimen geometry, we validated the modified test procedure by two different ways:

- By measuring K_{Ic} value for another material using the modified specimen geometry and comparing the results with the value measured on the standard specimen geometry.
- By evaluating K_{Ic} value of MP35N through J_{Ic} value, obtained by standard procedure, [R] [15] for J integral testing.

6.2.2.1. The test procedure

In our efforts to overcome some of the limitations in measuring K_{Ic} of commercially cold-drawn MP35N, we had to modify specimen geometry recommended by ASTM standard, [169,170]. For the reported yield strength and fracture toughness of the commercially drawn MP35N the minimum specimen size and configuration requirements according to the ASTM E399 are shown in Figure 6.15.
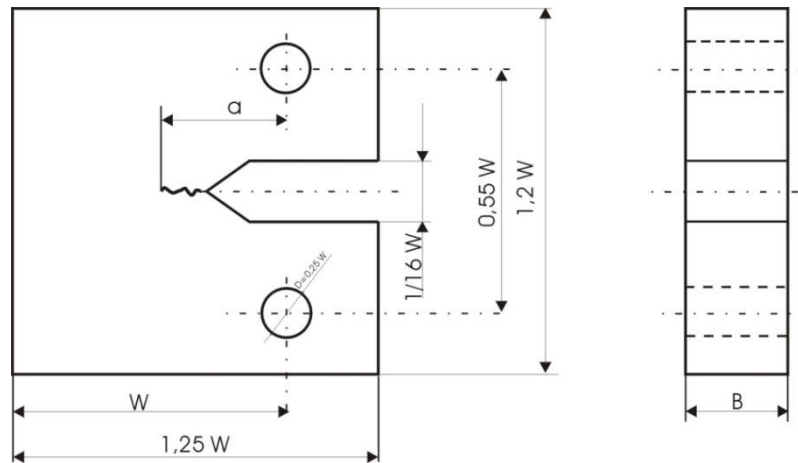
Figure 6.15. Compact tension specimen, [169]

It was impossible to obtain such a specimen from the available MP35N bar with 38.1 mm diameter for both CT and 3-point bend specimens. The proposed new specimen design is based on the standard ASTM compact tension specimen shape and geometry, and meets the criterion of small-scale yielding and plane strain conditions. All MP35N specimens described in this study were produced by Electric Discharge Machining (EDM).

Except for the specimen geometry, we followed all other procedures recommended by ASTM standard: a fatigue crack was initiated at the notch root (in a servo-hydraulic MTS machine), and the specimen was pulled to fracture (in a screw-driven Instron testing machine). The load-crack opening displacement curve was recorded, and the stress intensity at crack propagation (K_Q) was estimated using the 95% secant line.

Second procedure is based on the fact that K_{JIc} values, obtained by standard procedure for J integral testing, match standard K_{Ic} values.

A guess of the expected value of K_{Ic} (128 MPa$\sqrt{m}$) and the known yield strength value (σ_y=1440 MPa) for the unaged alloy were used to estimate the required thickness, $B=2.5 \cdot (K_{Ic}/\sigma_y)^2$=19.1 mm.

A sharp crack was introduced at the notch root by standard fatigue procedure with at least 15,000 cycles, producing crack initial length in the range of a_0=28.2-28.5 mm (a_0/W=0.55-0.56). This was performed for both aged and unaged samples while the specimens were in the unaged conditions. The specimens to be tested in the aged condition were subsequently aged in the standard way for 4 hours at 600°C. This eliminated the problem of irregular fatigue crack, obtained typically with pre-aged specimens.

The standard elastic-plastic testing of J integral and evaluation of K_{Ic} through J_{Ic} values, was performed using CT specimens, with thickness B=8 mm, and width W=25 mm, made of both aged and unaged samples.

One test was also carried out on Charpy (10x10x55 mm) pre-cracked specimen in unaged condition. Cracks were introduced by fatigue on MTS machine, which was also used for testing, according to ASTM E1820 standard procedure. All J integral tests were done at L-T orientation.

6.2.2.2. The KIc testing of MP35N with CT specimen

The plots of tensile load P versus crack opening displacement (COD), δ, are shown in Figure 6.16.

The K_{Ic} value was computed using the following formula:

$$K_{Ic}=P_Q \cdot f(a/W)/B\sqrt{W} \tag{6.12}$$

where f(a/W) stands for the geometry correction factor.

Using the average value of the crack length (a_0), measured in at least three locations, at ¼, ½, and ¾ of the thickness (B) and the critical load (P_Q), the critical value of the stress intensity was computed. Validity of test was checked using the formulas (1)-(2) and:

$$P_m/P_Q \leq 1.1; \qquad\qquad\qquad (6.13)$$

where P_m stands for the maximum load.

For the as-drawn unaged conditions (a=28.2 mm; B=19.0 mm, W=50.8 mm, P_m= 50.9 kN, P_Q=46.3 kN, K_{Ic}=124 MPa√m, σ_Y=1440 MPa):

P_m/P_Q=1.1;

W-a=22.6 mm;

$2.5(K_{Ic}/\sigma_y)^2$=19.1 mm;

so the standard conditions were satisfied.

For the as-drawn and aged conditions (a=28.5 mm; B=19.0 mm, W=50.8 mm, P_m=35.2 kN, P_Q=32.7 kN, K_{Ic}=98 MPa√m, σ_Y=1792 MPa):

P_m/P_Q=1.08;

W-a=22.3 mm;

$2.5(K_{Ic}/\sigma_y)^2$=7.5 mm;

so the standard conditions were also satisfied.
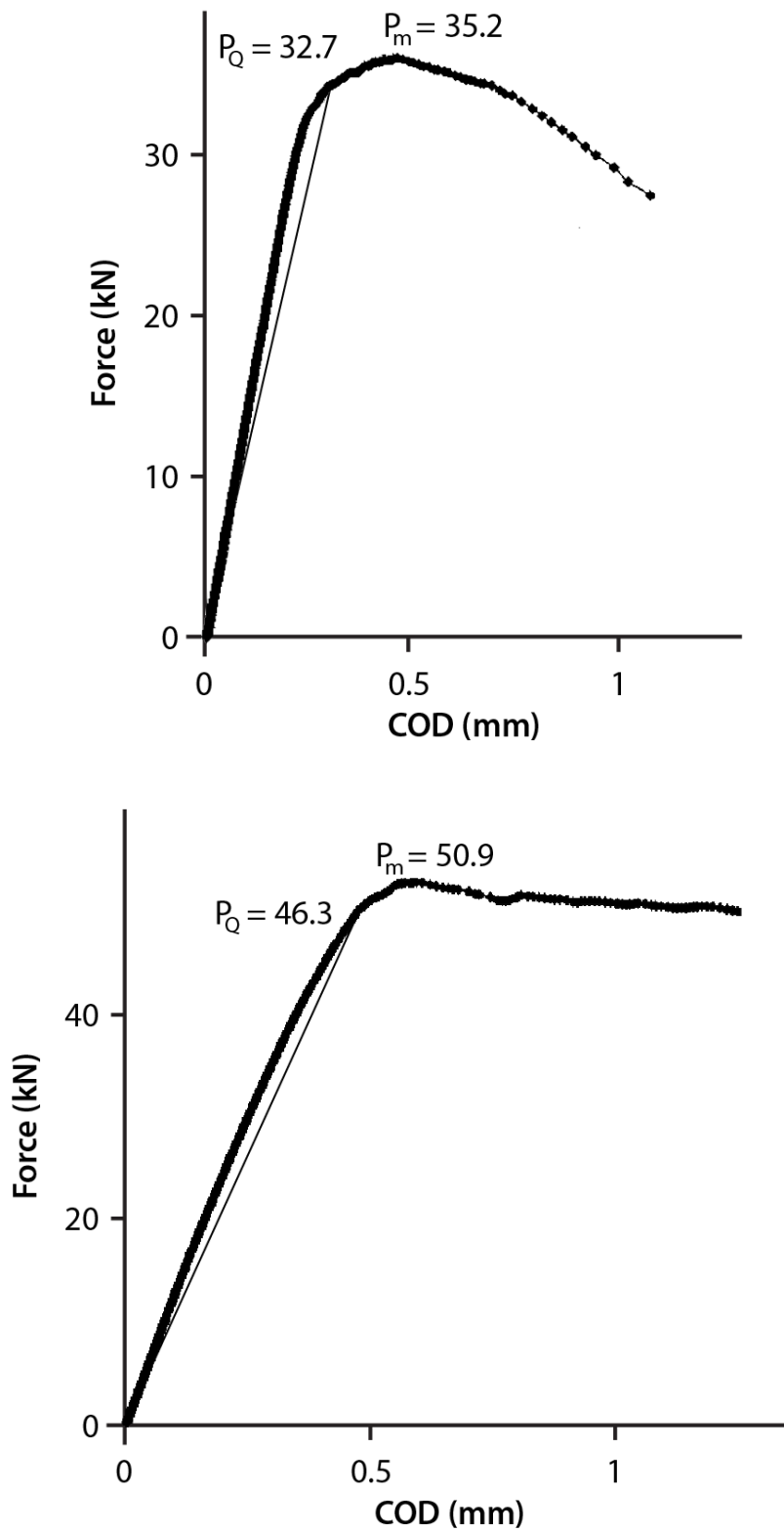
Figure 6.16. Load vs. COD a) as drawn MP35N; b) as drawn and aged MP35N.

6.2.2.3. The JIc testing of MP35N with standard specimen

The J_{Ic} values are obtained according to ASTM E1820 procedure and used to evaluate K_{JIc} by using the relation:

$$K_{JIc}=\sqrt{J_{Ic} \cdot E/(1-v^2)} \tag{6.14}$$

The results for K_{JIc} are given in Table 6.2. for CT specimens and in Table 6.3. for Charpy pre-cracked specimen.

Table 6.2. The measured K_{JIc} values for MP35N CT specimens (B=8.0 mm, W=25 mm)

Condition	Crack length a_0 (mm)	Yield strength σ_y (MPa)	Fracture toughness J_{Ic} (kPa·m)	Fracture toughness K_{JIc} (MPa√m)
as-drawn and unaged	12.1	1440	78.4-98.7	137-151
as-drawn and aged	12.4	1790	54.4-56.6	115-117

Table 6.3. The measured K_{JIc} values for MP35N pre-cracked Charpy specimen (B=10.0 mm, W=10 mm)

Condition	Crack length a_0 (mm)	Yield strength σ_y (MPa)	Fracture toughness J_{Ic} (kPa·m)	Fracture toughness K_{JIc} (MPa√m)
as-drawn and unaged	5.3	1440	98.4	157

Elastic-plastic fracture mechanics parameters are tested using three point bending specimen, and results are given as J-Δa static curve in graphical form, in Table 6.4. and Fig. 6.17.

Table 6.4. Data for J-R curve evaluation

unloading	Force F		Load line displacement		Slope at unloading	Crack enlogation (per step)	Crack enlogation (total)	Crack length ratio	Area	J integral
	Fmax	Fmin	max	min	tgα	Δa	Δa	a /W	A	
	(N)	*(N)*	*(mm)*	*(mm)*		*(mm)*	*(mm)*		*(Nm)*	*(kJ/m)*
1	8850	6250	0,365	0,320	57778	0	0,000	0,545	0,808	22,07
2	13050	9600	0,46	0,4	57500	0,024	0,024	0,547	1,040	66,91
3	15450	13200	0,535	0,495	56250	0,111	0,136	0,559	1,069	114,07
4	14850	12100	0,610	0,560	55000	0,115	0,250	0,570	1,136	166,10
5	11600	9700	0,665	0,630	54286	0,067	0,317	0,577	0,727	199,08
6	8550	6450	0,75	0,71	52500	0,171	0,488	0,594	0,856	239,96
7	6250	4200	0,87	0,83	51250	0,124	0,612	0,606	0,888	279,37
8	4750	3350	0,99	0,96	46667	0,497	1,109	0,656	0,660	315,56
9	2900	1550	1,13	1,1	45000	0,194	1,304	0,675	0,536	343,85
10	2300	650	1,32	1,28	41250	0,463	1,767	0,722	0,494	471,43
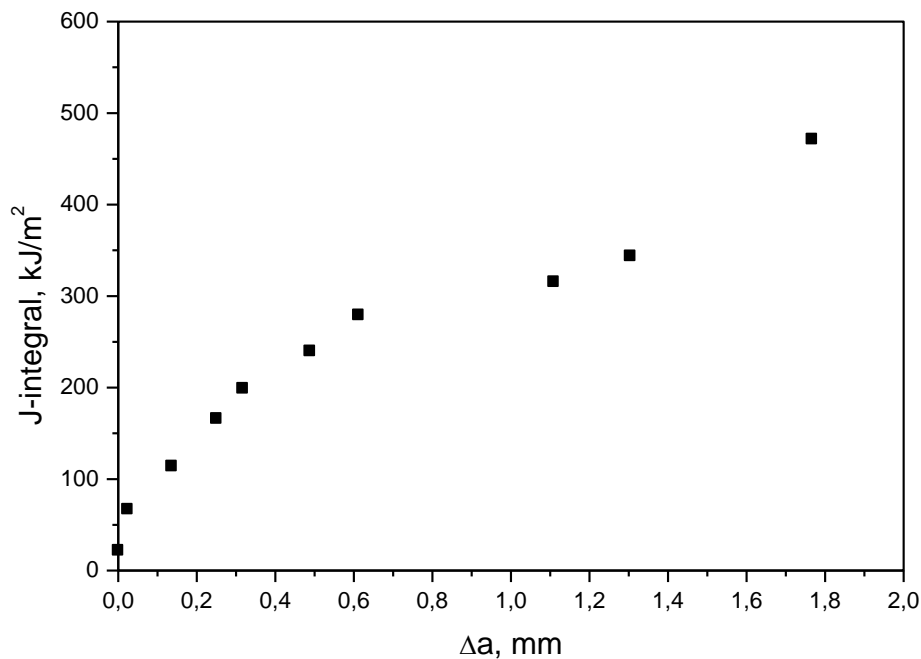
Figure 6.17. J-R curve.

6.2.3. Determination of biomaterials fracture parameters by using the final strength zone

In previous studies anisotropy effects were taken into account with different specimen orientation (T-T, L-T and T-L), [172,173]. In this analyses all experiments were performed in L-T direction. The standard static fracture mechanics testing was performed in order to evaluate a resistance of the aged and un-aged MP35N alloy to the stable crack growth and to investigate the influence of crack orientation. For MP35N fracture behaviour analysis, beside the standard 3 - point bending bars 10 mm width, as-drawn and un-aged state specimens, Charpy specimens without pre-crack were examined as well. Load-displacement diagrams were created, and J-R curve and J_{Ic} value obtained from them, [171].

In set of experiments done for this study the main purpose was to evaluate stretch zone width for MP35N alloy. For that purpose, SEM microphotographs of fracture surface for three specimens were captured.

For the sample without pre-crack it was not possible to observe stretch zone. For standard 3PB specimens it was possible to measure stretch zone widths. During each measuring procedure, SEM magnification must be such that both start and end of the final stretch zone are visible. In order to obtain a "local" critical stretch zone width, at least five measurements are necessary at each point.

Figure 6.18. shows fracture surface of specimen 01 exposed to dynamic load condition at relatively small magnification. Change of fracture surface microstructure from pre-notch toward the zone of stable crack propagation is shown at detail images.
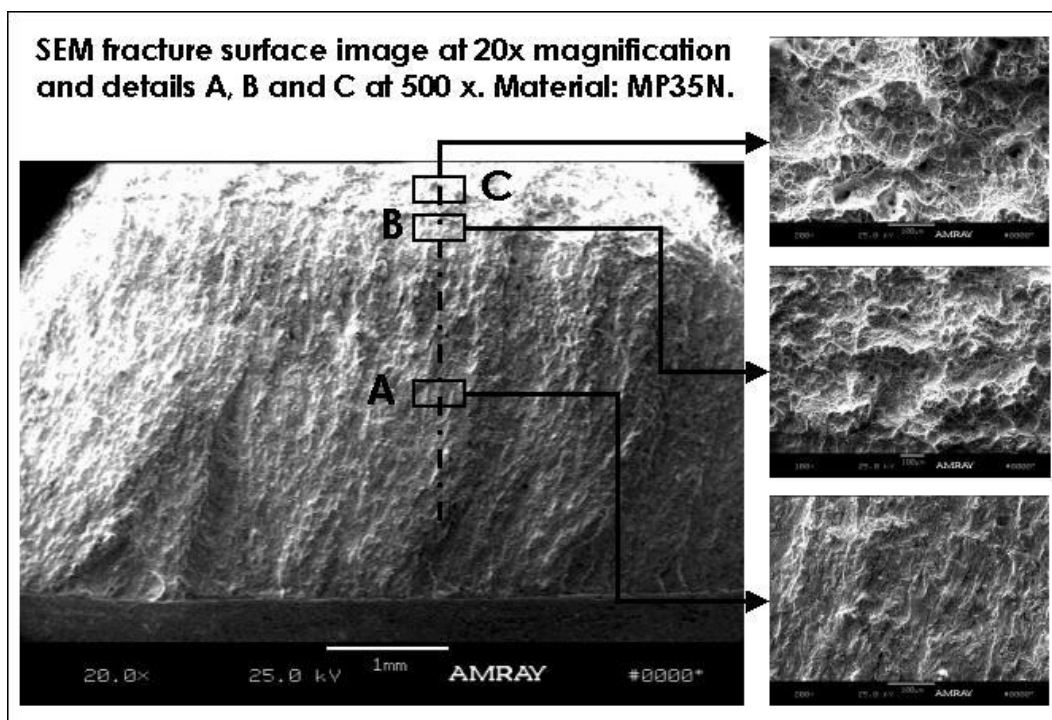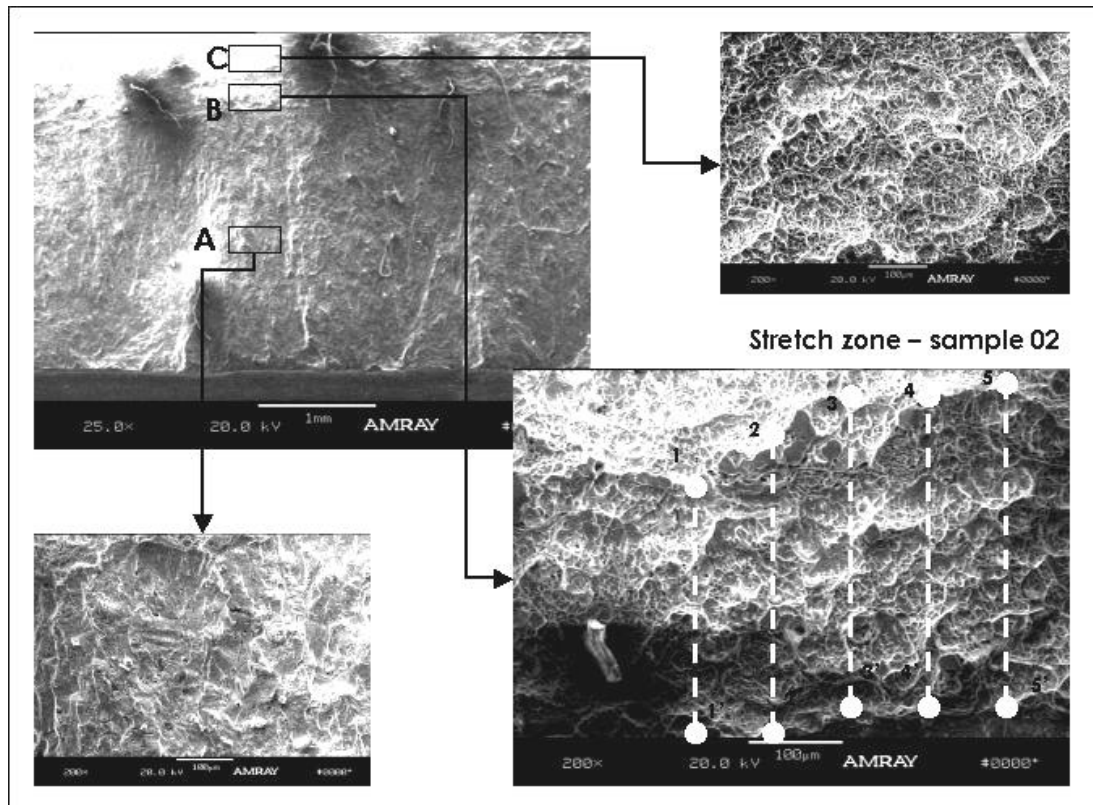

Figure 6.18. SEM image of fracture surface of 3 - point bending bar (MP35N): A – Fatigue crack, B – Stretch zone and C – Stable crack propagation.

Microstructure of stretch zone suggests that mixed loading conditions (elastic-plastic) are predominant around the crack tip at the stage of crack propagation. An inclusion at the beginning of the stretch zone is shown at Figure 6.19. (for the same test sample as in previous figure).
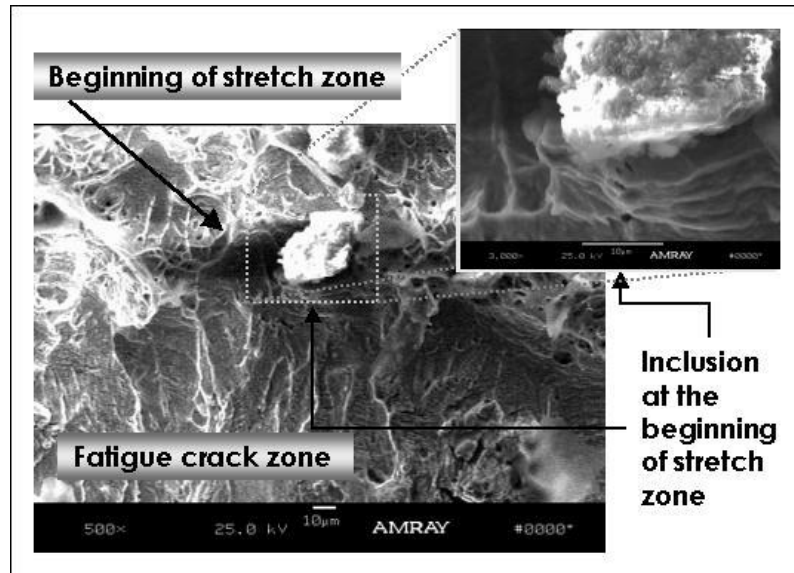
Figure 6.19. Stretch zone beginning.

Results for sample 2 is shown on Figure 6.20. One can notice equiaxed dimples in zone of stable crack propagation (Figure 6.20.b), which is usual way of microvoid coalescence when uniaxial load conditions are applied, but not for bending. Elongated dimples can be observed at sample 02 microphotographs.

From detail B one can measure 1-1', 2-2' … 5-5' distances and calculate the average SZW_L as:

$$SZW_L = \sum_{i=1}^{m} \frac{SZW_i}{m} \tag{6.15.}$$

where: m=5-10 and

SWZi is instantaneous value of SZW, i.e. equal to $\overline{11'}$, $\overline{22'}$, $\overline{33'}$ etc. (according to Figure 6.20.-B).

Measured values for sample 02 are shown in Table 6.5.

Table 6.5. SWZ$_i$ values according to Figure 6.20-B.

Section	1-1'	2-2'	3-3'	4-4'	5-5'	Average
SZW$_i$ [μm]	269	315	331	331	346	318

Figure 6.20. SEM image of fracture surface for 3-point bending bar for MP35N, test sample 02: A – Fatigue crack, B – Stretch zone and C – Stable crack propagation.

Average SZW is found to be 318μm. This parameter can be compared with the value of J integral during the stable crack growth initiation J$_i$, as shown in Figure 6.10.

Elastic-plastic fracture mechanics parameters were tested in three point bending specimen, and results are given as J- R curve in graphical form, as shown in Figure 6.17.

The obtained J_i value is 150 N/mm. The corresponding value for FSW is 220 μm, being cca. 70% of average measured value (318 μm, Table 6.5.). Also, if one uses 318 μm and obtains J_i cca. 200 N/mm from Fig. 6.17., the difference is still at the same level. Anyhow, having in mind the difference between J_i and J_{IC}, this is an acceptable error in predicting critical elasto-plastic fracture mechanics parameters.

CHAPTER 7

7.1 Numerical calculation of selected hip implant models

In case of area of orthopedy, there was always a significant interest in defining of acting stresses and loads. However, mathematical tools which were available for stress analysis in clasic mechanics were not suitable for calculations of extremely irregular structural characteristics of bones and implants. Thus the use of FEM represented a logical step due to its unique ability to determine the stress state of complex structures, loads and material behavior.

Even though it is approximative, this method is rather common in biomedicine, since obtaining the exact solution is not possible due to complex geometry, material properties and specificity of boundary conditions. Due to this, finite element method (FEM) became a widely used tool in orthopedic biomechanics, as a computational method suitable for determining of stresses and strain in any given point within a structure with arbitrary geometry and material complexity.

In order to describe real engineering problems which are used in numerical analysis, often a great number of equations is needed, hence topday FEM is mostly applied in form of software packages, such as ABAQUS (ABAQUS 6.5, Hibbit, Karlsson e Sorensen, Inc., Pawtucker, RI), which was used for numerical analysis in these thesis.

7.2 Selection of hip implant model

In accordance with hypotheses, and goals set during thesis development, numerical models were made of a hip prosthetic, in order to analyse material

behaviour of an implant during load in an ideal case, and also when there is a crack in the material. In this sense, simplifications of problems related to implanting of the prosthetic were performed in order to fulfil the requirements in terms of size. In a realistic case, there are many factors that influence the integrity of the prosthetic, such as state of bones, effects of corrosion and biocompatibility, but it is not possible to simulate all of these effects, since they depend on individual cases as well.[9] Numerical models were made with the purpose of simulating and analyzing the behavior of hip prosthetic, hence necessary approximations were performed in order to obtain the required results and to verify the model as accurately as possible.

For FEM analysis, performed in commercial software ABAQUS three-dimensional models of the prosthetic and stem were made based on real prosthetic components. Three types of prosthetic geometries were selected, wherein model 1 (Fig. 7.1.) and model 2 (Fig. 7.2.) are an integrated prosthetic type, i.e. acetabulum and stem are connected; and model 3 (Fig. 7.3.) represents a modular type, hence it is possible to represent the model using stem only. Shown in figure 7.4. is the acetabular component of a modular prosthetics.

Figure 7.1. Hip implant model 1

Figure 7.2. Hip implant model 2

Figure 7.3. Hip implant model 3 – prosthetic stem

Figure 7.4. Hip implant model 3 – prosthetic cup

Selected models were made of CoCrMo alloy, whose properties are given in tables 7.1 and 7.2 (Source: American Society for Testing and Mateirals (ASTM), 1992, F75-87, p42; F90-87, p47; F562-84, p150).

Table 7.1. Chemical composition

Element	Minimum	Maximum
Cr	27.0	30.0
Mo	5.0	7.0
Ni	--	2.5
Fe	--	0.75
C	--	0.35
Si	--	1.00
Mn	--	1.00
Co		

Table 7.2. Mechanical properties

Properties	CoCrMo
Tensile strength	655
Yield point (0.2 %), MPa	450
Elongation, %	8
Reduction area, %	8
Fracture point, MPa*	310

7.2.1. Loads on hip implant

From the standpoint of mechanics, each living body is considered as all other material bodies which are subjected to effects of other bodies.

The hip is located laterally and in front of the gluteal region, between the iliac tip and lies on the larger trochanter of the femur. In adults, tri pelvic bones are connected into the hip bones, the acetabulum, which is a part of the hip. Hip joint is located between the femoral and acetabular pelvic component and its primary function is to provide support to body weight in static and dynamic positions. It is located between the pelvis and the upper part of the femur. It is made of the pelvic bone with its circular indentation - acetabulum, in the femur head lies, and these strutures are mutually connected by ligaments. Hip joint's most important role is maintaining of balance [119, 120]. Pain in the hip can be caused by numerous reasons including anxiety, osteoarthritis, infection, trauma and genetics.

There are two main parts: femur head and acetabulum. Ligaments provide the stability of the joint itself. Cartilage and synovial fluid make movement easier, by coating and lubricating the joint, and by absorbing impact and nourishing the cartilage. Cartilage is important for transferring load through the joint with reduced friction. Hip joint is very mobile and enables a high level of stability and movement [119, 120]. The angle of femoral torsion represents the degree of frontal projection of the femoral neck in the frontal plane relative to the femur shaft. For adults, it ranges between 10 and 15 degrees, whereas at birth it is 40 degrees.
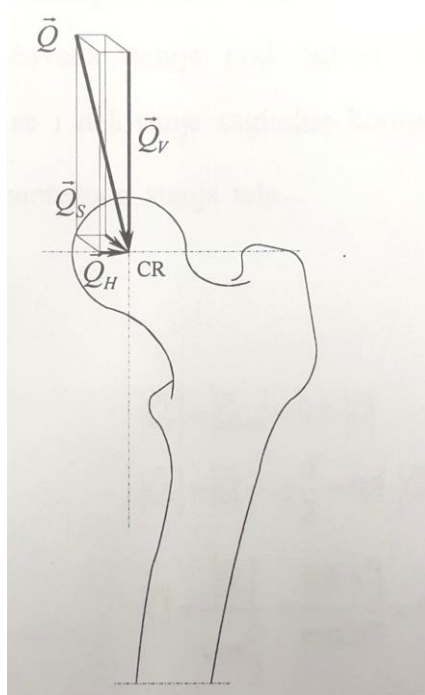
Figure 7.5. Load in hip joint. [119]
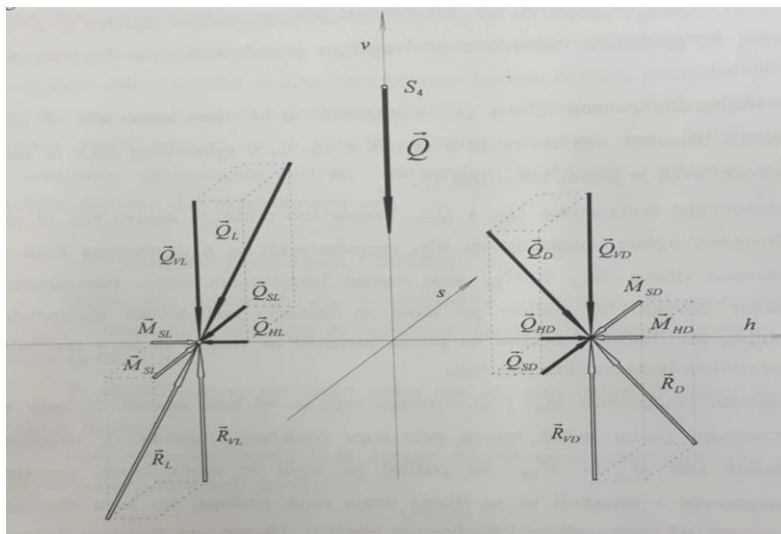
Figure 7.6. Spatial display of component forces which act in hip joints [119]

Hip forces occur due to the need to maintain balance between body weight and the tense state of abductor muscles. Force generation is affected by body weight, hip abductor muscle force (bending and straightening) and joint reaction force.

Load in the endoprosthetic is similar to the physiological load in hip joints. All loads in the acetabulum are transferred to the neck via endoprosthetic head, and then to the body of the femoral part of the endoprosthetic. Excentric load Q can be noticed, which causes significant bending in the femur neck, i.e. there are compressive presses in the cross-section, along with tension due to bending, shear and torsion [119, 120].

By comparison, the maximum forces on the knee and hip joints during different activities are shown in Table 7.3. [9,10].

Table 7.3. The maximum force on the hip joint

	The maximum force on the joint (A multiple of body weight)	
Activity	hip	knee
Walking on flat surface		
Slow	4.9	2.7
Normal	4.9	2.8
Fast	7.6	4.3
climbing the stairs	7.2	4.4
Coming down the stairs	7.1	4.4
climbing the steep surface	5.9	3.7
Coming down the steep surface	5.1	4.4

For further analysis, three types of load were selected in order to describe three ways of walking on a flat surface, normal, slow and fast walking types.

7.3 Development of numerical models

In this paper, implant models were developed in software package SolidWorks, after which they were imported into software package ABAQUS for further calculation and analysis.

SolidWorks is used for machine design and process automation, which are based on parametric modelling of solid bodies. It is also used as platform software for numerous programs.

For stress state and displacement analysis of a numerical model by finite element method, software package ABAQUS was used. It is used for modelling, analysis of mechanical components or assemblies and visualisation of analysis results obtained by finite element method. In addition, this software package has the possibility of analysing numerical models designed in another software.

7.3.1. Development of the geometric model

Prior to the analyzed structure discretization process itself, i.e. generating of the finite element mesh on the structure, it is necessary to define the geometry of the models on which numerical simulations will be performed. Software package ABAQUS has the ability to analyse numerical models made in another software, hence geometric models of implants were made in SolidWorks, and are shown in figures 7.6. - 7.9. Compared to the original models of real implant structure, certain approximations had to be introduced to the models themselves.
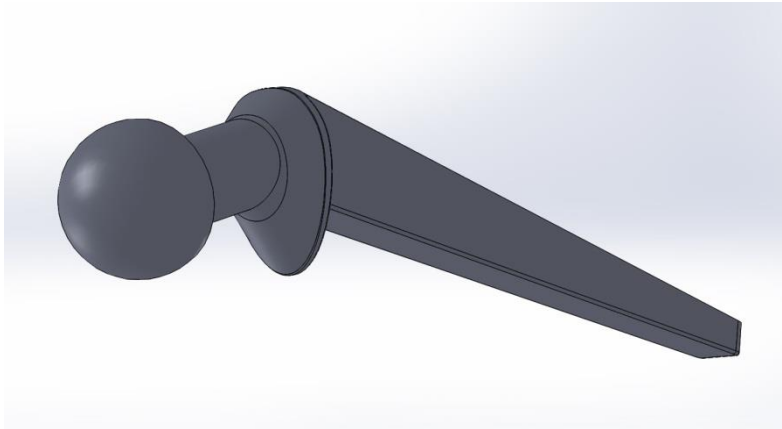
Figure 7.6. Hip implant 1 - solid model
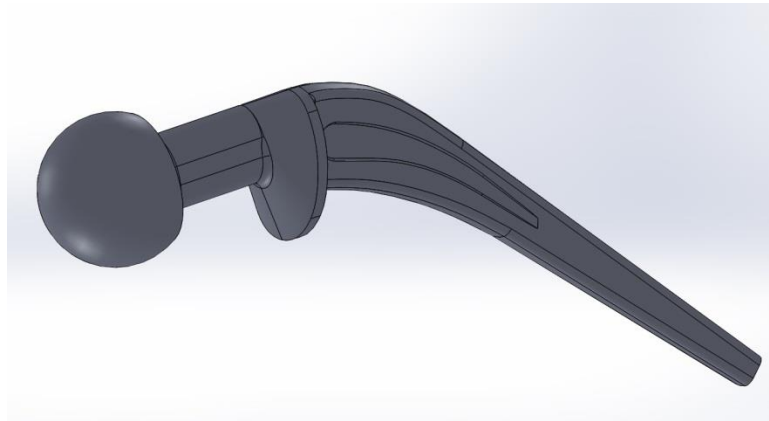
Figure 7.7. Hip implant 2 - solid model
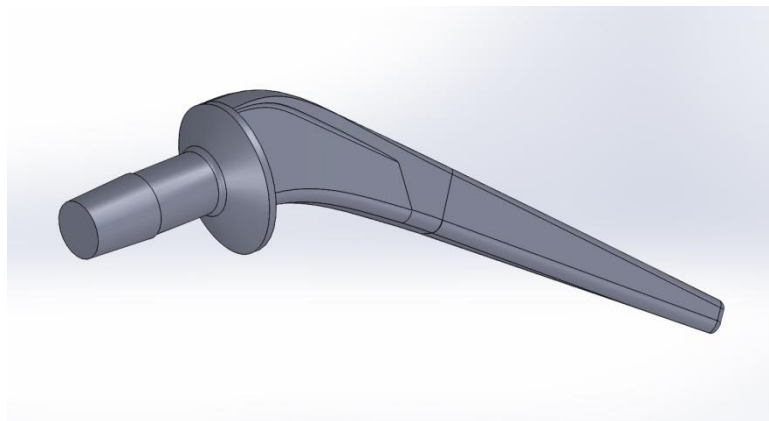
Figure 7.8. Hip implant 3 base - solid model

Figure 7.9. Hip implant 3 cup - solid model

The geometry of the stem has a significant effect on prosthetic performance. Stem with a smooth surface, generally speaking, reduces the stress concentration and enable significant fatigue resistance. Stem with a sharp or rugged surface enables good connection and prevents potential sliding of the joint. Level of stress concentration and tendency to fatigue fracture depend on the roughness of the stem surface.

Taking into account the complex geometry of the implant model which would affect mesh generation, and above all cause problems with placing of the crack in the material, it was necessary to introduce some more simplifications to the models. Additional simplification was performed on models 2 and 3 and shown in figures 7.10. - 7.12.
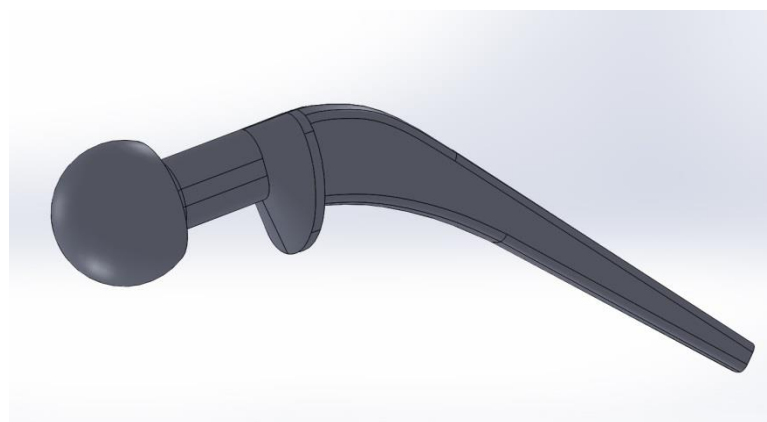
Figure 7.10. Hip implant model 2 – approximations on the solid model
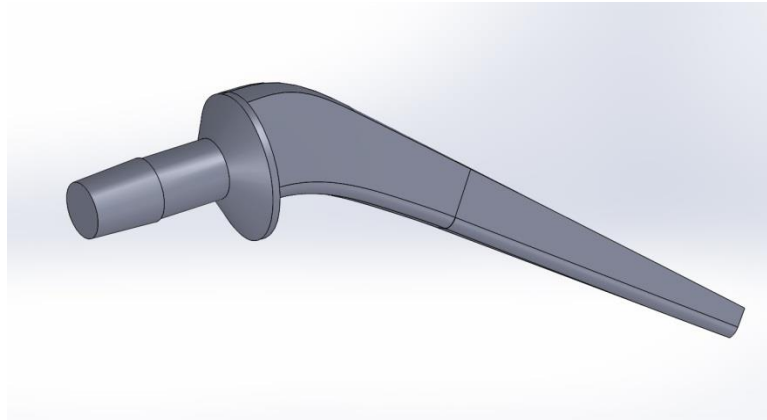
Figure 7.11. Hip implant model 3 – approximations on the solid model
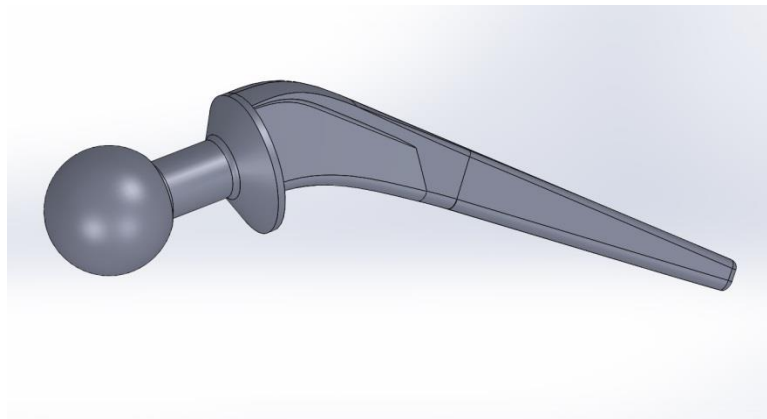
Figure 7.12. Hip implant model 3 assembly – approximation of the solid model

Dimensions of adopted geometrical models are given in the following figures, for model 1 - figure 7.13. for model 2 - figure 7.14. and for model 3 figures 7.15. and 7.16.
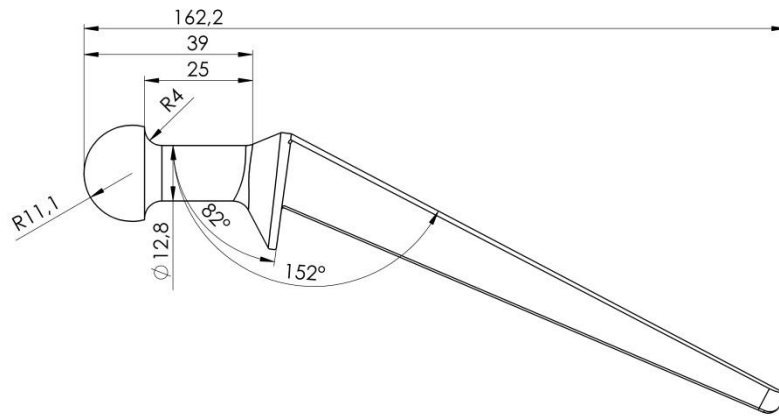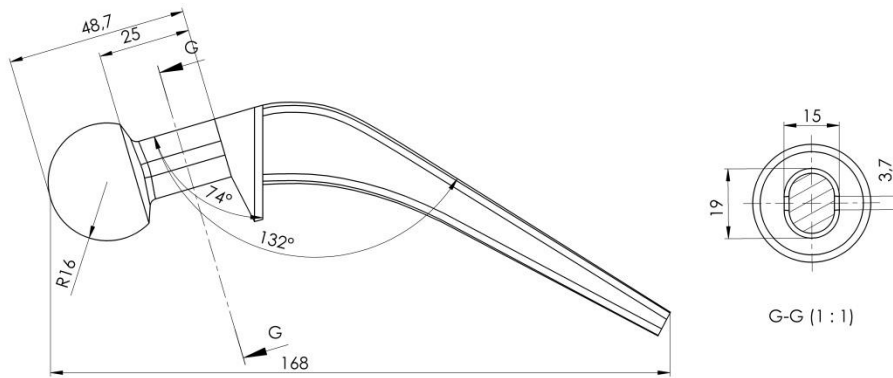
Figure 7.13. Hip implant 1 – dimensions
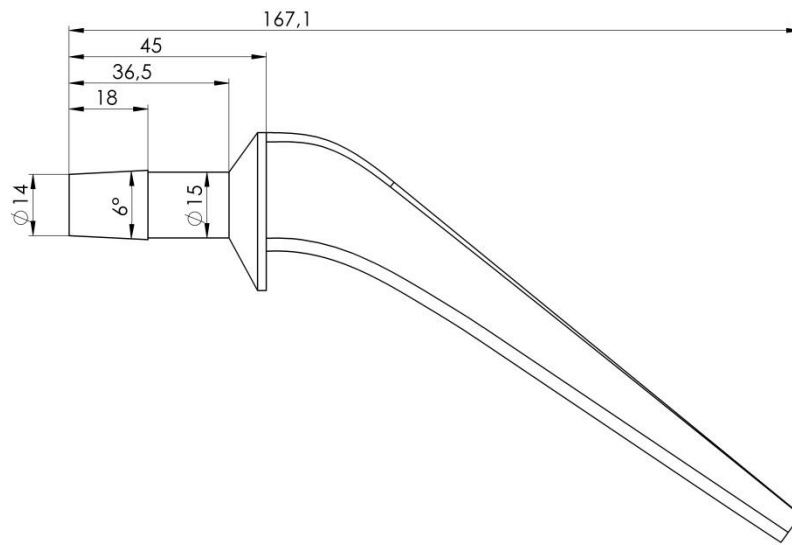

Figure 7.14. Hip implant 2 - dimensions
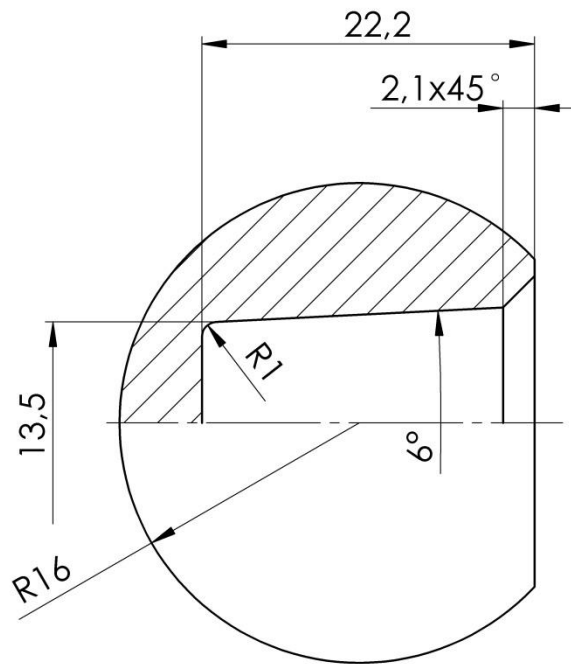
Figure 7.15. Hip implant 3 base - dimensions

Figure 7.16. Hip implant 3 cup - dimensions

A simplified alternative to the three-dimensional models is a a two-dimensional model which represents the mid-frontal plane only. Such a model is simple to develop, but does not take into account 3D behavior of implants. During the initiation of the FEM analysis, it is not recommended to immediately start developing the most complex model, but to adjust the model to the requirements of expected results. This, of course, requires the undestanding between model properties and expected results.

7.3.2. Defining of biomaterial model parameters

In a FEM model, each elements must have its corresponding elastic constants assigned to it, which are individually defined for every developed model. An isotropic linear elastic material requires two constants, i.e. the elasticity modulus and Poisson's ratio. This is the case for materials which are used in metal implants. Acrylic cement and plastic components can be included in this category only by rough approximation. Cortical bones can be considered as a linear elastic and transversely isotropic body, with reasonable amount of approximation.
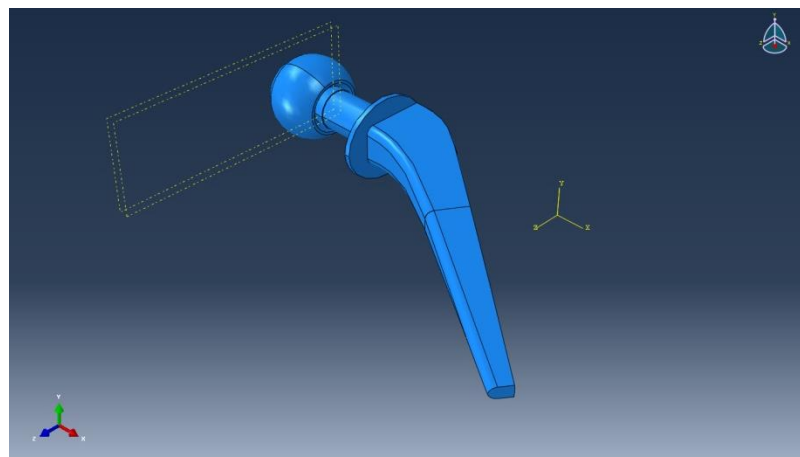

Figure 7.17. Hip implant – solid model in ABAQUS

After the geometric models are imported into a FEM analysis software, figure 7.17., it is necessary to define the material parameters for each model.

The constitutive relation which is chosen for the given problem requires the specification of two constants, Young's elasticity modulus and Poisson's ratio. Young's modulus represents the measure of material stiffness, whereas Poisson's coefficitne it the lateral contraction of a material subjected to longitudinal tension. When these coefficients are determined, it is easy do determine the mechanical behavior of an isotropic elastic material, for any strain. Values of coefficients used for this problem in all examples presented here, are given in Table 7.4.

Table 7.4. Values of coefficients used

Material	Elasticity modulus (GPa)	Poisson's ratio
CoCrMo	234	0.3

7.3.3. Establishing of boundary conditions and loads in models

FEM analysis requires a numerical description of all external loads affecting the structure (points in which they act, magnitude, direction). These loads are usually variable and are not always precisely defined, thus when using FEM analysis, a frequent question is which approach to use in order to obtain useful information. Selected prosthetic models are of the cement type, hence in a realistic case there would be a need to define real loads on the implant itself, along with the parameters of spongy bone in contact with the implant, as well as the properties of cement, so that realistic prosthetic displacement and stresses could be obtained in the bone which supports it. In addition, it would be needed to define a complex load which occurs in the hip

itself, which takes into account running, standing, sitting and falling stages, aside from walking.

In accordance with the initial hypotheses, certain approximations have been introduced regarding boundary conditions and loads of the model. Taking into account that only the behavior of metal structures is analyzed in terms of crack presence in the biomaterial, and based on the review of relevant literature in terms of the expected location of crack initiation, it was possible to introduce a fixed support approximation for the load bearing structure of the implant in the lower part which is in contact with the bone.

Real load which acts on the implant was introduced in two ways, as compressive load on prosthetic cup, i.e. a force which acts in a single point on the acetabular part of the prosthetic. Loads defined in this way actually represent an approximation of real hip implant behavior. Since real behavior acting on the hip is highest in the simulated direction, and in the first approximation of the bone-implant connection, a completely rigid connection can be assumed, thus defining of such boundary conditions in justified.

The applied approach to selecting of load is the use of representative load cases. This approach is particularly useful when there is need to study the effects of individual properties of prosthetic design by comparative analysis, or when load transfer mechanism need to be studied.

Three characteristic load types during the walking stage were selected, shown in table 7.3, for slow, normal and fast walking. In that sense, the values of the load range from minimum 4.9 TT to maximum 7.6 TT loads. For the purpose of numerical calculation, a person with a weight of 80 kg was selected, thus the expected loads on the implant were 3845.5 N, for slow and normal walking, i.e. 5964.5 N.

Taking into account the dimensions of the selected model implants, i.e. the dimensions of surfaces on which relevant forces act, compressive loads

were obtained, shown in table 7.5 for fast walking, i.e. the acting load of 5964.5 N.

Table 7.5. Hip implant models

Implant model	Area *(mm²)*	Compressive load on the implant *(MPa)*
Hip implant model 1	422	14.2
Hip implant model 2	376.6	15.8
Hip implant model 3 - base	154	38.7
Hip implant model 3 – base + cup	372	16

Shown in table 7.6. are the defined numerical models depending on the geometry and the load.

Table 7.6. Hip implant calculating models

CALCULATING MODELS	IMPLANT TYPE	ACTING LOAD
Model 1.1.	Hip implant model 1	Slow and normal walking on a flat surface
Model 1.2.	Hip implant model 1	Fast walking on a flat surface
Model 2.1.	Hip implant model 2	Slow and normal walking on a flat surface
Model 2.2.	Im Hip implant model 2	Fast walking on a flat surface

Model 3.1.	Hip implant model 3 - base	Slow and normal walking on a flat surface
Model 3.2.	Hip implant model 3 - base	Fast walking on a flat surface
Model 4.1.	Hip implant model 3 - base + cup	Slow and normal walking on a flat surface
Model 4.2.	Hip implant model 3 - base + cup	Fast walking on a flat surface

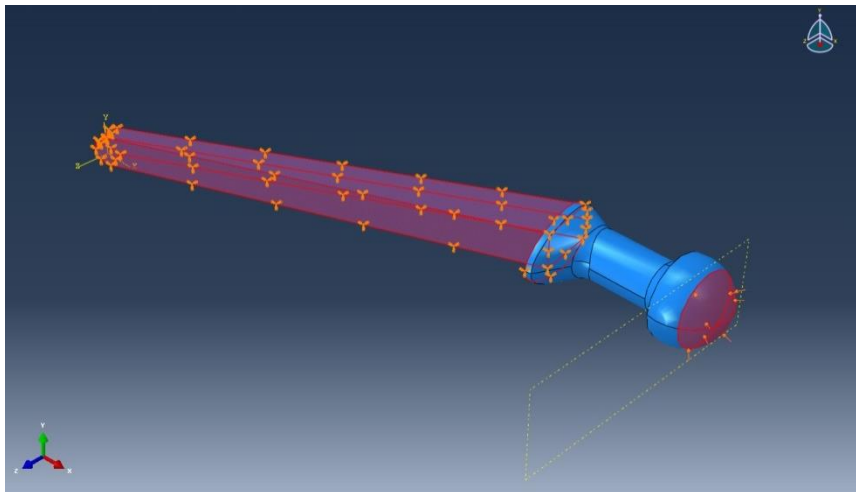After importing the implant model from SolidWorks into ABAQUS, loads and boundary conditions for each case were defined, as shown in figures 7.18. - 7.21.

Figure 7.18. Model 1 – boundary conditions and loads
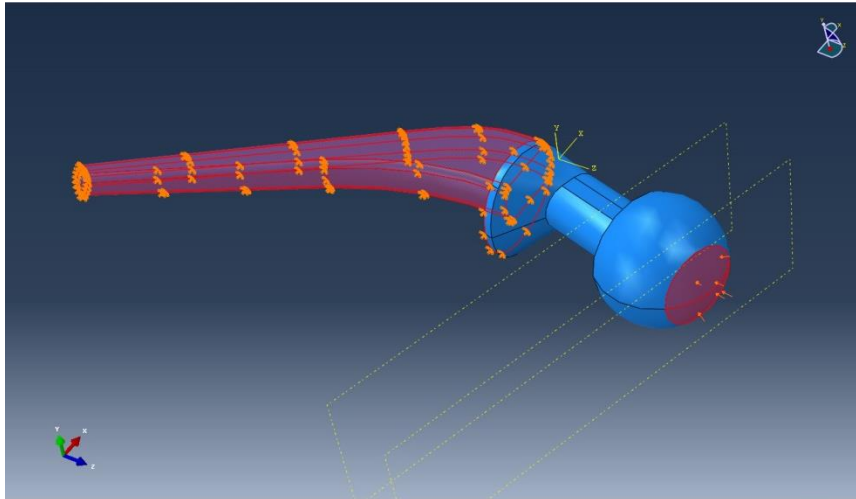
Figure 7.19. Model 2 – boundary conditions and loads
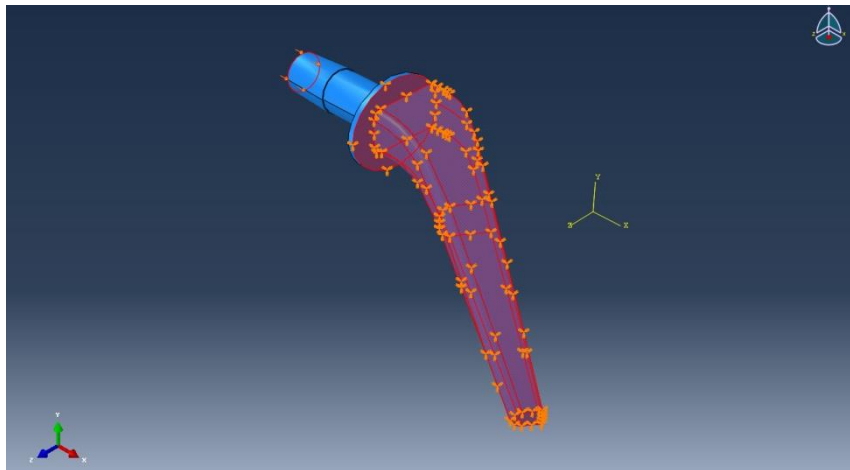
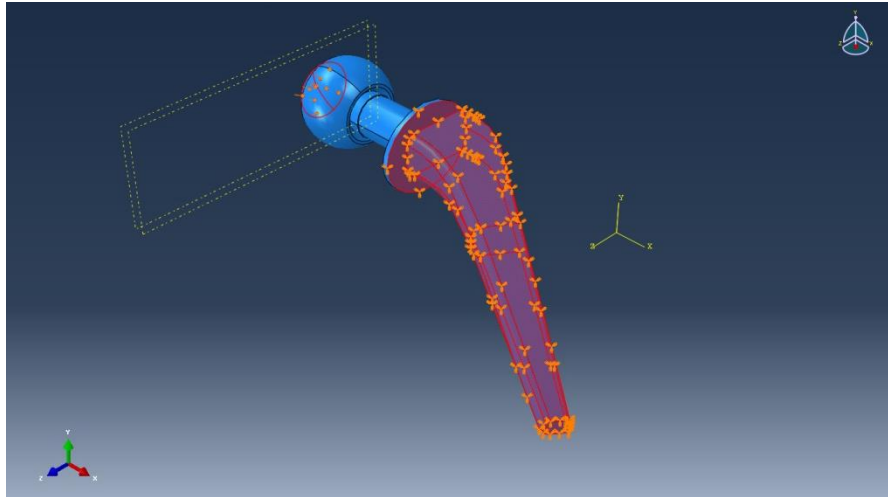*Figure 7.20. Model 3 – boundary conditions and loads*

Figure 7.21. Model 4 – boundary conditions and loads

7.3.4. Discretization of structure in numerical models

Conceptually, each detail of the structure can be represented by using sufficiently small elements, but in practice this is rarely profitable, hence the problem must be schematically described to a certain extent. Degree of structure fineness which is described by the mesh depends on the necessary information. It should be emphasized that the size of the mesh can greatly affect the accuracy of the results

A finite element mesh was generated as fine as possible, for a geometrical prosthetic model, wherein the goal was to generate high-quality mesh, selecting finer meshes wherever stress concentration was expected.

For the purpose of FEM analysis, two types of finite elements were selected, which adequately describe the behavior of complex three-dimensional structures, such as hip implants. Within the calculation, standard 3D stress elements types libraries were used, which are a part of the applied software package. Applied to all models were two types of 3D elements, an 8-node linear hex type element, with reduced integration and a 10-node tet type quadratic element.

Before the mesh was generated on solid models, it was necessary to divide each model into partitions, as shown in figures 7.22 - 7.25. in order to properly generate the FE mesh.
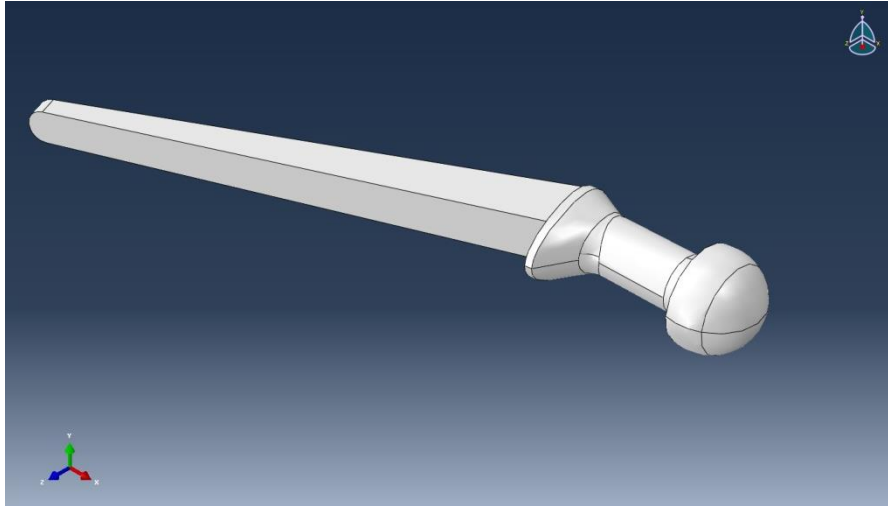

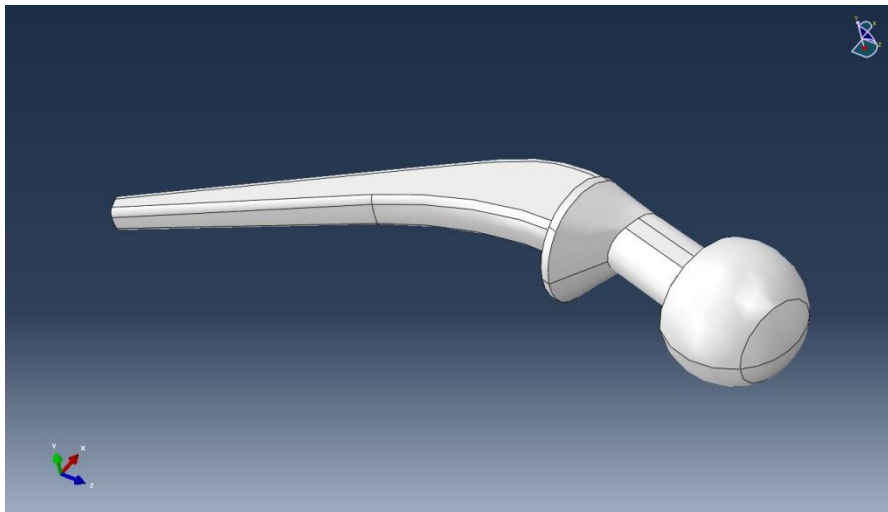*Figure 7.22. Model 1 – partitioning of the solid model*

Figure 7.23. Model 2 – partitioning of the solid model

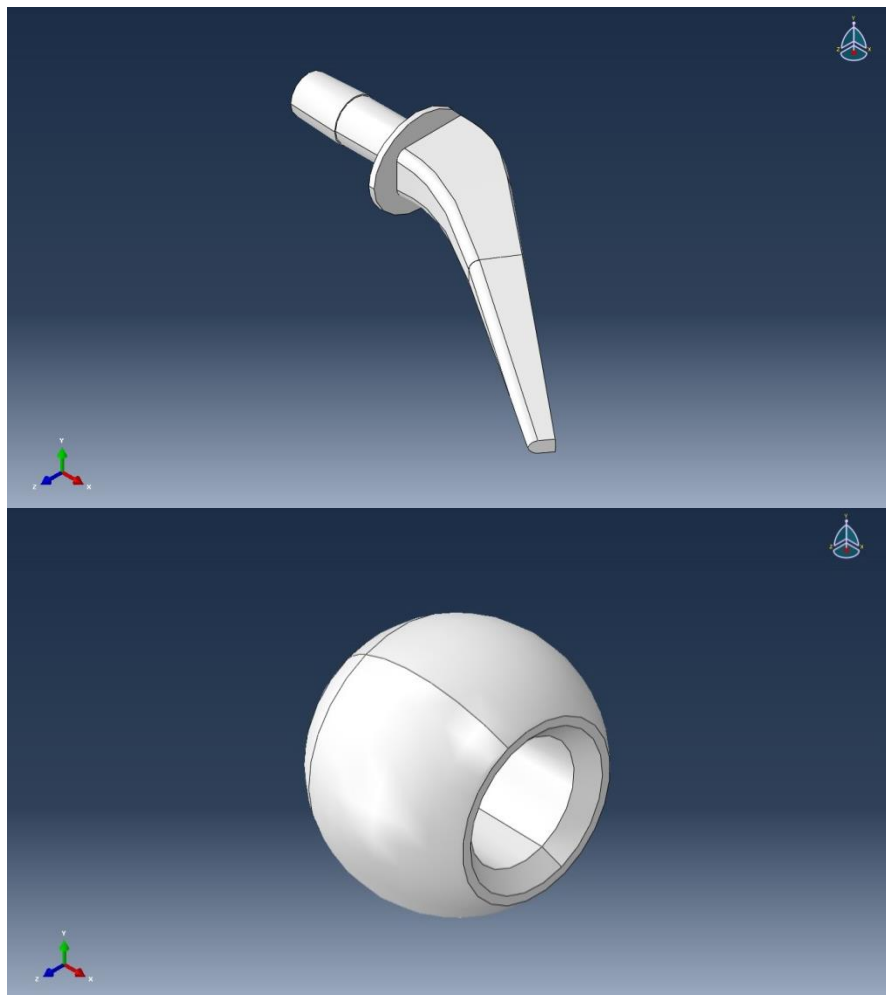*Figure 7.24. Model 3 – partitioning of the solid model*

Figure 7.25. Model 4 – partitioning of the solid model

After this, sweep and free techniques were used for mesh generation, in order to perform adequate discretization of the implant model structure. The appearance and parameters of discretization are given separately for each model in the following text.

Shown in table 7.7. are the discretization parameters for calculation model 1, which include the selected shape and number of elements and nodes.

Table 7.7. Model 1 - Discretization parameters

Model 1
Implant base:
Hexahedral type: (C3D8R) 8-node linear Reduced integration
Implant cup:
Hexahedral type: (C3D8R) 8-node linear Reduced integration *Tetrahedral type*: (C3D10) 10-node quadratic
Total number of elements: 7 253
Number of nodes: 9 708

Shown in figure 7.26 is the mesh of finite elements generated on the calculation model 1.
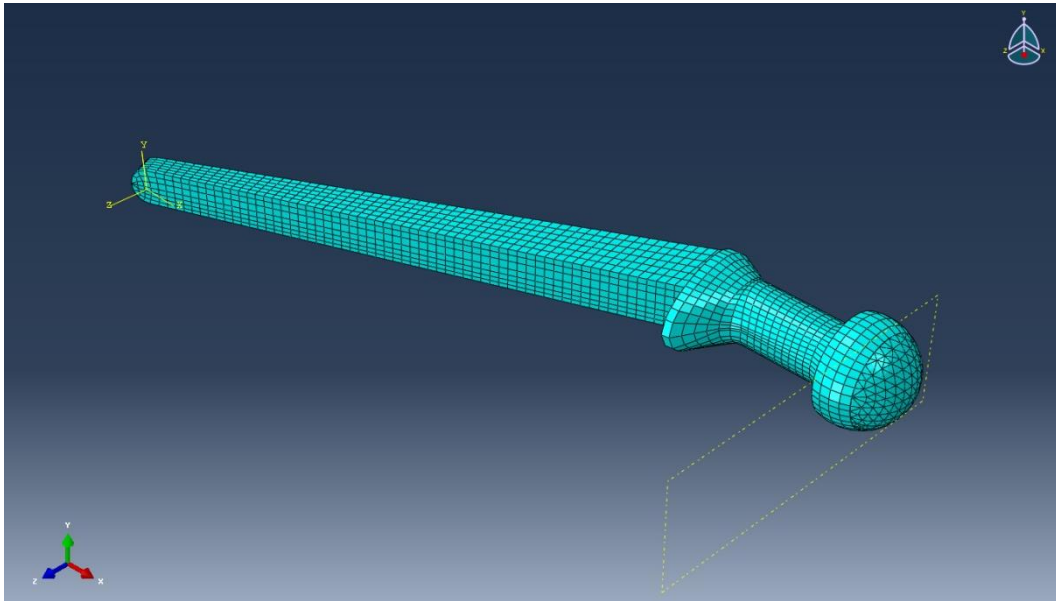

Figure 7.26 Model 1 - FE mesh

Shown in table 7.8. are the discretization parameters for calculation model 2, which include the selected shape and number of elements and nodes.

Table 7.8. Model 2 - Discretization parameters

Model 2
Implant base:
Hexahedral type: (C3D8R)
8-node linear
Reduced integration
Tetrahedral type: (C3D10)
10-node quadratic

Implant cup:
Hexahedral type: (C3D8R)
8-node linear
Reduced integration
Tetrahedral type: (C3D10)
10-node quadratic
Total number of elements: 11 510
Number of nodes: 17 191

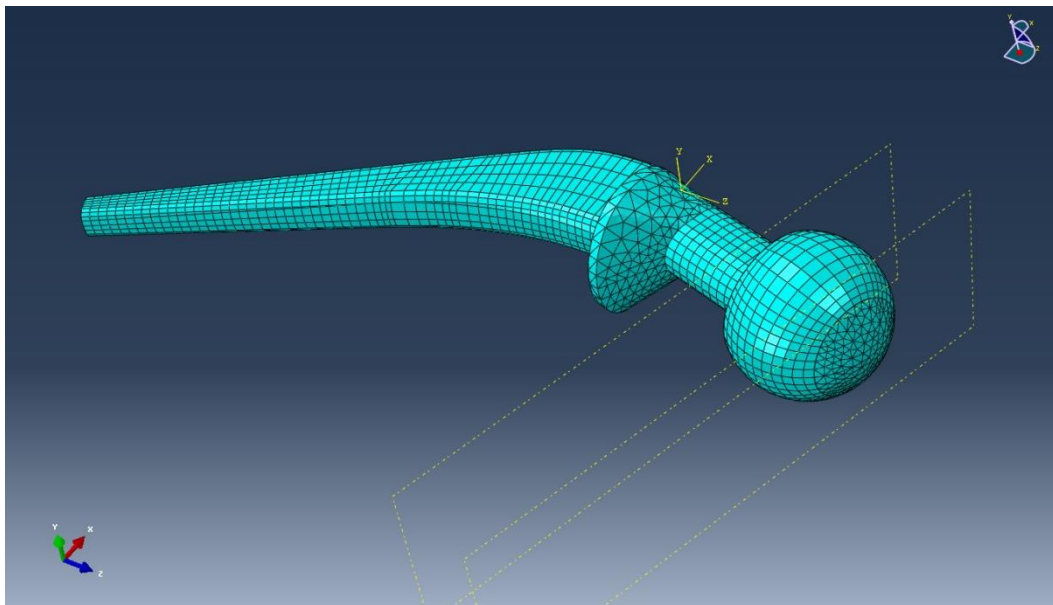Shown in figure 7.27 is the mesh of finite elements generated on the calculation model 1.

Figure 7.27. Model 2 - FE mesh

For this type of implant, it was necessary to generate a finer mesh at the transition from prosthetic stem to acetabular part of the implant, i.e. the expect

location of biomaterial damage, figure 7.28, and due to complex geometry for structural discretization, both types of finite elements were used.
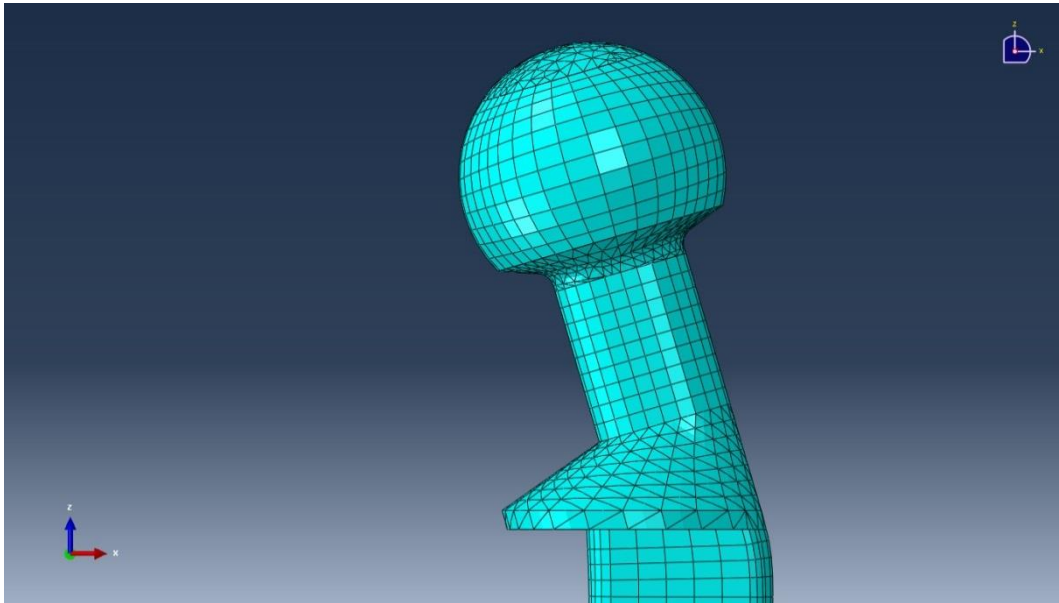

Figure 7.28. Model 2 – A detail of the FE mesh on the location where damage was expected to occur

Shown in table 7.9. are the discretization parameters for calculation model 3, which include the selected shape and number of elements and nodes.

Table 7.9. Model 3 - Discretization parameters

Model 3
Implant base:
Hexahedral type: (C3D8R)
8-node linear
Reduced integration
Tetrahedral type: (C3D10)
10-node quadratic

Total number of elements: 57 674
Number of nodes: 84 019

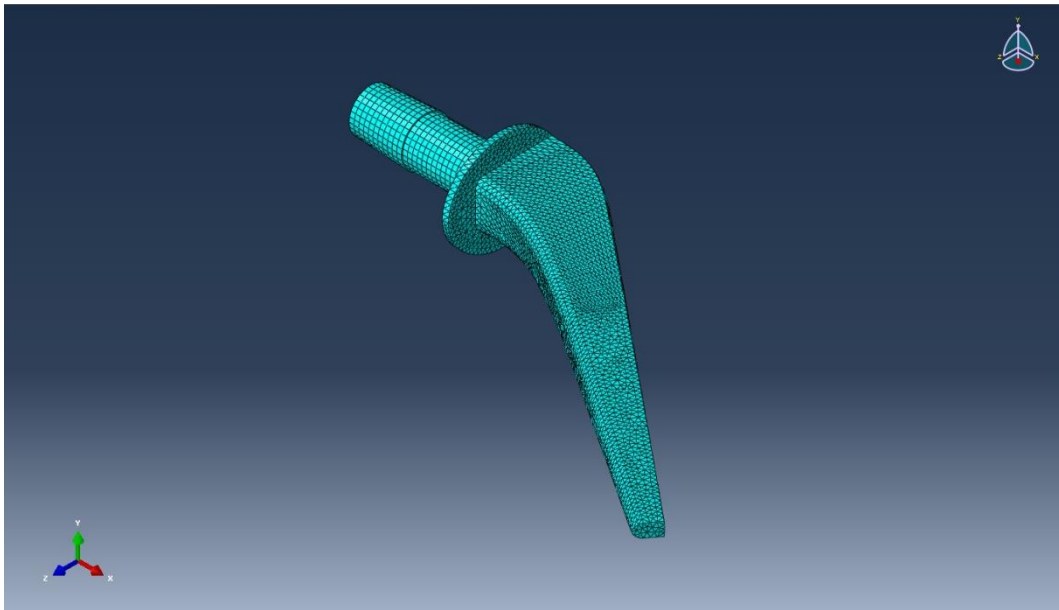Shown in figure 7.29 is the mesh of finite elements generated on the calculation model 3.

Figure 7.29. Model 3 - FE mesh

As with model 2, both types of selected finite elements were used in discretization, due to complex geometry, and the detailed view of the mesh is shown in figure 30, for the part where damage was expected.
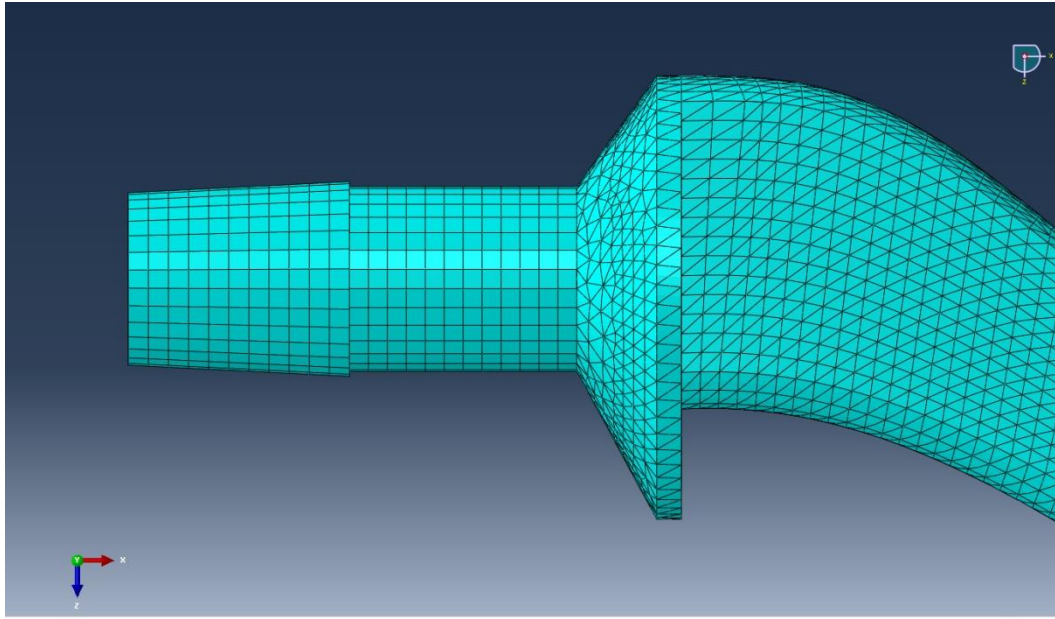
Figure 7.30. Model 3 – A detail of the FE mesh on the location where damage was expected to occur

Shown in table 7.10. are the discretization parameters for calculation model 4, which include the selected shape and number of elements and nodes.

Table 7.10. Model 4 - Discretization parameters

Model 4
Implant base:
Hexahedral type: (C3D8R)   8-node linear   Reduced integration   *Tetrahedral type*: (C3D10)   10-node quadratic
Implant cup:
• *Lower part*

Hexahedral type: (C3D8R) 8-node linear Reduced integration • *Upper part* *Tetrahedral type*: (C3D10) 10-node quadratic
Total number of elements: 62 098
Number of nodes: 91 044

As shown in table 7.10., the acetabulat prosthetic component was modeled using both types of elements, figure 7.31.
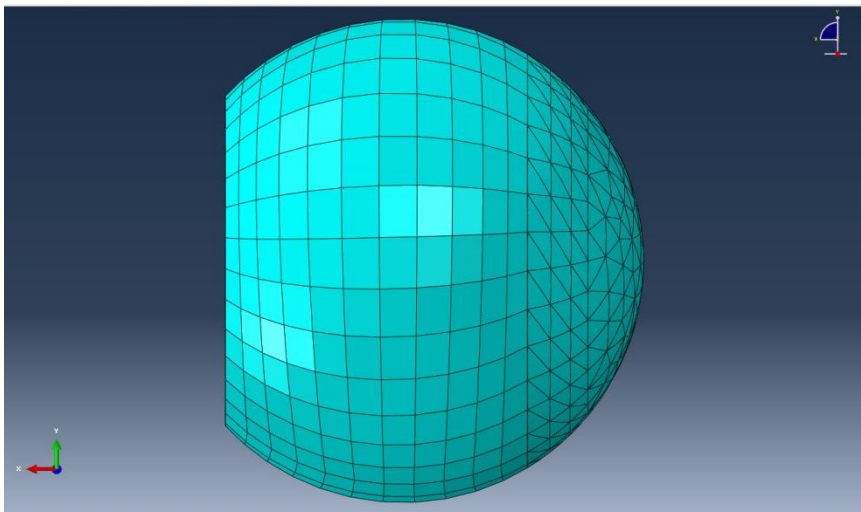

Figure 7.31. Application of hex and tet elements for the discrtization of acetabular component

Shown in figure 7.32 is the FE mesh for the calculation model 4, i.e. the assembly consisting of the base and cup of the modular hip prosthetic.
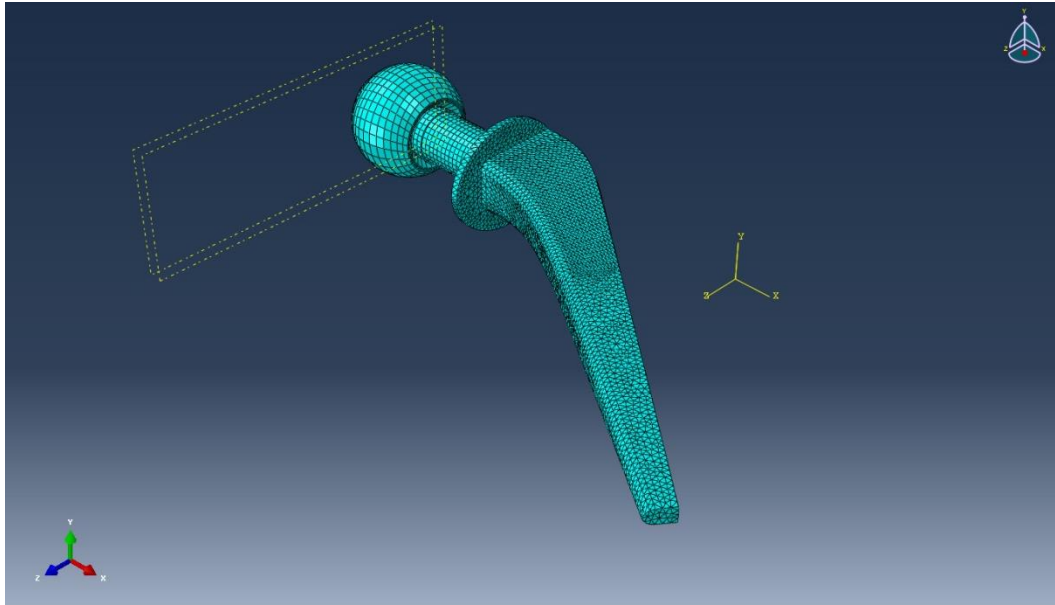
Figure 7.32. Model 4 - FE mesh of the assembly

Inner side of the cup can be considered As a critical location, where damage is expected to occur in the biomaterial in this model, since it is in constant contact with the prosthetic base, hence the discretization of this part of the model is also shown, in figure 7.33.
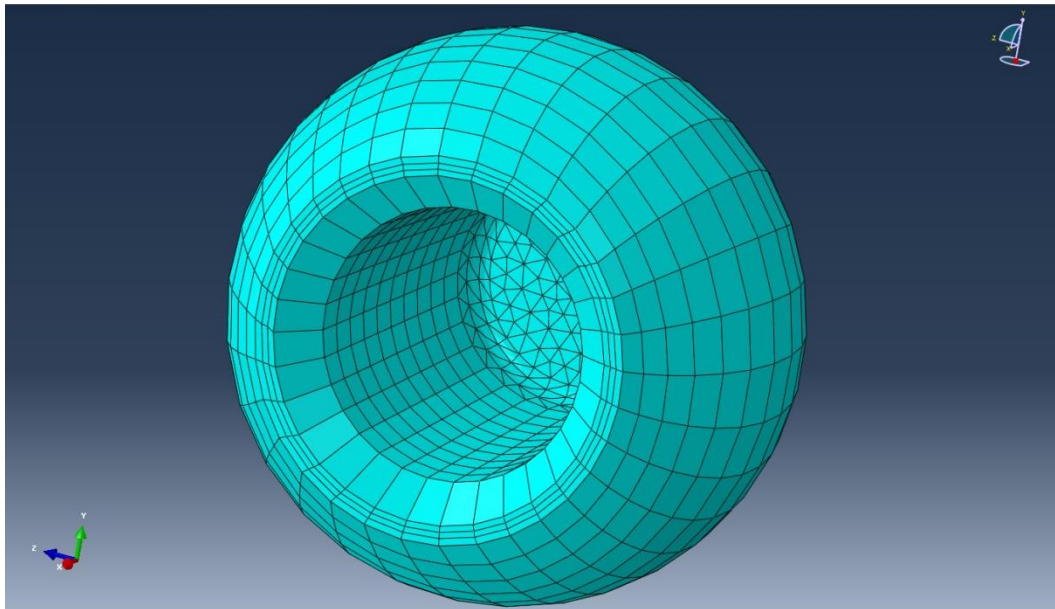

Figure 7.33. Model 4 – detailed view of the FE mesh at the contact between the cup and the base of the prosthetic.

7.4 Development of a model with a crack

It is important to observe that 3D modeling is significantly more complicated than 2D, thus reducing the problem to two dimensions is still common practice. It is necessary to emphasize that, unlike 2D problems, 3D problems require the use of commercial software with built-in elements. Commercial software packages have the possibility of simulating material behavior with a crack, by using sub-programs based on one of the above mentioned principles.[174-176] However, modeling of cracks and developing of methodologies for describing the discontinuity around the crack were the topic of numerous research in the recent years, which lead to developing of completely new calculation techniques. The most recent method which is applied to modeling of cracked material behavior is based on extended finite element method, X-FEM. [177-185]

Since X-FEM is very attractive for performing of assessment of tolerance to damage and simulation of crack growth curve on a complicated 3D geometry, multiple attempts were made to integrate X-FEM with existing FEM packages. During the problem analysis of cracked material behavior, sub-programs and software packages based on FEM were used, supported by the numerical package for FEM analysis, ABAQUS, above all others, Morfeo.

When predicting crack growth, the manner in which it will grow must be predicted, and then the mesh for a new configuration needs to be generated. Even when this is achieved, there is still a need to find a practical way to interpret the analysis results, in order to obtain sensible information about the crack configuration.

7.4.1. Application of XFEM method to crack growth simulation

In order to evaluate the influence of initial defects in material on strength and life of structures, finite element analysis is applied to cracks of various shapes, sizes and locations. In these analyses, FEM is limited, since changes in crack topology require additional generating of mesh domain. This represents a significant constraint and complicates crack growth simulation on complex geometries. Extended finite element method, X-FEM was developed in order to make calculations easier, which was required during positioning of arbitrary cracks within a finite element model.

Extended finite element method (XFEM) used enhancement functions as a means of displaying all forms of discontinuous behavior, such as crack displacement [186-189]. Enhancement functions are introduced into the displacement approximation for only a small number of finite elements, relative to the size of the whole domain. Additional degrees of freedom are introduced for all elements where the discontinuity is present, and in some cases - depending on the type of the selected function - into adjacent elements, which are then referred to as mixed elements [186-189].

Displacement approximation can be expressed in the following way, by applying enhancement functions:

$$u^h(x) = \sum_i N_i(x) \left[u_i + \sum_j v^j(x) a_i^j \right] \qquad (5.1)$$

The unity property is based on the fact that the sum of interpolation functions of finite elements equals one. Assuming that the unity property is fulfilled, additional enriching functions, i.e. improvement functions, can be given in displacement approximation. In this case, application of standard X-FEM displacement formulation approximate displacements as [186-189]:

$$u(\xi,\eta,\zeta) = \sum_i N_i(\xi,\eta,\zeta) U_i + \sum_i N_i(\xi,\eta,\zeta) H(\xi,\eta,\zeta) b_i +$$
$$\sum_i N_i(\xi,\eta,\zeta)\left(\sum_j \Psi_j(r,\theta) c_{ji}\right)$$

(7.1)

where $N_i(\xi,\eta,\zeta)$ are shape functions, $U_i \in \mathbf{R}^3$ are node displacement parameters for all nodes of a hexahedron element: 1~8, $b_i \in \mathbf{R}^3$ are parameters of jump function on jump nodes, and $c_{ji} \in \mathbf{R}^3 \times \mathbf{R}^4$ are parameters of the branching function for nodes at the crack tip. [186-189]

It is necessary during calculation to determine which mesh elements were divided by the crack and in which element the crack tip is located, taking into account that X-FEM does not approximate the entire domain. In this sense, an unequivocal identification of elements uses two functions on the level of sets (LS functions), which are based on level set (LS) method. [186-189]

Jump function H is defined as the sign of the level set φ:

$$H(\xi,\eta,\zeta) = \begin{cases} +1: \varphi(\xi,\eta,\zeta) > 0 \\ -1: \varphi(\xi,\eta,\zeta) < 0 \\ \pm 1: \varphi(\xi,\eta,\zeta) = 0 \end{cases}$$

(7.2)

It should be noticed that function $H(\xi,\eta,\zeta)$ is not well defined when $\varphi(\xi,\eta,\zeta) = 0$, $H(\xi,\eta,\zeta) = \pm 1$ and $[\![H(\xi,\eta,\zeta)]\!] = 2$ merely represents a suitable way of calculating of the jump function in points which are located at the crack surface. [186-189]

7.4.2. Calculation models of implants with a crack in the biomaterial

During the problem analysis of cracked material behavior, sub-programs and software packages based on XFEM were used, supported by the numerical package for FEM analysis, ABAQUS, above all others, Morpheo.

Taking into account that within the writing of this dissertation the emphasis was on material behavior analysis related to materials used for hip

prosthetics, and using FEM analysis results, the case of cracked implant behavior was analyzed for a previously made numerical models 1 and 2.

Based on literature analysis, it was assumed that in places where stem was connected to the acetabular part, wear or corrosion can occur in material, and as a result of that, material damage may occur, i.e. the appearance of cracks [60,62,63]. In accordance with that, the crack was placed on the geometrical implant model 1 as shown in Figure 7.34. and on the geometrical implant model 2 as shown in Figure 7.35.
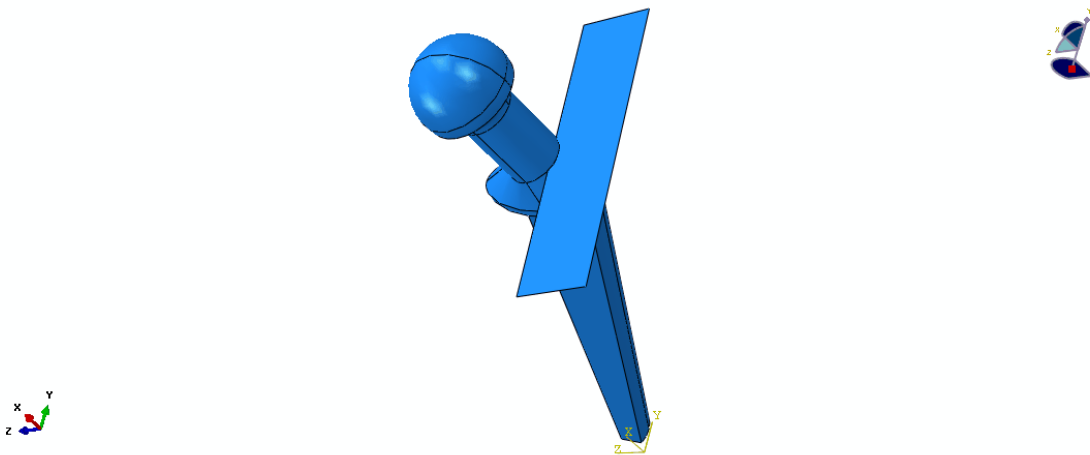

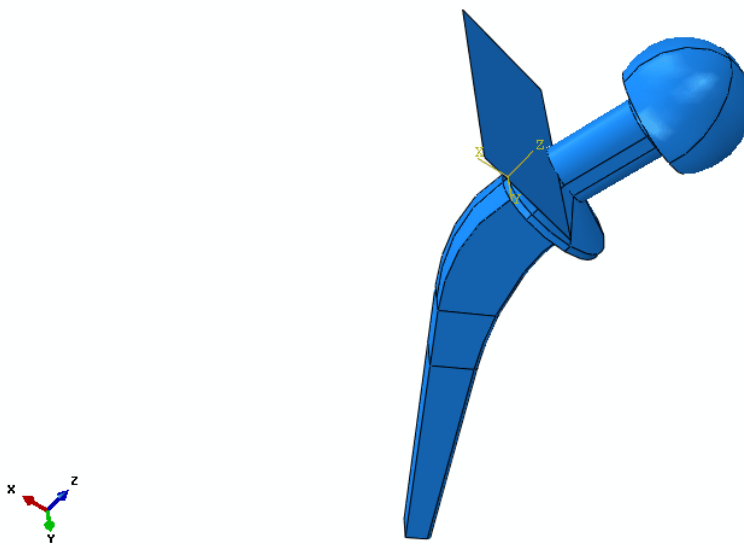*Figure 7.34. Model 1 – Schematic of placing the crack plane on the implant*

Figure 7.35. Model 2 – Schematic of placing the crack plane on the implant

During further model development and preparation for FEM analysis, generating of the mesh on the implant model was performed, with an initial crack, wherein there was a tendency to obtain a mesh as fine as possible.

Shown in Figure 7.36 is the implant model 1 and in Figure 7.37. is the implant model 2 with a generated mesh of finite elements and an initial crack in the critical area.
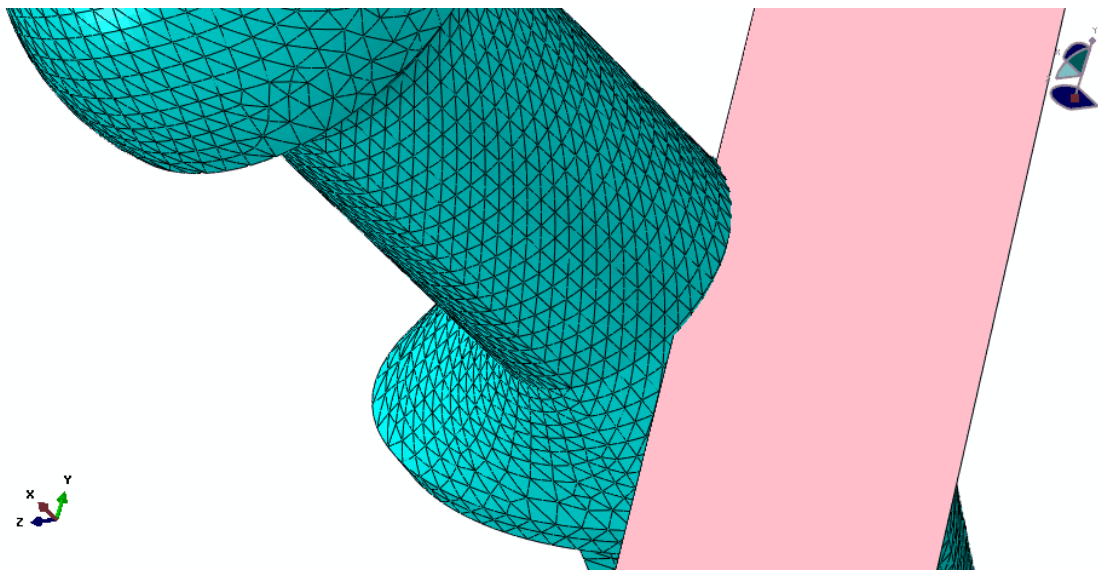

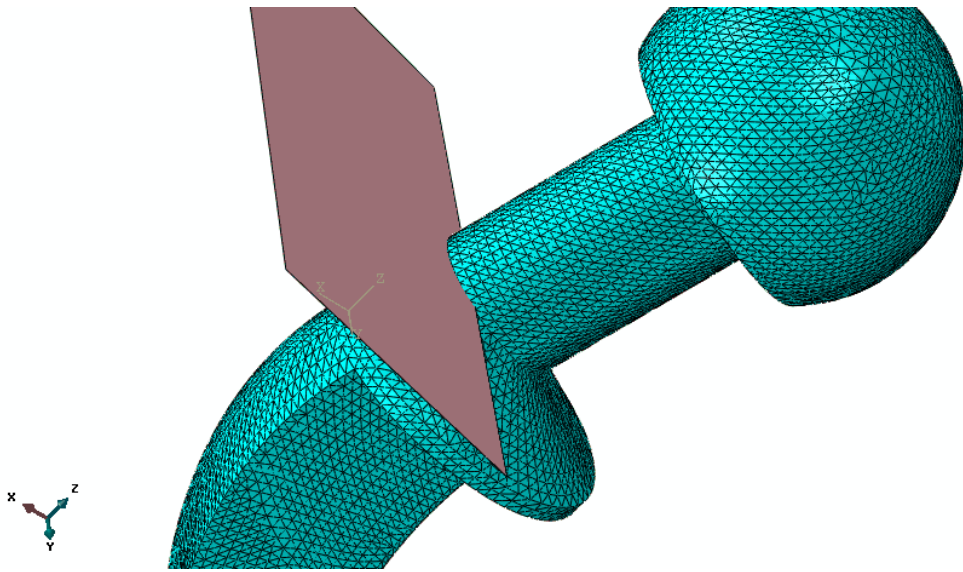*Figure 7.36. Model 1 – Display of a discretized implant model with a crack in the critical area*

Figure 7.37. Model 2 – Display of a discretized implant model with a crack in the critical area

CHAPTER 8

8.1 Analysis and discussion of the experimental and numerical results

8.1.1. Experimental analysis

Within experimental investigation presented in Chapter 6 two sets of experiments were carried out to determine the fracture mechanics parameters, first on standard test speciments for determination of fracture mechanics parameters for tested biomaterial, and second for determination of parameters using the final stretch zone method. All tests were done on MP35N multiphase Co Cr alloy, whose characteristics are also given in Chapter 6th.

Fracture toughness was measured in two directions P-T and T-T, based on the procedures defined by ASTM Standards E399 and E1820. Detailed testing and the results are presented in the Chapter sixth. The standard static fracture mechanics testing was performed in order to evaluate a resistance of the aged and unaged MP35N alloy to the stable (e.g. the blunting effect) and unstable crack growth and to investigate the influence of crack orientation. Final results of fracture toughness for tested biomaterial are shown in Table 8.1.

Table 8.1. The measured values of fracture toughness in MPa √m for a variety of conditions, the thickness and orientation

condition	orientation	K_c (thickness 3 mm)	K_c (thickness 8 mm)	K_{Ic}
HD	T-T	138	127	119
HDS	T-T	146	110	110
HD	L-T	147	132	125
HDS	L-T	142	115	96

One of the main tasks was to compare J_{Ic} values obtained from the J-R curves, with previouly obtained K_{Ic} values and also to evaluate both of them using standard single specimen technique. These results are also shown in Chapter 6, indicating good agreement with the K_{Ic} values obtained by using modified specimens.

The main purpose of impact testing was to evaluate the effects of loading rate to MP35N fracture behavior. The impact toughness evaluation on instrumented Charpy instrumented testing should enable better understanding of crack initation and growth processes due to its possibility to separate corresponding energies.

Table 8.2. Charpy instrumented testing

specimen	total energy (J) / corresponding K_{Ic}	crack initiation energy / K_{Ic}	crack growth energy / K_{Ic}
1	52.9 / 236	38.2 / 200	14.7 / 124
2	51.9 / 233	37.5 / 198	14.4 / 123

Another important task was to investigate the correlation between K_{Vtotal} and K_{Ic} and between $K_{Vgrowth}$ and J_{Id}. Finally, the Charpy instrumented testing was used for impact testing of pre-cracked specimens, in order to evaluate JId values and investigate further effects of orientation and aging on MP35N fracture behavior under impact load.

Results are given as J-Δa static curve in graphical form, Fig. 8.1. The J_{Ic}= 130 N/mm and corresponding K_{Ic}= 165 MPa$\sqrt{m}$ (for E = 210 GPa).
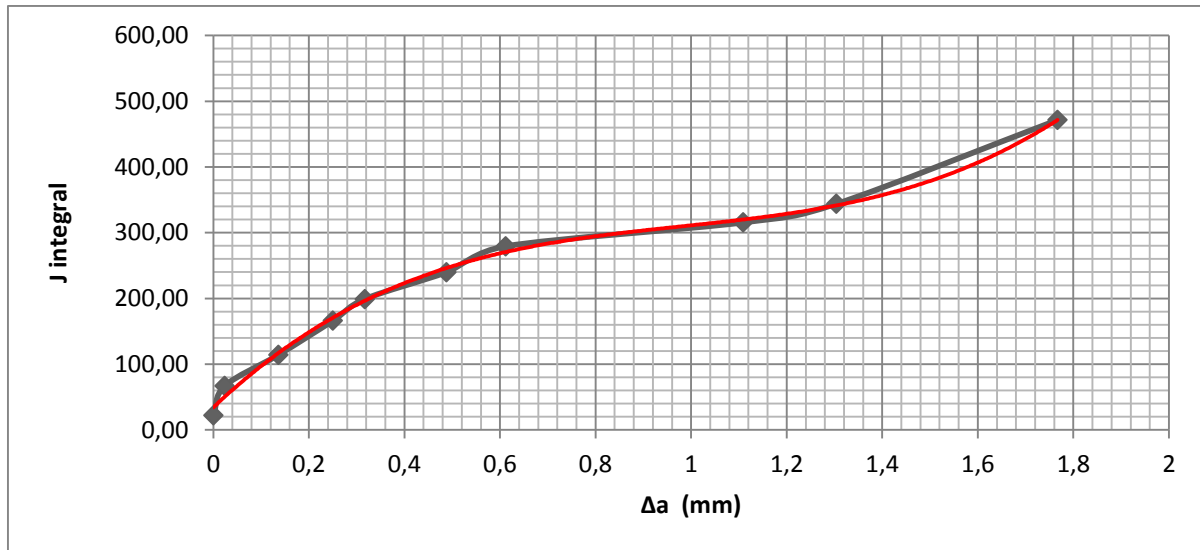
Figure 8.1. J - R curve for MP35N multiphase alloy.

The second criterion, i.e. comparison of the results for MP35N obtained using modified specimens with the results obtained by J_{Ic} testing, indicates that K_{JIc} values (ave. 147 MPa√m for the unaged and 117.5 MPa√m for the aged alloy) are somewhat higher than K_{Ic}(126 MPa√m for unaged and 98 MPa√m for the aged alloy). Even larger difference has been obtained for the pre-cracked Charpy specimen (K_{JIc}=159 MPa√ vs. 126 MPa√m).

According to the reference literature [172,173], more pronounced effect of anisotropy was observed for T-L crack configuration, since significantly lower fracture toughness values were obtained (84 MPa√m for the cold-drawn and 78 MPa√m for the cold-drawn and aged condition). Toughness decrease was attributed to the substantial grain boundary crack propagation in the T-L crack configuration.

The measurements from both the unaged and the aged samples with varying thicknesses and with the T-T crack configuration are summarized in referenced literature. [172,173] As the thickness of the sample was increased, the value of toughness approached an asymptotic value. The asymptotic value (K_{IC}) for the unaged material was about 120 MPa√m, while it was about 110

$MPa\sqrt{m}$ for the aged material. Note that some of the high values of toughness in previous reports can be easily reconciled as plane stress fracture toughness values, since they are comparable to the values presented in Figure 4. [172,173]
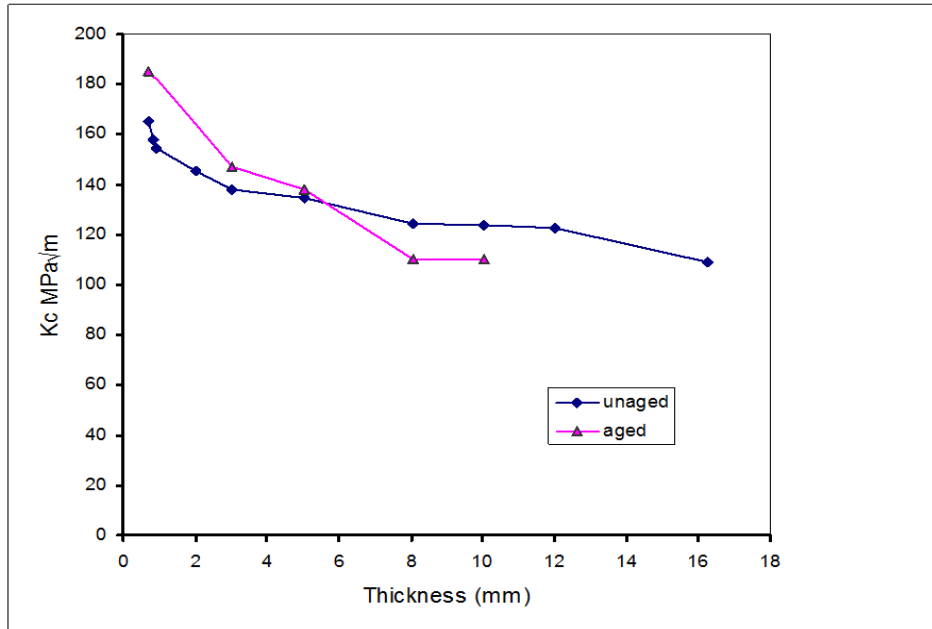

Figure 8.2. Influence of sample thickness on the fracture toughness of commercially drawn MP35N in both the unaged and the aged conditions[172,173]

As expected, the plane strain fracture toughness of the higher strength aged material is lower than that of the unaged material. However, the plane stress fracture toughness values of the aged material were significantly higher than those of the unaged material. It is striking that the relative toughness of the two conditions are switched between the two thicknesses, which correspond to near plane strain to near plane stress conditions. The condition of reduced toughness at increased yield strength is of course characteristic of all high strength alloys tested in plane strain.

The conventional explanation of this effect is that increased yield strength reduces the *volume* of the plastic zone at the tip of the crack. On this basis, it appears a reasonable hypothesis that in plane stress, where the plastic zone should be much larger in volume, the higher work done per unit volume,

in the higher strength aged condition, then offsets the increase in the volume of the plastic zone. This indicates a positive correlation between strength and toughness when the crack-tip process zone experiences plane stress conditions.

The fracture surfaces from these tests were examined in the scanning electron microscope (SEM). Figure 8.3. shows fracture surfaces from the 3-point bending bar for MP35N superalloy for three different magnification values. Appendix A. presents the results of all relevant SEM analysis, which, due to limited space will not be described in detail. The fracture surfaces in the T-T and L-T crack orientations indicate ductile shear fracture.

Microstructure of stretch zone suggests that mixed loading conditions (elastic-plastic) are predominant around the crack tip at the stage of crack propagation initiation. From results presented in Chapter 6, it is important to notice that SWZi average measured value is i318 μm. By applying stretch zone width determination method obtained values are for Ji 150 N/mm., and the corresponding value for FSW 220 μm, being 70% of average measured value.

By using SWZi average measured value (318 μm) and obtaining Ji (200 N/mm) from the Fig. 8.1. it can be shown that the difference is still at the same level.
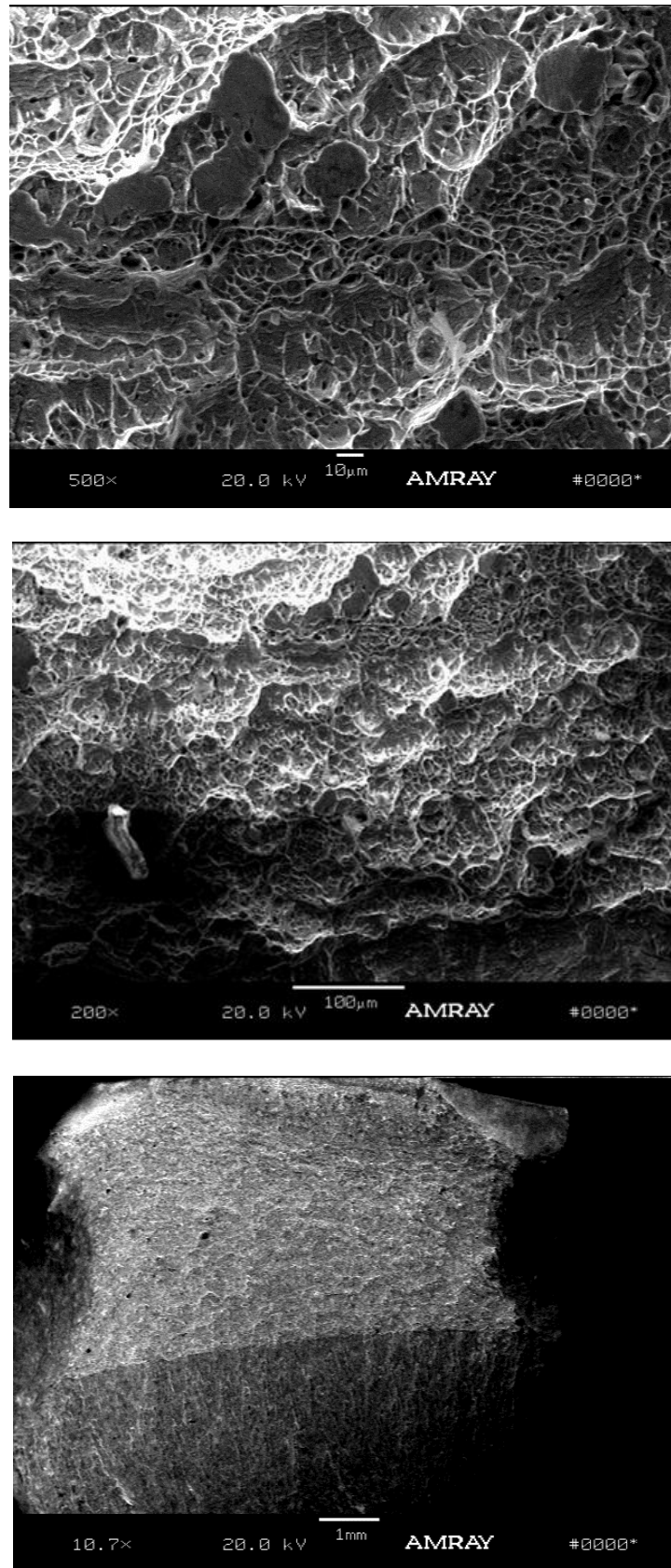
Figure 8.3. MP35N fracture surfaces from the scanning electron microscope (SEM)

The difference between initial blunting SZ (200 μm) and FSZ (220 μm), is obtained according to the slope of the curve in Fig. 8.1., in the following way: J_i (150 N/mm) divided by 2 × yield strength (cca. 3000 MPa, /4-6/), equals 20 μm.

It should be noted that the value of J_i obtained this way is not always precise enough, for it is possible to have greatly scattered measured values of critical stretch zone width.

These results indicate good agreement between measured values of critical stretch zone width, corresponding J_i parameter and fracture mechanics parameter J_{IC}.

8.1.2. Numerical analysis

Numerical analysis in this paper were performed on models that are made on the basis of selected types of hip implants, as described in Chapter 7. The analyzes were done in commercial software packages, Solid Works, Abaqus and Morpheo, with a detailed description of models also presented in the Chapter 7.

Numerical simulation included mechanical analysis of three different types of implants behavior, made of Co Cr alloy, where one of the implants is modular, so the analysis were made on the assembly of the prosthesis consisting of a stem and a cup, and also only on the stem of the prosthesis. Type of implants and materials are chosen based on literature review, or pursuant to the problems of preserving the integrity of the hip prosthesis which is to be examined. The same material was chosen as for the experimental tests described above.

To investigate the differense between results for standard define loads and real loads on implants that can appaere in practise, it is necessary to analyze the prosthesis under a body weight static loading, and under the maximum load that can occur during the walking cycle. Selected are Three

types of loadings on implant were selected, that can occur during walking on level ground, i.e. at slow, normal and fast walking speed. It can be assumed that the loads that occur in the phase of slow and normal walk are of similar value, so we have only two relevant loads for numerical analysis. So,the models are made of different geometries and accordingly to the selected the type of loading eight numerical models were created, defined in Table 7.6., for analysis of deformation and stress state of the implant during loading. Models are appropriately set with boundary conditions, for the bottom surface of the implant displacement is fixed in all degrees of freedom, and loads are applied in the define direction at the top of the femoral head prosthesis.

In the following disccution the three-dimensional stress states, calculated according to the Von Mises criterion, as well as three-dimensional displacement field depending on the applied loads on the implant are presented.

For numerical **MODEL 1.1.** Figure 8.4. shows the distribution of von Mises stress, while Figure 8.5. shows the strain analysis on an implant. Applied loads is 3845.5 *N* on the selected implant surface that is 422 mm². For this model standard element library is used, and the model is made by using the C3D8R and C3D10 element types. Total numer of elements is 7 253 and total numer of nodes is 9 708. For this analysis total CPU time is 7.300 and deformation scale factor for graphical representation is 500.

For numerical **MODEL 1.2.** Figure 8.6. shows the distribution of von Mises stress, while Figure 8.7. shows the strain analysis on an implant. Applied loads is 5964.5 N on the selected implant surface that is 422 mm². For this model standard element library is used, and the model is made by using the C3D8R and C3D10 element types. Total numer of elements is 7 253 and total numer of nodes is 9 708. For this analysis total CPU time is 6.000 and deformation scale factor for graphical representation is 500.
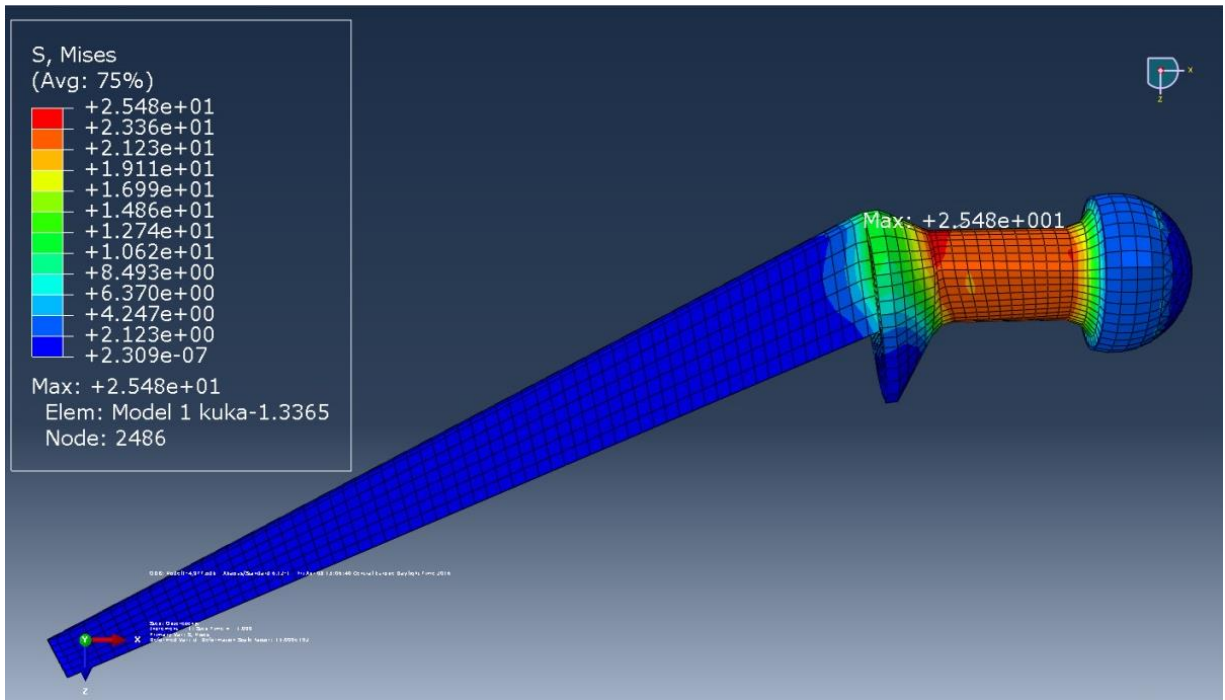
Figure 8.4. Numerical model 1.1. - von Mises stress distribution

Figure 8.5. Numerical model 1.1. - strain distribution

Figure 8.6. Numerical model 1.2. - von Mises stress distribution

Figure 8.7. Numerical model 1.2. - strain distribution

For numerical **MODEL 2.1.** Figure 8.8. shows the distribution of von Mises stress, while Figure 8.9. shows the strain analysis on an implant. Applied loads is 3845.5 N on the selected implant surface that is 376.6 mm². For this

model standard element library is used, and the model is made by using the C3D8R and C3D10 element types. Total numer of elements is 11 510 and total numer of nodes is 17 191. For this analysis total CPU time is 10.500 and deformation scale factor for graphical representation is 500.

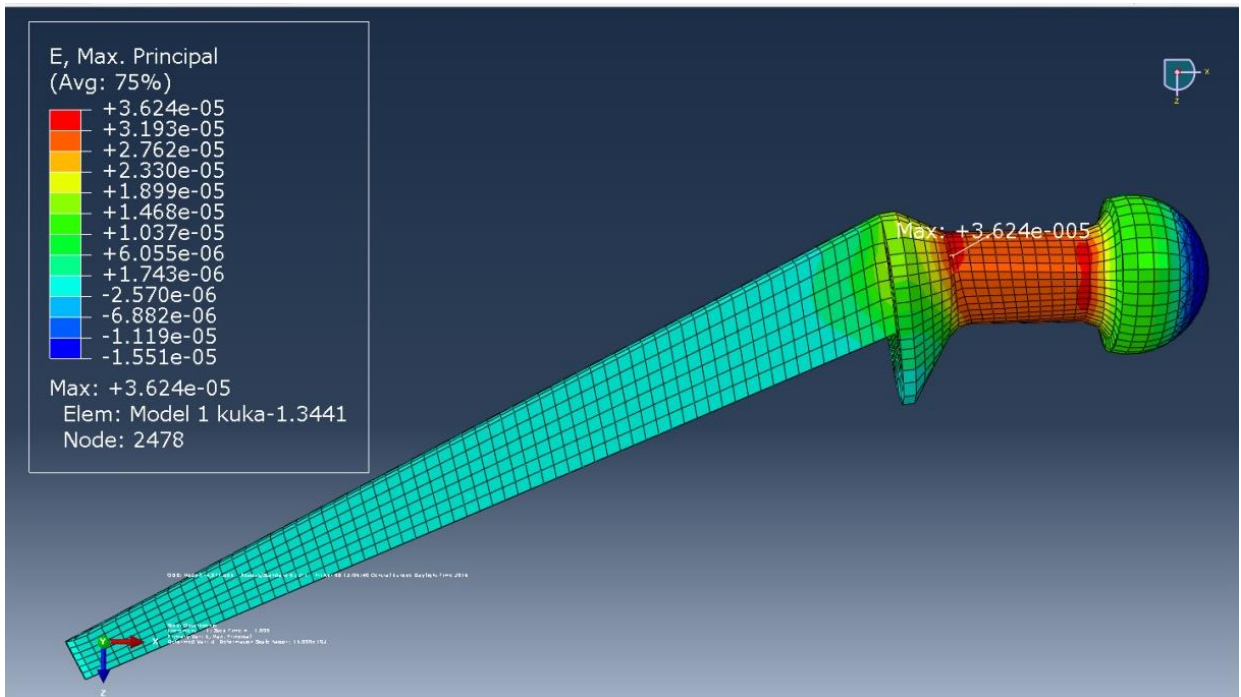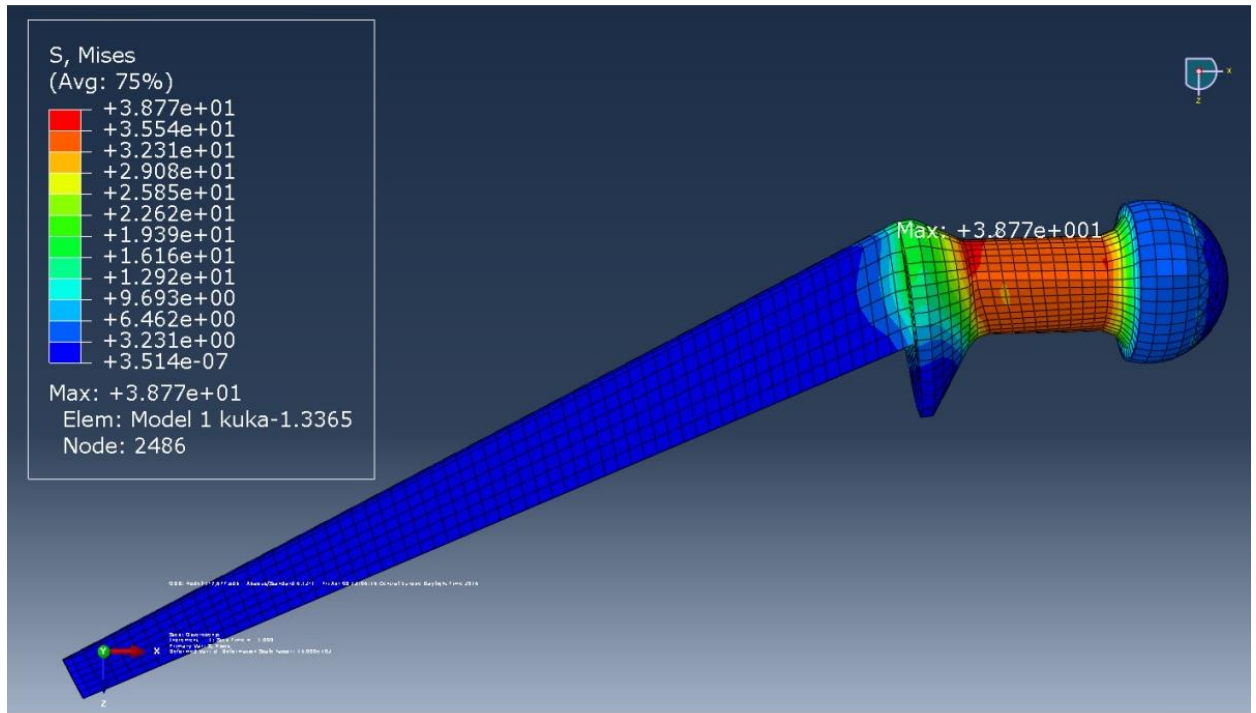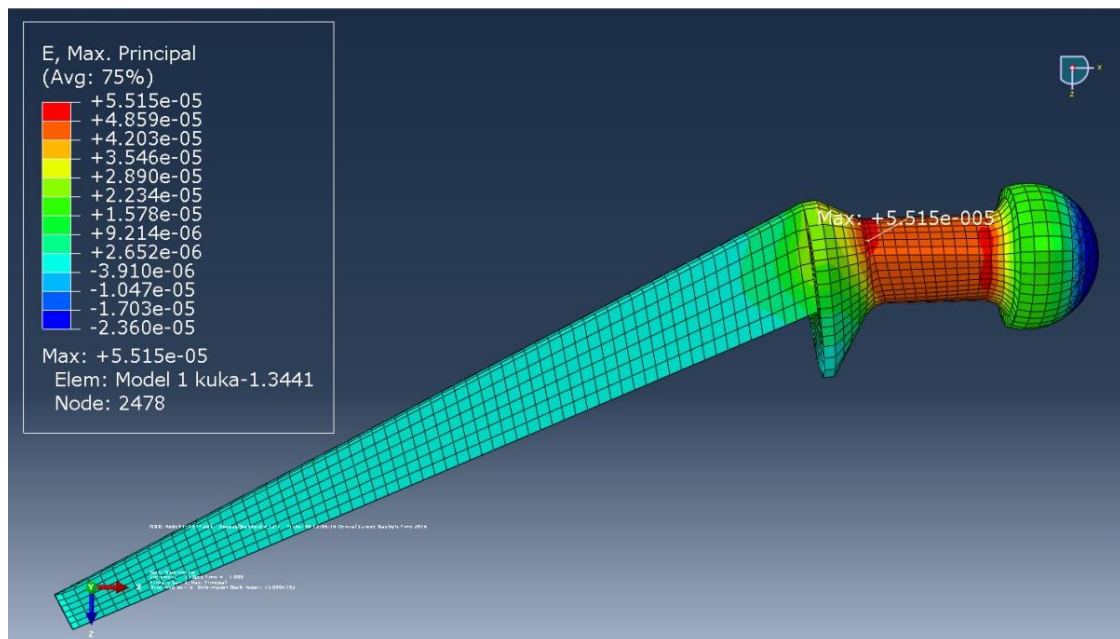*Figure 8.8. Numerical model 2.1. - von Mises stress distribution*

Figure 8.9. Numerical model 2.1. - strain distribution

For numerical **MODEL 2.2.** Figure 8.10. shows the distribution of von Mises stress, while Figure 8.11. shows the strain analysis on an implant. Applied loads is 5964.5 N on the selected implant surface that is 376.6 mm². For this model standard element library is used, and the model is made by using the C3D8R and C3D10 element types. Total numer of elements is 11 510 and total numer of nodes is 17 191. For this analysis total CPU time is 10.800 and deformation scale factor for graphical representation is 500.
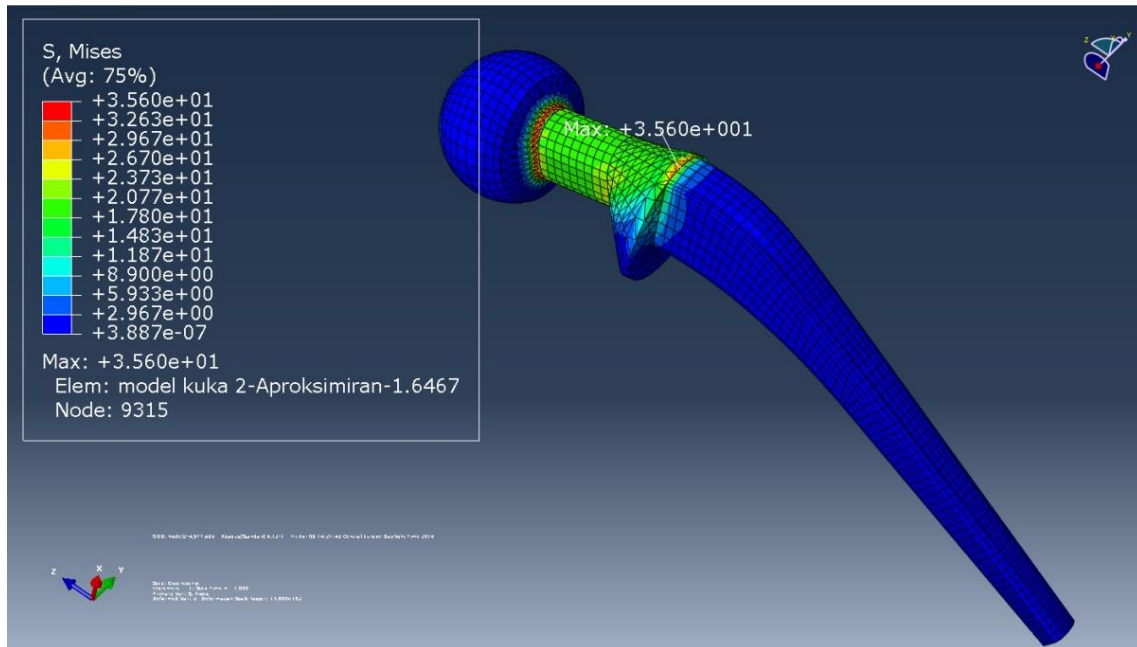

Figure 8.10. Numerical model 2.2. - von Mises stress distribution

Figure 8.11. Numerical model 2.2. - strain distribution

For numerical **MODEL 3.1.** Figure 8.12. shows the distribution of von Mises stress, while Figure 8.13. shows the strain analysis on an implant. Applied loads is 3845.5 N on the selected implant surface that is 154 mm². For this model standard element library is used, and the model is made by using the C3D8R and C3D10 element types. Total numer of elements is 57 674 and total numer of nodes is 84 019. For this analysis total CPU time is 77.500 and deformation scale factor for graphical representation is 500.

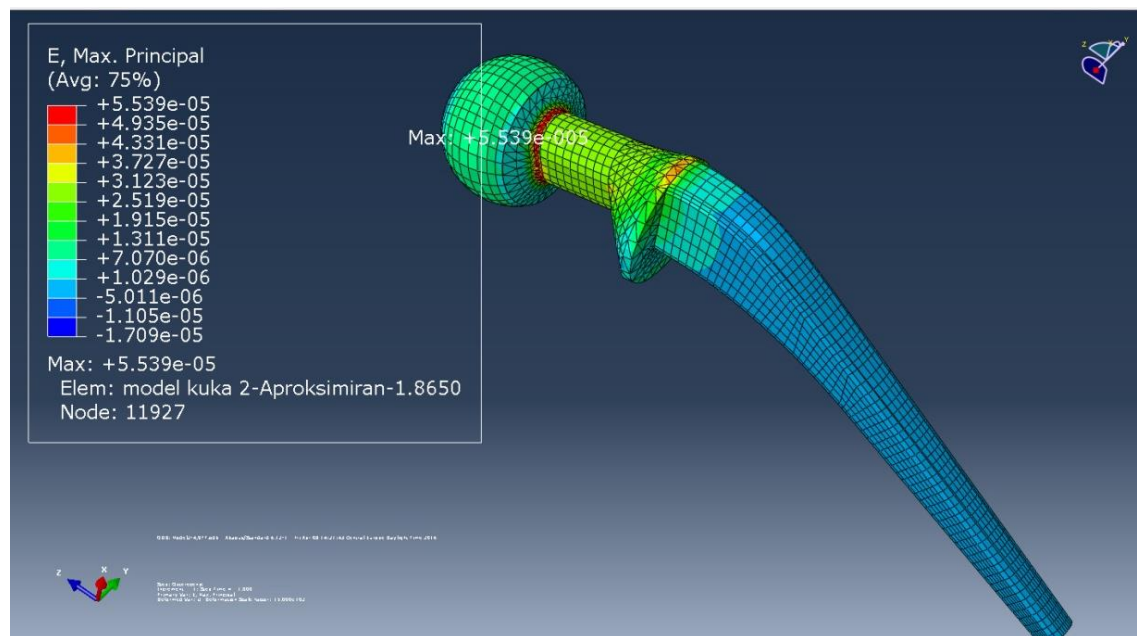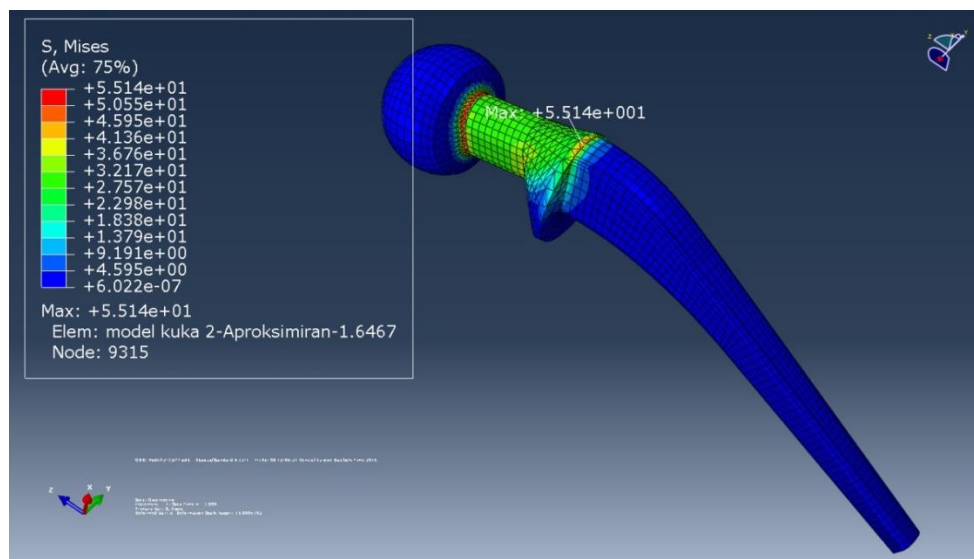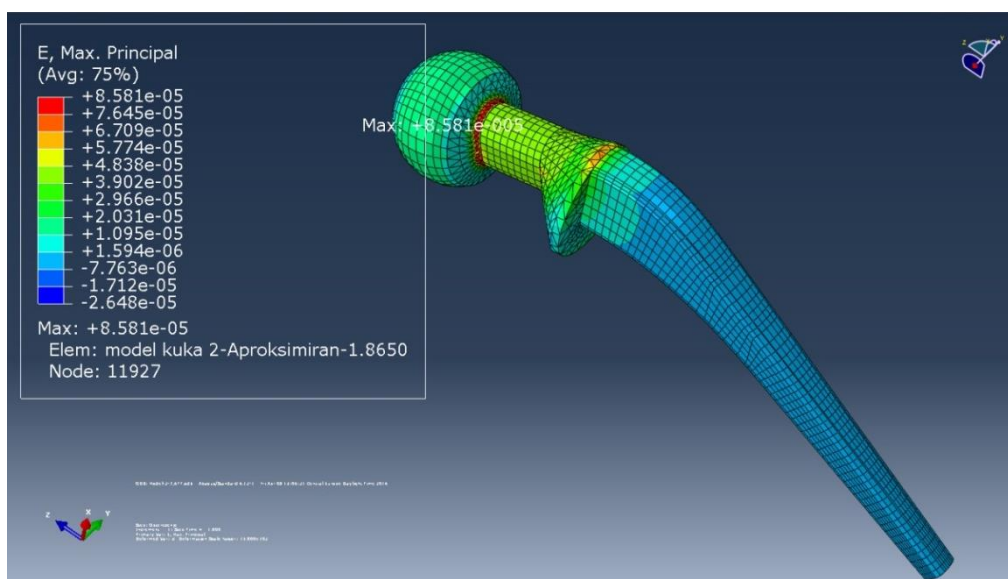*Figure 8.12. Numerical model 3.1. - von Mises stress distribution*

Figure 8.13. Numerical model 2.2. - strain distribution

For numerical **MODEL 3.2.** Figure 8.14. shows the distribution of von Mises stress, while Figure 8.15. shows the strain analysis on an implant. Applied loads is 5964.5 N on the selected implant surface that is 154 mm². For this model standard element library is used, and the model is made by using the C3D8R and C3D10 element types. Total numer of elements is 57 674 and total numer of nodes is 84 019. For this analysis total CPU time is 78.100 and deformation scale factor for graphical representation is 500.

For numerical **MODEL 4.1.** Figure 8.16. shows the distribution of von Mises stress, while Figure 8.17. shows the strain analysis on an implant. Applied loads is 3845.5 N on the selected implant surface that is 372 mm². For this model standard element library is used, and the model is made by using the C3D8R and C3D10 element types. Total numer of elements is 62 098 and total numer of nodes is 91 044. For this analysis total CPU time is 97.300 and deformation scale factor for graphical representation is 500.
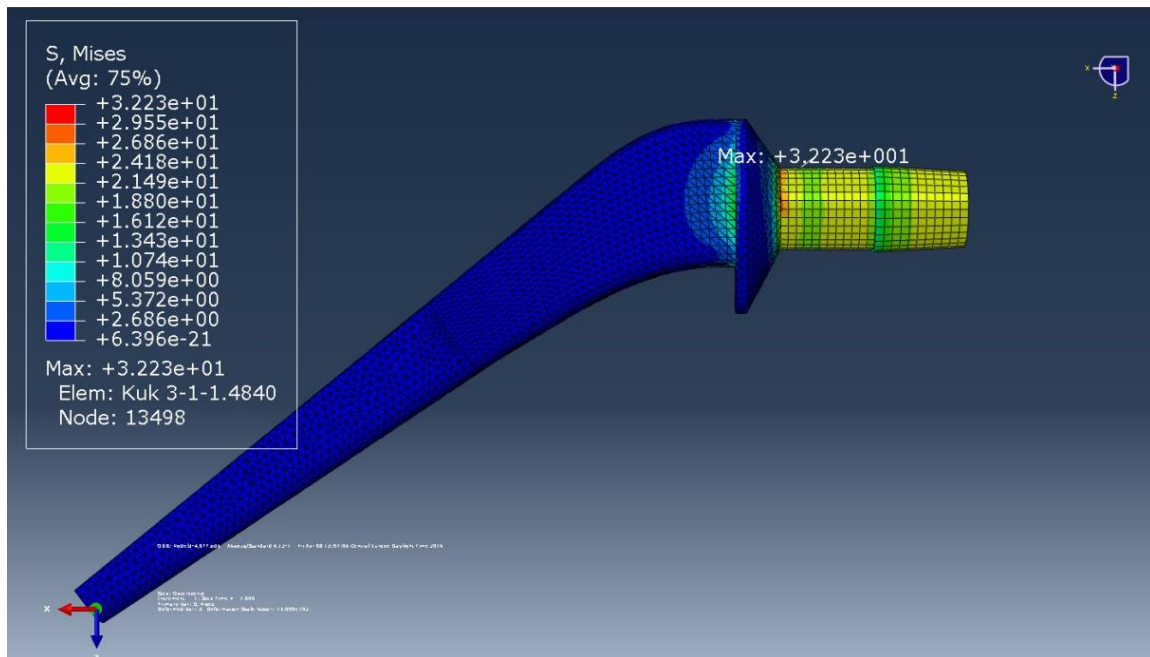

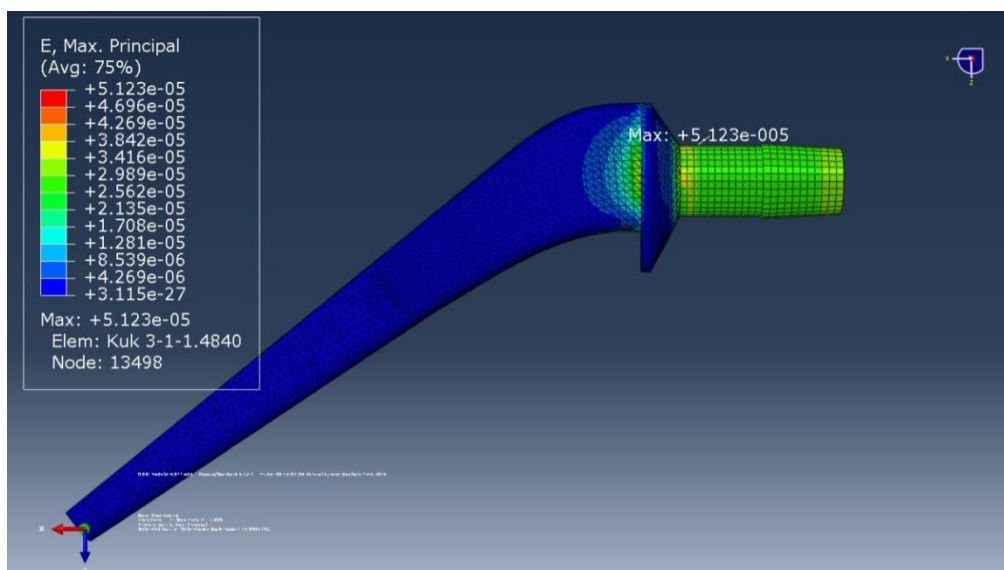*Figure 8.14. Numerical model 3.2. - von Mises stress distribution*
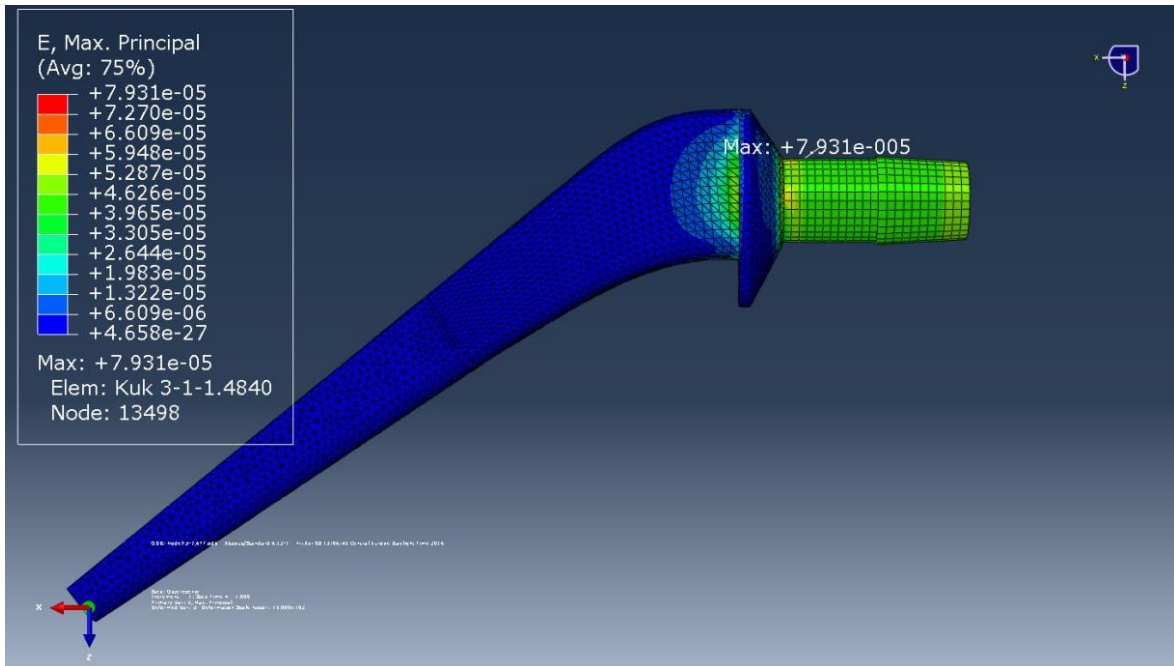
Figure 8.15. Numerical model 3.2. - strain distribution
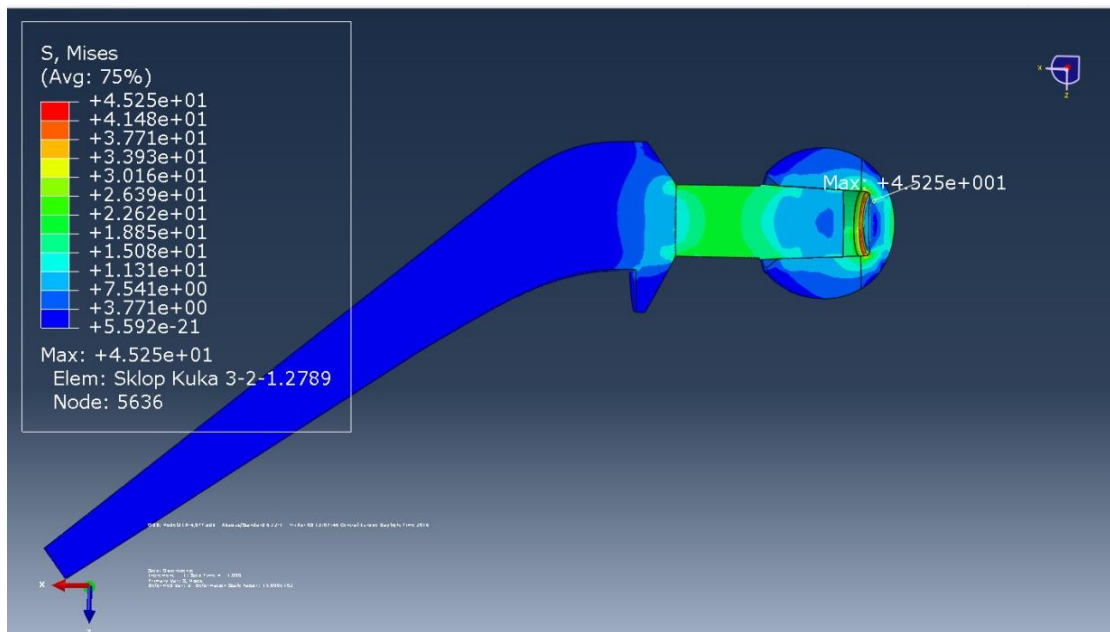
Figure 8.16. Numerical model 4.1. - von Mises stress distribution
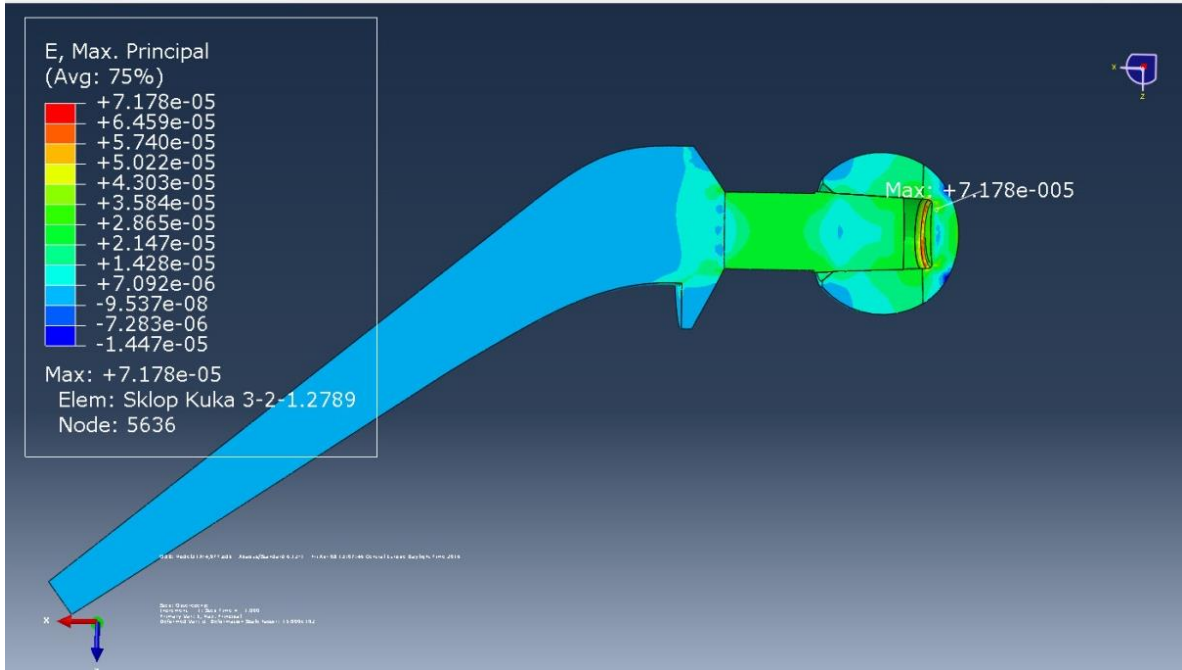
Figure 8.17. Numerical model 4.1. - strain distribution

Figure 8.18. shows the distribution of von Mises stress, while Figure 8.19. shows the strain analysis on an acetabular component.
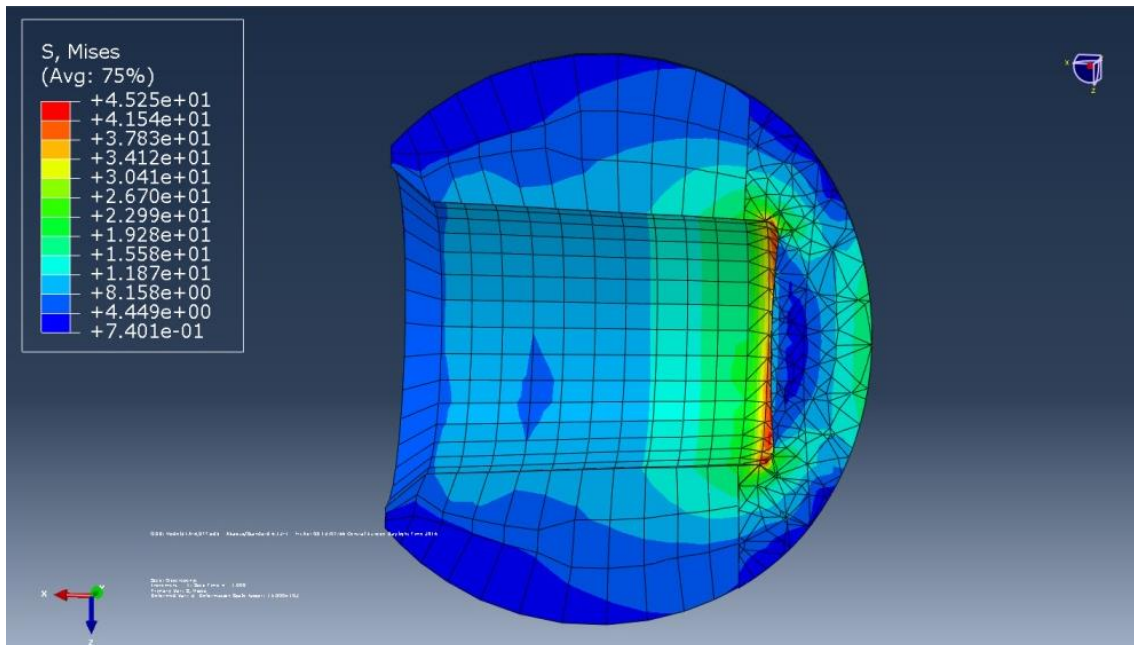
Figure 8.18. Numerical model 4.1. - von Mises stress distribution on acetabular component
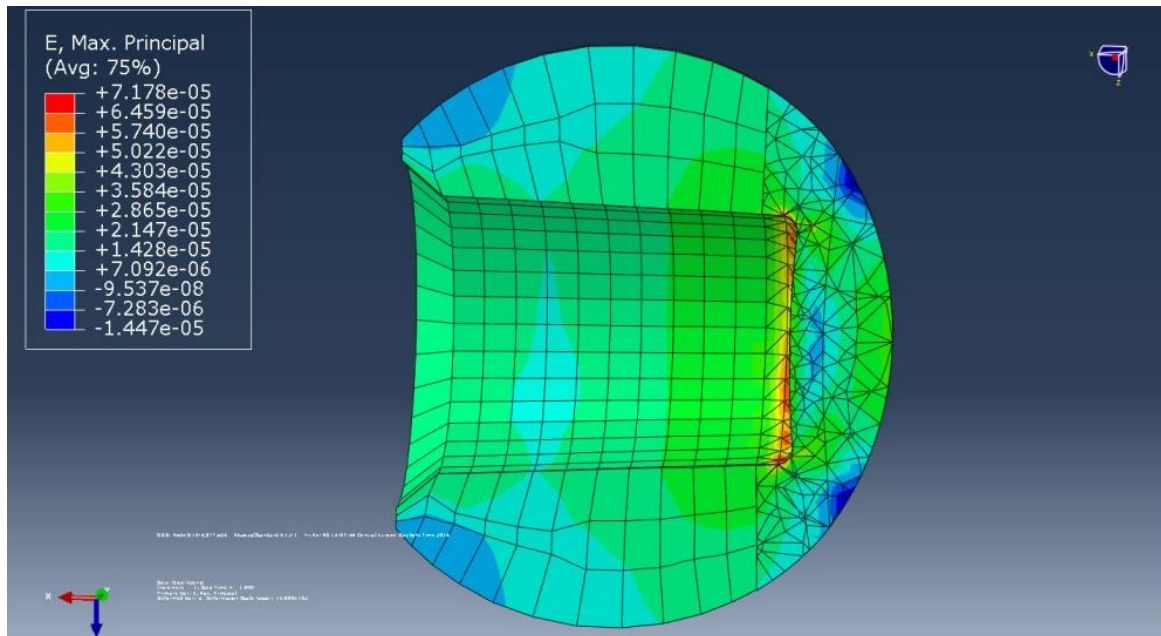
Figure 8.19. Numerical model 4.1. - strain distribution on acetabular component

For numerical **MODEL 4.2.** Figure 8.20. shows the distribution of von Mises stress, while Figure 8.21. shows the strain analysis on an implant. Applied loads is 5964.5 N on the selected implant surface that is 372 mm². For this model standard element library is used, and the model is made by using the C3D8R and C3D10 element types. Total numer of elements is 62 098 and total numer of nodes is 91 044. For this analysis total CPU time is 98.100 and deformation scale factor for graphical representation is 500.
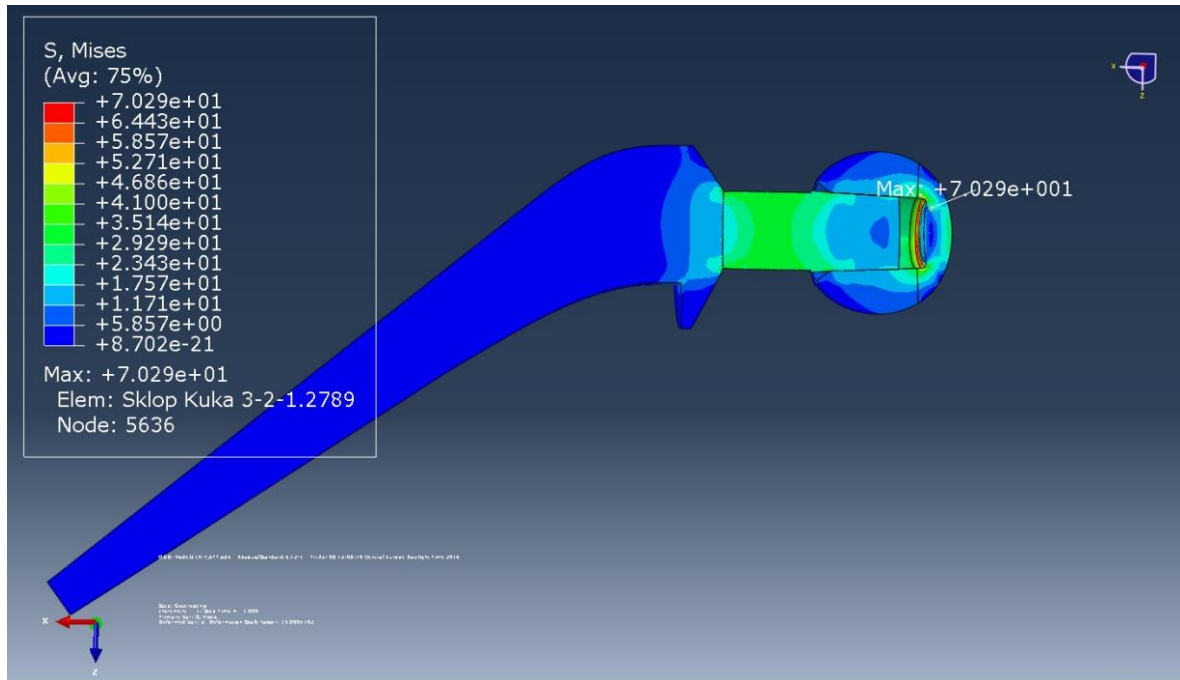
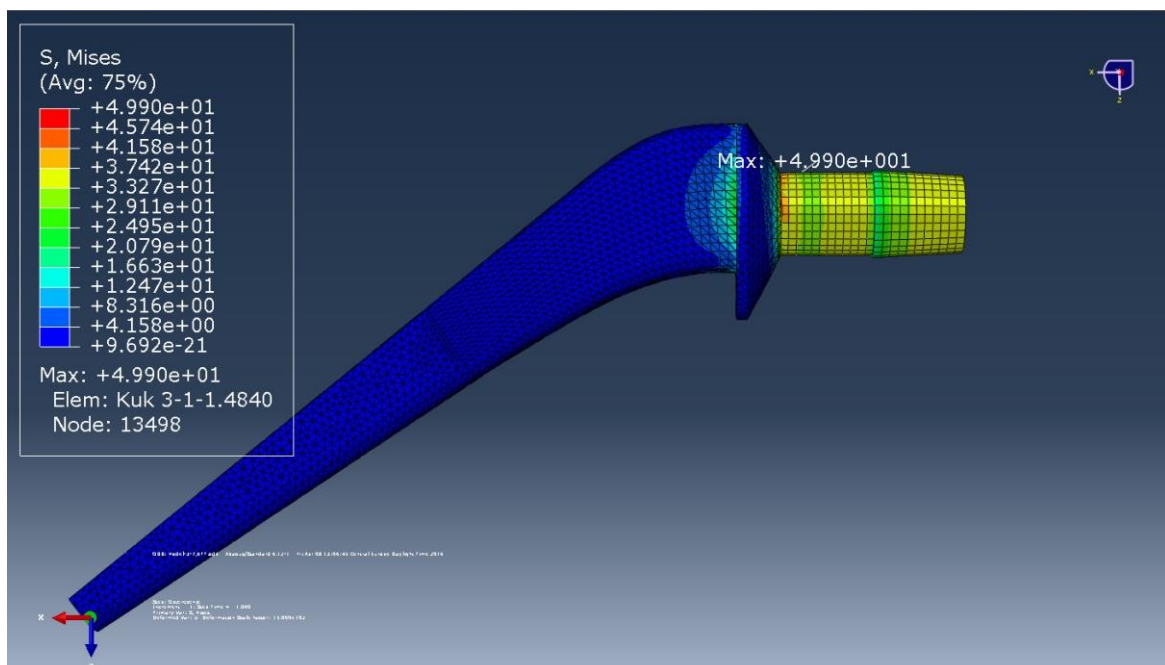*Figure 8.20. Numerical model 4.2. - von Mises stress distribution*
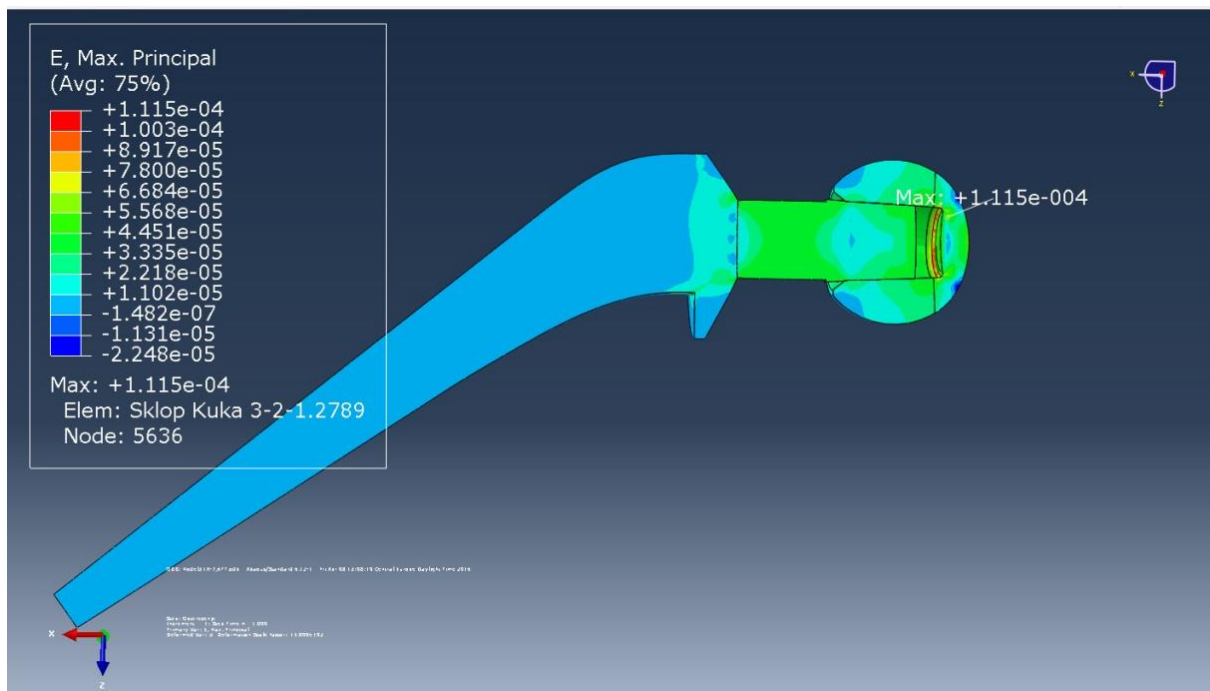
Figure 8.21. Numerical model 4.2. - strain distribution

Figure 8.22. shows the distribution of von Mises stress, while Figure 8.23. shows the strain analysis on an acetabular component.
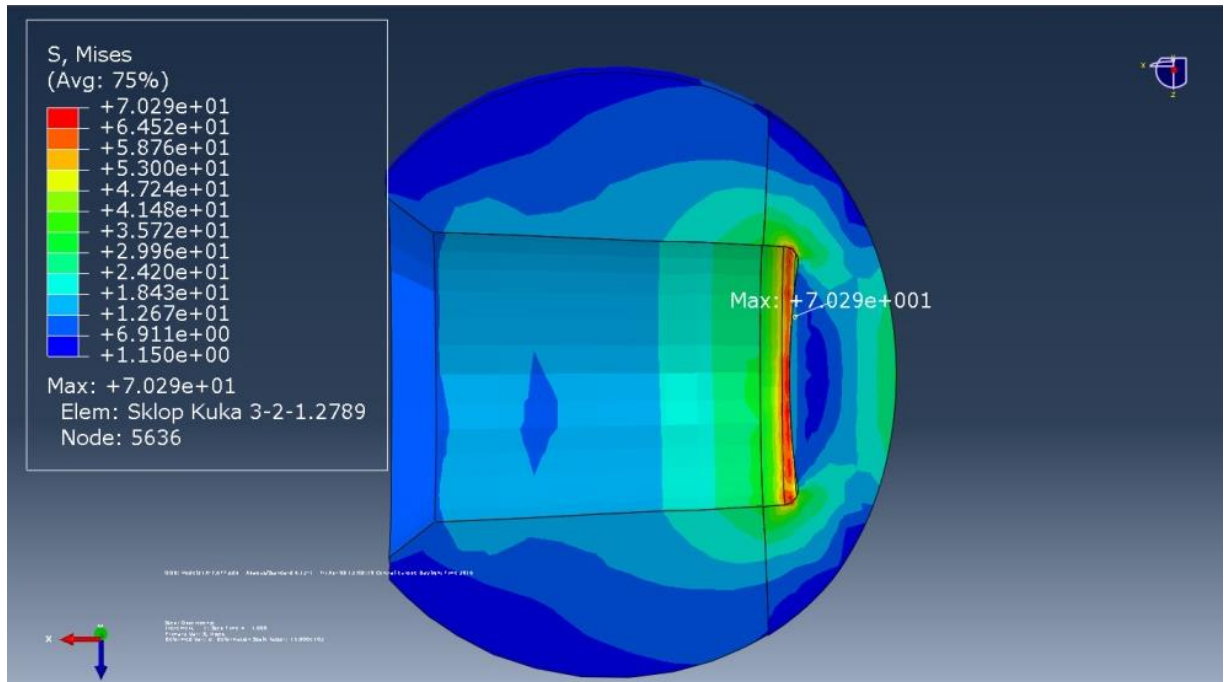
Figure 8.22. Numerical model 4.2. - von Mises stress distribution on acetabular component
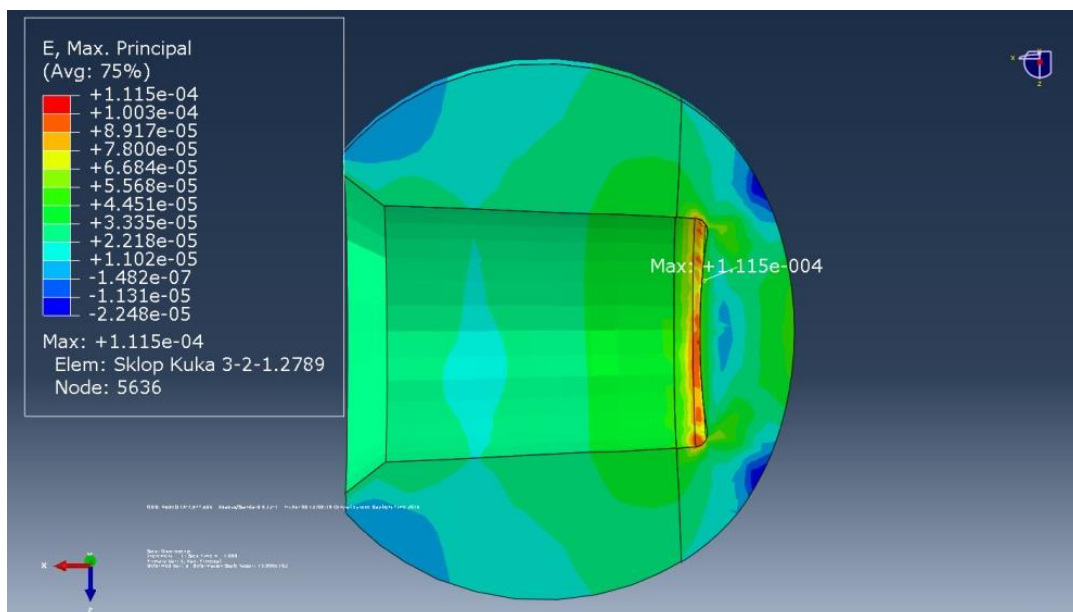
Figure 8.23. Numerical model 4.2. - strain distribution on acetabular component

Based on the analysis of obtained models parameters is clearly that for the model with the most complicated geometry (model 4) should be applied the largest number of finite elements to discretize the structure. Consequently, for

this numerical model the most CPU time was spent, almost ten times more than for the numerical model with simplest geometry (model 1).

Based on the stress field analysis for each of the individual numerical models, maximum stress values on each of the implants models are obtained, with two different types of load structure. The results are shown in Table 8.3.

Table 8.3. Results of numerical analysis

| NUMERICAL MODEL	LOAD ON IMPLANT (N)	VON MISES STRESS VALUE (MPa)
Model 1.1.	3845.5	254
Model 1.2.	5964.5	387
Model 2.1.	3845.5	356
Model 2.2.	5964.5	551
Model 3.1.	3845.5	322
Model 3.2.	5964.5	499
Model 4.1.	3845.5	450
Model 4.2.	5964.5	700

Referring to the analysis of stress and strain state on the numerical models, it can be concluded that the area of maximum stress and strain values is right on the expected places on implants geometry. Numerical simulations on models show that stress concentration occurs in precisely those areas where in practise on the implants of similar or the same geometry fatigue fracture occurred.

Based on these results, it is clear that the maximum stress value are appearing on the numerical model 4, right on the contact spot of stem and cup

of the hip prosthesis, which is actually in practice the most common spot where implant wear occurs. Taking into account that this is a modular type of prosthesis, analyses were performed just for the stem of the implant as well, and in this case there was a significantly lower stress field on the prosthesis. However, it should be noted that on the modular prosthesis type of numerical simulations obtained higher stress values than on the monblock type of prosthesis. A very common problem with the modular prosthesis is precisely corrosion or wear in areas where numerical simulations provide the highest stress value.

By comparative analysis of numerical results for two selected type of monoblock hip implants, it can be concluded that a significantly higher stress values are obtained for 2 compared to model 1, which is possible to explain by analysing the implant geometry, and loads acting on it. Precisely for this type of hip implant, structure integrity problems were perceived in practice, when there has been a fracture of hip prosthesis due to the existence of the crack in the biomaterial. By analysing the stress field on the numerical model 2 it can be concluded that the critical spots for the crack appearance in the biomaterial are exactly at the connection of the base and neck of the hip implant stem. Such spots are in the practices the most common locations for the occurrence of the cracks in biomaterials, which eventually lead to the weakening of the integrity of the prosthesis, or to failure.

Regarding to these observations further numerical analysis included numerical models of an implant with fatigue crack in the biomaterial, set just in spots of the highest stress concentration.

Crack propagation rate da/dN was obtained using Paris crack growth low, Eq. 5.32., Paris exponent n is 2.28, and Paris coefficient is 2.05 e^{-11}. Applied parameters for the numerical calculation of the fatigue crack propagation in biomaterial of an implant are given in Table 8.4.

Table 8.4. Numerical perameters for crack propagation behaviour

Implant biomaterial

CoCr superalloy

Crack growth low:

$$\frac{da}{dN}=C(\Delta K)^n$$

Numerical calculation parametars:

n = 2.28

C = 2.056e^{-11}

$Y_{ie.}$ = 1751

UTS = 1889

K_{Ie} = 3649

K_{IC} = 2780

The numerical analysis were done in numerical package Morpheo, which is based on application of extended finite element method, and is supported by numerical software for simulation and finite element analysis Abaqus.

Figures 8.24. and 8.25 show the critical area on the monoblock hip implant models in terms of the fatigue crack appearance, i.e. two numerical models with crack inserted and finite element mesh generated.

The initial crack was set on a spot where occurrence of fatigue and the micropitting it is expected. For two numerical models total calculation, i.e. numerical simulation of complite crack failure of an implant, lasted 12

calculation steps for implant 1 and 14 calculation steps for for implant 2. Figures 26.8 and 27.8. show the cracks propagation in the material.
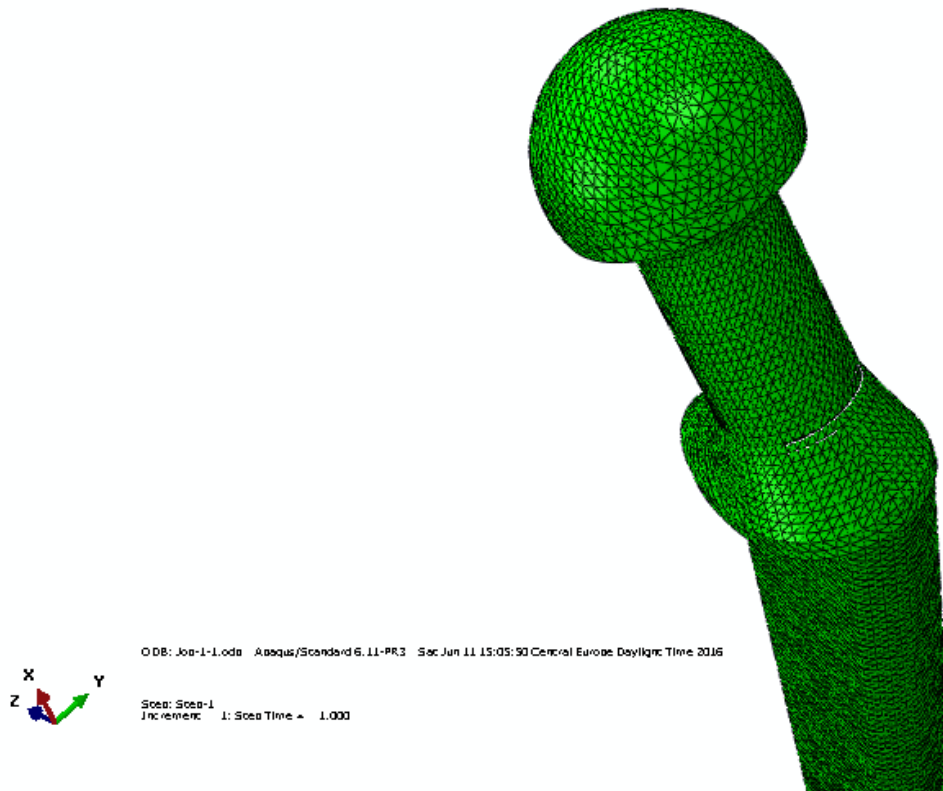
Figure 8.24. Numerical model 1 – initial crack in calculation step 1
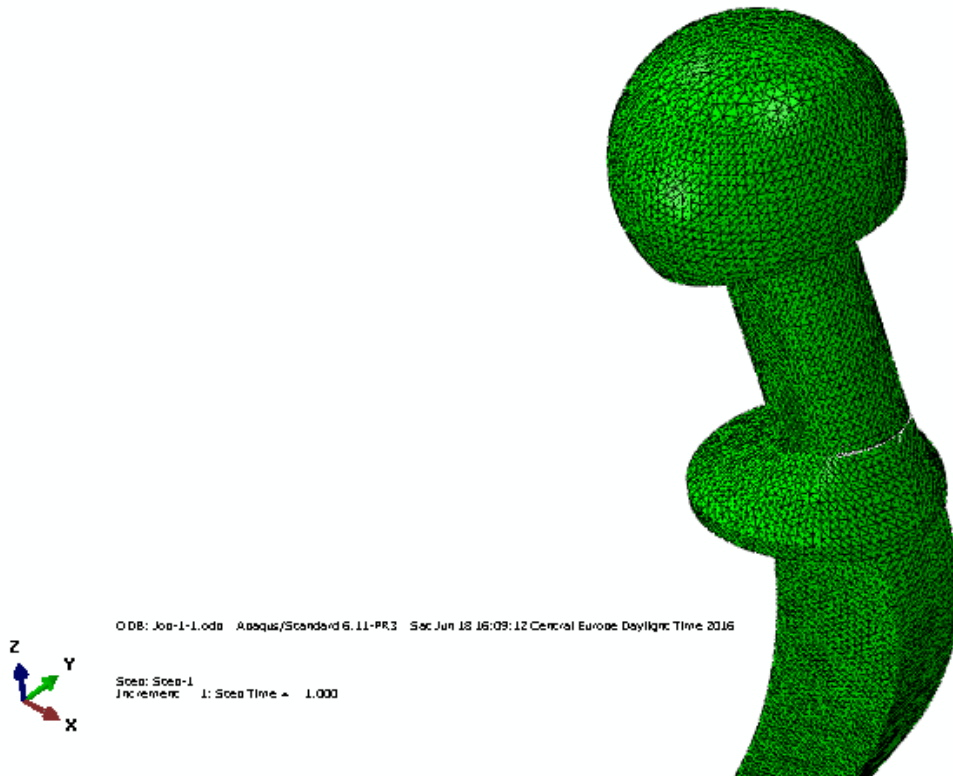
Figure 8.25. Numerical model 2 - initial crack in calculation step 1
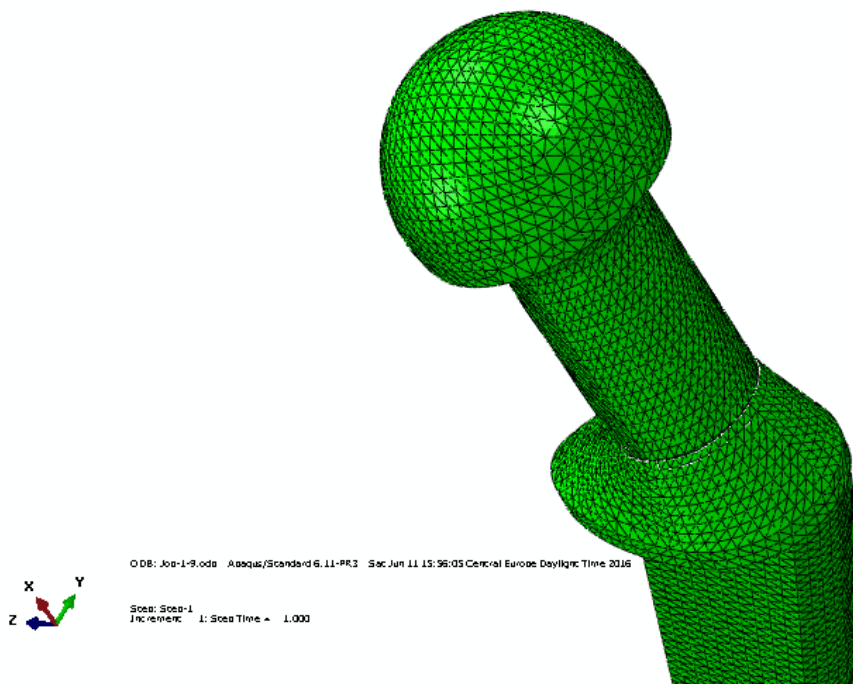
Figure 8.26. Numerical model 1 – crack propagation
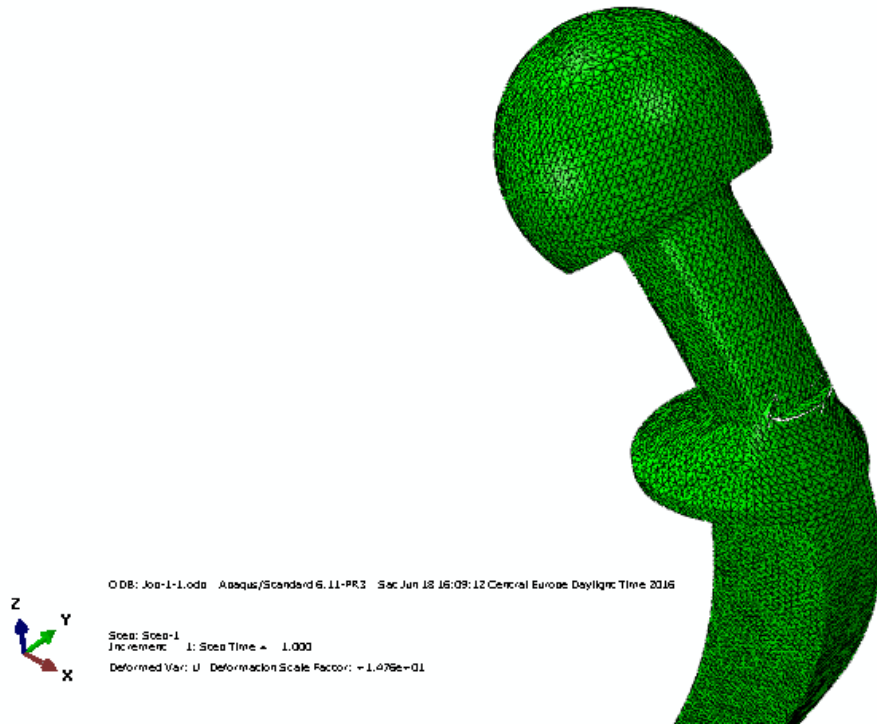
Figure 8.27. Numerical model 2 - crack propagation

Figures 8.28. and 8.29. show the expansion of cracks in the material and stress distribution at the critical crack length for first model.
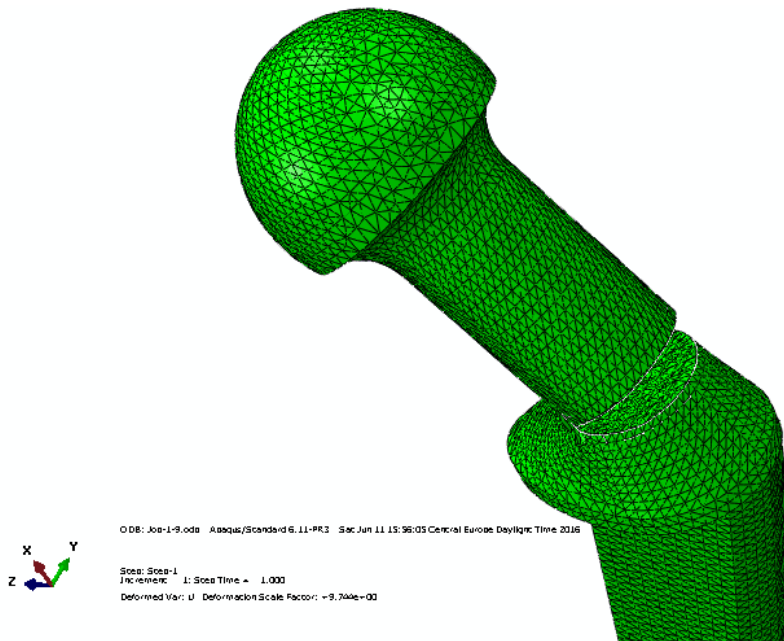
Figure 8.28. Numerical model 1 – critical crack length in calculation step 12
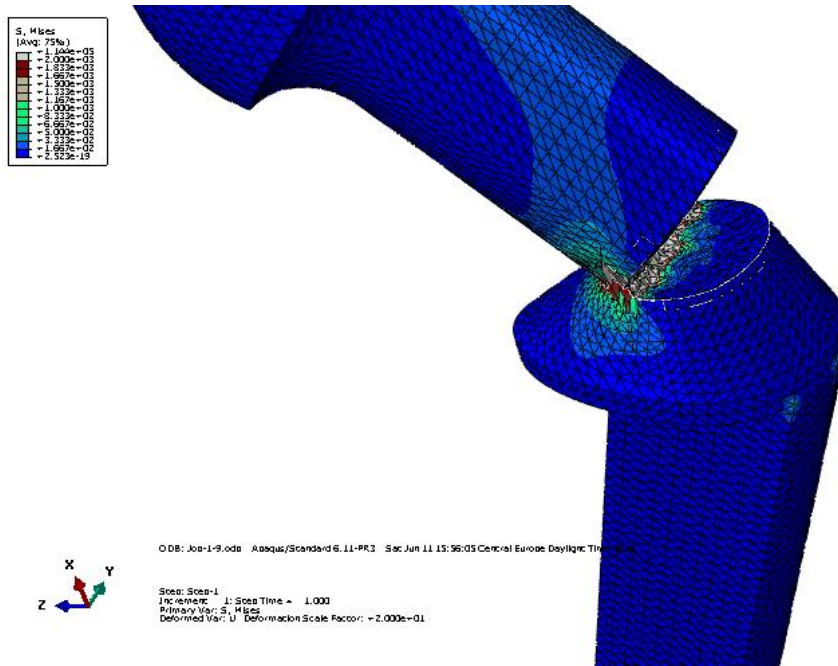
Figure 8.29. Numerical model 1 – Von Misses stress distribution

Figures 8.30. and 8.31. show the expansion of cracks in the material and stress distribution at the critical crack length for first model.
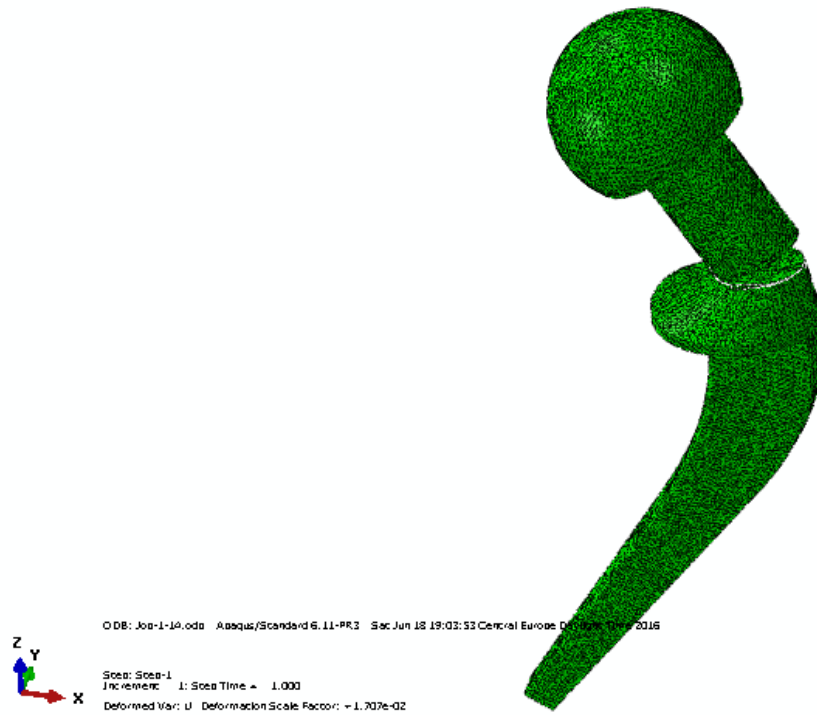
Figure 8.30. Numerical model 2 – critical crack length in calculation step 14
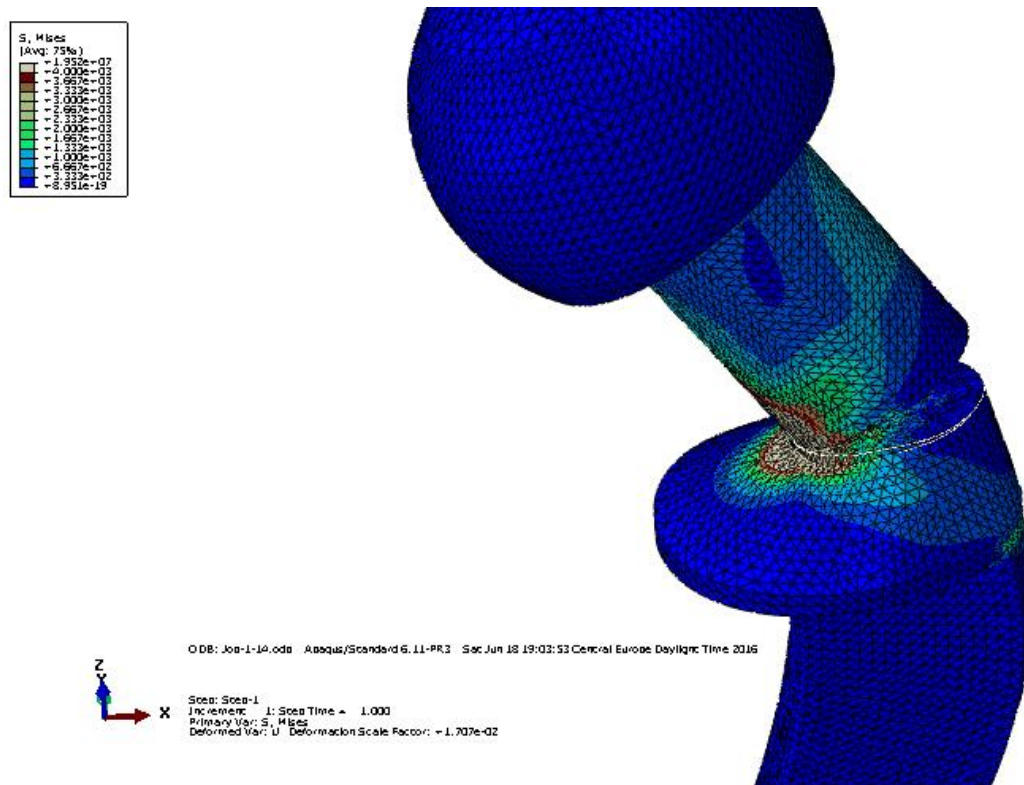
Figure 8.31. Numerical model 2 - Von Misses stress distribution

By applying numerical analysis on the model of an implant with crack fracture mechanics parameters were determined, i.e. value of the stress intensity factor K_I, K_{II} K_{III} i K_{ef}. It should be noted that all these values are determined for each calculation step. Based on theoretical considerations of the crack optening modes, it is clear that in this case of loading conditions on an implant, stress intensity factor values are much higher for the mode I than for modes II and III.

For each step of numerical calculation obtained stress intensity factors values K_I K_{II} and K_{III} are presented in Table 8.5. for model 1., and in Table 8.6. for model 2.

Table 8.5. K_i values for model 1

Calculation step	Crack length	K MPa√m		
		K_I	K_{II}	K_{III}
1	0.5	747.43	38.29	16.85
2	1	887.10	16.17	15.80
3	1.5	1042.62	21.98	7.93
4	2	1288.52	17.01	0.83
5	2.5	1556.34	16.65	6.69
6	3	1983.27	33.55	14.19
7	3.5	2716.15	37.63	22.28
8	4	3698.11	51.62	6.78
9	4.5	5806.34	109.64	33.78
10	5	10447.68	93.51	1.16
11	5.5	27257.73	989.75	193.49
12	6	114211.8	191.97	1148.49

Table 8.5. K_i values for model 2

Calculation step	Crack length	K MPa√m		
		K_I	K_{II}	K_{III}
1	0.3	4241.64	93.96	23.52
2	0.6	4922.05	23.22	7.22
3	0.9	5751.48	121.81	7.95
4	1.2	6691.27	13.70	16.00
5	1.5	8306.23	44.46	14.03
6	1.8	10037.27	105.37	12.22
7	2.1	12016.17	86.55	29.07
8	2.4	15465.3	82.59	80.06
9	2.7	20756.97	91.12	40.14
10	3	29100.4	8.46	26.06
11	3.3	44625.55	196.10	99.25
12	3.6	83769.63	238.65	125.97
13	3.9	203649	4138.50	1181.78
14	4.2	964839.2	34613.65	6764.18

It is possible to numerically predict number of walking cycles that will be critical if there is initial crack in implant, as shown on Figure 8.32. for model 1 and on Figure 8.33. for model 2.
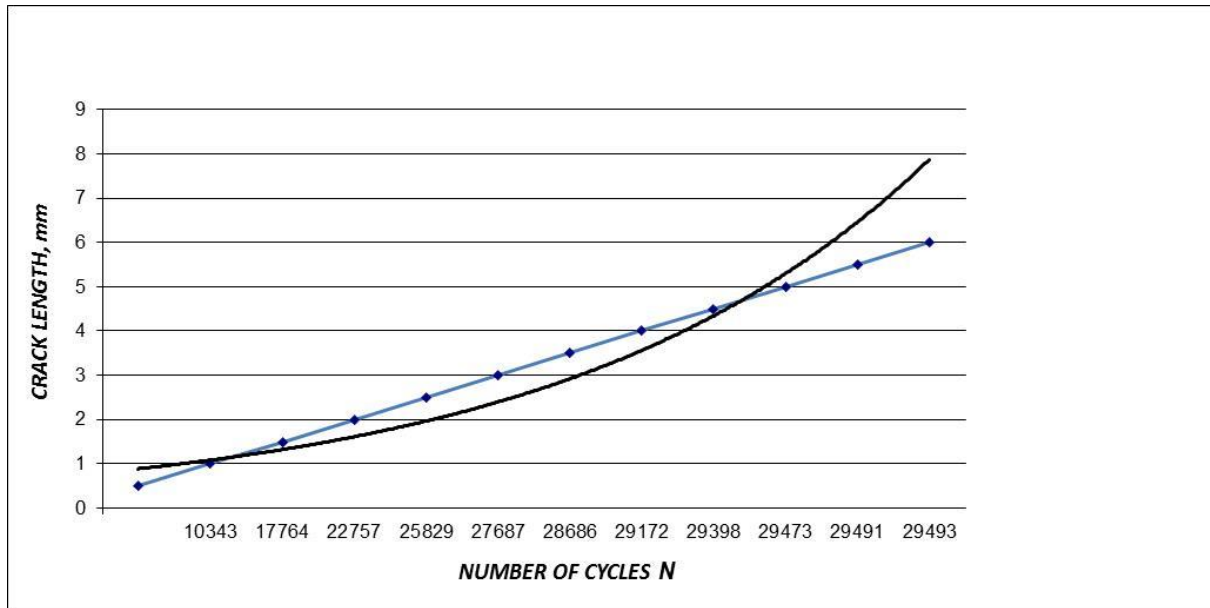
Figure 8.32. Structure integrity failure number of cycles for numerical model 1
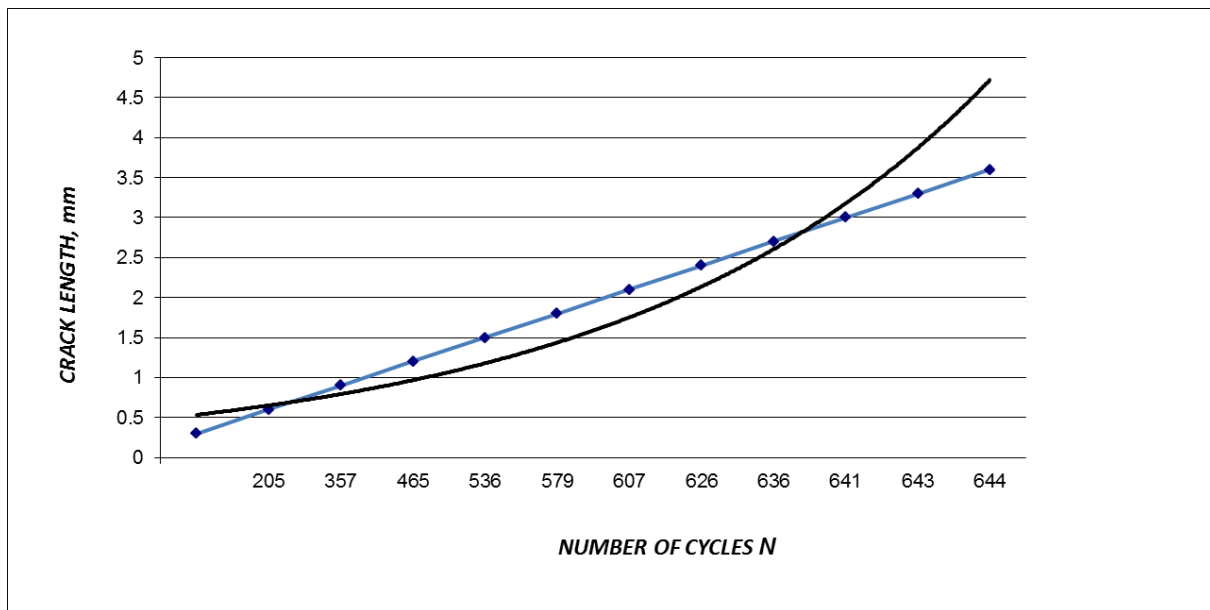
Figure 8.33. Structure integrity failure number of cycles for numerical model 2

It is recommended to assume an initial crack in a material in accordance with the fracture criteria K_{IC}, when crack growth occurs in case of $K_I \geq K_{IC}$, i.e. the linear elastic analysis fracture criteria.

Obtained values suggest that the hip prosthetic with an initial crack, subjected to a normal walking, i.e. which works under wlking cycle normal

conditions, will have a number of cycles equal to 29493 for model 1 and only 644 for model 2 before final fracture and prosthetic failure. Results were numerically and show the number of cycles after the crack was initiated, and with the application of numerical simulation, the number of cycles for which the prosthetic functions under normal conditions was determined, assuming there are no flaws in the material.

X-FEM had shown that it is an extremely efficient tool for numerical modelling of cracks in LEFM. Compared to standard FEM, X-FEM introduces significant improvements into numerical modelling of crack growth. Main advantages are that the finite element mesh does not need to be adjusted to crack boundaries (crack surface) in order to include geometric discontinuity, and that there is no need to regenerate the mesh in crack growth simulations.

It was shown that by applying modern numerical methods of biomaterial behaviour analysis it is possible to monitor three-dimensional crack behaviours in the material, as well as determining of characteristic fracture mechanics parameters.

CHAPTER 9

9.1 Conclusions

Generally speaking, as shown and discussed in this thesis, there are many influencing factors regarding integrity and life of hip implants. It is necessary to know precisely the loading, including variable stresses due to dynamic load, material properties and corrosion behaviour, including fracture mechanics properties, and stress distribution focused on concentration areas. Therefore, new, modern methods are needed for thorough analysis of this significant problem, starting from advanced experimental methods, using fracture mechanics approach to estimate structural integrity, and advance FEM numerical simulations, including fatigue crack growth, both in experimental and numerical research. It is also important to emphasize the need for mutual verification of experimental and numerical results.

More concretely, following conlusions cn be drawn, a for measurements and numerical analysis:

1) The plane strain fracture toughness of the commercially cold-drawn MP35N in all directions and configurations is high enough for crack resistance required for hip implant application.

2) Microstructure of stretch zone suggests that mixed loading conditions (elastic-plastic) are predominant around the crack tip at the stage of crack propagation initiation. The fracture surfaces in the T-T and L-T crack orientations indicate ductile shear fracture.

3) By applying stretch zone width determination method values are for J_i 150 N/mm, and the corresponding value for FSW 220 μm, being 70% of average measured value. Results indicate good agreement between measured values of critical stretch zone width, corresponding J_i parameter and fracture mechanics parameter J_{IC}.

4) The value of J_i obtained by stretch zone width determination method is not always precise enough, for it is possible to have greatly scattered measured values of critical stretch zone width.

5) FEM is reliable and powerful tool for stress-strain analysis of complex shaped implants, like artificial hip. It has been shown that by applying modern numerical methods to biomaterial behavior analysis, it is possible to monitor three-dimensional crack behavior in a material, as well as to determine fracture mechanics parameters.

6) Numerical simulation on developed models show that stress concentration occurs precisely in those areas, where in the examples from the practice, there was a fatigue fracture on the hip implant of very similar geometry. The areas on numerical models where there was maximum stress concentration coincide with the most common locations for the formation of cracks in biomaterials, which eventually lead to the weakening of the integrity of the prosthesis, or to failure.

7) A finite element analysis was performed using 3-dimensional models to examine the mechanical behaviour of the modular and block hip prosthesis at forces ranging from 3.5 to 6.0 kN. Results show that the force magnitudes acting on the implant are of interest, that according to implant biomaterial and design they can cause implant stress field changes, which can lead to structure integrity problems and implant failure.

8) the Extended finite element method (X FEM) provided good agreement of experimental and numerical result for the fatigue crack growth Ova metoda može dati dobre početne procene u smislu procene pouzdanosti, procene i integriteta implanta, a bez ispitivanja u in vivo uslovima.

9) During the optimization process in search of ideal biomaterials and geometry for hip replacement implants preclinical tests must be carried out in order to check whether new models can guarantee the mechanical resistance to the physiological load. It can be concluded that the application

of the finite element method (FEM) is good alternative approach to provide a preliminary results and overwiew of the mechanical properties of potential implant models.

10) Prevention of premature failure of orthopeadic hip implants has been a constant struggle for engineers. A multicentered study on the durability of implanted joint prostheses has clarified that the occurrence rate of either wear or breakage of the prostheses peaked during the 5-10 year period after implantation (Implant Committee of the Japanese Orthopedic Association, 2000).

11) The information provided in this thesis shows that mechanical and material issues are very important in the design and selection of materials for artificial hip implants. Failure of implants is due to mechanical reasons. Reviews of early fractures of femoral component made of Co-Cr alloy have identified several factors that contribute to catastrophic implant failure.

12) The ideal metal for a cemented component would have a high fatigue, yield and tensile strength, and corrosion resistance. Also, a high modulus of elasticity may be considered advantageous because it would reduce the strain in the cement around the component and decrease the risk of cement failure. On the other hand side, it would be disadvantageous because the bone may become so unloaded that disuse osteoporosis could develop, resulting in cement failure and subsequent loosening of the component.

13) Design parameters that should be considered for Co-Cr biomaterials are related to fatigue and fracture, corrosion, and wear. Prosthesis should be able to withstand 3 million cycles per year for an average individual. Fatigue analysis must take into consideration other factors that will prematurely weaken the material, such as corrosion and wear. In addition, combined effects of material failure modes working together should be considered.

Orthopedic biomechanics problems are not examine easily in vitro due to inaccessible locations and invasive methods. In order to obtain clinically useful models, the next step should involve the development of numerical models of the human bones in which the implant is located. It should be noted that the construction of these models is not an easy task, i.e. to get the most accurate results the first step would be scanning the human's hip for various patients, on what basis numerical models would be formed. Future work might also include design of numerical models that will take into account the impact of compound between human bones and hip implants, as well as simulation of the crack propagation in the cement biomaterial.

APPENDIX A

SEM analysis results
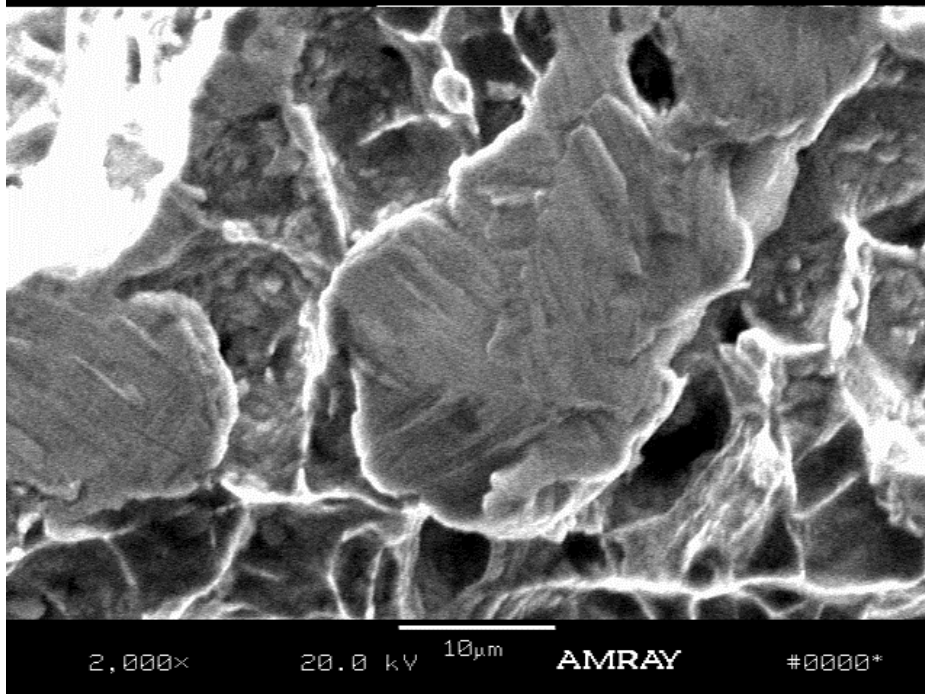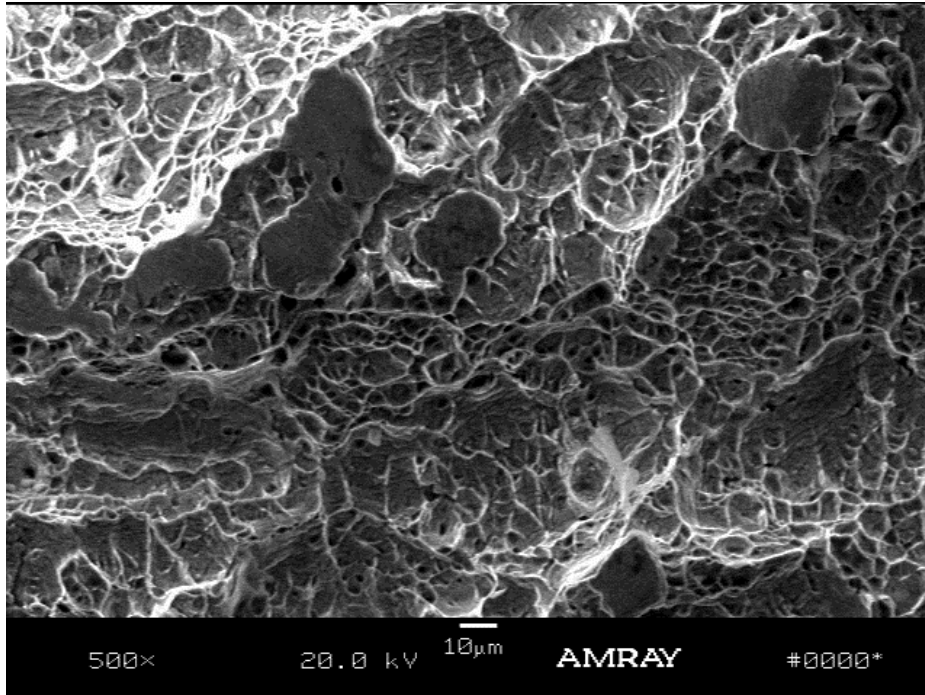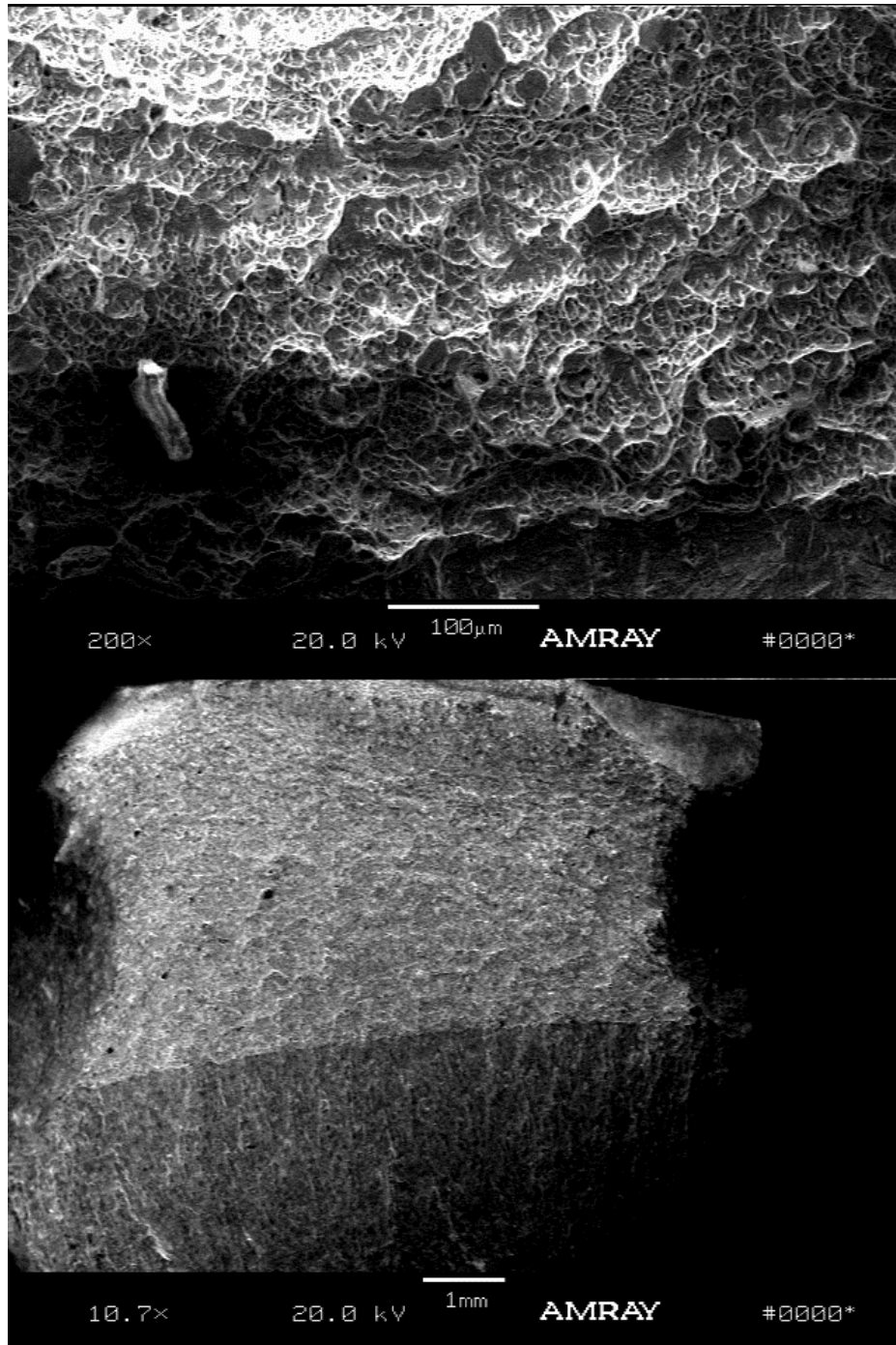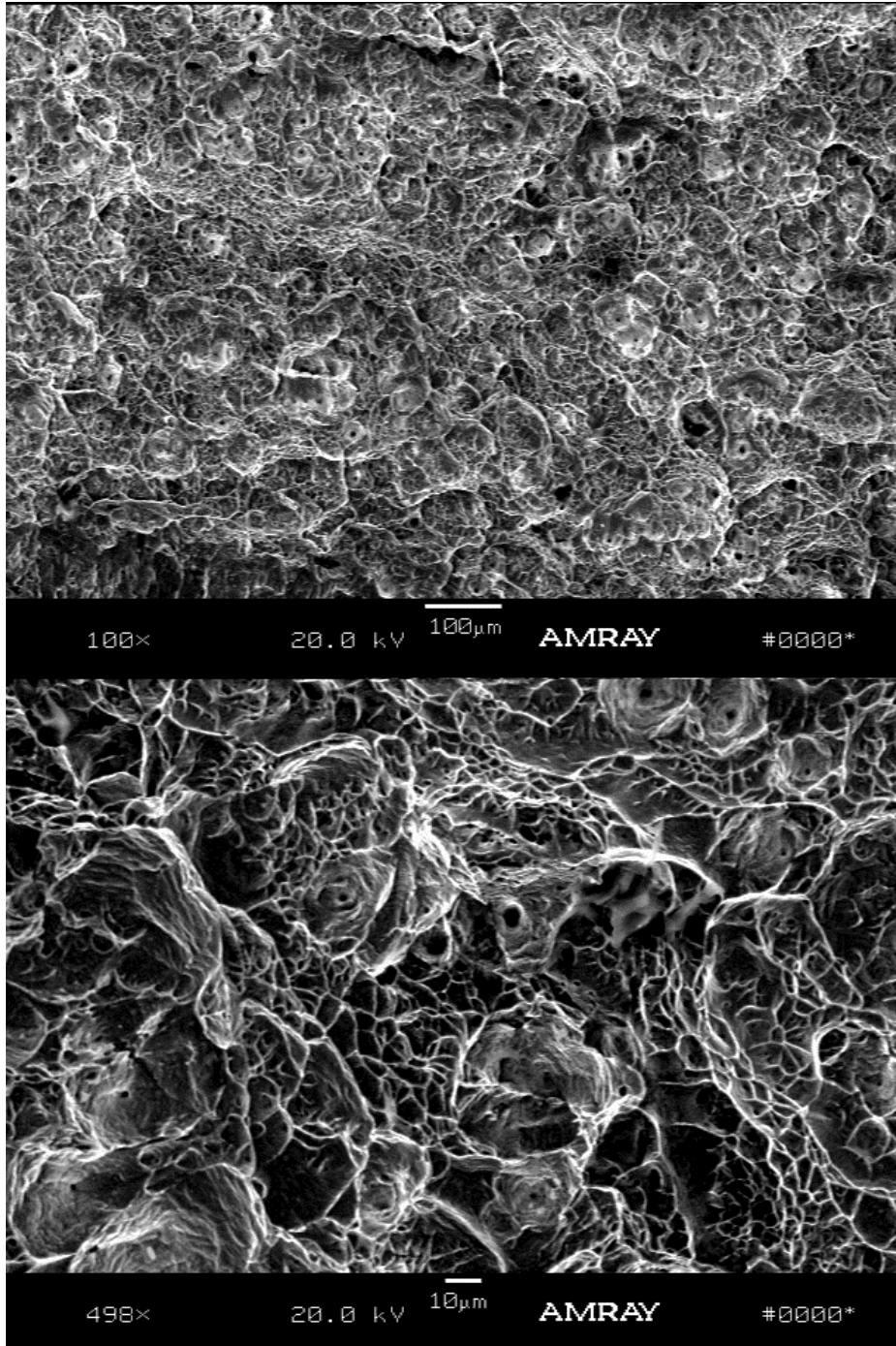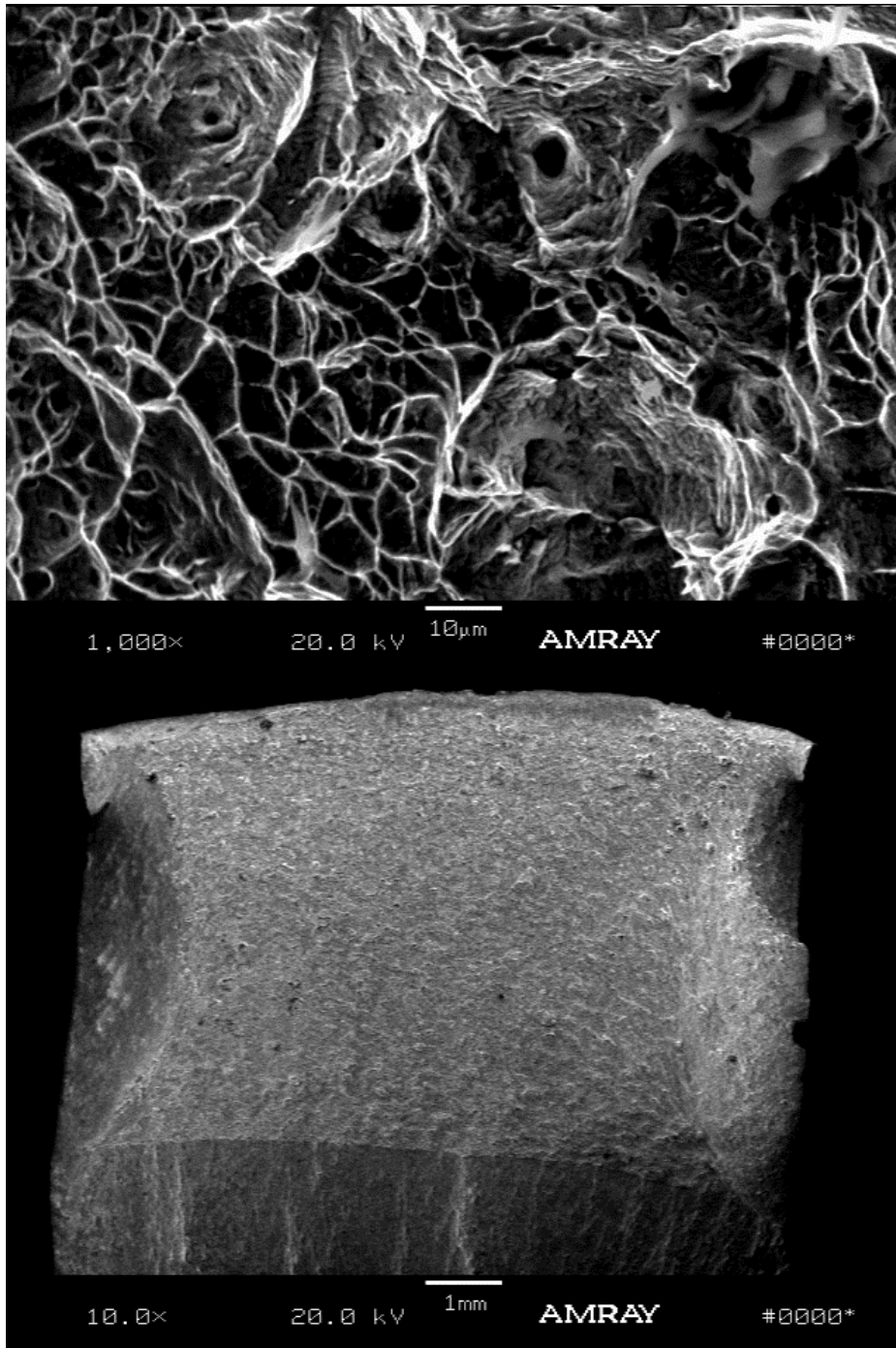
LITERATURE

1. J. Charnley, *Acrylic Cement in Orthopaedic Surgery*, E. S. Livingstone, Edinbourgh, 1970.

2. R.D. Beckenbaugh, D.M. Ilstrup, *Total hip arthroplasty*, Journal of Bone and Joint Surgery, 60 –A: 306-13, 1978.

3. Sir Walter Mercer, *Mercer's Orthopaedic Surgery*, Univ Park Pr, 8 Sub edition (February 1983)

4. J.B. Park, R.S. Lakes, *Biomaterials An Introduction* (Plenum Press, New York, 1992).

5. B.D. Ratner, A. S. Hoffman, F. J. Schoen, J. E. Lemons, *Biomaterials Science - An Introduction to Materials in Medicine*, Academic Press, San Diego, 1996.

6. Jeffrey N Katz, *Total joint replacement in osteoarthritis*, Best Practice & Research Clinical Rheumatology Vol. 20, No. 1, pp. 145–153, 2006.

7. W. Petty, *Total joint replacement*, W.B. Saunders Company, Philadelphia, 1991.

8. G. Bannister, *Primary total hip replacement*, The Surgeon Volume 1, Issue 6, pp. 332–341, 2003.

9. Katarina G. Čolić Fracture Behaviour Analysis Of Artificial Hip Biomaterials Doctoral Dissertation, Belgrade, 2012.

10. I. Milne, R.O. Ritcie, B. Karihaloo, *Comprehensive Structural Integrity,Vol. 9: Bioengineering* (Elsevier Ltd, Oxford, 2003).

11. A. Wang, A. Essner, *Three-body wear of UHMWPE acetabular cups by PMMA particles against CoCr, alumina and zirconia heads in a hip joint simulator*, Wear, 250, pp. 212–216, 2001.

12. T.P. Schmalzried, *et al.*, *The Mechanism of loosening of cemented acetabular components in total hip arthroplasty*, Clinical Orthopaedics, 274: pp. 60-77, 1992.

13. Schweizer M, Weber H, Schön R *Cobalt chromium molybdenum metal combination for modular hip prostheses*. Clin Orthop Relat Res. 1996 Aug;(329 Suppl):S35-47.

14. Toms AP, Marshall TJ, Cahir J, Darrah C, Nolan J, Donell ST, Barker T, Tucker JK. *MRI of early symptomatic metal-on-metal total hip arthroplasty: a retrospective review of radiological findings in 20 hips.* Clin Radiol. 2008 Jan;63(1):49-58. Epub 2007 Oct 24

15. Catelas I, Bobyn JD, Medley JB, Krygier JJ, Zukor DJ, Huk OL.*Size, shape, and composition of wear particles from metal-metal hip simulator testing: effects of alloy and number of loading cycles*. J Biomed Mater Res A. 2003 Oct 1;67(1):312-27.

16. B. Weisse, Ch. Affolter, G.P. Terrasi, G. Piskoty, S. Köbel, *Failure analysis of in vivo fractured ceramic femoral heads*, Engineering Failure Analysis Volume 16, Issue 4, pp. 1188–1194, 2009.

17. V. Good, K. Widding, G. Hunter, D. Heuer, *Oxidized zirconium: a potentially longer lasting hip implant*, Materials & Design Volume 26, Issue 7, pp. 618–622, 2005.

18. B.A.O. McCormack, P.J. Prendergast, *An analysis of crack propagation paths at implant/bone-cement interfaces*, Journal of Biomechanical Engineering, Vol. 118, pp. 579-585, 1996.

19. R. Huiskes, *Failed innovation in total hip replacement: Diagnosis and proposals for cure*, Acta Orthop Scand, 64 (6): pp. 699-716, 1993.

20. W. Pospula, *Total Hip Replacement: Past, Present and Future*, Kuwait Medical Journal, 36 (4), pp. 250-255, 2004.

21. Michael T. Manley, Kate Sutton, *Bearings of the Future for Total Hip Arthroplasty*, The Journal of Arthroplasty Vol. 23 No. 7 Suppl. 1, 2008.

22. Michael A. Mont *et al.*, *The Future of High Performance Total Hip Arthroplasty*, Seminars in Arthroplasty Volume 17, Issue 2, pp. 88–92, 2006.

23. George F. Chimento, Thomas P. Sculco, *Minimally Invasive Total Hip Arthroplasty*, Operative Techniques in Orthopaedics, Vol 11, No 4 (October), pp. 270-273, 2001.

24. Sakalkale DP1, Eng K, Hozack WJ, Rothman RH.*Minimum 10-year results of a tapered cementless hip replacement.* Clin Orthop Relat Res. 1999 May;(362):138-44.

25. W. Pompe *et al.*, *Functionally graded materials for biomedical applications*, Materials Science and Engineering A362, pp. 40–60, 2003.

26. N. Boudeau, D. Liksonov, T. Barriere, L. Maslov, J.-C. Gelin, Composite based on polyetheretherketone reinforced with carbon fibres, an alternative to conventional materials for femoral implant: Manufacturing process and resulting structural behaviour, Materials & Design Volume 40, pp. 148–156, 2012.

27. J.A. Simões, A.T. Marques, Design of a composite hip femoral prosthesis, Materials & Design Volume 26, Issue 5, pp. 391–401, 2005.

28. R. De Santis, L. Ambrosio, , L. Nicolais, Polymer-based composite hip prostheses, Journal of Inorganic Biochemistry.Volume 79, Issues 1–4, 30 April 2000, Pages 97–102

29. J.A. Simõesa, , A.T. Marquesb, G. Jeronimidisc, Design of a controlled-stiffness composite proximal femoral prosthesis. Composites Science and Technology, Volume 60, Issue 4, 1 March 2000, Pages 559–567

30. A. Sargeant, T. Goswami, *Hip implants – Paper VI – Ion concentrations*, Materials & Design Volume 28, Issue 1, pp. 155–171, 2007.

31. A. Sargeant, T. Goswami, *Hip implants: Paper V. Physiological effects*, Materials & Design Volume 27, Issue 4, pp. 287–307, 2006.

32. Catelas I, Medley JB, Campbell PA, Huk OL, Bobyn JD. *Comparison of in vitro with in vivo characteristics of wear particles from metal-metal hip implants*.J Biomed Mater Res B Appl Biomater. 2004 Aug 15;70(2):167-78.

33. St John KR, Zardiackas LD, Poggie RA.*Wear evaluation of cobalt-chromium alloy for use in a metal-on-metal hip prosthesis.* J Biomed Mater Res B Appl Biomater. 2004 Jan 15;68(1):1-14.

34. Witzleb WC1, Ziegler J, Krummenauer F, Neumeister V, Guenther KP.*Exposure to chromium, cobalt and molybdenum from metal-on-metal total hip replacement and hip resurfacing arthroplasty*. Acta Orthop. 2006 Oct;77(5):697-705.

35. Best SM, Porter AE, Thian ES et al (2008) Bioceramics: past, present and for the future. J Eur Ceram Soc 28(7):1319–132

36. Kontakis GM, Pagkalos JE, Tosounidis TI et al (2007) Bioabsorbable materials in orthopaedics. Acta Orthop Belg 73:159–169

37. Niinomi M, Nakai M, Hieda J (2012) Development of new metallic alloys for biomedical applications. Acta Biomater 8(11):3888–3903

38. Piskin E (1995) Biodegradable polymers as biomaterials. J Biomater Sci Polym Ed 6(9):775–795. doi:10.1163/156856295X00175

39. Sumayeh B. Abujaber, Adam R. Marmon, Federico Pozzi, James J. Rubano, Joseph A. Zeni Jr. Sit-To-Stand Biomechanics Before and After Total Hip Arthroplasty, The Journal of Arthroplasty Volume 30, Issue 11, November 2015, Pages 2027–2033

40. D.J. Simpson, A.P. Monk, D.W. Murray, H.S. Gill. Biomechanics in orthopaedics: considerations of the hip and knee.Surgery (Oxford) Volume 28, Issue 10, October 2010, Pages 478–482

41. Richard van Arkel, Andrew Amis. (i) Basics of orthopaedic biomechanics. Orthopaedics and Trauma.Volume 27, Issue 2, April 2013, Pages 67–75

42. Roy Abraham, Arthur L. Malkani, *Instability after Total Hip Replacement*, Seminars in Arthroplasty Volume 16, Issue 2, Pages 132–141, 2005.

43. Daniel P Nicolella et al. Probabilistic risk analysis of a cemented hip implant, Conference: American Society of Mechanical Engineers, Bioengineering Division (Publication) BED, Volume: 50, January 2001

44. Huiskes, Boeklagen. Mathematical Shape Optimization of Hip Prosthesis Design, 1989.

45. Chang, Williams, et al. Robust optimization of total joint replacements incorporating environmental variables, 1999

46. Monti Khatod et al. An Analysis of the Risk of Hip Dislocation with a Contemporary Total Joint Registry. Clinical orthopaedics and related research, Number 447, pp. 19–23, 2006.

47. ASTM F75 - 12 *Standard Specification for Cobalt 28 Chromium 6 Molybdenum Alloy Castings and Casting Alloy for Surgical Implants* (UNS R30075)

48. ASTM F139 - 08 *Standard Specification for Wrought 18Chromium 14Nickel 2.5Molybdenum Stainless Steel Sheet and Strip for Surgical Implants* (UNS S31673)

49. ASTM F1472 - 08e1 *Standard Specification for Wrought Titanium 6Aluminum 4Vanadium Alloy for Surgical Implant Applications* (UNS R56400)

50. ISO 7206-1:2008 Implants for surgery -- Partial and total hip joint prostheses -- Part 1: Classification and designation of dimensions

51. ISO 7206-2:2011 Implants for surgery -- Partial and total hip joint prostheses -- Part 2: Articulating surfaces made of metallic, ceramic and plastics materials

52. ISO 7206-4:2010 Implants for surgery -- Partial and total hip joint prostheses -- Part 4: Determination of endurance properties and performance of stemmed femoral components

53. ISO 7206-10:2003 Implants for surgery -- Partial and total hip-joint prostheses -- Part 10: Determination of resistance to static load of modular femoral heads

54. Predrag Djoredjevic, S. Kirin, A. Sedmak, E. Dzindo. Risk analysis in structural integrity, Structural Integrity and Life, 11(2) : 135-138, 2011.

55. Wolford LM1. Factors to consider in joint prosthesis systems. Proc (Bayl Univ Med Cent). 2006 Jul;19(3):232-8.

56. Cook SD, Kester MA, Harding AF, Brown TD, Sandborn PM.J Rehabil Metallurgical analysis of five failed cast cobalt-chromium-molybdenum alloy hip prostheses.Res Dev. 1986 Oct;23(4):27-36.

57. La Budde JK, Orosz JF, Bonfiglio TA, Pellegrini VD Jr.Particulate titanium and cobalt-chrome metallic debris in failed total knee arthroplasty. A quantitative histologic analysis. J Arthroplasty. 1994 Jun;9(3):291-304.

58. Michel Nganbe et al.Unusual Fatigue Failure of Cobalt Chrome Alloy Cementless Femoral Stem:Implant Retrieval and Biomechanical Analysis Journal of Medical and Biological Engineering,2009

59. M. Alvarez-Vera, J.H. Garcia-Duarte, A. Juarez-Hernandez, R.D. Mercado-Solis, A.G. Castillo, M.A.L. Hernandez-Rodriguez Failure analysis of Co–Cr hip resurfacing prosthesis during solidification Case Studies in Engineering Failure Analysis Volume 1, Issue 1, January 2013, Pages 1–5

60. Sedmak, A., Čolić, K., Burzić, Z., Tadić, S., Structural Integrity Assessment of Hip Implant Made of Cobalt-Chromium Multiphase Alloy, Structural Integrity and Life, 10(2) : 161-164, 2010.

61. Kohn DH, Ducheyne P, Cuckler JM, Chu AC, Radin S.Fractographic analysis of failed porous and surface-coated cobalt-chromium alloy total joint replacements. Med Prog Technol. 1994;20(3-4):169-77.

62. Lee E.W., Kim H. T., Early Fatigue Failures of Cemented, Forged, Cobalt-Chromium Femoral Stems at the Neck–Shoulder Junction,The Journal of Arthroplasty Vol. 16 No. 2 2001

63. Woolson S, Milbauer J, Bobyn JD, et al: Fatigue fracture of a forged cobalt-chromium-molybdenum femoral component inserted with cement: a report of ten cases. J Bone Joint Surg Am 79:1842, 1997

64. Evans EJ1, Benjamin M. The effect of grinding conditions on the toxicity of cobalt-chrome-molybdenum particles in vitro. Biomaterials. 1987 Sep;8(5):377-84

65. Devine TM, Wulff J. Cast vs. wrought cobalt-chromium surgical implant alloys. J Biomed Mater Res. 1975 Mar;9(2):151-67.

66. Dielert E, Milachowski K, Schramel P. The role of the alloy-specific elements iron, cobalt, chromium and nickel in aseptic loosening of total hip joint prosthesis[Article in German], Orthop Ihre Grenzgeb. 1983 Jan-Feb;121(1):58-63.

67. Ducheyne P, De Meester P, Aernoudt E. Performance analysis of total hip prostheses: some particular metallurgical observations. J Biomed Mater Res. 1980 Jan;14(1):31-40.

68. Michel R, Nolte M, Reich M, Löer F. Systemic effects of implanted prostheses made of cobalt-chromium alloys.Arch Orthop Trauma Surg. 1991;110(2):61-74.

69. Jacobs JJ, Skipor AK, Doorn PF, Campbell P, Schmalzried TP, Black J, Amstutz HC.Cobalt and chromium concentrations in patients with metal on metal total hip replacements. Clin Orthop Relat Res. 1996 Aug;(329 Suppl):S256-63.

70. Maezawa K1, Nozawa M, Hirose T, Matsuda K, Yasuma M, Shitoto K, Kurosawa H Cobalt and chromium concentrations in patients with metal-on-metal and other cementless total hip arthroplasty. Arch Orthop Trauma Surg. 2002 Jun;122(5):283-7. Epub 2002 Feb 28.

71. Merritt K, Brown SA.Distribution of cobalt chromium wear and corrosion products and biologic reactions. Clin Orthop Relat Res. 1996 Aug;(329 Suppl):S233-43.

72. Varano R1, Bobyn JD, Medley JB, Yue S.Effect of microstructure on the dry sliding friction behavior of CoCrMo alloys used in metal-on-metal hip implants. J Biomed Mater Res B Appl Biomater. 2006 Feb;76(2):281-6.

73. Jakobsen SS1, Danscher G, Stoltenberg M, Larsen A, Bruun JM, Mygind T, Kemp K, Soballe K., Cobalt-chromium-molybdenum alloy causes metal accumulation and metallothionein up-regulation in rat liver and kidney. Basic Clin Pharmacol Toxicol. 2007 Dec;101(6):441-6. Epub 2007

74. Della Valle AG, Becksaç B, Anderson J, Wright T, Nestor B, Pellicci PM, Salvati EA.Late fatigue fracture of a modern cemented [corrected] cobalt chrome stem for total hip arthroplasty: a report of 10 cases. J Arthroplasty. 2005 Dec;20(8):1084-8.

75. Lam LO, Stoffel K, Kop A, Swarts E.Catastrophic failure of 4 cobalt-alloy Omnifit hip arthroplasty femoral components. Acta Orthop. 2008 Feb;79(1):18-21. doi: 10.1080/17453670710014707.

76. Nimb L1, Gotfredsen K, Steen Jensen J.Mechanical failure of hydroxyapatite-coated titanium and cobalt-chromium-molybdenum alloy implants. An animal study. Acta Orthop Belg. 1993;59(4):333-8.

77. Decking R1, Reuter P, Hüttner M, Puhl W, Claes LE, Scharf HP.Surface composition analysis of failed cementless CoCr- and Ti-base-alloy total hip implants. J Biomed Mater Res B Appl Biomater. 2003 Feb 15;64(2):99-106.

78. Schmidt M, Weber H, Schön R. Cobalt chromium molybdenum metal combination for modular hip prostheses. Clin Orthop Relat Res. 1996 Aug;(329 Suppl):S35-47.

79. Parida P, Behera A, Mishra SC Classification of biomaterials used in medicine. Int J Adv Appl Sci 1(3):31–35(2012)

80. Patel NR, Gohil PP A review on biomaterials: scope, applications & human anatomy significance. Int J Emerg Techno Adv Eng 2(4):91–101(2012)

81. Williams DF The williams dictionary of biomaterials. Liverpool University Press. doi:10.5949/UPO9781846314438. (1999)

82. Khalid A. Syed, Rajiv Gandhi, Nizar N. Mahomed, THA for Failed Internal Fixation of Proximal Femur Fractures and Retained Hardware, Seminars in Arthroplasty 19, pp. 307-313, 2008.

83. Beim, G.M., Lavernia, C., Convey, F.R., Intramedullary plugs in cemented hip arthroplasty, Journal of Arthroplasty, 4, pp. 139-141 , 1989.

84. Jos Vander Sloten, Luc Labey, Remi Van Audekercke, Georges Van der Perre, Materials selection and design for orthopaedic implants with improved long-term performance, Biomaterials 19, pp. 1455-1459, 1998.

85. H. Malchau, P. Herberts, Prognosis of total hip replacement. Surgical and cementing technique in THR: A revision-risk study of 134,359 primary operations, rdScientific Exhibition presented at the 63Annual Meeting of the AAOS, 1996.

86. Damien P. Byrne, Kevin J. Mulhall and Joseph F. Baker; Anatomy & Biomechanics of the Hip; The Open Sports Medicine Journal, 2010, 4, 51-57

87. Varano R1, Bobyn JD, Medley JB, Yue S.The effect of microstructure on the wear of cobalt-based alloys used in metal-on-metal hip implants. Proc Inst Mech Eng H. 2006 Feb;220(2):145-59.

88. Wagner M, Wagner H. Medium-term results of a modern metal-on-metal system in total hip replacement. Clin Orthop Relat Res. 2000 Oct;(379):123-33.

89. Fisher J. et al., An in vitro study of the reduction in wear of metal-on-metal hip prostheses using surface-engineered femoral heads. Proc Inst Mech Eng H. 2002;216(4):219-30.

90. Daniel J, Ziaee H, Pradhan C, McMinn DJ. Systemic metal exposure in large- and small-diameter metal-on-metal total hip replacements. Orthopedics. Dec;31(12 Suppl 2) 2008.

91. K.-D. Kühn, *Bone Cements: Up-to-date comparison of physical and mechanical properties of commercial materials*, Springer Verlag New York , 2000.

92. E.W. Fritsch, *Static and Fatigue properties of two new low-viscosity PMMA bone cements improved by vacuum mixing*, Journal of Biomedical Materials Research, Vol. 32, pp. 451-456, 1996.

93. N. Verdonschot, R. Huiskes, *Mechanical effects of stem cement interface characteristics in total hip replacement*. Clinical Orthopaedics, 329:326-36, 1996a.

94. R. Huiskes, *Mechanical failure in total hip arthroplasty with cement*, Current Orthopaedics, 7, 239-247, 1993a.

95. T.P. Culleton, P.J. Prendergast, D. Taylor, Fatigue failure in the cement mantle of an artificial hip joint. Clinical Materials, 12: pp. 95-102, 1993.

96. Sotereanos NG, Engh CA, Glassman AH, Macalino GE, Engh CA Jr.Cementless femoral components should be made from cobalt chrome. Clin Orthop Relat Res. 1995 Apr;(313):146-53.

97. Nag S, Banerjee R (2012) Fundamentals of medical implant materials. In: Narayan R (ed) ASM handbook, vol 23, Materials for medical devices. ASM International, North Texas, pp 6–17

98. Harpal S. Khanuja et al. Cementless Femoral Fixationin Total Hip Arthroplasty; the journal of bone &joint surger. volume 93-a d number 5 d march 2, 2011

99. Park, J.B. "Hip Joint Prosthesis Fixation-Problems and Possible Solutions." The Biomedical Engineering Handbook: Second Edition, CRC Press LLC, 2000, 46.1 - 46.3

100.　　P.J. Gard, Fracs R. Iorio, W.L. Healy, Hip replacement: Choosing an implant, Operative Techniques in Orthopaedics Volume 10, Issue 2, pp. 94–101, 2000.

101.　　K. H. Chiu *et al.*, *Osteonecrosis of the Femoral Head Treated With Cementless Total Hip Arthroplasty*, The Journal of Arthroplasty Vol. 12 No. 6, 1997.

102.　　J.A. Johnson, *et al.*, *Fatigue of acrylic bone cement-effect of frequency and environment*, Journal of Biomedical Materials Research, Vol. 23, pp. 819-831, 1989.

103.　　Branko Ristić et al. Izbor biomaterijala u ortopedskoj hirurgiji;UDC:615.477::617.3-089-77

104.　　L.C. Zhanga, E.C.S Kiat, A. Pramanikc; A Briefing on the Manufacture of Hip Joint Prostheses; Advanced Materials Research Vols. 76-78 (2009) pp 212-216

105. Stuart Goodman; Bearing Surfaces for Joint Replacement: New Materials or New Problems; DOI 10.1007/978-1-4614-8999-3_2, © Springer Science+Business Media NewYork 2014

106. Buford A., Goswami T., Review of wear mechanisms in hip implants: Paper I – General, Materials and Design 25 (2004) 385–393

107. M. Slonaker, T. Goswami, Review of wear mechanisms in hip implants: PaperII–ceramics IG004712, Materials and Design, 25, pp. 395–405, 2004.

108. Yerby SA1, Taylor JK, Park J, Shackelford JF.Corrosion at the interface. A possible solution to cobalt-chrome heads on titanium alloy stems. J Arthroplasty. 1996 Feb;11(2):157-62.

109. K. Colic, A. Sedmak, N. Gubeljak, M. Burzic, S. Petronic, Experimental analysis of fracture behavior of stainless steel used for biomedical applications, Integritet i vek konstrukcija (Structural Integrity and Lifre). 2012, Vol. 12 No. 1, pp. 59-63, 2012.

110. D. M. Brunette, P. Tengvall, M. Textor, P. Thomsen, Titanium in Medicine, Springer, Berlin, 2001.

111. Tompkins GS, Lachiewicz PF, DeMasi R. A prospective study of a titanium femoral component for cemented total hip arthroplasty. J Arthroplasty. 1994 Dec;9(6):623-30

112. Marti A. Cobalt-base alloys used in bone surgery. Injury. Dec;31 Suppl 4:18-21. 2000

113. Bridgeport DA, Brantley WA, Herman PF Cobalt-chromium and nickel-chromium alloys for removable prosthodontics, Part 1: Mechanical properties. J Prosthodont. 1993 Sep;2(3):144-50.

114. Holzwarth U, Thomas P, Kachler W, Göske J, Schuh A. [Metallurgical differentiation of cobalt-chromium alloys for implants]. [Article in German] Orthopade. 2005 Oct;34(10):1046-7, 1049-51.

115. Gómez M, Mancha H, Salinas A, Rodríguez JL, Escobedo J, Castro M, Méndez M.Relationship between microstructure and ductility of

investment cast ASTM F-75 implant alloy. J Biomed Mater Res. Feb;34(2):157-63. 1997

116.   Vallittu PK, Kokkonen M.*Deflection fatigue of cobalt-chromium, titanium, and gold alloy cast denture clasp*. J Prosthet Dent. 1995 Oct;74(4):412-9.

117.   Vallittu PK, Luotio K.*Effects of cobalt-chromium alloy surface casting on resistance to deflection fatigue and surface hardness of titanium*. Int J Prosthodont. 1996 Nov-Dec;9(6):527-32.

118.   Price JW. Elevated chromium levels and prosthetic joint implants. J Am Osteopath Assoc. 2011 Sep;111(9):548-50.

119.   V.C. Mow, W.C. Hayes, Basic Orthopaedic Biomechanics, 2nd edition, Lippincott - Raven, Philadelphia, 1997.

120.   R. Bruce Martin, David B. Burr, Neil A. Sharkey (Eds.), Skeletal Tissue Mechanics, Springer, New York, 1998

121.   P.J. Prendergast, Bone Mechanics Handbook, Bone prostheses and implants, CRC Press, New York, 2000.

122.   M. A. L. Hernandez-Rodriguez, J. A. Ortega-Saenz, G. R. Contreras-Hernandez, „Failure analysis of a total hip prosthesis implanted in active patient", Journal of the Mechanical Behavior of Biomedical Materials 3, pp. 619–622, 2010.

123.   Al Jabbari Y1, Fournelle R, Ziebert G, Toth J, Iacopino A.Mechanical behavior and failure analysis of prosthetic retaining screws after long-term use in vivo. Part 2: Metallurgical and microhardness analysis. J Prosthodont. 2008 Apr;17(3):181-91. Epub 2007 Nov 28.

124.   Swarts E, Miller SJ, Keogh CV, Lim G, Beaver RJ.Fractured Whiteside Ortholoc II knee components. J Arthroplasty. 2001 Oct;16(7):927-34.

125.   Kaled Legweel, Aleksandar Sedmak, Katarina Čolić, Miloš Milošević, Nenad Mitrović, Žarko Mišković, Sergej Hloch, Experimental

and numerical research of mechanical behaviour of titanium alloy hip implant, Technical Gazette ISSN 1330-3651 (print) ISSN1848-6339 (Online), Vol. 24/No. 3, 2017., DOI: 10.17559/TV-20160219132016

126. Jesus Chao, Victor Lopez, „Failure analysis of a Ti6Al4V cementless HIP prosthesis", Engineering Failure Analysis 14, pp. 822–830, 2007.

127. S. Griza et al., Fatigue failure analysis of a specific total hip prosthesis stem design, International Journal of Fatigue 30, pp. 1325–1332, 2008.

128. Gosheger G1, Goetze C, Hardes J, Joosten U, Winkelmann W, von Eiff C.The influence of the alloy of megaprostheses on infection rate. J Arthroplasty. 2008 Sep;23(6):916-20. doi: 10.1016/j.arth.2007.06.015. Epub 2008 Feb 13.

129. Szuszczewicz ES, Schmalzried TP, Petersen TD.Progressive bilateral pelvic osteolysis in a patient with McKee-Farrar metal-metal total hip prostheses. J Arthroplasty. 1997 Oct;12(7):819-24.

130. M. Sumita, Corrosion fatigue and fretting corrosion fatigue. In: "Metallic Biomaterials-Fundamentals and Applications," eds. M. Sumita, Y. Ikada and T. Tateishi, IPC, Tokyo, pp. 233 270. 2000

131. G. Bergmann, F. Gracichen, A. Rohlmann, Hip joint loading during walking and running measured in two patients, Journal of Biomechanics, vol 26, pp. 969-990, 1993.

132. G. Bergmann et al., Hip contact forces and gait patterns from routine activities, Jour. of Biomechanics 34, pp. 859-871, 2001.

133. S. Griza et al., „Design aspects involved in a cemented THA stem failure case", Engineering Failure Analysis Volume 16, Issue 1, pp. 512–520, 2009.

134. S. Griza, , M. Reis, Y. Reboh, A. Reguly, T.R. Strohaecker. Failure analysis of uncemented total hip stem due to microstructure and neck

stress riser. Engineering Failure Analysis Volume 15, Issue 7, October 2008, Pages 981–988

135.   Rui B. Ruben, Paulo R. Fernandes, João Folgado, On the optimal shape of hip implants, Journal of Biomechanics Volume 45, Issue 2, pp. 239–246, 2012.

136.   Tirupathi R. Chandrupatla, Ashok D. Belegundu, Introduction to Finite Elements in Engineering, Prentice Hall, 2012.

137.   J. N. Reddy, An Introduction to the Finite Element Method, McGraw-Hill: New York, 2005.

138.   K.J. Bathe, Finite Element Procedures in Engineering Analysis, Prentice Hall , Englewood Cliffs, 1982.

139.   A.Z. Senalp, O. Kayabasi, H. Kurtaran, Static, dynamic and fatigue behavior of newly designed stem shapes for hip prosthesis using finite element analysis, Materials and Design, 28, pp. 1577–1583, 2007.

140.   Brummitt K, Hardaker CS, McCullagh PJ, Drabu KJ, Smith RA Effect of counterface material on the characteristics of retrieved uncemented cobalt-chromium and titanium alloy total hip replacements.Proc Inst Mech Eng H. 1996;210(3):191-5.

141.   Piotr Niesłony, Wit Grzesik, Piotr Laskowski, Jan Sienawski. Numerical and Experimental Analysis of Residual Stresses Generated in the Machining of Ti6Al4V Titanium Alloy. 2nd CIRP Conference on Surface Integrity (CSI), Procedia CIRP, Volume 13, 2014, Pages 78–83

142.   David Bennett, Tarun Goswami, Finite element analysis of hip stem designs, Materials & Design, Volume 29, Issue 1, 2008, Pages 45–60

143.   E. Pyburn, T. Goswami, Finite element analysis of femoral components paper III–hip joints, Materials and Design, 25, pp. 705–713, 2004.

144.   Manish Paliwal, D. Gordon Allan, Peter Filip, „Failure analysis of three uncemented titanium-alloy modular total hip stems", Engineering Failure Analysis Volume 17, Issue 5, pp. 1230–1238, 2010.

145.   N Nuño, M Amabili. Modelling debonded stem–cement interface for hip implants: effect of residual stresses. Clinical BiomechanicsVolume 17, Issue 1, January 2002, Pages 41–48

146.   Makarand G. Joshi, Suresh G. Advani, Freeman Miller, Michael H. Santare, Analysis of a femoral hip prosthesis designed to reduce stress shielding, Journal of Biomechanics 33, pp. 1655-1662, 2000.

147.   S Gross, E.W Abel, A finite element analysis of hollow stemmed hip prostheses as a means of reducing stress shielding of the femur, Journal of Biomechanics, Volume 34, Issue 8, August 2001, Pages 995–1003

148.   Maroš Hrubina, Zdeněk Horák, Radek Bartoška, Leoš Navrátil, Jozef Rosina Computational modeling in the prediction of Dynamic Hip Screw failure in proximal femoral fractures Journal of Applied Biomedicine. Volume 11, Issue 3, 2013, Pages 143–151

149.   I. Balac, K. Colic, M. Milovancevic, P. Uskokovic, M. Zrilic, Modeling of the Matrix Porosity Influence on the Elastic Properties of Particulate Biocomposites, FME Transactions. 2012, Vol. 40, No. 2, pp. 81-86 ISSN 1451-2092, 2012.

150.   J. Geringer, L. Imbert, K. Kim Computational Modelling of Biomechanics and Biotribology in the Musculoskeletal System, 13 – Computational modeling of hip implants, Biomaterials and Tissues, Woodhead Publishing Limited, 2014, Pages 389–416

151.   R. Huiskes, E. Y. S. Chao - A Survey of Finite Element Analysis in Orthopedic Biomechanics, The First Decade; J. Biomechanics Vol. 16, No 6.,1983

152.   PJ Prendergast Clinical Finite element models in tissue mechanics and orthopaedic implant design Biomechanics Volume 12, Issue 6, September 1997, Pages 343–366

153.   Huiskes, Hollister From Structure to Process, From Organ to Cell: Recent Developments of FE-Analysis in Orthopaedic, 1993

154.   Zohar Yosibasha, , , Alon Katza, Charles Milgromb, Toward verified and validated FE simulations of a femur with a cemented hip prosthesis. Medical Engineering & Physics. Volume 35, Issue 7, July 2013, Pages 978–987

155.   Javad Hazrati Marangalou, Keita Ito, Bert van Rietbergen. A new approach to determine the accuracy of morphology–elasticity relationships in continuum FE analyses of human proximal femur. Journal of Biomechanics. Volume 45, Issue 16, 15 November 2012, Pages 2884–2892

156.   A.F. Bower, Applied Mechanics of Solids, CRC Press, 2009.

157.   G. T. Mase, G. E. Mase, Continuum Mechanics for Engineers 2nd ed., CRC Press, Florida, 1999.

158.   T. Belytschko, T. Black, Elastic crack growth in finite elements with minimal remeshing, International Journal for Numerical Methods in Engineering, Vol. 45, No. 5, pp. 601-620, 1998.

159.   N. Moës, J. Dolbow, T. Belytschko, A finite element method for crack growth without remeshing, International Journal for Numerical Methods in Engineering, Vol. 46, No. 1, pp. 131-150, 1999.

160.   B.L. Karihaloo, Q.Z. Xiao, Modelling of stationary and growing cracks in FE framework without remeshing: a state-of-the-art review, Computers & Structures, Volume 81, Issue 3, pp. 119-129, 2003.

161.   T.L. Anderson, Fracture Mechanics: Fundamentals and Applications, 3rd ed, CRC Press, London, 2005.

162.   D. Broek, Elementary Engineering Fracture Mechanics, 3rd Edition, Martinus Nijhoff Publishers, The Hague, 1982.

163.   E.E. Gdoutos, Fracture Mechanics An Introduction, Springer, Netherlands, 2005.

164.   A. Sedmak, Primena mehanike loma na integritet konstrukcija, Mašinski fakultet, Beograd, 2003.

165.   Schijve J., Fatigue of Structuresand Materials, Springer, 2009.

166.   Bullen W.P., Head A.K., Wood W.A., Structural changes during the fatigue of metals. Proc. Roy. Soc., Vol. A216, 1953, p. 332.

167.   G. Pluvinage, Fracture and Fatigue Emanating from Stress Concentrators, Springer, Dordrecht, 2004.

168.   GC, Macdonald Fracture mechanics applied to engineering problems – strain energy density fracture criterion. Eng Fract Mech 1974;6:361–86

169.   ASTM E399-06, Standard Test Method for Linear-Elastic Plane Strain Fracture Toughness of Metallic Materials

170.   ASTM E1820-08, Standard Test Method for Measurement of Fracture Toughness

171.   Khaled Legweel, Aleksandar Sedmak, Katarina Colic, Zijah Burzic, Lana Gubeljak. Final stretch zone width determination for mp35n multiphase alloy. Structural Integrity and Life, 15(3) : 163-167, 2015.

172.   E.M. Shaji, S.R. Kalidindi, R.D. Doherty, A.S. Sedmak, Plane strain fracture toughness of MP35N in aged and unaged conditions measured using modified CT specimens, Materials Science and Engineering A 340, pp. 163-169, 2003.

173.   E.M. Shaji, S.R. Kalidindi, R.D. Doherty, A.S. Sedmak, Fracture properties of multiphase alloy MP35N, Materials Science and Engineering A 349, pp. 313-317, 2003.

174.   E. Giner, N. Sukumar, J.E. Tarancón, F.J. Fuenmayor, An Abaqus implementation of the extended finite element method, Engineering Fracture Mechanics , Volume 76, Issue 3, February 2009, Pages 347–368

175.   Jianxu Shi, David Chopp, Jim Lua, N. Sukumar, Ted Belytschko , Abaqus implementation of extended finite element method using a level set representation for three-dimensional fatigue crack growth and life predictions, Engineering Fracture Mechanics, Volume 77, Issue 14, September 2010, Pages 2840–2863

176.   Grbović A., Rašuo B., Vidanović N., Perić M., Simulation of Crack Propagation in Titanium Mini Dental Implants (MDI), FME Transactions, Volume 39, No 4, 2011, pp. 165-170.

177.   Jay Oswald, Robert Gracie, Roopam Khare, Ted Belytschko, An extended finite element method for dislocations in complex geometries: Thin films and nanotubes, Computer Methods in Applied Mechanics and Engineering, Volume 198, Issues 21–26, pp. 1872-1886, 2009.

178.   J. Dolbow, N. Moës, and T. Belytschko, "Discontinuous enrichment in finite elements with a partition of unity method," Finite elements in analysis and design, vol. 36, no. 3, pp. 235–260, 2000.

179.   Li Ming Zhou, Guang Wei Meng, Feng Li, and Shuai Gu, "A Cell-Based Smoothed XFEM for Fracture in Piezoelectric Materials," Advances in Materials Science and Engineering, vol. 2016, Article ID 4125307, 14 pages, 2016. doi:10.1155/2016/4125307

180.   Fei Liu, Li-qiang Zhao, Ping-li Liu, Zhi-feng Luo, Nian-yin Li, and Pei-shan Wang, "An Extended Finite Element Model for Fluid Flow in Fractured Porous Media," Mathematical Problems in Engineering, vol. 2015, Article ID 604212, 10 pages, 2015. doi:10.1155/2015/604212

181.   Youshi Jiang, Jinzhou Zhao, Yongming Li, Hu Jia, and Liehui Zhang, "Extended Finite Element Method for Predicting Productivity of Multifractured Horizontal Wells," Mathematical Problems in Engineering, vol. 2014, Article ID 810493, 9 pages, 2014. doi:10.1155/2014/810493

182.   Wei Li, Huangjian Yi, Qitan Zhang, Duofang Chen, and Jimin Liang, "Extended Finite Element Method with Simplified Spherical Harmonics Approximation for the Forward Model of Optical Molecular Imaging," Computational and Mathematical Methods in Medicine, vol. 2012, Article ID 394374, 10 pages, 2012. doi:10.1155/2012/394374

183.   Nicolas Moës,Ted Belytschko, Extended finite element method for cohesive crack growth, Engineering Fracture Mechanics, Volume 69, Issue 7, May 2002, Pages 813–833

184.   Stolarska, D.L. Chopp Modeling thermal fatigue cracking in integrated circuits by level sets and the extended finite element method, International Journal of Engineering Science, Volume 41, Issue 20, December 2003, Pages 2381–2410

185.   N. Sukumar, N. Moes, P. B. Moran, and T. Belytschko, "Extended finite element method for three-dimensional crack modeling," International Journal of Numerical Methods in Engineering, vol. 48, pp. 1549–1570, 2000.

186.   T. Belytschko and T. Black, "Elastic crack growth in finite elements with minimal remeshing," International Journal for Numerical Methods in Engineering, vol. 45, no. 5, pp. 601–620, 1999.

187.   N. Moës, J. Dolbow, and T. Belytschko, "A finite element method for crack growth without remeshing," International Journal for Numerical Methods in Engineering, vol. 46, no. 1, pp. 131–150, 1999

188.   S. Mohammadi, Extended finite element method for fracture analysis of structure, Blackwell Publishing Ltd., Oxford, UK, 2008.

189.   Yazid Abdelaziz, Abdelmadjid Hamouine, A survey of the extended finite element, Computers & Structures, Volume 86, Issues 11–12, pp. 1141-1151, 2008.

BIOGRAFIJA AUTORA

Kaled M. B. Legweel rođen je 7.3.1972 u mestu Sebha u Libiji. Oženjen je i državljanin je Libije.

Osnovnu i srednju školu je završio u mestu Ghordah, Shati u Libiji. Diplomirao je 1997. godine na University of Sebha, Libija. Master rad završio je 2005. godine na University of Newcastle Upon Tyne, England, Faculty of Science, Agriculture and Engineering, Department of Automation and Control. Radio kao inženjer Održavanja u General Electronic Company, Tripoli, Libija, 1995-1996. Godine. Radi na Sebha High Institute, Sebha, Libija, od 1996. godine.

Upisao je doktorske studije na Mašinskom fakultetu Univerziteta u Beogradu 2009. godine. Tokom izrade teze bavio se problemima mehanike loma, primenom numeričkih metoda i radom u laboratorijama Mašinskog fakulteta Univerziteta u Beogradu. Objavio je više naučnih i stručnih radovima različitih kategorija na konferencijama i u časopisima.

Прилог 1.

Изјава о ауторству

Потписани Kaled M. B. Legweel

број индекса

Изјављујем

да је докторска дисертација под насловом

Утицај биоматеријала на интегритет и век вештачког кука

- резултат сопственог истраживачког рада,
- да предложена дисертација у целини ни у деловима није била предложена за добијање било које дипломе према студијским програмима других високошколских установа,
- да су резултати коректно наведени и
- да нисам кршио/ла ауторска права и користио интелектуалну својину других лица.

Потпис докторанда

У Београду, 21.06.2016.

_____

Прилог 2.

Изјава о истоветности штампане и електронске верзије докторског рада

Име и презиме аутора Kaled M. B. Legweel

Број индекса

Студијски програм

Наслов рада Утицај биоматеријала на интегритет и век вештачког кука

Ментор Проф. др Александар Седмак

Потписани/а Kaled M. B. Legweel

Изјављујем да је штампана верзија мог докторског рада истоветна електронској верзији коју сам предао/ла за објављивање на порталу **Дигиталног репозиторијума Универзитета у Београду.**

Дозвољавам да се објаве моји лични подаци везани за добијање академског звања доктора наука, као што су име и презиме, година и место рођења и датум одбране рада.

Ови лични подаци могу се објавити на мрежним страницама дигиталне библиотеке, у електронском каталогу и у публикацијама Универзитета у Београду.

Потпис докторанда

У Београду, 21.06.2016.

_____

Прилог 3.

Изјава о коришћењу

Овлашћујем Универзитетску библиотеку „Светозар Марковић" да у Дигитални репозиторијум Универзитета у Београду унесе моју докторску дисертацију под насловом:

Утицај биоматеријала на интегритет и век вештачког кука

која је моје ауторско дело.

Дисертацију са свим прилозима предао/ла сам у електронском формату погодном за трајно архивирање.

Моју докторску дисертацију похрањену у Дигитални репозиторијум Универзитета у Београду могу да користе сви који поштују одредбе садржане у одабраном типу лиценце Креативне заједнице (Creative Commons) за коју сам се одлучио/ла.

1. Ауторство

2. Ауторство - некомерцијално

3. Ауторство – некомерцијално – без прераде

4. Ауторство – некомерцијално – делити под истим условима

5. Ауторство – без прераде

6. Ауторство – делити под истим условима

(Молимо да заокружите само једну од шест понуђених лиценци, кратак опис лиценци дат је на полеђини листа).

Потпис докторанда

У Београду, 21.06.2016.

_____

1. Ауторство - Дозвољавате умножавање, дистрибуцију и јавно саопштавање дела, и прераде, ако се наведе име аутора на начин одређен од стране аутора или даваоца лиценце, чак и у комерцијалне сврхе. Ово је најслободнија од свих лиценци.

2. Ауторство – некомерцијално. Дозвољавате умножавање, дистрибуцију и јавно саопштавање дела, и прераде, ако се наведе име аутора на начин одређен од стране аутора или даваоца лиценце. Ова лиценца не дозвољава комерцијалну употребу дела.

3. Ауторство - некомерцијално – без прераде. Дозвољавате умножавање, дистрибуцију и јавно саопштавање дела, без промена, преобликовања или употребе дела у свом делу, ако се наведе име аутора на начин одређен од стране аутора или даваоца лиценце. Ова лиценца не дозвољава комерцијалну употребу дела. У односу на све остале лиценце, овом лиценцом се ограничава највећи обим права коришћења дела.

4. Ауторство - некомерцијално – делити под истим условима. Дозвољавате умножавање, дистрибуцију и јавно саопштавање дела, и прераде, ако се наведе име аутора на начин одређен од стране аутора или даваоца лиценце и ако се прерада дистрибуира под истом или сличном лиценцом. Ова лиценца не дозвољава комерцијалну употребу дела и прерада.

5. Ауторство – без прераде. Дозвољавате умножавање, дистрибуцију и јавно саопштавање дела, без промена, преобликовања или употребе дела у свом делу, ако се наведе име аутора на начин одређен од стране аутора или даваоца лиценце. Ова лиценца дозвољава комерцијалну употребу дела.

6. Ауторство - делити под истим условима. Дозвољавате умножавање, дистрибуцију и јавно саопштавање дела, и прераде, ако се наведе име аутора на начин одређен од стране аутора или даваоца лиценце и ако се прерада дистрибуира под истом или сличном лиценцом. Ова лиценца дозвољава комерцијалну употребу дела и прерада. Слична је софтверским лиценцама, односно лиценцама отвореног кода.